VOLUME 78 JULY 4, 1974 NUMBER 14

JPCHAx

THE JOURNAL OF PHYSICAL CHEMISTRY

PUBLISHED BIWEEKLY BY THE AMERICAN CHEMICAL SOCIETY

THE JOURNAL OF

PHYSICAL CHEMISTRY

AMERICAN CHEMICAL SOCIETY, *1155 Sixteenth St., N.W., Washington, D. C. 20036*

Books and Journals Division

JOHN K CRUM *Director*
RUTH REYNARD *Assistant to the Director*

CHARLES R. BERTSCH *Head, Editorial Processing Department*
D. H. MICHAEL BOWEN *Head, Journals Department*
BACIL GUILEY *Head, Graphics and Production Department*
SELDON W. TERRANT *Head, Research and Development Department*

 Published biweekly by the American Chemical Society at 20th and Northampton Sts., Easton, Pa. 18042. Second-class postage paid at Washington, D. C., and at additional mailing offices.

All manuscripts should be sent to *The Journal of Physical Chemistry*, Department of Chemistry, University of Minnesota, Minneapolis, Minn. 55455.

Additions and Corrections are published once yearly in the final issue. See Volume 77, Number 26 for the proper form.

Extensive or unusual alterations in an article after it has been set in type are made at the author's expense, and it is understood that by requesting such alterations the author agrees to defray the cost thereof.

The American Chemical Society and the Editor of *The Journal of Physical Chemistry* assume no responsibility for the statements and opinions advanced by contributors.

Correspondence regarding accepted copy, proofs, and reprints should be directed to Editorial Processing Department, American Chemical Society, 20th and Northampton Sts., Easton, Pa. 18042. Head: CHARLES R. BERTSCH. Editorial Assistant: JOSEPH E. YURVATI.

Advertising Office: Centcom, Ltd., 50 W. State St., Westport, Conn. 06880.

Business and Subscription Information

Send all new and renewal subscriptions *with payment* to: Office of the Controller, 1155 16th Street, N.W., Washington, D. C. 20036. Subscriptions should be renewed promptly to avoid a break in your series. All correspondence and telephone calls regarding changes of address, claims for missing issues, subscription service, the status of records, and accounts should be directed to Manager, Membership and Subscription Services, American Chemical Society, P.O. Box 3337, Columbus, Ohio 43210. Telephone (614) 421-7230.

On changes of address, include both old and new addresses with ZIP code numbers, accompanied by mailing label from a recent issue. Allow four weeks for change to become effective.

Claims for missing numbers will not be allowed (1) if loss was due to failure of notice of change in address to be received before the date specified, (2) if received more than sixty days from date of issue plus time normally required for postal delivery of journal and claim, or (3) if the reason for the claim is "issue missing from files."

Subscription rates (1974): members of the American Chemical Society, $20.00 for 1 year; to nonmembers, $60.00 for 1 year. Those interested in becoming members should write to the Admissions Department, American Chemical Society, 1155 Sixteenth St., N.W., Washington, D. C. 20036. Postage to Canada and countries in the Pan-American Union, $5.00; all other countries, $6.00. Air freight rates available on request. Single copies for current year: $3.00. Rates for back issues from Volume 56 to date are available from the Special Issues Sales Department, 1155 Sixteenth St., N.W., Washington, D. C. 20036.

Subscriptions to this and the other ACS periodical publications are available on microfilm. Supplementary material not printed in this journal is now available in microfiche form on a current subscription basis. For information on microfilm or microfiche subscriptions, write Special Issues Sales Department at the address above.

Notice to Authors last printed in the issue of June 6, 1974

THE JOURNAL OF

PHYSICAL CHEMISTRY

Volume 78, Number 14 July 4, 1974

JPCHAx 78(14) 1339–1446 (1974)
ISSN 0022-3654

COMMUNICATIONS TO THE EDITOR

■ Supplementary and/or miniprint material for this paper is available separately, in photocopy or microfiche form. Ordering information is given in the paper.

* In papers with more than one author, the asterisk indicates the name of the author to whom inquiries about the paper should be addressed.

AUTHOR INDEX

Editorial

In the days when Sam Lind edited this *Journal* from one side of the Minnesota mall, and Jack Tate the *Physical Review* from the other, keeping up with science was simpler. The former added 3 in. to the shelf each year at a cost of $10.00, the latter 4 to 5 in. for $15.00, in those happier pre-WWII years; and each published all the news that was fit to print in its respective field within 3–6 months of submission. Now we publish 8–9 in. a year; the *Physical Review* runs in sections and even our esteemed sister the *Journal of Chemical Physics* adds a couple of feet; subscription prices and page charges are best not mentioned; and though new specialized journals break out each month to drain the overflow, the time lag to publication currently peaks at about 6 months for our Journal, and bimodally at about 6 and 18 months for the *Journal of Chemical Physics*. In short, few chemists can carry the burden of cost, shelf space, and time to read the journals they wish to follow—they can hardly carry the issues home to read.

The ACS, like other societies which publish scientific journals, has given considerable study to these problems; staff, editors, authors, readers, and members have been involved in consultations to seek means whereby these burdens can be effectively brought under control, and current reading of science brought back from a harassed duty to a relaxed pleasure. In this issue we have the privilege of presenting a paper by Professor Ernest Eliel which admirably discusses the problems and the nature of the approaches which the ACS is trying out in several of our journals. We urge our readers to give this paper careful study. And further, we ask readers and authors and all friends of this Journal to assist us in our experiments to determine optimal use of these experimental methods of publishing. The ACS Books and Journals Division staff has worked and is working hard and effectively on improving the mechanical methods; the effective use of the formats available is up to *us*, the editors, authors, and readers of the Journal.

We have since 1972 utilized both the microfilm and microfiche resources discussed by Professor Eliel; in 1972 6.66% of the papers in JPC included some microform material, averaging overall 0.43 microform pages and 5.49 printed pages, while in 1973 11.71% of the papers used microform, the overall average running 0.86 microform and 4.92 printed pages. (Incidentally, the 1973/1972 comparison shows the effect of the computer-based photocomposition technique which was first used in 1973 with an accompanying type-style change; not only is the cost of composition reduced, but each printed page holds some 11% more material.) We are grateful to the many authors whose thoughtful and responsive cooperation has helped us to develop the use of these formats while adhering to the policy that the identification of material to be published in microform must always be a matter of agreement between the editor and the author. We stress the fact that the microform-published material is not "buried;" it is readily available from the ACS, and moreover in several hundred libraries; a certain number of individual subscribers avail themselves of the microfiche edition. In the 1974 issues we shall also, like our sister publication the *The Journal of Organic Chemistry*, be experimenting with the miniprint format. (See pp 1368 of this issue.)

Our experience convinces us that a significant amount of material can appropriately be placed in the microform/miniprint format; that one cannot delineate the two types of material by a formula; and that the best use of the printed-plus-microform format will be achieved when the author looks forward to such use *as he originally composes his paper*, and plans the structure of his paper with this format in mind.

Some types of material commonly present in physical chemical papers of course come to mind: details about purification of materials, or about apparatus; those structure-factor tables, or long tables of rotational-line frequencies; extensive tables of resulting data (which can be published in absolutely complete detail in microform while a graph on the printed page better shows the nature and trend of the data); mathematical derivations, which can be summarized in the printed page and fully detailed in microform, with computer programs where appropriate; those lengthy arguments which give the logical reasoning leading to a vibrational assignment, or testing out a hypothetical reaction mechanism, which can be similarly treated.

We bespeak your help in making full and wise use of this format. When you next write a paper for us, consider what material you can put in microform, and how to refer to it or summarize it in print. When next you do the essential and generous and gratefully appreciated favor of reviewing a paper for us, let the author and the editor have your suggestions as to possible microform material. Point out to the director of your institutional library the value of the microform editions (either microfilm or microfiche). And let us have your thoughts and reactions as you read articles and find that we have put too much, or too little, in microform.

The rewards, which our calculations show to be not impossible of achievement, include a reasonable cost, sensible shelf-space demand, a reduction of publication time lag, better coverage of our field, and—by no means least in our opinion—a more readable journal.

Bryce Crawford, Jr., Editor

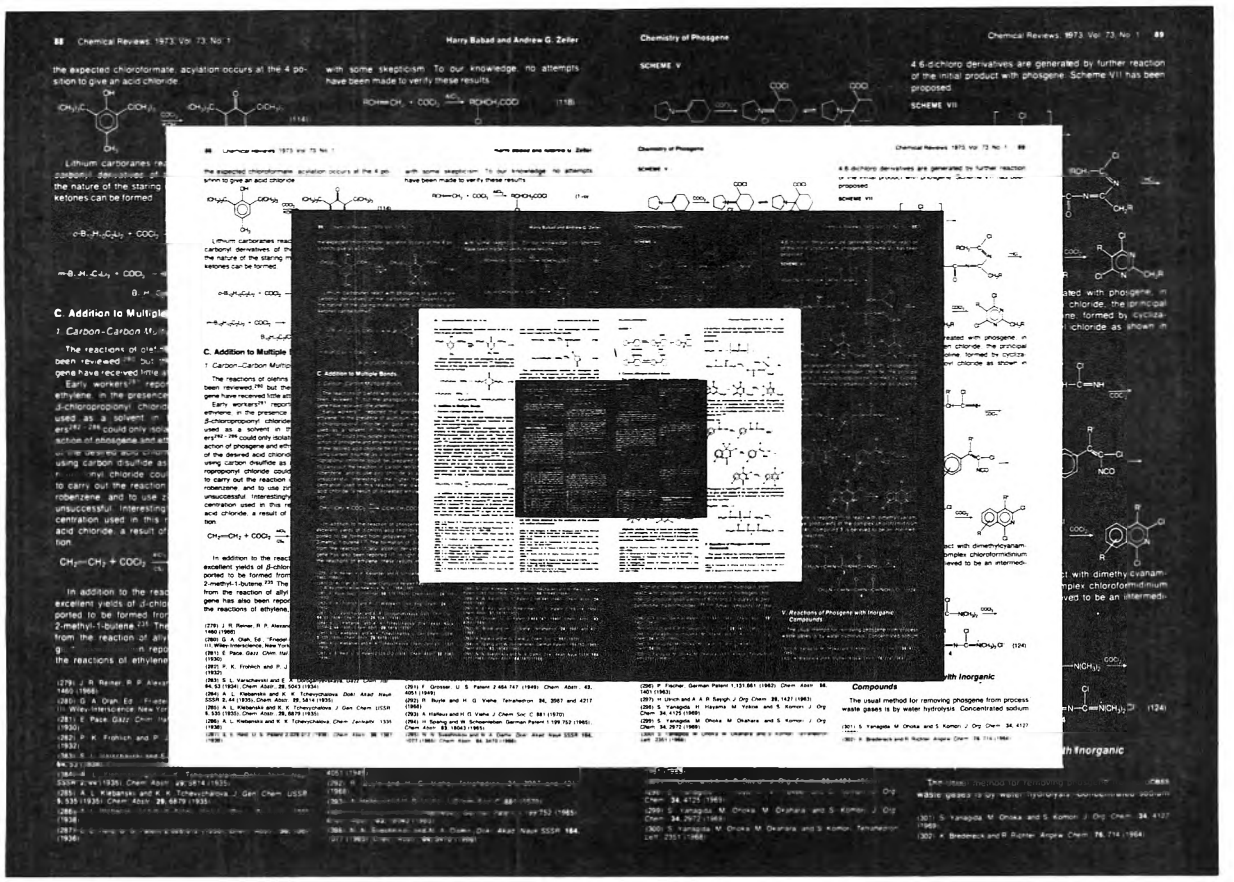

INFORMATION IMPLOSION!

The ACS Journal Microform Program

One of the steps being taken by ACS Publications to reduce new chemical information to manageable proportions is the adoption of microform techniques for storage and publication.

We are using both microfilm and microfiche.

MICROFILM: Most of the ACS periodical publications are now available on **microfilm**, 16 mm or 35 mm, negative or positive, open reel or special cartridge. Back issues—back to Volume 1 for many journals—are available. Subscriptions to current volumes also are available; the **microfilm** is supplied at year's end.

Current subscriptions to **microfilm** editions of journals include a subscription to "hard copy" issues of the journal. **Microfilm** subscriptions are on a lease basis that specifically grants the subscriber a license to make unlimited numbers of photocopies for internal use.

Microfilm editions contain supplementary materials–such as tables, charts, computer printouts, and the like–that are not printed in the regular hard copies. They thus constitute the most complete version of each journal.

MICROFICHE: The supplementary materials which are included at the end of each year in the current microfilm editions of the journals are also available on 105 x 148 mm negative **microfiche** cards.

Journal users can obtain material supplementary to an article, on **microfiche**, soon after publication by following the ordering instructions given at the end of the article.

Microfiche cards containing supplementary material are available on a subscription basis for five journals that have a substantial, continuing volume of such material—these five are Journal of the American Chemical Society, Journal of Organic Chemistry, Journal of Physical Chemistry, Inorganic Chemistry, and Journal of Chemical & Engineering Data. Most, but not necessarily all, issues of these journals have supplementary material. **Microfiche** subscriptions are not available on other ACS publications.

Microfilm edition subscribers receive all **microfiche** cards for the particular journal to which they subscribe and thus do not need to special-order any **microfiche** cards for that journal.

Note: Single issues of journals and entire articles are not available either on microfilm or on microfiche.

To: Special Issues Sales
American Chemical Society
1155 16th St., N.W., Washington, D.C. 20036

Please send me full information on the ACS Journal microform program.

Name _____

Title _____

Address _____

_____

THE JOURNAL OF
PHYSICAL CHEMISTRY

VOLUME 78, NUMBER 14 JULY 4, 1974

Aspects of the Information Explosion

Ernest L. Eliel

W. R. Kenan, Jr. Laboratories of Chemistry, University of North Carolina, Chapel Hill, North Carolina 27514
(Received March 18, 1974)

Certain aspects of the "information explosion" are presented: the function of scientific publishing, the financial picture of scientific journals, the role of various kinds of microform and miniprint, the subdivision of papers into "to-be-printed" and "to-be-archived" parts. Alerting and retrieval services based on computer-readable abstract information are discussed briefly.

> "The difficulty seems to be, not so much that we publish unduly in view of the extent and variety of present day interests, but rather that publication has been extended far beyond our present ability to make real use of the record. The summation of human experience is being expanded at a prodigious rate, and the means we use for threading through the consequent maze to the momentarily important item is the same as was used in the days of square-rigged ships." V. Bush, 1945

The problem Bush, Director of the Office of Scientific Research and Development in World War II, pointed out almost 30 years ago continues to plague us more than ever. Under the impact of generous public support, science, since World War II, has flourished as never before, and with that have come enormous amounts of new information. On the whole, this is clearly a good thing: no one wants to stop the flow of knowledge. Yet that very flow can drown us: knowledge which is not properly accessible is useless knowledge and it can even be worse than useless, acting as a source of confusion and discouragement.

The information explosion is serious in all areas of science and, indeed, in all areas of knowledge. However, as chemists we are particularly involved and also particularly concerned for several reasons. One is that chemistry, more than many sciences, depends on past knowledge—the existing art must be repeated but must not be accidentally and expensively rediscovered. Another reason is that in Chemical Abstracts we have perhaps the world's best basis for information retrieval and at the same time a great stimulus for improving retrieval strategy.

But before going into abstracting, let us consider the genesis of the information, the scientific paper. In essence, the written scientific literature has three purposes: to inform or *alert* those who are working in the same field, to *educate* those who are working in related fields and want to expand their horizons, and to serve an *archival* function for posterity who, in later years, may wish to retrieve details of information accumulated and stored earlier.

In the old days scientists interchanged information by writing each other letters. There are now too many of us to make this kind of information exchange efficient, so we have printed journals and editors and referees to decide what should go into them. But there is one thing in common between letters and articles: they require reduction of an experimental observation and/or interpretation to the written word. Herein lies the first bottleneck. Many scientists and engineers do not know how to write clearly and concisely. As a result the written record is more difficult to read than it should be and both its informational and educational functions are impaired.

I like to illustrate the source of the difficulty of reducing experimental observations and interpretations to clear prose with an anecdote which reaches back over 20 years when my wife was secretary of the Mathematics Department at a major university. At that time the movie "Hamlet" with Laurence Olivier was being shown and my wife encouraged one of the graduate students to see it. The next day she asked him how he had liked it. "Not very much," he said, "I got bored and walked out in the middle. But, now I am bothered because I shall never know how the story ended." My wife, in shock, asked him if he had not read Hamlet in school or at least in college, where he had been an engineering undergraduate. The answer: "No, I took English for engineers."

Looking at my students' laboratory reports I feel that while the situation has improved over the years, it is still far from perfect. There is much room for better education in English and the ability to write—a skill which should be taught in high school rather than in college. Sugges-

tions have been made to get around the writing problem by employing ghost writers for lab reports and papers. Personally I doubt this will work, for I know how I feel myself when I write up a paper of work I have done years before and with which I no longer have close contact. Of course, there is a reward for good writing: more people read one's papers. It is a talent which contributes to scientific success.

Let us return to the information process. Let us assume that the paper is written in understandable form and that it is scientifically sound and has been accepted by referees and the editor. (This is not the place to discuss the scientific editing process except to say that, if an editor has budgetary limitations on the number of pages he can publish, he has at present only three choices: to tighten his publication standards and accept fewer papers, to ride herd on his authors to be briefer—which is very difficult—or to let publication delays become longer.) The next step is for the paper to be printed. That is a costly process. Just to set a page in type, *e.g.*, in The Journal of the American Chemical Society (JACS), costs approximately $54. Since JACS contains about 9000 pages per year, this amounts to $486,000. This figure represents about 45% of the total budget, with printing, editorial costs, subscription fulfilment costs, and overhead accounting for the rest. Unfortunately, printing and paper costs have been skyrocketing. JACS was produced in 1972 at a deficit of $105,000. If neither page charges nor subscription rates are increased, the deficit will rise to $321,000 in 1976. This clearly cannot be allowed to happen, for there are no subsidies, public or private, to cover such deficits. In fact, it has been computed that at constant subscription rates, the *total* deficit of all the American Chemical Society journals in 1976 would be over $675,000, which would constitute a loss calculated to be about $6.50 per member to be compared with total present dues of $28. Since there are many competing claims for the Society's dues, it is highly unlikely that *ca.* 25% of the dues income will be allocated to subsidizing the publications program, much as some members may consider such a subsidy desirable.

Before considering remedies, let us take a look at the income side of the ledger. There are four sources of revenue: member subscriptions, nonmember subscriptions, advertising, and page charges. Member subscriptions are a limited source of revenue. JACS, at a subscription price of $22, had nearly 10,000 member subscribers in 1973. This is a large number (amounting to nearly 10% of the membership) but, unfortunately, it has been steadily declining in the last 5 years. Between 1971 and 1973 total journal subscriptions for ACS journals by members declined over 8%, from *ca.* 67,000 to *ca.* 61,500. Since 1969 when the member subscription rate to JACS was increased from $16 to $22, the number of member subscriptions has dropped from 12,900 to 9800. One might expect the situation to be more favorable with nonmember subscriptions since libraries can ill afford to do without the major journals, but this is unfortunately not the case. In 1972 the ACS increased most nonmember subscription prices by 50%. The total number of nonmember subscriptions in 1973 as compared to 1971 has dropped 6.7%; for JACS the drop has been from 6100 to 5600.

We come to the conclusion that subscription income is precarious. What about the other two sources? Advertising is not a major factor in most specialized technical journals (as distinct from general ones, such as Science and Physics Today), with a few exceptions (*e.g.*, Analytical Chemistry). In any case, the state of technical advertising is parlous. We are left with the most undesirable source of income: page charges. Where, in the past, an author would receive a honorarium for his efforts, he must now pay a penalty to see his work published. Of course, it is not expected that the author will pay this charge out of his own pocket. It is really a hidden government or industrial subsidy; it is expected that the sponsor of the work pays for the page charge. Page charges are high. They amount to $50 per page in ACS journals; in AIP (American Institute of Physics) journals they are now $70. The payment of page charges is not mandatory and if (and only if!) the work an author publishes is not sponsored, he may (and legitimately should) ask for a waiver of page charges. In fact nearly 40% of the authors in ACS journals do just that. In the American Chemical Society, authors who do not pay page charges are not penalized: the editor does not know about payment when he accepts the paper and authors who do not pay are not discriminated against. The situation is otherwise in AIP journals. Although editors of AIP journals also accept papers purely on their scientific merits, only a limited number of pages are allocated to authors who do not pay page charges. As a result, a paper that might take 6–7 months to appear if page charges are paid is delayed by about 1 year to a total of 18–21 months from submission to publication. Clearly, page charges are at best a necessary evil.

What can be done to keep scientific journals viable? One experiment which has been carried out with The Journal of Medicinal Chemistry and Inorganic Chemistry is to use socalled "cold type," *i.e.*, to type a master copy from which printing plates are then made photographically rather than to set the type in a conventional way. The savings in this process are substantial, as much as $15–20 or approximately one-third of composition costs. The product is quite pleasing, in fact, it is distinguishable from a typeset product only by the lack of a flush ("justified") right margin. It should be stressed that this process is entirely different from producing journals by photographing the author's manuscript and making plates from it. The latter process tends to produce poor copy (since authors' manuscripts tend to be esthetically imperfect) and low information density. In the "cold type" process the manuscript is retyped on a special typewriter with a variety of symbols by a trained operator and is illustrated by an expert draftsman.

Another way of saving composition cost is by computer composition—the so-called "photon process." Both typewriter and computer composition reduce cost by a one-time fixed factor but obviously do not contain the expansion of the literature.

Let us return from the digression of journal economics to the more general problem of the information explosion. Not only do journals get more expensive, there are also more of them and they are getting fatter. The problems of journal economics and of what might be called the "information burial" (it both buries us and gets buried) are, of course, closely related. If the amount of material printed per unit time remained constant, costs should increase roughly with inflation and one might expect that libraries, and perhaps even individuals, could keep up. In fact, however, at least up to now, there has been nearly exponential growth. As a result, not only have journals become fatter but there have been more of them. Library budgets are unable to keep up with the situation. Nor can any individual's reading and comprehension power.

One might suggest that the remedy is for editors to accept fewer papers for publication, but this is clearly a dangerous course. If a paper is novel and if the work reported is valid and scientifically sound, the only legitimate reason to reject the paper is that it is of no interest ("irrelevant") and that argument is, of course, not infrequently used. But it is a dangerous argument, as might be illustrated by a story related to me by Milton Burton, the Director Emeritus of the Radiation Laboratory at the University of Notre Dame. It occurred around 1940 or 1941, shortly before the U.S. entered the war, and concerns a thesis by a graduate student of Professor Benedetti Pichler's at New York University. The topic of the thesis was "The Attainable Limits of Microanalysis of Rare Earth Elements." What could be more useless and uninteresting than the trace analysis of an obscure group of elements? There was some thought (fortunately discarded) that the thesis should be rejected on the basis of "irrelevance," to use a fashionable expression. Yet, only a few months later, after the inception of the Manhattan Project, the thesis became so important that it was classified, for the now obvious reason that rare earth elements turned out to be fission products and their analysis, on the ultramicro scale, proved to be most important for studying the fission process in the preliminary experiments prior to achieving a chain reaction.

We might ask if there is any way of streamlining information so that it becomes both less expensive to print and easier to absorb. The American Chemical Society has studied this problem for some time through a special "Committee on Improved Publication Formats" of which the author of this article is a member and the editor of this journal is chairman. Some of the thinking which went into this study and likely developments resulting from it may be of interest. They are largely what one might call "evolutionary" though a far more "revolutionary" scheme is now being experimented with in Europe.

In attempts to improve publication formats, one might focus on the fact that only a certain fraction of each scientific article, varying perhaps between 10 and 70%, depending on the article, is of real educational value to the average reader. The remainder is of interest only to the few experts in the specific field of the article or to those later investigators who, in posterity, wish to retrieve certain specific information from the article. Thus one might make a case that only the generally interesting material should be printed in bound and hard-cover form whereas the rest should be "archived," *i.e.*, photographed directly from manuscript and put out in the form of microfilm, microfiche, miniprint, or several of these media.

There are, of course, difficulties with such a scheme. It requires a tremendous educational campaign to get authors to understand how they should divide their manuscripts into "to be printed" and "to be archived" parts. It requires great efforts on the part of editors to help in this educational process and, eventually, after a transitional period, to insist that a reasonable division between these two portions be adhered to by the author. Also, even the most optimistic estimates contemplate savings of only 30–50% in the size of the printed version. However, even that much would save a great deal of printing cost and would make it much easier for the reader to digest the essential part of the paper.

If this development comes about, we foresee that there might be three kinds of subscriptions. One would be a hard-cover, printed, core version only, mainly for the use of individuals. The second one would be the core version *plus* all supplementary material in the form of microfiche supplied *with* each journal. This version would be suitable for smaller libraries and for those few demanding individuals who feel they need the entire journal. It would, of course, be considerably more expensive than the core version only, but the cost might not be higher than that of the present library subscriptions, since filming costs less than the expensive process of printer composition. Fiche readers are available inexpensively, at a cost of about $100 and are thus well within financial reach of even a small college library. However, this version would *not* be adequate for a large library for two principal reasons: one is that fiche is *not* a suitable permanent archival form for a large library because of storage and loss problems, and the second is that it would *not* be sold with the right to make offprints. Thus a large library would probably subscribe to the third or "deluxe" version which includes all of the above plus reels of microfilm which are supplied at regular intervals, whenever there is enough material (printed plus supplemental) to fill a reel. This version would also confer the right to make enlarged offprints. Microfilm is, of course, in any case the library medium of the future because of its much smaller storage volume, because of the ease with which modern cassette 16-mm microfilm can be inserted into a self-engaging microfilm reader, unwound, and read and the ease with which enlarged printout can be produced from it. I hasten to add that all ACS journals are in fact available in microfilm format and that those journals containing an appreciable amount of supplemental material also make such material available in fiche form. So far, however, authors have made very limited use of this medium (see below).

This proposed system has one major advantage and one major drawback. The drawback is the obvious high cost of the "deluxe" journal editions which the major libraries would have to defray. The present cost of JACS on microfilm (including the hard-cover edition) is $275 per year, compared to the library price of the hard-cover edition alone of $66; it includes the right to make off-prints. There is no question that there will be major budgetary problems for the large libraries beyond those already plaguing us. The advantage is that we may, under this scheme, be able to abandon the nonmember *vs.* member subscription dichotomy. At the moment, JACS costs $22 to Society members, $66 to nonmembers. The Society is trying to keep the member's price low because of the belief that journals provide an important educational function and that individual subscriptions should therefore be encouraged. One problem in this, however, is cheating. Despite the membership subscription pledge introduced in 1973 and despite the overprint on member subscription journals, there is evidence that member's current journals are leaked to libraries with resulting loss of income to the Society. Under the new scheme, separate member subscription prices could eventually be abolished—the price of the printed version would be roughly the member price, that of the printed-plus-fiche version would be roughly that of the nonmember price, and the complete version would sell at a price comparable to the present microfilm subscription.

One of the drawbacks of the hard cover–microfilm–microfiche scheme is that a reader would have to own a microfiche reader to read the journal (or any particular article therefrom) in its entirety and that the current information package (as distinct from the microfilm which is

issued only every few months when a reel is complete), would come in two separate forms: the hard-cover journal and the microfiche. And, although microfiche readers are not very expensive, cost is of some consideration and so is the convenience (or inconvenience) of using them. There exists therefore at the present time something of a "chicken-and-egg" situation: authors are not anxious to place their data in the supplemental (fiche) material because they think (with some justification at this moment in time) that it cannot be instantly retrieved; libraries are less than anxious to buy the microform because the overwhelming percentage of material (over 95%) is still published in hard-cover form. The conclusion has therefore been reached that the microform should be included in the journal itself in the form of miniprint. This means that no separate vehicle (such as fiche) is used and that the material can be read with a good hand lens, available for a few dollars. The scheme, which has already become operative on an experimental basis in The Journal of Organic Chemistry (*cf.* the Jan 11, 1974 issue, pp 8-10, 12, 18, 19), involves miniprinting the less essential parts of a paper directly from the author's manuscript at a reduction of 9:1, *i.e.*, nine manuscript pages to one journal page. Such material is easily readable with a good lens; it can be read with the naked eye (albeit with some difficulty) by a reader with good vision.

The savings are considerable. There will be hardly any typesetting costs for photographed minipages (this saving will be partly passed on to the author who will pay no page charges) and there will be a saving in printing and paper for miniprinted pages of some help, since the material which fits on one miniprinted page would normally occupy about 2-4 typeset pages. It will, however, be necessary for authors to revise their writing habits quite extensively. This point has already been mentioned, but it is true to an even greater extent in the miniprinted journal since it is contemplated that more than half of a typical article, including much of the experimental part, will be miniprinted. This almost obliges the author to write his article in two parts, part A which will contain the essential information (essentially a very long abstract of perhaps two to four printed pages) and part B (miniprinted) which will contain all the details (*cf.* The Journal of Organic Chemistry, Vol. 35, pp 3591-3646, 1970).

Making journals available with miniprint inserts is not to do away with microfilm. The microfilm editions of the journals containing the complete article (both printed and miniprinted version) will be retained. The miniprinted part, which, in the hard cover, is reduced at a scale of 9:1, in the microfilm version will continue to be filmed at one page to a frame. This means that full-size print-out of supplemental pages can be made from the microfilm—an important point since there is, at present, no good way of getting full-sized replica from miniprinted copy. Thus, in fact, the miniprinted journal should stimulate, rather than supplant, the distribution of microfilm to libraries.

One incidental point of concern is that legible miniprint can be made only from clean and neatly typed authors' manuscripts. This will no doubt encourage the use of tape-typewriters in manuscript production, since clean corrections can readily be made with such typewriters.

The proposed European ("revolutionary") scheme of information abbreviation is currently being experimented with in *Chemie-Ingenieur-Technik*. In this scheme it is contemplated that the only printed version of a paper will be a synopsis, about one page in length—essentially a summary with a few pictures or formulas. This synopsis will also serve as the abstract of the paper in the abstract journals, such as Chemical Abstracts. The full paper will be microfilmed from author's copy and will be available only in the microfilmed version. In the author's opinion, this scheme has serious dangers in that it might well destroy what I like to call the "edifying" purpose of the journal article (others call it "browsing") and might possibly kill the whole tenuous process of transmittal of scientific thought and thereby the progress of science altogether.

The final part of this paper will be dedicated to the problem of information retrieval. Chemical Abstracts is probably the world's most outstanding medium for retrieving scientific information but the process has become increasingly more costly and time-consuming because the amount of information is so vast. Chemical Abstracts themselves have been vigorous in adopting new methods and applying new technology. Their entire indexes (author, subject, formula, patent, etc.)—and the indexes are, of course, the key to access to the system—are now produced by computer, as is about 40% of the text of the abstracts. The responsibility for abstracting and indexing is being spread to other national groups through agreements with the Germans and the British, hopefully also with the French and the Japanese and perhaps some day even with the Russians. Many abstracts are made from page proof, before the published paper even appears, thus bringing CA more up-to-the-minute. But even with all this cooperation and most modern methods of technology total costs inexorably increase, although the processing cost *per abstract* has decreased in terms of dollars adjusted for inflation.

An investigator in any field would like to find out, as quickly as possible, any new developments in his field. It used to be fashionable to read Chemical Abstracts to this end, but the task has become too burdensome for most people. There is now a publication called "Current Contents" which reproduces the tables of contents of a large number of chemical journals published each month. The ACS publishes a similar pamphlet, called "ACS Single Article Announcements," relating to its own journals with which comes a service to order reprints of any article listed. But these services are not tailored to individual interests, they require a total scanning of *all* titles for items of concern. More individually tailored services have been developed for what I call the "alerting" function of the secondary or abstract services.

One of these is "Chemical Titles." Chemical Titles (CT) also prints the tables of contents of the journals it scans each week, using a so-called "Coden" (letter abbreviation) to characterize each journal. Along with this comes an author index (with cross reference to the tables of contents) and a so-called "keyword index" in which the title of each article is printed in numerous different permuted ways so that each one of several key words of the title of the article may come up as the first word. This index is alphabetical and also has cross reference to the tables of contents. Thus if one wants to find all papers with the word "conformation" in the title he needs only to look under "conformation" to find cross references to all the pertinent journal articles (identified by Coden and page number) there.

CT still involves a lot of work in its use and it has the draw-back of only listing those terms which occur in the *title*. Often, important concepts in a scientific paper do not occur in the title. To remedy these two shortcomings,

Chemical Abstracts Service in Columbus has created "Chemical Abstracts Condensates." This service comes only in the form of computer tapes and contains, for each article, not only the full citation, including the title but also key words selected from both the title and the abstract text.

This computer tape can be played against an "author profile" of key concepts, author names, etc., and thus a computer retrieval can be made, in the form of print-out cards or CRT display, of *all* articles containing, in the title or key words, or as authors, the terms prescribed by the user of the service. There are several computing centers in the USA that provide this kind of service: for example, at Illinois Institute of Technology, at the University of Georgia, at the University of Pittsburgh, at Indiana University; there are also a number of such services abroad. The service is quite cheap, about $200–300 for a year's subscription. The reason for the low cost is that a service center can play a CAS Condensate tape against the profiles of several hundred customers and retrieve the information they want all at one time. Also, if the profile is not initially satisfactory, because it does not retrieve all the desired information, or because it provides too much information ("false drops"), the profile can readily be modified from one week to the next.

The situation for retrieving back information is much less satisfactory. First, Chemical Abstracts Condensate tapes only go back to July 1968. Second, the cost of playing a number of condensate tapes against one profile is infinitely greater than playing one tape against a multiplicity of profiles because of the obvious access problem. Third, an error in the retrospective profile can vitiate the output and correction of such an error is very expensive. Finally, whereas a delay of a couple of days in the mails of alerting information is not serious, retrieval information is usually wanted within a few hours, while an experiment is in progress in the laboratory, and that is unfortunately not yet possible at the present time.

There exists another alerting service, provided by a privately owned organization in Philadelphia called the Institute for Scientific Information (ISI). ISI has its own abstracting service; it does not abstract as many journals as CAS but only those *ca.* 2500 journals it considers most important for chemistry (actually these journals contain about 90% of all chemical information). That is a slight drawback; it also makes the system more parochial. But there is a trade-off: ISI profiles, in addition to concepts, authors, organizations, etc., may also have, as input, citation to a given author's work or citations to a given article or book. In this way, all work derivative from an original paper or from the work of a given man can be retrieved.

In conclusion, it seems evident that problems of information storage, dissemination, and retrieval are very serious indeed. Unless these problems are solved, they may well choke off the entire progress of science, regardless of anything else that may happen, by turning science into a Tower of Babel. However, the author is optimistic that, if the information problems are tackled as vigorously as other problems in science have been, viable solutions will in due time be found. The Chemical Abstracts Service has done a very good job in illuminating the way, but much more remains to be done, one of the most urgent problems being that of storing information in such a way as to produce rapid computer access to a large amount of material.

Acknowledgment. The author is indebted to Dr. D. H. M. Bowen for providing some of the data cited and to Dr. R. J. Rowlett, Jr., for a critical reading of the manuscript. This paper is based on a Sigma Xi lecture given at the University of North Carolina on November 20, 1973.

Rate Constants for Reactions of Methylene with Carbon Monoxide, Oxygen, Nitric Oxide, and Acetylene

Allan H. Laufer* and Arnold M. Bass

Physical Chemistry Division, National Bureau of Standards, Washington, D. C. 20234 *(Received January 23, 1974)*

Publication costs assisted by the National Bureau of Standards

Rate constants for some reactions of triplet and singlet methylene have been measured by means of the flash photolysis of ketene with product analysis by gas chromatography. Rate constants for reactions of triplet methylene with NO, O_2, and C_2H_2 in helium are $1.6 \pm 0.1 \times 10^{-11}$, $1.5 \pm 0.1 \times 10^{-12}$, and $7.5 \pm 1.0 \times 10^{-12}$ cm^3 molecule^{-1} sec^{-1}, respectively, over the pressure range of at least 50–700 Torr. The rate constant of triplet CH_2 with CO in 700 Torr of helium was $\leq 1.0 \times 10^{-15}$ cm^3 molecule^{-1} sec^{-1}. Rate constants for reaction of singlet CH_2 with NO, O_2, CO, and CH_2CO were $<4 \times 10^{-11}$, $<3 \times 10^{-11}$, $<9 \times 10^{-12}$, and $3.2 \pm 1.2 \times 10^{-11}$ cm^3 molecule^{-1} sec^{-1}, respectively. The triplet CH_2 reactions were measured relative to $^3CH_2 + {}^3CH_2 \rightarrow C_2H_2 + (H_2 \text{ or } 2H)$. The rate constants for singlet CH_2 were relative to $^1CH_2 + He \rightarrow {}^3CH_2 + He$.

Introduction

The reactions of the methylene species have received increasing attention during the past few years after the spate of reviews[1] about a decade ago. Following the descriptive results obtained earlier, recent work has been directed toward quantitative studies including the energetics of both singlet and triplet methylene as well as the differences in reactivity between these species. Rate constants for quenching of $^1CH_2$ to $^3CH_2$[2] and for reaction with several organic compounds have been measured.[3a] Bell[3b] has deduced a whole series of rate constants of singlet methylene, and rates of hydrogen abstraction by $^3CH_2$ have been predicted based upon a BEBO calculation.[4]

Interpretation of reaction mechanisms involving methylene has been complicated by the lack of quantitative information on the relative amounts of singlet and triplet species present during the reaction. Efforts have been made to scavenge either the singlet or triplet and examine the product distribution resulting from the reaction of the remaining moiety. Two reagents, CO and O_2, have been extensively used to remove $^3CH_2$ from reaction mixtures. Quantitative rate data are not available for these reactions although recent evidence[5] suggests the collision efficiency of CO with $^3CH_2$ to be $<10^{-5}$, which disagrees with earlier evidence for a rapid reaction.[6] Further, the reaction has been found to be pressure dependent, and at low pressures (<50 Torr) excess CO does not completely eliminate $^3CH_2$ reactions.[7]

The scavenging ability of O_2 with respect to $^3CH_2$, initially observed about 20 years ago,[8] has been widely utilized to examine the chemistry of $^1CH_2$. Reaction of $^3CH_2$ with O_2 is estimated to be much more rapid than it is with CO. In fact, the collision efficiency of O_2 toward $^3CH_2$ is about 10^4 times greater than with CO, suggesting an overall collision efficiency of about 1 in 10. NO, though not used extensively to suppress reactions of $^3CH_2$, has been utilized in CH_2 containing systems to eliminate complicating alkyl radical reactions.[9] The effect of NO upon the chemistry of CH_2 systems has not been examined systematically.

Flash photolysis of ketene has been shown to be an excellent source of CH_2.[3a] Addition of inert gas to the system produces only $^3CH_2$ which reacts to produce C_2H_2 and trace quantities of methylacetylene and allene.[3a] These products are all amenable to analysis by gas chromatography. Addition of a chemical species which can react with $^3CH_2$ reduces the yield of hydrocarbon products. The reduction in products due to the reaction of $^3CH_2$ with the additive leads to a value for the rate constant of this reaction provided the rate constant of the competing reaction (the combination of methylene) is known.

In this study we have examined the CH_2 system and have obtained rate constants for the reaction of $^3CH_2$ with NO, O_2, CO, and C_2H_2. In addition we have been able to deduce several rate constants for the reactions of $^1CH_2$.

Experimental Section

The vacuum-ultraviolet flash photolysis and gas chromatographic analysis system has been previously described in detail.[10] Very briefly, the flash apparatus consists of a quartz reaction vessel placed inside a 3000-J flash chamber. The photoflash, produced by a pulsed discharge through N_2, had a 1/e decay time of about 5 μsec. Following the flash, samples for chromatographic analysis were rapidly withdrawn from the center of the reaction vessel through a sampling valve, and injected into the chromatograph. The products, CH_4, C_2H_2, methylacetylene, and allene, were separated on a 7-m, 6-mm o.d. stainless steel column packed with 30% (w/w) squalane on Chromosorb P. Results of a "typical" run are shown in Figure 1a. The final large peak is due to cyclopropane which was added to the original mixture as an internal standard. At the concentrations used, the cyclopropane was inert as evidenced by the same product distribution with and without its presence.

Ketene, whose preparation and purification have been reported,[11] was utilized as the source of methylene. O_2 and CO were obtained commerically and mixed with ultrapure He at high pressure. Samples of the mixture were metered into the reaction vessel at pressures of several mTorr. NO was also commercially obtained and purified by repeated degassing and subsequent storage over silica

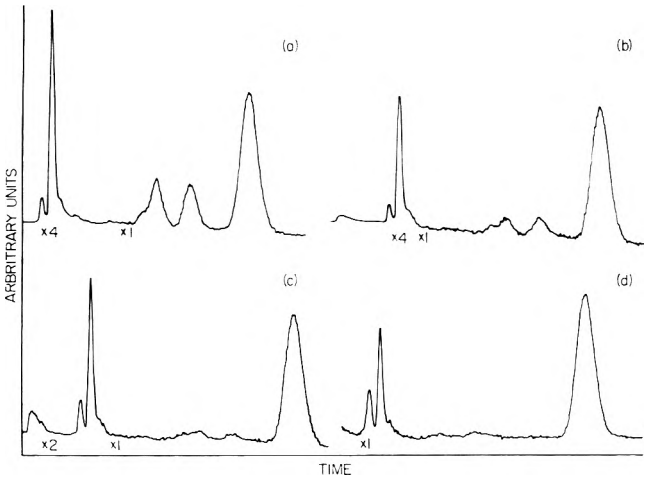

Figure 1. Chromatographic analysis of a "typical" run: (a) initial conditions 40 mTorr of CH_2CO, 700 Torr of He, and 1.5 mTorr of cyclopropane. The peaks are due to CH_4, C_2H_2, methylacetylene, allene, and cyclopropane, respectively. (b) A plus 50 mTorr of NO. (c) A plus 100 mTorr of NO. (d) A plus 150 mTorr of NO.

gel. Samples of NO were obtained by condensing initially at −196° and collection of the initial fraction upon warming. The NO was diluted with ultrapure helium so that samples in the mTorr range could be placed in the reaction vessel.

In a typical series of runs, several mTorr of ketene, mixed with helium, was admitted to the reaction vessel which was then pressurized with ultrapure helium. The procedure for mixing samples has been described.[10] After the appropriate mixing time, the sample mixture was flash photolyzed and a 5-cm^3 sample withdrawn and injected into the chromatograph. The procedure was repeated several times, with a new sample mixture time, to ascertain accurately the initial product distribution. Succeeding experiments were performed in the same manner except that NO, O_2, or CO were added in known quantities prior to flashing. "Raw" data are shown, as a function of increasing additive, in Figures 1b, 1c, and 1d.

Results

As previously mentioned, the rate constants were obtained from the observed *decrease* in the yield of C_2H_2 with increasing additive. It was very important, therefore, to determine the linearity of the vpc response to C_2H_2. At concentrations required for our analyses, the response of the flame detector was not, in fact, linear with sample pressure; presumably due to loss of C_2H_2 on the column material. The instrument was calibrated in the pressure region of typical yields of product which were from 0.06 to 1.8 mTorr (1.9×10^{12}–5.8×10^{13} molecules cm^{-3}). The true acetylene yields were then obtained from the calibration curve.

In the absence of additive the products of the flash photolysis of ketene were predominantly acetylene, methylacetylene, and allene. The latter products arise from the reaction of $^3CH_2 + C_2H_2$ as evidenced by the rapid disappearance of the substituted acetylene with even very small pressures of additive. The total yield of $^3CH_2$ was determined from

$$^3CH_2 = 2[C_2H_2] + 3[C_3H_4]$$

where C_3H_4 is the sum of the methylacetylene and allene.

TABLE I: Summary of Rate Constants of Methylene

Reaction	Rate constant, cm^3 molecule^{-1} sec^{-1}
$^3CH_2 + C_2H_2 \rightarrow C_3H_4$	$7.5 \pm 1.0 \times 10^{-12}$
$^3CH_2 + NO \rightarrow$ products	$1.6 \pm 0.1 \times 10^{-11}$
$^3CH_2 + O_2 \rightarrow$ products	$1.5 \pm 0.1 \times 10^{-12}$
$^3CH_2 + CO \rightarrow$ products	$\leq 1.0 \times 10^{-15}$
$^1CH_2 + CH_2CO \rightarrow C_2H_4 + CO$	$3.2 \pm 1.2 \times 10^{-11}$
$^1CH_2 + NO \rightarrow$ products	$<4 \times 10^{-11}$
$^1CH_2 + O_2 \rightarrow$ products	$<3 \times 10^{-11}$
$^1CH_2 + CO \rightarrow$ product	$<9 \times 10^{-12}$

Ethylene was detected with a yield which increased with a decrease in pressure of inert gas. We assume that the CH_2 produced, as a result of the photodissociation, is in a singlet state (see Discussion). Since the quenching of $^1CH_2$ to CH_2 by He (the pressurizing gas) has a rate constant of 3×10^{-13} cm^3 molecule^{-1} sec^{-1},[3a] the absence of $^1CH_2$ is assured at high helium pressures. The absence of C_2H_4 at high pressure is further indication that the reaction

$$^3CH_2 + CH_2CO \longrightarrow C_2H_4 + CO \qquad (1)$$

is indeed quite slow, in agreement with Lee, *et al.*,[12] who obtained a value for $k_1 \cong 10^{-17}$ cm^3 molecule^{-1} sec^{-1}. At lower helium pressures, $^1CH_2$ is not deactivated and can react with ketene to produce C_2H_4, *via*

$$^1CH_2 + CH_2CO \longrightarrow C_2H_4 + CO \qquad (2)$$

It was initially required to determine the rate constant for

$$^3CH_2 + C_2H_2 \longrightarrow C_3H_4 \qquad (3)$$

since it constituted an important sink for $^3CH_2$. In the absence of products other than C_2H_2 and the two C_3H_4 isomers, a rate constant for reaction 3 was calculated using a rate constant for the combination of two $^3CH_2$ radicals of 5.3×10^{-11} cm^3 molecule^{-1} sec^{-1}.

$$^3CH_2 + {}^3CH_2 = C_2H_2 + (H_2 \text{ or } 2H) \qquad (4)$$

The desired rate constant was obtained from a determination of the product yields. The model included, initially, reactions 3 and 4 for which the time-dependent equations are

$$d(CH_2)/dt = -2k_4(CH_2)^2 - k_3(CH_2)(C_2H_2) \qquad (A)$$

$$d(C_2H_2)/dt = k_4(CH_2)^2 - k_3(CH_2)(C_2H_2) \qquad (B)$$

$$d(C_3H_4)/dt = k_3(CH_2)(C_2H_2) \qquad (C)$$

The usual steady-state assumption is invalid in the flashed system and, therefore, the unknown rate constant, k_3, was calculated by obtaining a numerical solution to eq A, B, and C utilizing the Runge-Kutta method. The step size in the calculation was 10^{-6} sec. The calculated value for k_3 is tied to the observed final product yields of C_2H_2 and C_3H_4. Since C_2H_4 is not a product at high inert gas pressure, the reaction of $^3CH_2$ with CH_2CO (reaction 1) was not included in the calculation. The result was $k_3 = 7.5 \pm 1.0 \times 10^{-12}$ cm^3 molecule^{-1} sec^{-1}. The value of k_3 was found to be independent of added helium from 20 to 700 Torr and was used in all subsequent calculations. At lower pressures, particularly at 20 Torr, the increase in C_2H_4 associated with reaction 2 did not affect the calculation since we were only interested in the fate of the $^3CH_2$ species. Limits have not been placed upon k_3 but will be discussed separately later.

The addition of NO as a scavenger requires the addition of reaction 5 to reactions 1, 3, and 4 to complete the mechanism.

$$CH_2 + NO \longrightarrow [CH_2NO] \quad (5)$$

We were not able to isolate the addition product of (5) but simply observed a decrease in the products of reactions 3 and 4 which were attributed to (5). Based upon such a mechanism, a calculated bimolecular rate constant for (5) expressed as the unweighted average of 19 determinations was $k_5 = 1.6 \pm 0.1 \times 10^{-11}$ cm^3 molecule^{-1} sec^{-1}. In this as well as the remainder of the rate constants, the error is the statistical deviation of the mean itself. The value for k_5 was independent of both the helium pressure from 20 to 700 Torr and of NO over the pressure range of 7.7 to 150 mTorr. The initial CH_2 concentration was varied from ~1.3 to 9.5 mTorr.

Initial studies using O_2 as a scavenger for $^3CH_2$ indicated that greater quantities of O_2 than NO were needed to remove similar amounts of C_2H_2. Therefore, all the experiments involving O_2 were performed at higher concentrations, in the range from 25 to 202 mTorr of additive. The rate constant, expressed as an average of 27 determinations, was also independent of helium pressure from 50 to 700 Torr, and was found to be $1.5 \pm 0.1 \times 10^{-12}$ cm^3 molecule^{-1} sec^{-1}.

Efforts were made to reduce the C_2H_2 yield by adding CO, a reported excellent scavenger for $^3CH_2$.[13] At the highest pressures of helium used in this study, 700 Torr, the effect of added CO at pressures as high as 1 Torr resulted in only a very slight reduction of C_2H_2. The combination of $^3CH_2$ to yield C_2H_2 proceeded virtually unhampered at all CO pressures from 50 to 400 mTorr. The rate constant we determined can only be expressed as a limiting value based on the observable reduction in C_2H_2. The rate constant so determined is $\leq 1.0 \times 10^{-15}$ cm^3 molecule^{-1} sec^{-1}. The large concentrations of CO required to reduce the observed C_2H_2 may cause complications which are not readily discernable, e.g., possible physical quenching of $^1CH_2 \rightarrow {}^3CH_2$ resulting in increased C_2H_2 relative to the initial value, and further work on this system was not performed.

Reactions of $^1CH_2$

As previously mentioned, the yield of C_2H_4 was found to vary with total pressure. It has been suggested that the formation of C_2H_4 is due to reaction 2, which involves singlet CH_2. To examine this hypothesis, we added up to 100 mTorr of NO to a mixture of ketene and helium at a total pressure of 20 and 50 Torr and examined the yields of both C_2H_4 and C_2H_2. The presence of NO decreases the C_2H_2 to about 4% of its initial value while the C_2H_4 remains virtually unchanged suggesting different precursors. In the determination of the rate constants of reactions of $^1CH_2$ with ketene, it was assumed that small quantities of additive do not affect the quenching of $^1CH_2$ to $^3CH_2$. In the same way as we determined rate constants of $^3CH_2$ we can obtain values for rate constants of $^1CH_2$ with respect to the deactivation of $^1CH_2$ by He. Based upon eight determinations, k for reaction 2 was determined to be $3.2 \pm 1.2 \times 10^{-11}$ cc molecule^{-1} sec^{-1} or about one in every ten collisions. The time scale of this reaction was much shorter than for the reactions of $^3CH_2$. In fact, with respect to the $^1CH_2$ chemistry, the reaction was essentially complete in 800 nsec necessitating a much smaller step size in the Runge–Kutta calculation than used in calculation of triplet rate constants. Further, since our flash duration is the order of 5 μsec, the reaction was complete during the flash itself which would lead to a large error.

We assumed, for calculation purposes, the instantaneous photolysis of substrate to produce the primary fragment, in this case, $^1CH_2$. We then calculated the removal of $^1CH_2$ by all of the known reaction paths. Since the flash is of finite duration, the model is not realistic. Alternatively, we may determine experimentally the decay in the flash intensity and assume that the total CH_2 is generated during the complete lifetime of the flash. If we divide the flash lifetime into equal time periods, 10 nsec, for example, then the fraction of the total CH_2 produced in each time interval is equal to the fraction of the total area under the curve for the corresponding time interval. We can now "feed" into the reaction mixuture the CH_2 produced as a function of time while the CH_2 produced earlier during the flash has already partially reacted. The results of these calculations indicate that, although the reaction was complete during the flash, the rate constant did not require any correction and the product distribution remained the same as before.

With the rate constant for (2) determined, we were able to obtain limiting values for the reaction of $^1CH_2$ with several inorganic additives.

$$^1CH_2 + X \longrightarrow [CH_2X] \quad (6)$$

where X = NO, CO, or O_2. Where X = NO, the upper limit for k_6 is 4×10^{-11} cc molecule^{-1} sec^{-1}. Similarly, where X = CO, $k_6 \leq 9 \times 10^{-12}$ cc molecule^{-1} sec^{-1}. In the case of O_2 as the reactant in eq 6, $k_6 \leq 3 \times 10^{-11}$ cc molecule^{-1} sec^{-1}. The rate constants can only be expressed as upper limits since we could not determine the effect of either NO, CO, or O_2 on the efficiency of the intersystem crossing of $^1CH_2 \rightarrow {}^3CH_2$. The decrease in C_2H_4, which is the observed process, is the sum of at least two processes: *i.e.*, reaction with CH_2 and quenching of $^1CH_2$.

Discussion

Methylene radicals were generated from the photolysis of ketene in the wavelength region from 180 (the cutoff of the quartz cell) to 360 nm which is the long wavelength edge of the ketene absorption. The major fraction of the photolysis took place between 180 and 190 nm where the ketene absorption is quite large,[3a] while at longer wavelengths the absorption is significantly weaker. At the energies utilized for the decomposition, the primary process results predominantly in production of singlet CH_2. It is known that photolysis of CH_2CO in the region of 270–290 nm produces almost exclusively the $^1CH_2$[14] and since higher lying states of the CH_2CO molecule are singlets,[15] conservation of spin would suggest production of $^1CH_2$ rather than $^3CH_2$. Further, reaction of $^1CH_2$ with H_2 to produce CH_3 is relatively rapid ($k \leq 1.5 \times 10^{-12}$ cm^3 molecule^{-1} sec^{-1})[3a] while $^3CH_2 + H_2$ is quite slow (5×10^{-14} cm^3 molecule^{-1} sec^{-1}).[3a] In the presence of H_2, the CH_2 produced in the flash is completely converted to CH_3.[10] The absence of C_2H_2 strongly suggests the absence of $^3CH_2$ as a product of the primary photolysis. In these experiments, we are unable to distinguish between the two possible singlet states of CH_2($\tilde{a}^1A_1$ or $\tilde{b}^1B_1$).

The reaction of $^3CH_2$ with C_2H_2 produces methylacetylene and allene in a ratio of about 1:2. The rate constant derived in this work clearly represents the sum of the rate constants of the two reactions. Since C_2H_2 is, itself, a

product of the photolysis fragments, the formation of C_3H_4 does not become significant until later times when the rate of combination of $^3CH_2$ is reduced and the only fate of $^3CH_2$ can be reaction with C_2H_2 since reaction with ketene is very slow. The postulated intermediate of reaction 3, which should possess triplet character to conserve spin, may result in either $H_2C{=}C{=}CH_2$ or $H_3C{-}C{\equiv}CH$ depending on the shift of the labile hydrogen atom to either adjacent carbon atom. The reaction of methylene with acetylene has been examined and, in a matrix where $^3CH_2$ clearly predominates, allene was found to be the major product.[16a] In a gas-phase study,[16b] the methylacetylene:allene ratio was 1.5, independent of total pressure and added O_2 or NO. Since inert gas was not used the results indicate the importance of singlet methylene even though some contribution of $^3CH_2$ cannot be totally eliminated. The present work does not provide insight into the mechanism of the reaction and speculation is not warranted. In view of the rapid rate constant determined for reaction 3 we suggest that C_2H_2 would be useful as a "scavenger" of $^3CH_2$ in mixed singlet–triplet systems.

The suppression of $^3CH_2$ reactions by added CO, originally suggested by DeGraff and Kistiakowsky,[13] has been confirmed recently.[5] The latter results, however, indicated that the collision efficiency of CO toward $^3CH_2$ was surprisingly low in comparison to the presumption of high reactivity of $^3CH_2$ toward CO.[6] Our results are in agreement with those of Montague and Rowland[5] who estimated a collision efficiency of $\leq 10^{-5}$ for reaction of $^3CH_2$ + CO. Although our rate constant is also expressed as a limiting value, $\leq 1.0 \times 10^{-15}$ cm^3 molecule^{-1} sec^{-1}, its magnitude is quite comparable with the low overall efficiency previously reported. Within the inherent limitations of our value for reaction of $^3CH_2$ with CO, the ratio of the reactivities of O_2 relative to CO with respect to $^3CH_2$ is $\geq 10^3$, not inconsistent with previous estimates of 10^4.[5] Complications in the CH_2–O_2 system caused by reaction to produce CO[8a,17]

$$^3CH_2 + O_2 \longrightarrow \text{products (CO, } CO_2\text{, and } H_2\text{)} \qquad (7)$$

among other products, is of minor influence on the rate constant determination since reaction of $^3CH_2$ with CO is so slow.

The reaction of $^3CH_2$ with NO is 10 times more effective than with O_2 and is, by far, the best "scavenger" for radicals studied. The experimental conditions were such that the initial ratio of NO/CH_2 was >5 in all cases. As the reaction progresses, following the flash, the effective ratio increases drastically as the CH_2 is removed by more than one path. Now, even if the reaction between CH_2 and NO were to produce an intermediate, which in principle could also react with CH_2 and remove C_2H_2, the concentration of the unknown species would be small relative to the NO. Nevertheless, if we assume that $^3CH_2$ reacts with the intermediate with the same k as with NO, then the largest error is caused in those runs where NO/CH_2 is small, *i.e.*, a factor of 5. In this situation

$$^3CH_2 + NO \longrightarrow A + B \qquad (8)$$

the error caused by reaction with both A and B would result in a calculated rate constant which is 40% higher than the "true" value. Since, however, the calculated value of k_8 is independent of NO pressure, probability of reaction of $CH_2(^3\Sigma)$ with products (such as A and B) is remote.

There are no numbers in the literature with which to compare our value but it is noteworthy that C_2O, in its $(X^3\Sigma)$ state, reacts with NO about 135 times more rapidly than with O_2.[18] In both situations, C_2O and CH_2 reaction with NO, an adequate mechanism for the reaction has not been reported. In the absence of a close examination for intermediates or products, speculation as to a mechanistic interpretation of the CH_2–NO reaction would not be productive.

Reactions of $^1CH_2$

The ratio we obtain for $k_6/k_2 = 0.28$ is only in fair agreement with earlier values of 0.14[16] and 0.10[5] for the comparable reactions. The differences lie in our method for determining k_6. It has been indicated that stabilization of the complex formed by reaction of $^1CH_2$ with CO

$$^1CH_2 + CO \longrightarrow CCH_2O^* \qquad (9)$$

is not complete at the pressures used in our study and, in fact, only 50% is stabilized at pressures of 840 Torr or higher.[5] If the decomposition of CCH_2O^* results in $^1CH_2$, the competition between quenching of the singlet by He to produce triplet CH_2 *vs.* further reaction with ketene favors production of $^3CH_2$. In this case we would observe a decrease in C_2H_4 yield attributable to (6) thereby suggesting a higher value for the rate constant.

In the low-intensity, steady-state photolysis of ketene, addition of O_2 and CO may remove $^3CH_2$. With this technique and making the same assumptions which we have, *i.e.*, that (1) all the C_2H_4 observed is the result of reaction 2 and that (2) reduction in the yield of C_2H_4 is caused by added inert gases such as He resulting in quenching of $^1CH_2$ to $^3CH_2$

$$^1CH_2 + M \longrightarrow CH_2(^3\Sigma) \qquad (10)$$

Cox and Preston[19] obtained a ratio of $k_{10}/k_2 = 0.018$ where M = He. Based on $k_{10} = 3.0 \pm 0.7 \times 10^{-13}$ cm^3 molecule^{-1} sec^{-1} [3a] and our value for $k_2 = 3.2 \pm 1.2 \times 10^{-11}$ cm^3 molecule^{-1} sec^{-1}, the ratio derived from the flash photolysis work is again in agreement, within the expressed error limits, with the low-intensity data.

As previously mentioned, the error limits quoted are the standard deviations of the mean which reflect mainly the uncertainty in the gas chromatographic analysis; other experimental errors are probably small. An error in the value of the "reference" rate constant[3a] will affect our values linearly as will an error in the determination of the CH_2 yield. The latter may be caused by reactions of CH_2 which result in a nondetected high molecular weight product.

Acknowledgment. This reaseach has been supported, in part, by NASA.

References and Notes

(1) (a) H. M. Frey, *Progr. React. Kinet.*, **2**, 131 (1964); (b) J. A. Bell, *Progr. Phys. Org. Chem.*, **2**, 1 (1964); (c) W. B. DeMore and S. W. Benson, *Advan. Photochem.*, **2**, 219 (1964); (d) W. Kirmse, "Carbene Chemistry," 2nd ed, Academic Press, New York, N. Y., 1971.
(2) $^3CH_2$ refers to the ground triplet state of $CH_2(\tilde{X}\,^3\Sigma_g^-)\,^3B_1$ and $^1CH_2$ to the lowest singlet state of $CH_2(\tilde{a}\,^1A_1)$.
(3) (a) W. Braun, A. M. Bass, and M. Pilling, *J. Chem. Phys.*, **52**, 5131 (1970); (b) J. A. Bell, *J. Phys. Chem.*, **75**, 1537 (1971).
(4) R. W. Carr, Jr., *J. Phys. Chem.*, **76**, 1581 (1972).
(5) D. C. Montague and F. S. Rowland, *J. Amer. Chem. Soc.*, **93**, 5381 (1971).
(6) R. A. Cox and R. J. Cvetanovic, *J. Phys. Chem.*, **72**, 2236 (1968).
(7) K. Dees and D. W. Setser, *J. Phys. Chem.*, **75**, 2240 (1971).
(8) (a) A. N. Strachan and W. A. Noyes, Jr., *J. Amer. Chem. Soc.*, **76**, 3258 (1954); (b) H. M. Frey, *ibid.*, **82**, 5947 (1960).
(9) (a) M. L. Halberstadt and J. R. McNesby, *J. Amer. Chem. Soc.*, **89**, 3417 (1967); (b) G. Z. Whitten and B. S. Rabinovitch, *J. Phys. Chem.*, **69**, 4348 (1965).

(10) A. M. Bass and A. H. Laufer, *Int. J. Chem. Kinet.*, **V**, 1053 (1973).
(11) R. L. Nuttall, A. H. Laufer, and M. V. Kidlay, *J. Chem. Thermodyn.*, **3**, 167 (1971).
(12) P. S. T. Lee, R. L. Russell, and F. S. Rowland, *Chem. Commun.*, 18 (1970).
(13) B. A. DeGraff and G. B. Kistiakowsky, *J. Phys. Chem.*, 71, 3984 (1967).
(14) J. W. Calvert and J. N. Pitts, "Photochemistry," Wiley, New York, N. Y., 1967, p 392.
(15) H. Basch, *Theor. Chim. Acta*, **28**, 151 (1973).
(16) (a) M. E. Jacox and D. E. Milligan, *J. Amer. Chem. Soc.*, **85**, 278 (1963); (b) T. Terao, N. Sakai, and S. Shida, *ibid.*, **85**, 3919 (1963).
(17) R. L. Russell and F. S. Rowland, *J. Amer. Chem. Soc.*, **90**, 1671 (1968).
(18) D. G. Williamson and K. D. Bayes, *J. Amer. Chem. Soc.*, **89**, 3390 (1967).
(19) R. A. Cox and K. F. Preston, *Can. J. Chem.*, **47**, 3345 (1969).

Photolysis of Diazo-*n*-propane. A Route for the Photochemical Activation of Propylene

Juan M. Figuera,* Ernesto Fernández, and María J. Avila

Instituto de Química Física "Rocasolano," Serrano 119, Madrid-6, Spain *(Received January 22, 1974)*

Publication costs assisted by Consejo Superior de Investigaciones Científicas

Diazo-*n*-propane and diazo-*n*-propane-*1*-^{14}C have been photolized in gas phase with Pyrex glass as a filter. A reaction mechanism is proposed that explains the product distribution and its pressure dependence. Vibrationally excited propylene is formed as an intermediate. The experimental rate constant for the predominant decomposition path (C–C scission) of propylene has been evaluated, $k_{C-C} = 0.23 \times 10^8$ sec^{-1} (20 mm pressure). RRKM calculations performed allowing a gaussian distribution of propylene internal energy gave 99 ± 6 kcal mol^{-1} as more probable internal energy in propylene. This figure corresponds to 68 ± 10% of the total energy available for partitioning being carried by the carbene moiety as internal energy. ART theory was used to calculate the rate constant for the combination of methyl and vinyl, $k_{400K} = 4.62\text{–}15.5 \times 10^7$ M^{-1} sec^{-1} (*i.e.*, the reverse process of the unimolecular propylene decomposition).

Introduction

The chemistry of carbenes has received considerable attention in recent years.[1] However, the reactivity of alkylcarbenes in gas phase is not completely understood. The initial purpose of this work was to study the ethylcarbene.

Several methods are available[2-4] for generating carbenes. We have chosen the long wavelength photolysis of diazo-*n*-propane for the following reasons. It is expected that the carbene is formed in its first singlet state, free of appreciable amounts of the triplet ground state.[5-8] Herzberg[5] showed that in the photolysis of diazomethane singlet methylene is initially formed and then, decay to the triplet species can be collisionally induced. In ethylcarbene, the intramolecular insertion of the divalent carbon provides an alternative escape for the molecule, that can avoid the crossing to the triplet surface if the reaction is fast enough, as MO calculations indicate.[9] On the other hand, the carbene should be formed smoothly in one step (*i.e.*, in a concerted mode), as the transition that corresponds to the long wavelength absortion of diazoalkanes raises the molecule to a dissociative state (antibonding between carbon and nitrogen).[10]

In this work, we have tried to accumulate enough evidence to sketch the mechanism of the reaction of ethylcarbene in gas phase, Carbon-14 labeling was used to confirm some details of the proposed mechanism.

Once the mechanism was outlined, it was clear that the photolysis of diazo-*n*-propane afforded a simple and convenient way for the activation of propylene. The unimolecular decomposition of this species was subsequently studied by RRKM[11] techniques that afforded data on the reverse reaction *via* ART[12] and also about the partition of energy between the fragments produced in the photolysis.

Experimental Section

Diazo-n-propane. Diazo-*n*-propane was prepared from *n*-propylamine and pulegone by the method of Adamson and Kenner.[13] The diazopropane formed in the reaction was passed successively through a reflux condenser, an ice-cooled spiral trap, and a U-tube packed with KOH pellets and was finally collected in a trap cooled with a slush of Dry Ice and acetone. The product was further purified by distillation in a grease-free vacuum line.

The ir spectrum of diazo-*n*-propane in gas phase at 20 mm was recorded with a Perkin-Elmer, Model E-125, spectrophotometer. The spectrum showed a very strong band at 2050 cm^{-1}, characteristic of the diazo group, and no significant bands between 1300 and 400 cm^{-1}.

Diazo-n-propane-1-^{14}C. Diazo-*n*-propane-*1*-^{14}C was prepared in the previously described mode from *n*-propylamine-*1*-^{14}C. The amine was synthesized from propionic-*1*-^{14}C acid (The Radiochemical Centre, Amershan, England; 0.5 mCi, 35 mCi/m*M*) through the preparation of the amide and its reduction with titrated solutions of H_4LiAl[14] using standard techniques. The amine was isolated as the corresponding chlorhydrate, saturating the ether solution previously obtained with gaseous HCl.[15]

Photolysis. Photolyses were carried out at room temper-

ature in cylindrical Pyrex vessels of about 350 ml provided with a water-cooled jacket. The surface-to-volume ratio was about 1 cm^2/ml. The light source was a Hannovia Model 679A36 mercury lamp.

The initial pressure of diazo-*n*-propane in the vessels ranged from 1 to 84 mm. Experiments with diazo-*n*-propane-*1*-^{14}C were performed at 6, 10, and 20 mm of initial diazocompound pressure. Another series of photolyses were performed on mixtures of diazo-*n*-propane-*1*-^{14}C and propylene in the ratio 1:1 at total initial pressures of 6, 10, and 20 mm. Experiments were performed until complete decomposition, checked by disappearance of the 2050-cm^{-1} band in the ir spectrum of the irradiated mixture. A grease-free vacuum line was used throughout.

Analysis. Analysis was by gas chromatography. A HP Model 5750 gas chromatograph with hot-wire detector was used. The analogical signal of the detector was digitalized with a V to F converter (HP Model 2712A), and its output pulse train fed into an electronic counter (Nuclear Chicago Model 8735).

Through simple calculations the area of the peaks was computed in arbitrary units. In some of the analysis a Perkin-Elmer fractometer 116-E was used; in this case integration of peaks was carried out with a Perkin-Elmer Model D26 integrator. Helium was the flow gas in all cases, except in the analysis of hydrogen where argon was used.

The columns used for the various products along with the conditions were as follows: a 3.1 m × 0.4 cm column of 30–40 mesh active carbon for hydrogen (51°); a 7.5 m × 0.64 cm column of 60–80 mesh silica gel for hydrocarbons up to 1-butene (programmed temperature); a 8 m × 0.64 cm column of 20% β,β'-oxidipropionitrile on 60–80 mesh Chromosorb P (room temperature) for higher hydrocarbons; a 12 m × 0.64 cm column of 25% dimethylsulfolane for hydrocarbons (0°). Several other columns were occasionally used.

Products were identified by comparison of their retention times with those of authentic samples in at least two different columns. Besides, acetylene and cyclopropane were collected at the gas-chromatograph outlet and identified by their gas-phase ir spectra.

The inlet system to the chromatograph employed a multi-way gas-sampling valve, to which a glass trap could be connected. The trap was filled in the vacuum line with a known fraction of the mixture to be analyzed and then connected to the inlet system. Grease-free joints were used throughout. In most cases only products condensable at 77 K were analyzed, but in a few the whole photolysis mixture was analyzed.

Calibration factors were determined by analysis of measured amounts of pure compounds.

Radioactivity Measurements. Radiogas chromatography was used. A Berthold proportional counter of 80 ml was coupled to the gas chromatograph. Methane was added to the carrier, in the ratio 1:2, to form the counting gas. The associated electronics was from Nuclear Chicago. A single channel analyzer was used to improve the signal-to-noise ratio. The system integrated and printed the counting rate every 10 sec. These data coupled to the chromatographic data gave after some manipulation the relative specific activity of the hydrocarbons.

The products were carried directly inside the counter (*i.e.*, no combustion or cracking was effected); therefore, their presence inside the counter chamber may slightly alter its efficiency. Although the deviations observed are small (see Table I), strictly only activities within one product can be compared.

TABLE I: Molar Activity of the Main Products of Diazo-*n*-propane-*1*-^{14}C, Photolyzed Pure and Mixed with Propylene[a]

Diazo-*n*-propane-*1*-^{14}C initial pressure, mm	Propylene initial pressure, mm	Molar activity[b]		
		Ethylene	1-Butene	1,5-Hexadiene
6	No	1.06	1.10	2.11
10	No	1.07	1.17	1.9
20	No	1.10	1.14	1.94
3	3	1.03	0.84	1.54
5	5	0.88	0.73	1.3
10	10	0.92	0.83	1.36

[a] See Experimental Section. [b] The molar activity of the products is referred to the activity of propylene found in each experiment; the initialy added propylene has been discounted in the calculation in order to obtain consistent figures. The results represent averages of at least three independent runs. Ethane showed no traces of activity.

Results

Experiments with Unlabeled Diazo-n-propane. The yield of the different hydrocarbons formed in the gas-phase photolysis of diazo-*n*-propane has been plotted against initial pressure in Figures 1–3.[16] The yields are expressed as mole per cent of the initial diazo compound.

Propylene is the main reaction product. Ethylene, 1-butene, ethane, 1,5-hexadiene, and cyclopropane are formed in amounts exceeding 1%, at least in some experiments. The rest of the identified products, hydrogen, methane, propane, acetylene, 1-pentene, and 2,3-dimethylbutane, are formed in yields smaller than 1%. The data for these products are only of semiquantitative accuracy. 2,3-Dimethylbutane and hydrogen were not systematically analyzed and their results have not been plotted.

In the following equations we have labeled with an asterisk the position where the carbon-14 would be if the experiments were run with a labeled diazo compound, but only in the equations relevant to the subsequent discussion. In molecules with geometrically equivalent positions, the position of the label has been arbitrarily assigned to one of them.

Initial Step. We assume (see Introduction) that the primary photochemical process is the formation of ethylcarbene in its first singlet state

$$CH_3CH_2{}^*CHN_2 \xrightarrow{h\nu} CH_3CH_2{}^*CH\uparrow\downarrow + N_2 \qquad (1)$$

We wish to show that the molecular fragmentation, necessary to explain the final product distribution, is best explained as taking place from excited propylene and not from the carbene, as might have been thought.

First, compare our results with those obtained by Frey, *et al.*, for the photolysis of 3,3'-dimethyldiazirine.[4c] In that work, the carbene presumably formed was the 1,1'-dimethylcarbene. This carbene has no C–H bonds in the γ position and, therefore, it cannot give cyclopropane by intramolecular insertion of the divalent carbon.[1c] For both systems the product distribution and pressure effects are similar. This similarity is easily understood if both reactions occur, at least partially, through a common intermediate, the vibrationally excited propylene

$$CH_3CH_2CH\uparrow\downarrow \longrightarrow [CH_3CH{=}CH_2]^* \qquad (2)$$

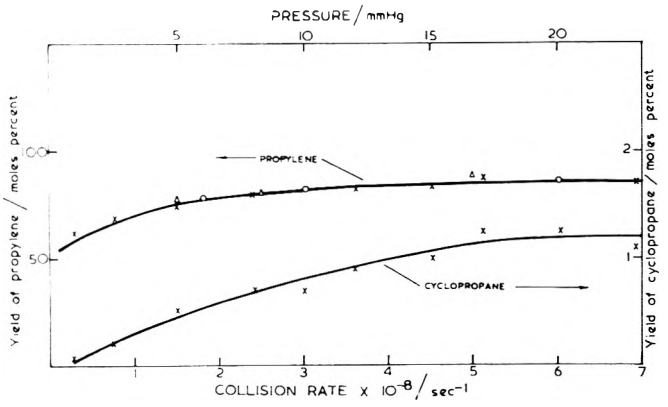

Figure 1. Photolysis of diazo-*n*-propane. Plot of propylene and cyclopropane yields as a function of collision rate and diazo-*n*-propane initial pressure: ×, experiments with pure diazo-*n*-propane; O, experiments with diazo-*n*-propane-*1*-^{14}C; Δ, experiments with diazo-*n*-propane-*1*-^{14}C diluted with propylene (the added propylene has been substracted in the plot.

On the other hand, INDO and MINDO/2 calculations of the coordinate of the reaction methylcarbene → ethylene show practically no barrier of energy for the conversion through the singlet surface.[9] Preliminary calculations[9c] for the reaction ethylcarbene–propylene show a similar lack of barrier. Therefore, a rate for this reaction higher than the collision rate can be expected. The only reaction that may compete with this hydrogen migration is the γ insertion, but its participation seems to be minor (see below). Involvement of excited propylene seems to be the most reasonable alternative.

Vibrationally Excited Species. (*a*) *Cyclopropane.* The yield of cyclopropane from diazo-*n*-propane in the high-pressure region is more than three times the amount obtained from 3,3′-dimethyldiazirine. Furthermore, in this work the yield of this product increased with increasing pressure (see Figure 1), while the opposite behavior was found in Frey's work. These effects are rationalized in eq 3, where ω represents the rate of deactivating collisions, and other reactions of

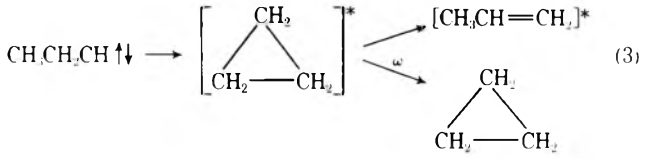

(3)

excited cyclopropane have been neglected.

(*b*) *Propylene.* The pressure effect on propylene yield is also characteristic of a vibrationally excited species. With increasing pressure only the yield of propylene (and of the small amount of cyclopropane present) increases, while the opposite behavior is found in the other products (see Figures 1–3). This result suggests that these other products are formed from propylene by fragmentation and subsequent reaction of the fragments. Equations 4–6 correspond to the decomposition processes of propylene that are thermochemically more favored. Equation 7 corresponds to the collisional deactivation.

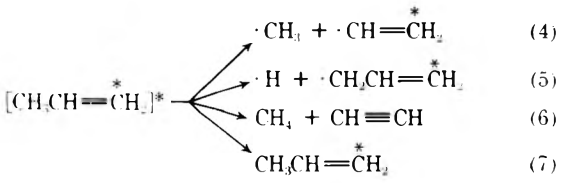

(4)
(5)
(6)
(7)

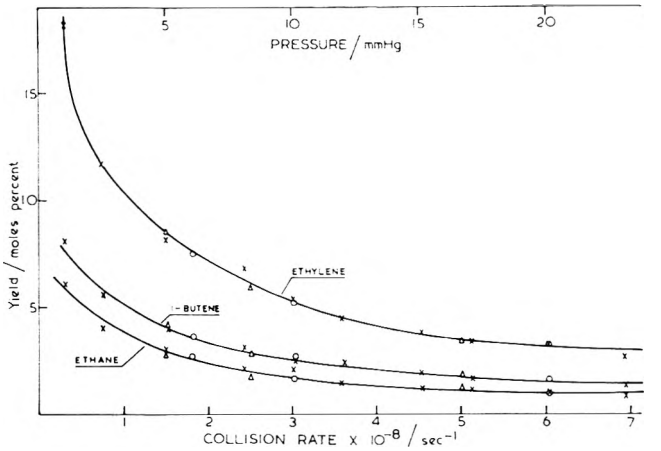

Figure 2. Photolysis of diazo-*n*-propane. Plot of ethane, ethylene, and 1-butene yields as a function of diazo-*n*-propane initial pressure: ×, experiments with pure diazo-*n*-propane; O, experiments with diazo-*n*-propane-*1*-^{14}C; Δ, experiments with diazo-*n*-propane-*1*-^{14}C diluted with propylene.

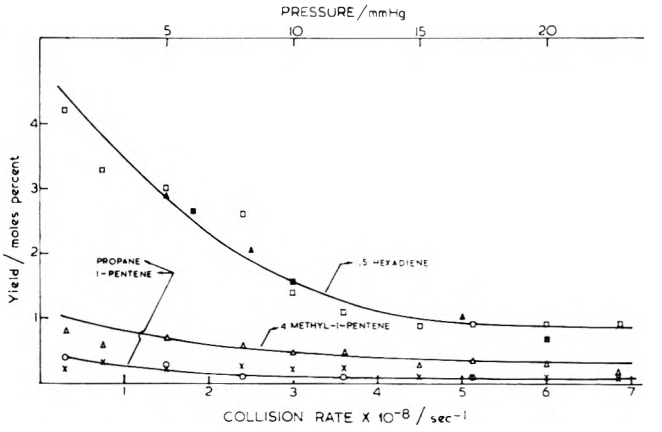

Figure 3. Photolysis of diazo-*n*-propane. Plot of 1,5-hexadiene (pure diazo-*n*-propane □, diazo-*n*-propane-*1*-^{14}C ■, diazo-*n*-propane-*1*-^{14}C diluted with propylene ▲), 4-methyl-1-pentene Δ, propane ×, and 1-pentene O against collision rate and pressure.

Only trace amounts of acetylene have been found and, therefore, the reaction represented by eq 6 can be ruled out. Equation 4 represents the path that accounts for most of the fragmentation products (see below), the rest being explained by reaction 5.

Radical Reactions. The reaction scheme is shown in Chart I.

(*a*) *Atomic Hydrogen.* Molecular hydrogen can be produced by abstraction, eq 8. The hydrogen donor is, most likely, propylene. Then, eq 8 is an additional source of allyl; although a minor one as the amount of hydrogen found is small.

Addition to propylene should give predominantly isopropyl, the product of terminal addition,[17] eq 9.

The preferred decomposition pathway of this chemically activated isopropyl radical is the C–H splitting that gives back the reactants. The products of the collisionally deactivated isopropyl that can be expected under the experimental conditions used are those formed by disproportionation (eq 10), recombination (eq 11), combination with methyl (eq 12), with allyl (eq 13) and with vinyl (eq 14).

We have identified (see Figure 3) 4-methyl-1-pentene, the product of eq 13, although this product can be formed

Chart I

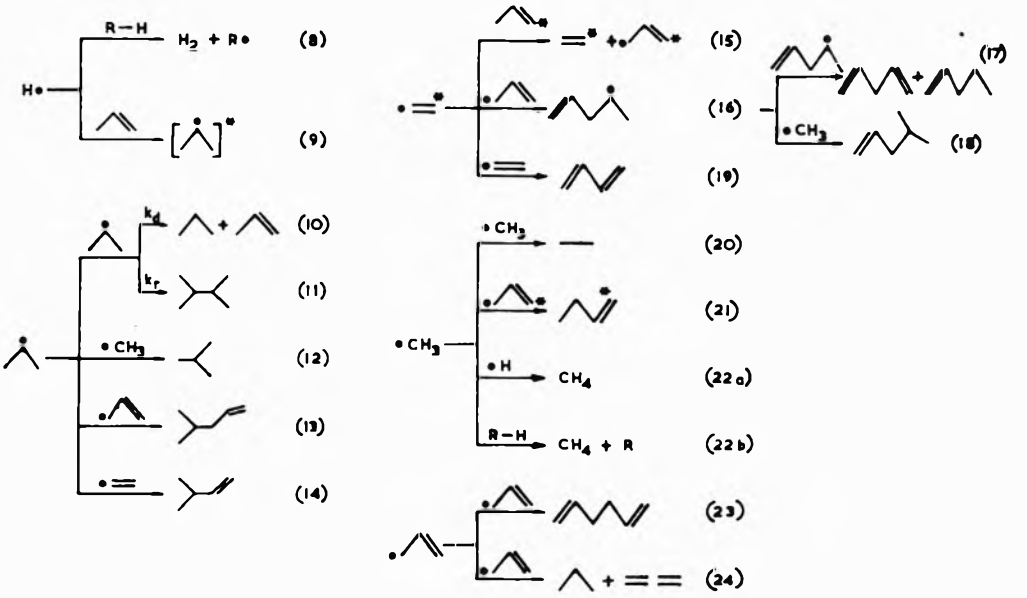

by a different pathway (see below). We failed to identify isobutane, due probably to analytical difficulties (peak overlapping), and 3-methyl-1-butene. This last product is probably formed in amounts undetectable by our analytical technique. It will be shown that most of the vinyl reacts by abstraction.

We have identified 2,3-dimethylbutane and propane. However, the amount of propane is larger than that predicted by the accepted value of $k_d/k_r = 0.64$,[18] indicating the presence of another source of propane.

We may conclude from the small proportion of products that can be ascribed to reactions of atomic hydrogen that C–H scission is a minor fragmentation of the vibrationally excited propylene.

(*b*) *Vinyl Radical.* Abstraction, eq 15, is the main vinyl reaction. In Figure 4 the ratio vinyl/methyl (see eq 26 and 27) has been plotted against initial diazo-*n*-propane pressure. Only eq 15 has been used to compute the total vinyl formed. The ratio is close to the expected value of one, derived from eq 4. The ratio ethylene/allyl is also close to one (see Figure 4). This result is to be expected if eq 15 is the main source of allyl.

Addition of vinyl to propylene may give another radical (nonterminal addition being neglected), eq 16. This radical may undergo several reactions. We found only 1-pentene and 4-methyl-1-pentene (see Figure 3). The first could be formed by disproportionation, eq 17, and the second by combination with methyl, eq 18. The last is also formed by eq 13.

We looked for butadiene, the product of recombination, eq 19. We did not find any, and eq 19 can be ruled out.

(*c*) *Methyl and Allyl.* Ethane, 1-butene, and 1,5-hexadiene are explained by combination reactions, eq 20, 21, and 23. These products, together with ethylene, account for more than 90% of the fragmentation products (*i.e.*, excluding propylene and cyclopropane). Methane, which is formed in small amounts (*i.e.*, less than 1%) can be formed by combination with hydrogen, or by abstraction, eq 22.

We have obtained a value of 1.57 ± 0.18, pressure independent, for the ratio of cross combination to recombination, $k_{21}/(k_{20}k_{23})^{1/2}$.

We have performed a careful search for allene, which may be formed by disproportionation of allyl, eq 24. No trace of this product could be found. This evidence sets a higher limit of 0.01 (evaluating roughly our detection limits) for the ratio of disproportionation to combination of allyl radical. The reported value for this ratio is 0.008 at 164–190°.[19]

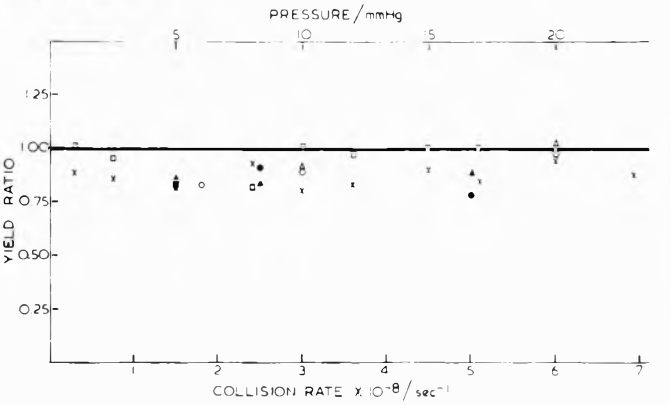

Figure 4. Plot of vinyl/methyl (experiments with pure diazo-*n*-propane ×, experiments with diazo-*n*-propane-*1*-^{14}C ○, experiments with diazo-*n*-propane-*1*-^{14}C diluted with propylene ○) and of ethylene/allyl (pure diazo-*n*-propane □, diazo-*n*-propane-*1*-^{14}C △, diazo-*n*-propane-*1*-^{14}C diluted with propylene ▲) against collision rate and initial pressure. The horizontal line corresponds to the expected value. Allyl = 1-butene + 2(1,5-hexadiene).

Experiments with Diazo-n-propane-1-^{14}C. Experiments were run with pure diazo-*n*-propane-*1*-^{14}C and with 1:1 mixtures of diazo-*n*-propane-*1*-^{14}C and propylene. In these experiments we analyzed ethane, ethylene, propylene, 1-butene, and 1,5-hexadiene. The results have been plotted against collision rate (see Figures 1–4).[16] The addition of propylene does not influence the product distribution, in agreement with the proposed mechanism.

The molar activity found in the different products is in Table I. The activities are relative to that of propylene, and in the experiments with added propylene the amount added has been deduced. In this way activities from the different runs can be compared.

The experiments with pure diazo-*n*-propane-*1*-^{14}C support further the mechanism outlined. According to eq 1 and 2, propylene should be labeled in carbon one and with the same molar activity than the original diazo-*n*-propane-*1*-

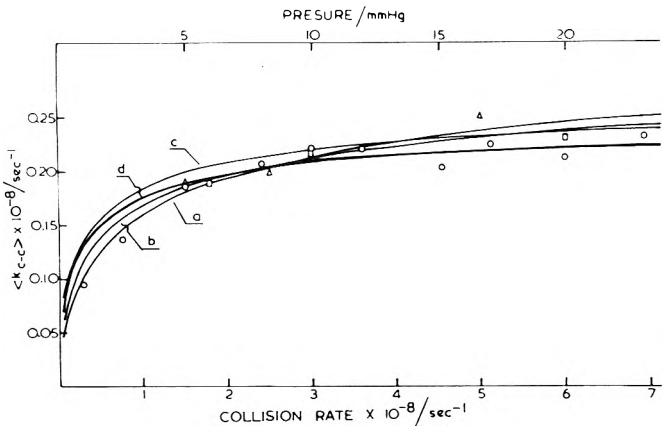

Figure 5. Plot of the rate constants of propylene C-C scission against collision rate and pressure (experiments with pure diazo-*n*-propane O, experiments with diazo-*n*-propane-*1*-^{14}C □, experiments with diazo-*n*-propane-*1*-^{14}C diluted with propylene Δ. The RRKM calculated curves use model I+, E_0 = 81.09 kcal mol^{-1} and the parameters: curve a, E_{MP} = 93.1 kcal mol^{-1} and σ = 6 kcal mol^{-1}; curve b, E_{MP} = 94.1 and σ = 5; curve c, E_{MP} = 95.1 and σ = 4; curve d, E_{MP} = 94.9 and σ = 4.

^{14}C. The self-consistency of the following arguments confirm this point. Vinyl radical, see eq 4, should also be formed with identical activity and also ethylene, eq 15. On the other hand, allyl should also contain the same activity, see eq 5 and 15. Therefore, 1-butene formed by eq 21 should also have identical activity, while 1,5-hexadiene should have twice as much, as its formed from two allyl molecules, eq 22. However, ethane that is formed from methyl radical by eq 4 and 20 should show no activity.

In Table I it can be observed that the experimental data agree with the above predictions within experimental uncertainty.

The relative contribution of the C-H scission of propylene to the reaction can be estimated in the experiments with added propylene. As the propylene "competes" with the active (formed by eq 2) in eq 15, the molar activity of allyl should be reduced, and consequently, those of 1-butene and 1,5-hexadiene. However, if most of the allyl is formed by C-H splitting, eq 5, the effect of the added propylene would be negligible.

The data of Table I show that introduction of propylene in the ratio 1:1 decreases the activity of 1-butene by 30% and that of 1,5-hexadiene by 29%. These results do not rule out the participation of the C-H scission in the propylene unimolecular decomposition but confirm our earlier interpretation that the C-C splitting dominates the reaction under the actual experimental conditions.

Rate Constants of Unimolecular Decomposition of Propylene. The specific rate of C-C splitting of activated propylene, $\langle k_{C-C} \rangle$, in this system is given by eq 25, where the

$$\langle k_{C-C} \rangle = \omega D_{C-C}/S \qquad (25)$$

amount of stabilized product is S = propylene. The amount of decomposition (D_{C-C}) may be calculated through the computation of vinyl or methyl

$$\text{methyl} = 2\text{ethane} + 1\text{-butene} \qquad (26)$$

$$\text{vinyl} = \text{ethylene} \qquad (27)$$

The vinyl to methyl ratio has been plotted against collision rate[16] in Figure 4. This ratio is rather close to one, the value expected from the mechanism. The vinyl deficit indicates that participation of vinyl in secondary reactions is higher than that of methyl. In any case, the reactions used in the computations account for more than 90% of the fragmentation products. Equation 26 will be employed in the computation of experimental $\langle k_{C-C} \rangle$.

The collision rate of the vibrationally excited propylene with the bath molecules (*i.e.*, diazo-*n*-propane) was calculated from kinetic theory (see Appendix). Unit collision efficiency of deactivation of propylene was assumed. The deactivation rate calculated for the propylene having a Boltzmann distribution of velocities at 20° is ω/P = 3.02 × 10^7 collisions sec^{-1} Torr^{-1}. The experiments were run to complete diazo-*n*-propane decomposition. Therefore, the collision rate of the propylene in a bath of completely decomposed diazo-*n*-propane may be approximated by a bath composed of a equimolecular mixture of nitrogen and propylene. Under these conditions the rate at 20° is ω/P = 3.33 × 10^7 collisions sec^{-1} Torr^{-1} and, therefore, we took the initial value as a reasonable approximation in the subsequent calculations. In the experiments with added propylene the total collision rate was calculated as the sum of the collisions with diazo-*n*-propane and the added propylene.

The experimental $\langle k_{C-C} \rangle$ values are plotted in Figures 5-7 against the collision rate.

The relationship between the experimentally observed unimolecular rate constants and the microscopic unimolecular rate constants for C-C decomposition of a propylene molecule with internal energy content E, $k_{C-C}(E)$, is given by

$$\langle k_{C-C} \rangle = \int_{E_0}^{\infty} \frac{k_{C-C}(E)}{k_{C-C}(E) + k_{C-H}(E) + \omega} f(E)\, d\epsilon \Big/ \int_0^{\infty} \frac{1}{k_{C-C}(E) + k_{C-H}(E) + \omega} f(E)\, d\epsilon \qquad (28)$$

where $k_{C-H}(E)$ represents the contribution of the C-H splitting.[20]

The rate constants, $k(E)$, were calculated using the RRKM theory,[11] as revised by Wieder and Marcus.[21] All the internal vibrations of propylene were allowed to be active degrees of freedom. The details of the rate and energy distribution calculations, including the necessary molecular vibrational assignments and the thermochemistry, are given in the Appendix. We assumed $f(E)$ to be a Gaussian;[22] therefore, for a given model there are only two adjustable parameters for fitting the calculated curves to the experimental data, E_{mp}, the most probable energy of the excited propylene, and the dispersion of $f(E)$. Some typical calculated curves are shown in Figure 5.

Energy Partitioning in Diazo-n-propane Photolysis. Three different sets of calculations have been performed that encompass the standard deviations quoted for the experimental Arrhenius parameters used to select the activated complex models (see Appendix and Table II). The curves in Figure 5 represent typical results for one of the sets.

The parameters E_{mp} = 99 ± 6 kcal mol^{-1} and σ = 5 ± 1.5 kcal mol^{-1} encompass the best fits obtained with the different sets of calculations and make allowance of the dispersion of the experimental points.

If the isomerization of ethylcarbene is faster than the collision rate as should be for a unimolecular process with no activation energy,[9] the more probable energy of ethylcarbene can be obtained subtracting from the E_{mp} of propylene the heat of the reaction at 0 K, see eq 2.[23] We obtained E_{mp}(ethylcarbene) = 43 ± 6 kcal mol^{-1}.

TABLE II: Molecular Models Used in the Calculations[a]

Propylene	Complex[b] I−	Complex[b] I	Complex[b] I+	Methyl	Vinyl
		Vibrational Assignments, cm^{-1}			
3090		3272		3002(2)	3019
3013		3184		3184	3272
2954(2)		3019		1503(2)	2989
2992		3002(2)		611	1623
2933		2989			1444
1474		1420(2)			943
1378		1444			825
1443		611			1050
1419		1623			995
1652		1050			
1298		995			
1172	153	145.5	160		
428		943			
920		825			
912	310(2)	250(2)	200(2)		
578	250(2)	200(2)	150(2)		
963					
991					
1045					
225					
		Principal Moments of Inertia, g cm^{-2}			
$I_A = 101.6 \times 10^{-40}$	$I_A = 101.6 \times 10^{-40}$		$I_A = 5.92 \times 10^{-40}$		$I_A = 29.17 \times 10^{-40}$
$I_B = 87.75 \times 10^{-40}$	$I_B = 87.75 \times 10^{-40}$		$I_B = I_C = 2.96 \times 10^{-40}$		$I_B = 25.13 \times 10^{-40}$
$I_C = 19.20 \times 10^{-40}$	$I_C = 19.20 \times 10^{-40}$				$I_C = 4.05 \times 10^{-40}$
		Symmetry Numbers (σ)			
1	1		6		1
		Calculated Standard Molar Entropies[c] ($S°$) at 293.16 K, cal K^{-1} mol^{-1}			
62.953	70.326		46.242		55.709

[a] See Appendix. [b] Only wave numbers that differ from those of model I has been listed for models I+ and I−. [c] The electronic degeneracy of the radicals ($g_i = 2$) is included in the calculations.

TABLE III: Calculated (ART)[a] High Pressure Rate Parameters of Unimolecular Decomposition of Propylene (Thermal Activation) $CH_3CH{=}CH_2 \rightarrow CH_3\cdot + \cdot CH{=}CH_2$

Temperature, K	Log A, sec^{-1}	E_∞, kcal mol^{-1}	$k_{1\infty}$, sec^{-1}
	14.90	85.94	8.81×10^{-33}
400	15.27	83.51	4.46×10^{-31}
	15.66	83.71	8.41×10^{-31}
	15.51	87.47	4.10×10^{-9}
800	15.90	85.09	4.57×10^{-8}
	16.30	85.32	9.88×10^{-8}
	15.60	87.86	2.53×10^{-4}
1000	16.00	85.48	2.09×10^{-3}
	16.40	85.72	4.65×10^{-3}
	15.67	88.21	6.96
1300[b]	16.07	85.84	4.37×10^{1}
	16.47	86.09	9.99×10^{1}

[a] For each temperature the upper row uses model I− and E_0 = 83.75 kcal mol^{-1}, the middle row model I and E_0 = 81.09, and the lower row I+ and E_0 = 81.09. [b] This temperature has been included to show how well our models reproduce the experimental Arrhenius parameters (see Appendix).

TABLE IV: Calculated (ART)[a] High Pressure Rate Parameters for the Combination Reaction $CH_3\cdot + \cdot CH{=}CH_2 \rightleftarrows CH_3CH{=}CH_2$

Temperature, K	Log A, M^{-1} sec^{-1}	E_∞, kcal mol^{-1}	$k_{D\infty}$, M^{-1} sec^{-1}
	7.81	0.34	3.61×10^{7}
298.16	8.16	0.54	5.87×10^{7}
	8.54	0.72	1.02×10^{8}
	8.14	0.86	4.62×10^{7}
400	8.51	1.09	8.23×10^{7}
	8.90	1.29	1.55×10^{8}
	9.00	3.16	1.37×10^{8}
800	9.40	3.44	2.87×10^{8}
	9.80	3.67	6.21×10^{8}
	9.29	4.35	2.19×10^{8}
1000	9.69	4.64	4.75×10^{8}
	10.09	4.88	1.06×10^{9}
	9.63	6.14	3.99×10^{8}
1300	10.03	6.44	8.95×10^{8}
	10.43	6.68	2.05×10^{9}

[a] For each temperature the upper row uses model I−, the middle row model I, and the lower row model I+. In every case the critical energy has been taken as zero.

The calculated available energy for partitioning between ethylcarbene and and nitrogen in the photolysis of diazo-*n*-propane is 62.5 kcal mol^{-1} (see Appendix). This value coupled with the E_{mp}(ethylcarbene) gives 68 ± 10% of the available energy being carried out by the carbene moiety.

ART Calculations. We have calculated the high-pressure (thermal) rate constants, k_∞, for the unimolecular decomposition of propylene and for the reverse reaction, the combination of methyl and vinyl, through absolute rate theory (ART).[12] see Tables III and IV. The calculation details are in the Appendix.

The calculated rate constant for the recombination of methyl and vinyl radicals at 400 K is 4.62-15.5 × 10^7 M^{-1} sec^{-1}. Using a similar approach Hase and coworkers[24] have calculated that the recombination rates of several alkyl radicals range from 9.5 × to 10^7 to 1.1 × 10^{10} at 400 K. Therefore, according to our values, the vinyl radical combines at a rate comparable to that of the slower alkyl

radicals. This rate correlates with a relatively tight activated complex (see Appendix) and a comparatively low A factor for the unimolecular decomposition of propylene. The A factors for the vibrator models of activated complex of alkane decomposition range at 1000 K from $10^{16.4}$ to $10^{17.8}$ sec^{-1} against our calculated $10^{15.67}$–$10^{16.47}$ sec^{-1} for the propylene decomposition. Then, although there seems to be a trend in our values toward a tighter activated complex, our error limits overlap the values reported and no definitive conclusions can be obtained.

It should be remembered that recombination rates calculated with the present approach are significantly smaller than experimental and estimated recombination rates.[24] Therefore, only correlation with rates calculated in the same way is significant.

Acknowledgment. We thank Professor J. M. Gamboa, head of our Department, for the facilities granted that made this work possible; also Mr. A. Gomez for the ir spectra. One of us thanks Instituto de Cultura Hispanica and C.S.I.C. for scholarships.

Appendix

RRKM Calculations. The vibrational frequency assignment for propylene has been taken from the literature.[25] The activated complex assignments were chosen under the constraint that they should reproduce the Arrhenius preexponential factor of Chappell and Shaw[26] (RRKM results depend only on the A factor and not on the exact model of the activated complex[27]). Three models have been evaluated; model I corresponds to the A factor reported and models I+ and I− to the A factor plus and minus one standard deviation (see Table II).

The critical energy E_0 can be calculated from the experimental activation energy E_∞, using absolute rate theory, by eq 31.[28] Application of model I to the calculation of the average energy of the complex $\langle E^+ \rangle$ gives E_0 = 81.09 kcal mol^{-1} if E_∞ is taken as 85.84 kcal mol^{-1}. Using E_∞ = 88.27 kcal mol^{-1} (*i.e.*, the mean value plus one standard deviation) and model I− one obtains E_0 = 83.75 kcal mol^{-1}. With E_∞ = 83.47 kcal mol^{-1} (*i.e.*, the mean value minus one standard deviation) and model I+ one obtains E_0 = 78.47 kcal mol^{-1}.

However, the discrepancy between activation energies calculated from shock tube experiments and low temperature data is well documented in diatomic molecules.[29] The lower activation energy (and rate constant) obtained at higher temperatures is adscribed to a depletion of the higher vibrational levels by the reaction, the V-V transfer not being able to reestablish the equilibrium quota.[30] The relevance of this effect in polyatomics, where the V-V transfer is favored by the presence of several vibrational modes, is difficult to assess.

The lack of low-temperature kinetic data[31] forces us to choose between the E_0 value that can be derived from the estimated standard bond dissociation energy, $DH°(CH_2{=}CH\text{---}CH_3)$ = 97 kcal mol^{-1},[32] and those extrapolated from the shock tube Arrhenius parameters. However, the mentioned DH° is much higher than the value for C-H splitting $DH°(CH_2{=}CH\text{-}CH_2\text{---}H)$ = 87.1 kcal mol^{-1},[33] and therefore, very hard to reconcile with our experimental data that favors C-C over C-H rupture, and has been left out. Of the values derived from the experimental Arrhenius parameters, E_0 = 78.47 kcal mol^{-1} has been discarded as unrealistic (*i.e.*, too far from the estimated values). Then, E_0 = 81.09 and E_0 = 83.75 kcal mol^{-1} are the values used in the calculations. See Figures 5-7.

ART Calculations.[12,28] High-pressure rate constants of methyl vinyl recombination and unimolecular propylene decomposition were calculated by eq 29. The frequency

$$k_\infty = A_\infty \exp(-E_\infty/RT) \tag{29}$$

factor A_∞ was calculated from eq 30, where L^* is the path

$$\ln A_\infty = \ln (L^* ekT/h) + \Delta S^*/R - \Delta n \tag{30}$$

degeneracy Δn is the increment in moles (counted from reactants toward activated complex), and the rest of the symbols have their usual meaning. The activation energy E_∞ was calculated by eq 31, where E_0 is the critical energy

$$E_\infty = E_0 + \langle E^* \rangle - \langle E \rangle + RT \tag{31}$$

for reaction, $\langle E^* \rangle$ is the average internal energy of the complex, and $\langle E \rangle$ is the average internal energy of the reactants. The term RT corresponds to the contribution of the degree of freedom of the reaction coordinate that has not been included in $\langle E^+ \rangle$.

The vinyl and methyl models used in the calculations of recombination rates are listed in Table II; the principal moments of inertia employed for the activated complex were those of propylene (calculated from standard bond distances and angles).

The ratio of the products of the principal moments of inertia of reactant and complex were taken as one in the propylene decomposition calculations.

The different thermodynamical quantities have been calculated from the models by standard statistical-mechanics equations.

Calculation of the Total Energy Available for Partitioning. The total energy that can be partitioned between nitrogen and ethylcarbene in the photolysis of diazo-*n*-propane will be the sum of the light absorbed by the reactant, the thermal energy of the reactant, and the exothermicity of the reaction at 0 K.

The contribution of thermal energy was neglected. The distribution of energies absorbed by the diazo-*n*-propane can be calculated as follows. The ratio of light intensity absorbed I_{ab} to incident I_0 is given by eq 32 as a function

$$I_{ab}/I_0 = 1 - 10^{-A} \tag{32}$$

of the absorbance A. For absorbance lower than 0.1 eq 32 can be approximated by

$$I_{ab}/I_0 = 2.303A \tag{33}$$

If Beer's law is obeyed the absorbance is proportional to diazo-*n*-propane concentration. Therefore, the ratio $(I_{ab}/I_0)_{\lambda_2}/(I_{ab}/I_0)_{\lambda_2}$, where λ_1 and λ_2 are two different wavelengths, will be concentration independent as long as eq 33 holds. This ratio, for the wavelengths of interest, was obtained from the spectrum of diazo-*n*-propane in cyclohexane (gas- and liquid-phase spectra of diazo compounds are similar[34]). Experimental conditions were such as to ensure that 33 was obeyed. The relative incident light, I_0, was obtained from data furnished by Hannovia Co., the manufacturer of the lamp used. These data give almost identical spectral distribution as that the emission reported by Calvert and Pitts[35] for medium-pressure mercury lamps. The number of molecules with energy equal to that of the absorbed photon, $n(E)$, shou.d be proportional to the intensity absorbed, I_{ab}, at the corresponding wave-

TABLE V: Distribution of the Energy Absorbed by Diazo-*n*-propane in the Photolysis Experiments

nm	$n(E)$,[a] I_{ab}	E, kcal mol^{-1}
546.1	5.08	52.17
435.8	75.00	65.38
404.5	14.55	70.44
366.0	5.36	77.85

[a] Normalized to 100. As Pyrex was used as filter, the diazo-*n*-propane only absorbs light significantly at the wavelengths considered.

TABLE VI: Parameters Used in Collision Calculations

	σ, cm $\times$ 10^8	ϵ/k, K
Diazo-*n*-propane[a]	7.1	400
Propylene[b]	4.67	303
Vinyl[c]	5.061	205
Methyl[c]	3.796	144
Nitrogen[b]	3.68	92

[a] Estimated values. [b] Reference 36. [c] Parameters of ref 36 for the corresponding hydrocarbons.

length. The $n(E)$ for the range of interest are listed in Table V. The average energy E absorbed by diazo-*n*-propane was calculated as $\bar{E} = \Sigma En(E)/\Sigma n(E)$ and equals 66.1 kcal mol^{-1}.

As it has been mentioned before, from this average energy has to be subtracted the energy that is converted into potential energy of the fragments when diazo-*n*-propane decomposes, in order to obtain the energy available for partitioning. This energy has been approximated as the difference in standard heat of formation of products and reactant, and was found to be 3.6 kcal mol^{-1} (endothermic).[36] Then, a value of 62.5 kcal mol^{-1} for the average energy available for partitioning is found.

Calculation of Collision Rates.[37,38] Collision rates were calculated by the standard kinetic relationship (34),

$$\omega_{AB} = \left(\frac{S_A + S_B}{2}\right)^2 \left(\frac{M_A + M_B}{M_A M_B}\right)^{1/2} (8\eta kT)^{1/2} N_B \quad (34)$$

where S is the effective collision diameters, M the molecular weight, and N_B the concentration of B molecules. The S_{AB} values are estimated from Lennard-Jones hard-spheres diameters σ_{AB} by

$$S_{AB}^2 = \sigma_{AB}^2[\Omega^{2,2}(T^*)] \quad (35)$$

The collision integral $\Omega^{2,2}$ is a function of the reduced temperature T^*. The reduced temperature is calculated by eq 36, where ϵ/k is the force constant and the other symbols have their usual meanings.

$$T^* = kT[(\epsilon/k)_A(\epsilon/k)_B]^{-1/2} \quad (36)$$

The parameters used are listed in Table VI.

Supplementary Material Available. Figures 6 and 7 will appear following these pages in the microfilm edition of this volume of the journal. Photocopies of the supplementary material from this paper only or microfiche (105 $\times$ 148 mm, 24$\times$ reduction, negatives) containing all of the supplementary material for the papers in this issue may be obtained from the Journals Department, American Chemical Society, 1155 16th St., N.W., Washington, D. C. 20036. Remit check or money order for $3.00 for photocopy or $2.00 for microfiche, referring to code number JPC-74-1348.

References and Notes

(1) (a) J. A. Bell, *Progr. Phys. Org. Chem.*, **2**, 1 (1964); (b) H. M. Frey, *Progr. React. Kinet.*, **2**, 132 (1964); (c) W. Kirmse, "Carbene Chemistry," 2nd ed, Academic Press, New York, N. Y., 1971.

(2) (a) H. M. Frey and G. B. Kistiakowsky, *J. Amer. Chem. Soc.*, **79**, 6373 (1957); (b) H. M. Frey, *J. Chem. Soc.*, 2293 (1962); (c) D. W. Setser and B. S. Rabinovitch, *Can. J. Chem.*, **40**, 1425 (1962); (d) P. B. Shevlin and A. P. Wolf, *J. Amer. Chem. Soc.*, **88**, 4735 (1966); (e) C. L. Kibby and G. B. Kistiakowsky, *J. Phys. Chem.*, **70**, 126 (1966); (f) J. M. Figuera, *An. Quim.*, **67**, 209 (1971).

(3) (a) H. Staudinger and R. Endel, *Ber. Deut. Bot. Ges.*, **46**, 1437 (1913); (b) R. A. Holroyd and F. E. Blacet, *J. Amer. Chem. Soc.*, **79**, 4830 (1957); (c) D. P. Chong and G. B. Kistiakowsky, *J. Phys. Chem.*, **68**, 1793 (1964); (d) S. Y. Ho, I. Unger, and W. A. Noyer, *J. Amer. Chem. Soc.*, **87**, 2297 (1965); (e) R. W. Carr, Jr., and G. B. Kistiakowsky, *J. Phys. Chem.*, **70**, 118 (1966).

(4) (a) H. M. Frey and I. D. R. Stevens, *Proc. Chem. Soc.*, 79 (1962); (b) H. M. Frey and I. D. R. Stevens, *J. Amer. Chem. Soc.*, **84**, 2647 (1962); (c) H. M. Frey and I. D. R. Stevens, *J. Chem. Soc.*, 3514 (1963); (d) E. Schmitz, D. Habish, and A. Stark, *Angew. Chem.*, **75**, 723 (1963); (e) M. J. Amrich and J. A. Bell, *J. Amer. Chem. Soc.*, **86**, 292 (1964); (f) H. M. Frey and I. D. R. Stevens, *J. Chem. Soc.*, 1700 (1965).

(5) (a) G. Herzberg and J. Shoosmith, *Nature, (London)*, **183**, 1801 (1959); (b) G. Herzberg, *Proc. Roy. Soc., Ser. A*, **262**, 291 (1961); (c) G. Herzberg and J. W. C. Johns, *ibid.*, **295**, 107 (1966).

(6) (a) J. F. Harrison and L. C. Allen, *J. Amer. Chem. Soc.*, **91**, 807 (1969); (b) C. F. Bender and H. F. Schaefer, III, *ibid.*, **92**, 4984 (1970); (c) C. F. Bender, H. F. Schaefer, III, D. R. Franceschetti, and L. C. Allen, *ibid.*, **94**, 6888 (1972).

(7) (a) E. Wasserman, V. J. Kuck, R. S. Hutton, and W. A. Yager, *J. Amer. Chem. Soc.*, **92**, 7491 (1970); (b) E. Wasserman, V. J. Kuck, R. S. Hutton, E. D. Anderson, and W. A. Yager, *J. Chem. Phys.*, **54**, 4120 (1971).

(8) G. Herzberg and J. W. C. Johns, *J. Chem. Phys.*, **54**, 2276 (1971).

(9) (a) V. Menendez and J. M. Figuera, *Chem. Phys. Lett.*, **18**, 426 (1973); (b) M. Martin, V. Menendez, and J. M. Figuera, to be submitted for publication; (c) N. Bodor and M. J. S. Dewar, *J. Amer. Chem. Soc.*, **94**, 9103 (1972).

(10) R. Hoffman, *Tetrahedron*, **22**, 539 (1966).

(11) (a) R. A. Marcus and O. K. Rice, *J. Phys. Chem.*, **55**, 894 (1951); (b) R. A. Marcus, *J. Chem. Phys.*, **20**, 359 (1952); (c) the approximation of G. Z. Whitten and B. S. Rabinovitch, *J. Chem. Phys.*, **38**, 2466 (1963), has been used.

(12) S. Glasstone, K. J. Laidler, and H. Eyring, "The Theory of Rate Processes," McGraw-Hill, New York, N. Y., 1941.

(13) D. W. Adamson and J. Kenner, *J. Chem. Soc.*, 1551 (1937).

(14) (a) H. C. Brown, *Org. React.*, **5**, 469 (1951); (b) J. A. Krynitsky, J. E. Johnson, and H. W. Carhart, *Anal. Chem.*, **20**, 311 (1948).

(15) G. Brauer, "Handbook of Preparative Inorganic Chemistry," Vol. 1, Academic Press, New York, N. Y., 1963, p 280.

(16) The collision rate (see Appendix) has been included in the plots in order to be able to compare experiments with and without added propylene. For the latter, the points have been plotted against collision rate. The pressure scale is not applicable to these cases.

(17) (a) W. E. Falconer and W. A. Sunder, *Int. J. Chem. Kinet.*, **3**, 395 (1971); (b) W. E. Falconer and W. A. Sunder, *ibid.*, **4**, 315 (1972); (c) B. S. Rabinovitch and D. W. Setser, *Advan. Photochem.*, **3**, 1 (1964).

(18) J. A. Kerr and A. F. Trotman-Dickenson, *Progr. React. Kinet.*, **1**, 109 (1961).

(19) D. G. L. James and S. M. Kambanis, *Trans. Faraday Soc.*, **65**, 1350 (1969).

(20) If $k_{C-H}(E) \ll k_{C-C}(E)$ or $k_{C-H}(E) \ll \omega$, then the rate constant $k_{C-H}(E)$ can be omitted in eq 28. We have calculated that with a C–H splitting model that gives $\langle k_{C-C}\rangle/\langle k_{C-H}\rangle \approx 2.5$, the error introduced if we make $k_{C-H}(E) = 0$ is about 3% at 20 mm pressure and about 10% at lower pressures. Our results indicate that the ratio of the average rate constants should be higher and, therefore, the $k_{C-H}(E)$ terms in eq 28 have been left out.

(21) (a) G. M. Wieder and R. A. Marcus, *J. Chem. Phys.*, **37**, 1835 (1962); (b) E. V. Waage and B. S. Rabinovitch, *Chem. Rev.*, **70**, 377 (1970).

(22) F. H. Dorer, E. Brown, J. Do, and R. Rees, *J. Phys. Chem.*, **75**, 1640 (1971).

(23) The heat of reaction at 0 K has been taken as the difference in standard heat of formation of propylene and ethylcarbene, calculated by MINDO/2: $\Delta H(0\text{ K}) = \Delta H_f^\circ$(ethylcarbene) $- \Delta H_f^\circ$(propylene) = 56 kcal mol^{-1}.

(24) W. L. Hase, R. L. Johnson, and J. W. Simons, *Int. J. Chem. Kin.*, **4**, 1 (1972).

(25) J. W. Simons, B. S. Rabinovitch, and F. H. Dorer, *J. Phys. Chem.*, **70**, 1076 (1966).

(26) G. A. Chappell and H. Shaw, *J. Phys. Chem.*, **72**, 4672 (1968), have found the following expression for the unimolecular C–C splitting of propylene in shock tubes (at about 1300 K): $k = 10^{16.07 \pm 0.40}\exp(-85.84 \pm 2.37/RT)$.

(27) Z. B. Alfassi, S. W. Benson, and D. M. Golden, *J. Amer. Chem. Soc.*, **95**, 4784 (1973).

(28) (a) P. J. Robinson and K. A. Holbrook, "Unimolecular Reactions."

Wiley, New York, N. Y., 1972, p 152; (b) J. M. Perez, J. M. Figuera, and V. Menendez, *An. Fis.*, **69**, 233 (1973).
(29) R. L. Belford and R. A. Strehlow, *Ann. Rev. Phys. Chem.*, **20**, 247 (1969).
(30) J. H. Kiefer, *J. Chem. Phys.*, **57**, 1938 (1972).
(31) Under ordinary pyrolysis conditions propylene undergoes bimolecular initiation, and no direct information about the unimolecular decomposition can be obtained: (a) M. Simon and M. H. Back, *Can. J. Chem.*, **48**, 317 (1970); (b) *ibid.*, **48**, 3313 (1970).
(32) S. W. Benson, "Thermochemical Kinetics," Wiley, New York, N. Y., 1968, p 215.
(33) Obtained using the most recent value for the standard heat of formation of allyl, ΔH_f° = 40 kcal mol^{-1}; D. K. Sen Sharma and J. L. Franklin, *J. Amer. Chem. Soc.*, **95**, 6562 (1973).
(34) R. K. Brinton and D. H. Volman, *J. Chem. Phys.*, **19**, 1394 (1951).
(35) J. G. Calvert and J. N. Pitts, "Photochemistry," Wiley, New York, N. Y., 1967, p 696.
(36) Heats of formation were calculated by MINDO/2, trough a minimization procedure. The results will be published elsewhere.
(37) J. O. Hirschfelder, C. F. Curtiss, and R. B. Bird, "Molecular Theory of Gases and Liquids," Wiley, New York, N. Y., 1954.
(38) (a) D. W. Setser and B. S. Rabinovitch, *Can. J. Chem.*, **40**, 1425 (1962); (b) S. P. Pavlou and B. S. Rabinovitch, *J. Phys. Chem.*, 75, 2171 (1971).

Isothermal Flash Photolysis of Hydrazine

M. Arvis,* C. Devillers, M. Gillois,

DRA/SRIRMa, C.E.N. Saclay, B.P. No. 2, 91190 Gif Sur Yvette, France

and M. Curtat

G.R.C.P.C., Faculté des Sciences, 86000 Poitiers, France *(Received November 12, 1973)*

Publication costs assisted by C.E.N. de Saclay

The flash photolysis of hydrazine diluted in an excess of inert gas (isothermal photolysis) has been reinvestigated using a long path cell and a flash of shorter duration ($t_{1/2} \approx 5$ μsec) than previously employed. Under these conditions the well-known absorption of NH_2 is observed in addition to two new transients: the 336-nm absorption band of NH ($t_{1/2} \approx 18$ μsec) and a continuous absorption detectable at 400 nm whose intensity increases in the ultraviolet ($t_{1/2} \approx 10$ μsec). The time dependence of the NH_2 radical concentration has been monitored by kinetic spectrophotometry at 597.6 nm and compared with the evolution of the same radical in the NH_3–helium system. The comparison demonstrates the existence of a secondary formation of NH_2 attributed to the reaction $H + N_2H_3 \rightarrow 2NH_2$; the secondary formation is limited and this is believed to be the result of the fast disappearance of N_2H_3 radicals by the reaction $N_2H_3 + N_2H_3 \rightarrow$ products. The assignment of the short-lived continuous absorption to N_2H_3 is discussed on the basis of this interpretation.

Introduction

The photodissociation of hydrazine by photons whose wavelength is about 200 nm can be interpreted in terms of the four energetically probably primary events

$$N_2H_4 \xrightarrow{h\nu} NH_2 + NH_2 \qquad \Delta H = 61 \text{ kcal} \qquad (1)$$

$$\xrightarrow{h\nu} N_2H_3 + H \qquad \Delta H = 76 \text{ kcal} \qquad (2)$$

$$\xrightarrow{h\nu} N_2H_2 + H_2 \qquad \Delta H = 26 \text{ kcal} \qquad (3)$$

$$\xrightarrow{h\nu} NH + NH_3 \qquad \Delta H = 50 \text{ kcal} \qquad (4)$$

The first studies on the continuous photolysis of hydrazine did not definitely establish the relative roles of these different processes[1,2] although the observation of NH_2[3] during the flash photolysis of N_2H_4 suggested that reaction 1 was important. More recent work on the continuous photolysis of hydrazine[4-7] indicates that the major primary event is reaction 2. Thus, Schurath and Schindler[7] measured the following quantum yields in the photolysis at 206.2 nm: $\phi_2 = 0.97 \pm 0.1$, $\phi_3 < 0.05$. These values show that the contribution of reaction 1 is small under these conditions.

The last observation led us to investigate the origin of NH_2 in the isothermal flash photolysis of hydrazine by following the formation and decay of this radical using its intense 597.6-nm absorption band. The ammonia system, in which the kinetic behavior of NH_2 is now well established,[8,9] was used as a reference. In addition an attempt was made to detect any weakly absorbing transients formed in the photolysis by using long absorption paths (up to 16 m).

Experimental Section

The flash photolysis apparatus was equipped with two parallel, 1-m long, silica lamps in which an electric discharge (5000 J, 8 × 7.7 μF, 13 kV) produced a 5-μsec (at half-intensity) polychromatic light pulse. The photolysis cell, 55-mm i.d., contained a multiple reflection mirror system based on the White principle.[10] The lamps and cell were enclosed in an aluminum reflector. A 1-m optical path was obtained by eliminating the mirror system and the 0.5-m path by masking half of the cell with black paper.

Transient absorption spectra were recorded on a Hilger

E 742 spectrograph using a 100-J capillary spectroflash lamp ($t_{1/2} \approx 3$ μsec). The same capillary lamp was used as the light source for kinetic spectrophotometry but was supplied in this case from a pulse-forming network producing an almost flat pulse of light whose intensity was constant within a few per cent during 450 μsec (energy stored in the capacitance network ≈ 700 J). After traversing the photolysis cell, the light was dispersed in a 3.4-m Jarrel-Ash spectrograph provided with an exit slit and then received on a photomultiplier (56 UVP, La Radiotechnique). The linearity of the photomultiplier response to intense signals was ensured by a chain of large capacitances. A convenient signal-to-noise ratio was obtained using a 100-μm entrance slit and a 150-μm exit slit. Under these conditions the slit function was measured with a narrow emission line and is represented in Figure 1. The differences observed between the measured and calculated curves are attributed to a stigmatic defect of the apparatus. Wavelengths shorter than 550 nm were eliminated using a filter placed in front of the entrance slit. Wavelengths longer than 700 nm were not detected due to the rapid decrease of the photomultiplier sensitivity in the red.

Hydrazine was distilled over CaO in the presence of inert gas (argon) thus reducing the water content to less than 1%. Before use the liquid was pumped for several minutes at room temperature. Ammonia (Matheson, 99.99%) was used without further purification. Inert gases (argon, helium) were admitted into the vacuum line after passing through a molecular sieve column. In the case of helium the column was cooled to liquid nitrogen temperature. Analysis of the small concentrations of photolysis products (H_2, N_2, NH_3) was carried out after separation of condensable products in a liquid nitrogen trap. Uncondensable products, H_2, N_2, and argon, were then introduced into the gas chromatograph (13× molecular sieve column, flowing gas argon). Condensable products were transferred into a 1-cm spectrophotometer cell fitted with a side arm. Ammonia was determined with a Cary 14 spectrophotometer using the structured far-uv absorption spectrum of this gas; during the measurements the partial pressure of the excess hydrazine was maintained at a constant low value by plunging the side arm in an ice bath. The validity of this procedure was checked using synthetic mixtures of known composition.

Owing to the strong adsorption of hydrazine on Pyrex or silica walls a standard procedure was adopted for the preparation of hydrazine–inert gas mixtures. The 5-l. bulb used for the preparation was first "poisoned" with a hydrazine pressure of 6 Torr. After 1 hr this gas was rapidly pumped out and a fresh charge introduced to the required pressure followed by 500 Torr of inert gas. The gases were allowed to mix for at least 1 hr before introduction into the photolysis cell where the mixture was photolyzed within 30 to 40 sec.

Results

1. Preliminary Study by Kinetic Spectroscopy in the Range 290–650 nm. The photolysis of a mixture containing a partial pressure of 1.17 Torr of hydrazine in 100 Torr of argon permitted the observation of the 336-nm absorption of the NH radical ($A^3\Pi \leftarrow X^3\Sigma^-$, half-life 18 μsec) and the fine structured absorption spectrum of NH_2 in the visible during several hundred microseconds.

A continuous absorption was detected between 400 and

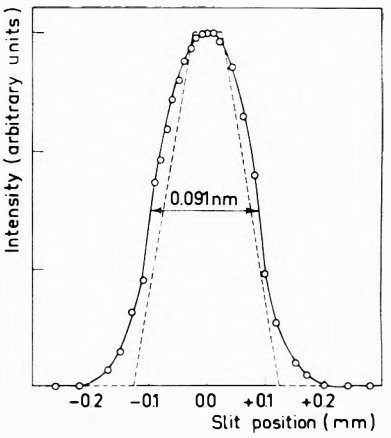

Figure 1. Slit function of the spectrograph used to follow the kinetics of the 597.6-nm band of NH_2: full line, measured; dashed line, calculated from slit width (spectrograph dispersion 0.495 Å/mm).

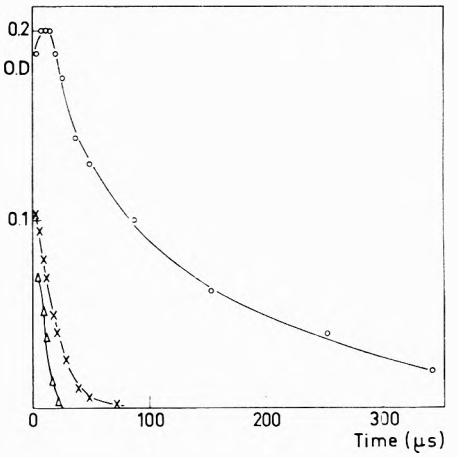

Figure 2. Time variation of the transients detected in the flash photolysis of the mixture N_2H_4–argon (1.17 Torr–100 Torr): O, NH_2 (598 nm); ×, NH (336 nm); Δ, continuous absorption (290 nm). The optical densities are those measured directly on the photographic plate.

290 nm (half-life about 10 μsec). Its intensity increased in strength toward the ultraviolet but was only 0.07 o.d. at the shortest wavelength of observation (290 nm). The poor reflectivity of the mirrors combined with the increasing intensity of the N_2H_4 absorption made observations impossible at shorter wavelength.

The variation with time of the three absorption spectra is represented in Figure 2. The optical densities are plotted directly from the microdensitometer traces. No absorptions were detected at longer delays.

The analysis of the final products gave $[N_2] = 1.7 \pm 0.2 \times 10^{-6}$ *M*, $[H_2] = 2.2 \pm 0.2 \times 10^{-6}$ *M*, and $[NH_3] = 2.7 \pm 0.2 \times 10^{-6}$ *M* which corresponds to the decomposition of 3×10^{-6} *M* of N_2H_4, *i.e.*, 5% of the initial concentration of hydrazine.

2. Rate of Formation and Decay of the NH_2 Radical. The absorption spectrum of NH_2 in the visible ($^2A_1 \leftarrow {}^2B_1$) is composed of a large number of partially resolved vibrational bands.[11] The particularly intense 597.6-nm band used to monitor the NH_2 concentrations may contain one or several saturated rotational lines. In such a case the Beer–Lambert law is not applicable[12] and the measured optical density is not proportional to the con-

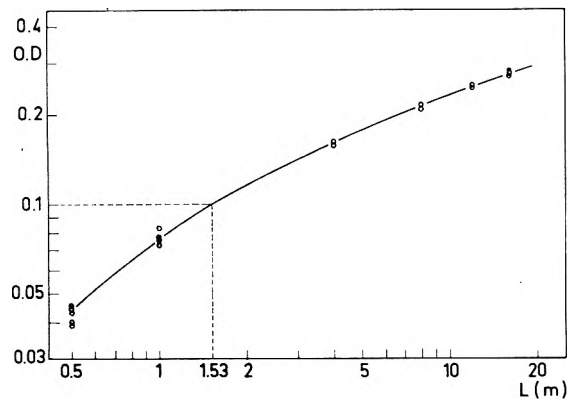

Figure 3. Optical density of NH_2 absorption as a function of length of the optical path. (The optical density is measured 55 μsec after the photolytic flash: λ 597.6 nm, N_2H_4 1.17 Torr, helium 100 Torr.)

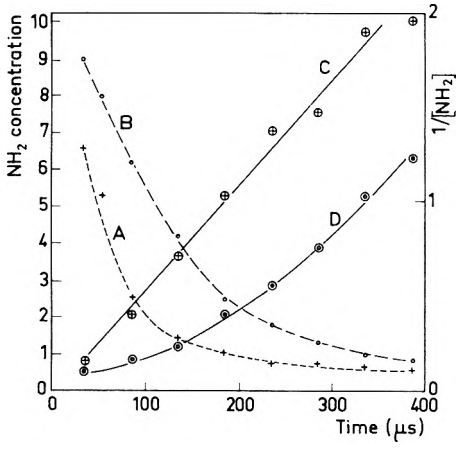

Figure 4. Time variation of the NH_2 concentration in the photolysis of (A) NH_3 (6 Torrs)-helium (100 Torr); (B) N_2H_4 (1.17 Torr)-helium (100 Torr); (C and D) are plots of the inverse of NH_2 on the same time scale ((C) NH_3 system, (D) N_2H_4 system). Concentrations are expressed in relative units (see text).

centration of the absorbing species.[13] Similar conclusions have been reached in some recent works on the photolysis[14] and the radiolysis[8] of gases, and the well-known relation

$$\mathrm{OD} = \epsilon c l \qquad \text{(I)}$$

has been replaced by

$$\mathrm{OD} = (\epsilon c l)^n \qquad (n < 1) \qquad \text{(II)}$$

to take into account the effect of saturation, n being a constant in the range of concentrations studied. Relation II was empirically justified by plotting log D as a function of log l, the straight line obtained having a slope of less than one. In particular, Gordon, *et al.*,[8] found $n = 0.77$ for NH_2, l varying from 0.4 to 2 m. Under our conditions and with l varying from 0.5 to 16 m such a plot is not linear (Figure 3). The value of n equals 0.8 for small values of l ($0.5 < l < 1$ m) but reaches 0.4 for the longest optical paths used. No attempt will be made to obtain an analytical formulation of the relation $D = f(l)$ represented by the plot of Figure 3; instead the concentrations of NH_2 will be expressed as relative values obtained directly from Figure 3 (for example, a measured optical density of 0.10 corresponds to $[NH_2] = 1.53$ in relative units).

The time dependence of the relative concentrations of NH_2 is represented in Figure 4 for the two systems NH_3-

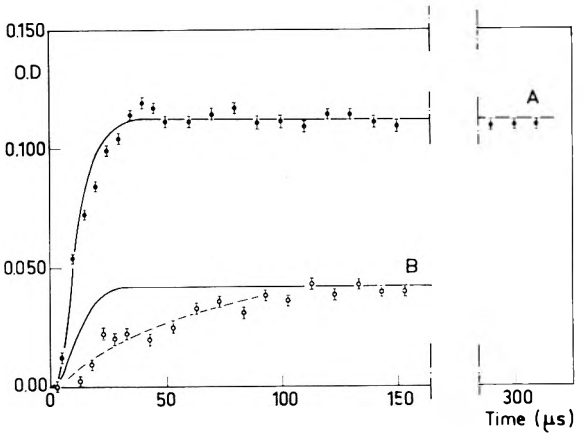

Figure 5. Time variation of NH_2 optical density (A) NH_3-helium (0.36 Torr-6 Torr), (B) N_2H_4-helium (1.95×10^{-2} Torr-60 Torr). The full lines correspond to the function $\int_0^t I(t)\,dt$, $I(t)$ being the intensity of the photolytic light as a function of time, and are normalized to the observed plateau values.

helium (6 Torr-100 Torr), curve A, and N_2H_4-helium (1.2 Torr-100 Torr), curve B. Curves C (NH_3-helium) and D (N_2H_4-helium) show the variation with time of the inverse of the relative concentrations. Comparison of curves A and B immediately suggests a secondary formation of NH_2 in the hydrazine photolysis (slower rates of disappearance in spite of higher concentrations). Such a secondary formation has been exemplified at very low concentrations of NH_2 where the rates of reaction can be higher than the duration of the photolytic flash. Figure 5, curve B, shows the variation (formation) of the NH_2 concentration for the mixture N_2H_4 (1.95×10^{-2} Torr)-helium (60 Torr); it is compared to the variation of NH_2 in the mixture NH_3 (0.36 Torr)-helium (6 Torr), curve A, where no significant decay of NH_2 occurs during the observation period. The form of curve A compares favorably with that expected for the formation of a primary species as represented by the function $\int I(t)\,dt$ ($I(t)$ = intensity of the flash as a function of time). Curve B clearly shows a 100-μsec risetime indicating, within experimental error, that part of NH_2 formation is a secondary process.

Discussion

The data presented here and obtained with the use of a long optical path clearly contain some new information relative to the isothermal photolysis of hydrazine. Thus the appearance of a continuum and of the 336-nm absorption of NH has not been previously mentioned in the literature. It appears necessary to examine the origin of the continuum and of the NH radical before discussing any secondary process of NH_2 radical formation.

1. The Continuum. The most reasonable assignments are certainly N_2H_2, N_2H_3, or N_2H_4*. The first, N_2H_2, is incompatible with the accumulated information on the lifetime of this species. Identified as one of the products resulting from the action of a microwave discharge on N_2H_4, it can be trapped at liquid nitrogen temperature and detected by mass spectroscopy after warming.[15,16] Moreover, its electronic spectrum has been recorded in absorption at about 175 nm in a cell separated from the discharge by a trap cooled at $-78°$.[17]

The assignment of the continuum to the electronic spectrum of unthermalized hydrazine is a second possibility. Such an assignment was proposed by Husain and Norrish in discussion of the adiabatic flash photolysis of

N_2H_4[18] where a similar continuum was observed on a longer time scale and where the temperature was higher ($\approx$1500°K). Following this hypothesis the disappearance of the absorption under our experimental conditions could be interpreted as the thermal relaxation of the corresponding molecule in a time comparable to that of the photolytic flash, *i.e.*, 5 μsec. This assignment is however difficult to support because of the structureless absorption spectrum of hydrazine[3] which suggests that photon excitation leads uniquely to dissociation.

It therefore appears reasonable to attribute this absorption to N_2H_3. Several modes of disappearance have been proposed for this radical

$$N_2H_4 + N_2H_3 \longrightarrow \text{products} \quad (5)$$

$$H + N_2H_3 \longrightarrow 2NH_2 \quad (6)$$

$$N_2H_3 + NH_2 \longrightarrow NH_3 + N_2H_2 \quad (7)$$

Reaction 5 is accepted as the principal mode of disappearance of N_2H_3 at low radical concentrations.[19-21] Reaction 6 was proposed to explain the high concentrations of NH_2 observed when H atoms react with hydrazine at large $[H]/[N_2H_4]$ ratios.[22,23] Reaction 7 can explain part of the isotopic scrambling of molecular N_2 formed during photolysis of mixtures of ^{15}N- and ^{14}N-labeled hydrazines.[20] Neglecting reactions re-forming hydrazine the initial concentration of the N_2H_3 radical, $[N_2H_3]_0$, can be estimated from the amount of N_2H_4 decomposed, *i.e.*, $[N_2H_3]_0 \approx 3 \times 10^{-6}$ *M*. The half-life of the continuous absorption, 10 μsec, is 5 μsec higher than the duration of the photolytic flash; the difference, if used as a half-time of reaction 5 gives $2k_5 = 1/[N_2H_3]_0 t_{1/2} \approx 0.7 \times 10^{11}$ M^{-1} sec^{-1}. The value $2k = 1.2 \times 10^{11}$ M^{-1} sec^{-1} has been measured for the bimolecular disappearance of NH_2.[8] Also supporting the assignment of the continuum to N_2H_3 is the recent assignment of a continuous absorption with maximum at 200 nm to the isoelectronic radical HO_2.[13]

2. *Origin of the NH Radical.* Formation of NH by the reaction

$$NH_2 + NH_2 \longrightarrow NH + NH_3 \quad (8)$$

can be eliminated by comparing the fast rate of its disappearance ($t_{1/2} \approx 18$ μsec) to the measured rate of NH_2 decay. Furthermore, reaction 8 was observed in the photolysis of ammonia at low pressures (total pressure less than 1 Torr)[24] but under our conditions the radical is not detectable in the photolysis of NH_3 (total pressure 100 Torr) where NH_2 radical concentrations are of the same order of magnitude as in the hydrazine photolysis. An extinction coefficient ϵ 40,000 M^{-1} cm^{-1} [25] has been proposed for the 336-nm absorption of NH. From the oscillator strength of the transition[26,27] a similar value, $\epsilon \approx$ 50,000 M^{-1} cm^{-1}, can be calculated for the unresolved Q branch of the O-O transition. This gives an estimate of about 3×10^{-9} *M* for the maximum NH concentration in the present experiment; such a small concentration may come from N_2H_4 by the photochemical reaction

$$N_2H_4 \xrightarrow{h\nu} NH + NH_3 \quad (4)$$

However, a preliminary experiment on the adiabatic flash photolysis of N_2H_4 (1.2 Torr) suggests another possibility. It has been observed that under these conditions and at short delays the continuous absorption is 2.5 times greater in intensity than under isothermal conditions, the increase being associated with a corresponding increase in NH intensity although the NH_2 absorption is unchanged. Thus the correlation between the continuous absorption and NH intensities may be the result of the secondary photolysis of N_2H_3

$$N_2H_3 \xrightarrow{h\nu} NH + NH_2 \quad (9)$$

the small yield estimated for NH being associated with a negligible NH_2 formation.

3. *Formation of the NH_2 Radical. Ammonia Photolysis.* The NH_2 radicals formed in this system are of primary origin

$$NH_3 \xrightarrow{h\nu} NH_2 + H$$

The kinetic of their disappearance has been described by the two competitive reactions

$$NH_2 + NH_2 \longrightarrow \text{products} \quad (10)$$

$$NH_2 + H + M \longrightarrow NH_3 + M \quad (11)$$

The variation of $1/[NH_2]$ as a function of time is linear (Figure 4) from 40 μsec where the photolytic formation is terminated up to 400 μsec. Such a linear plot has been obtained in the pulse radiolysis of NH_3 at the lowest pressure used (250 Torr);[3] it corresponds to the predominance of reaction 10, $2k_{10} = 1.2 \times 10^{11}$ M^{-1} sec^{-1} over reaction 11, $k_{11} = 2.2 \times 10^{12}$ M^{-1} sec^{-1}. The disagreement which was pointed out in the Experimental Section between our relation OD = f($[NH_2]$) and that of Gordon, *et al.*,[8] does not allow us to use their ϵ_{NH_2} value to evaluate the absolute NH_2 concentrations. However such an estimate can be made from the rate constant k_{10} and the slope of curve C on Figure 4. In fact, the relative NH_2 concentrations $[NH_2]_{rel}$ used in Figure 4 are proportional to the absolute concentrations $[NH_2]_{abs}$: $[NH_2]_{rel} = K[NH_2]_{abs}$ from which it follows that the slope *s* of curve C can be related to the bimolecular rate constant k_{10} by

$$s = 2k_{10}/K$$

the expression being analogous to the relation $s = 2k/\epsilon l$ used when Beer's law is applicable and the relative unit of concentration is the measured optical density. Taking $k_{10} = 0.6 \times 10^{11}$ M^{-1} sec^{-1}, *K* is then equal to 2.17×10^7 and the relative unit of concentration used on Figure 3 corresponds to 0.46×10^{-7} *M*. Using this value to estimate the empirical coefficient ϵ in the relation $D = (\epsilon cl)^n$ in the part of Figure 3 where *n* is close to the value 0.77 obtained by Gordon, *et al.*, we obtain $\epsilon \approx 1100$ M^{-1} cm^{-1} which may be compared with the value $\epsilon \approx 774$ M^{-1} cm^{-1} obtained by these authors. The discrepancy can certainly be explained by experimental factors such as slit function and positioning, variation of line widths in the 597.6 nm band as a function of pressure, or nature of diluant gas but needs more experimental investigation to be elucidated.

Hydrazine Photolysis. A rise time longer than expected for a primary species is observed in the photolysis of N_2H_4 at low partial pressure (2×10^{-2} Torr of hydrazine, 60 Torr of helium, Figure 5). On the other hand comparison of curves A and B of Figure 4 clearly shows that between 0 and 250 μsec the rates of disappearance of NH_2 are slower in the mixtures containing hydrazine than in those containing ammonia in spite of higher concentrations in the former. This result is unexpected since the presence of other radicals in the system (N_2H_3, NH) would favor a higher rate of disappearance. These observations are therefore the result of a fast secondary formation of NH_2. A process such as

$$N_2H_4 \xrightarrow{h\nu} N_2H_4^* \quad (12)$$

followed by

$$N_2H_4^* \xrightarrow{} 2NH_2 \quad (13)$$

$$N_2H_4^* \xrightarrow{+M} N_2H_4 \quad (14)$$

can explain the slow rise time observed in Figure 5. The evidence for the existence of a long-lived excited state of hydrazine (triplet N_2H_4?) is however small. The reaction

$$H + N_2H_4 \longrightarrow NH_2 + NH_3 \quad (15)$$

has been proposed to explain the emission $^2A_1 \rightarrow {}^2B_1$ of NH_2 observed when high H atoms concentrations react with hydrazine.[22] Such a reaction is however a minor process[2] compared to

$$H + N_2H_4 \longrightarrow H_2 + N_2H_3 \quad (16)$$

Two values for k_{16} can be found in the literature ($k = 1.3 \times 10^{10} \exp(-2500/RT)\ M^{-1}\ sec^{-1}$,[23] $k = 3.5 \times 10^8 \exp(-2000/RT)\ M^{-1}\ sec^{-1}$).[21] If one considers that reaction 16 is the limiting process in the formation of NH_2 by (15) its time of half reaction is thus approximately equal to the half rise time of NH_2. Taking $[N_2H_4] = 1.46 \times 10^{-6}\ M$ (0.02 Torr), $T = 300°K$, and using the largest value for k_{16} one gets $\tau_{1/2} \approx 3 \times 10^{-3}$ sec. This value is incompatible with the observed formation of NH_2, 100 μsec under these conditions.

The possibility of a fast disappearance of the N_2H_3 radicals discussed earlier suggests a third possible origin of NH_2 which has been proposed by Ghosh and Bair[22]

$$H + N_2H_3 \longrightarrow 2NH_2 \qquad \Delta H = 15 \text{ kcal} \quad (17)$$

A consideration of the enthalpy difference between the reaction paths

$$H + N_2H_3 \rightleftharpoons N_2H_4^* \xrightarrow{+M} N_2H_4 \quad (18)$$

$$NH_2 + NH_2 \rightleftharpoons N_2H_4^* \xrightarrow{+M} N_2H_4 \quad (19)$$

has led to the conclusion[28] that stabilization by (18) needs pressures several orders of magnitude greater than by (19). Comparing the pressure where reaction 19 does not lead exclusively to stabilization (5-10 Torr[9]), with the range of pressures where it does (250-1500 Torr[8]) it appears reasonable to conclude that at the helium pressure of 100 Torr reaction 17

$$H + N_2H_3 \longrightarrow 2NH_2 \quad (17)$$

is favored in comparison with

$$H + N_2H_3 \xrightarrow{+M} N_2H_4 \quad (20)$$

The maximum NH_2 concentration produced in the photolysis of 1.95×10^{-2} Torr of hydrazine, $2.3 \times 10^{-8}\ M$ represents 1.6% of the initial hydrazine concentration. The amount of hydrazine decomposed at this pressure is not known but can be estimated approximately from the percentage decomposition measured at 1.2 Torr, 5%, which does not take into account the possible reformation of N_2H_4 by

$$N_2H_3 + N_2H_3 \longrightarrow N_2H_2 + N_2H_4 \quad (21)$$

and

$$NH_2 + NH_2 \xrightarrow{+M} N_2H_4 \quad (19)$$

It follows that the formation of NH_2 represents less than 1/6 of the hydrazine dissociated into H and N_2H_3 indicating that the major part of H and N_2H_3 disappear by other reactions than (17). Further, the estimate of 3×10^{-3} sec made for the half-time of reaction 16

$$H + N_2H_4 \longrightarrow H_2 + N_2H_3 \quad (16)$$

suggests that the process limiting the formation of NH_2 is rather reaction 5

$$N_2H_3 + N_2H_3 \longrightarrow \text{products} \quad (5)$$

which is in agreement with the fast bimolecular disappearance of N_2H_3 suggested earlier.

Conclusion

In spite of the difficulties associated with the determination of NH_2 concentrations due to deviation from Beer's law it can be concluded that this species plays only a minor role in the photolysis of hydrazine, a conclusion consistent with other recent results on N_2H_4 photolysis. The delayed formation of the NH_2 radical is well accounted for at least on a semiquantitative basis by the competition between

$$N_2H_3 + N_2H_3 \longrightarrow \text{products}$$

and

$$H + N_2H_3 \longrightarrow 2NH_2$$

However it should be pointed out that the role of a possible long-lived excited state of hydrazine cannot be entirely eliminated and that the definitive attribution to N_2H_3 of the continuous absorption detected at shorter delays will need more experimental evidence.

References and Notes

(1) L. F. Audrieth and R. A. Ogg, "The Chemistry of Hydrazine," Wiley, New York, N. Y., 1951.
(2) W. A. Noyes, Jr., and P. A. Leighton, "The Photochemistry of Gases," Reinhold, New York, N. Y., 1941.
(3) D. A. Ramsay, *J. Phys. Chem.*, **57**, 415 (1953).
(4) A. N. Terenin, *Chem. Abstr.*, 3058*b* (1962).
(5) L. J. Stief, V. J. De Carlo, R. J. Mataloni, *J. Chem. Phys.*, **46**, 592 (1967).
(6) L. J. Stief and V. J. De Carlo, *J. Chem. Phys.*, **49**, 100 (1968).
(7) U. Schurath and R. N. Schindler, *J. Phys. Chem.*, **74**, 3188 (1970).
(8) S. Gordon, W. Mulac, and P. Nangia, *J. Phys. Chem.*, **75**, 1087 (1971).
(9) J. D. Salzman and E. J. Bair, *J. Chem. Phys.*, **41**, 3154 (1964).
(10) J. White, *J. Opt. Soc. Amer.* **32**, 285 (1942).
(11) K. Dressler and D. A. Ramsay, *Phil. Trans.*, **A251**, 553 (1959).
(12) G. Porter, "Rates and Mechanisms of Reactions," Tome II, Interscience, New York, N. Y., 1963, p 1082.
(13) C. J. Hochanadel, J. A. Ghormley, and P. J. Ogren, *J. Chem. Phys.*, **9**, 4426 (1972).
(14) A. B. Callear and W. J. R. Tyerman, *Trans. Faraday Soc.*, **62**, 371 (1966).
(15) J. N. Foner and R. L. Hudson, *J. Chem. Phys.*, **28**, 719 (1958).
(16) J. N. Foner and R. L. Hudson, *J. Chem. Phys.*, **29**, 442 (1958).
(17) A. Trombetti, *Can. J. Phys.*, **46**, 1005 (1968).
(18) D. Husain and R. G. W. Norrish, *Proc. Roy. Soc., Ser. A*, **273**, 145 (1963).
(19) L. J. Stief and V. J. De Carlo, *J. Chem. Phys.*, **44**, 4638 (1966).
(20) L. J. Stief, *J. Chem. Phys.*, **52**, 4841 (1970).
(21) M. Schiavello and G. G. Volpi, *J. Chem. Phys.*, **37**, 1510 (1968).
(22) P. K. Ghosh and E. J. Bair, *J. Chem. Phys.*, **45**, 4738 (1966).
(23) M. Gehring, K. Hoyermann, H. G. Wagner, and J. Wolfrum, *Ber. Bunsenges. Phys. Chem.*, **75**, 1287 (1971).
(24) K. A. Mantei and E. J. Bair, *J. Chem. Phys.*, **49**, 3248 (1968).
(25) O. Schnepp and K. Dressler, *J. Chem. Phys.*, **32**, 1682 (1960).
(26) R. G. Bennet and F. W. Dalby, *J. Chem. Phys.*, **32**, 1716 (1960).
(27) W. H. Smith and H. S. Liszt, *J. Quant. Spectrosc. Radiat. Transfer*, **11**, 45 (1971).
(28) U. Schurath, Diplomarbeit, Bonn, 1966.

Flash Photolysis of Potassium Tris(oxalato)cobaltate(III)

L. Cordemans, J. D'Olieslager, J. Hendrix, and S. De Jaegere*

Laboratorium voor Analytische en Anorganische Scheikunde, Universiteit te Leuven, Celestijnenlaan 200 F, B-3030 Heverlee, Belgium *(Received July 24, 1972; Revised Manuscript Received November 26, 1973)*

Publication costs assisted by the Laboratorium voor Analytische en Anorganische Scheikunde

Aqueous solutions of 10^{-5} to 10^{-4} *M* $K_3Co(C_2O_4)_3 \cdot 3.5H_2O$ in 3×10^{-3} *M* oxalic acid were flash irradiated. The results demonstrate the formation of two intermediary species, X and Y. Both decay in a monomolecular process, with rate constants $k_X = 20$ sec^{-1} and $k_Y = 87$ sec^{-1}. The spectra of both species are given. Arguments are given to prove that X is formed by photodecomposition of Y. The thermal decomposition of Y leads to the formation of the $C_2O_4 \cdot^-$ radical, which will either react very fast with $Co(C_2O_4)_3^{3-}$, or, when no $Co(C_2O_4)_3^{3-}$ is left after the flash, disappear by reaction with another $C_2O_4 \cdot^-$ species.

Introduction

The photoreduction of the trisoxalato complexes of trivalent transition metals such as Fe(III), Co(III), and Mn(III) has been extensively studied for the past years.[1] Most of the conclusions on the actual reduction mechanism result from data on iron oxalate. A survey of the literature on the reduction of Co(III) and Mn(III) oxalates reveals a more or less general tendency to preconceive a similar if not an identical decomposition mechanism.

Although most of the data seem to confirm this assumption, there is no clear proof that indeed the same reactive species are present. Some of the conclusions on $Fe(C_2O_4)_3^{3-}$ can nevertheless be very valuable in the interpretation of specific data on the photoreduction of the other oxalato complexes.

This paper reports on new flash photolysis data for $Co(C_2O_4)_3^{3-}$. Their kinetic analysis shows that two primary intermediate species have to be considered. Their relative importance depends on the reaction conditions.

$Co(C_2O_4)_3^{3-}$ was preferred over $Fe(C_2O_4)_3^{3-}$ because it has the advantage of yielding reaction intermediates with spectra which overlap only partially with those of the initial and final products, as will be shown in this work.

Literature Survey on the Photoreduction of Cobalt and Iron Oxalates

In view of their importance it seems logical to include the data on the photoreduction of $Fe(C_2O_4)_3^{3-}$ in this survey. A detailed investigation of the photolysis of $Fe(C_2O_4)_3^{3-}$ by Parker[2,3] led to the well-known mechanism

$$Fe(C_2O_4)_3^{3-} \xrightarrow{h\nu} \cdots \longrightarrow Fe(C_2O_4)_2^{2-} + C_2O_4^{\cdot-} \quad (1)$$

$$C_2O_4^{\cdot-} + Fe(C_2O_4)_3^{3-} \longrightarrow Fe(C_2O_4)_2^{2-} + 2CO_2 \quad (2)$$

Later, the photolysis of $Fe(C_2O_4)_3^{3-}$ was reinvestigated by Parker and Hatchard,[4] and their flash photolysis experiments proved that the earlier mechanism could not explain the observed transient signals. Reaction 2 was not observed. They then proposed an intermediate species that either could be a ferrooxalate ion attached to an oxalate radical or a ferrioxalate-oxalate radical. An alternative would be the formation of a binuclear complex

$$[Fe^{II}(C_2O_4^{2-})_2\text{-}C_2O_4^{\cdot-}\text{-}Fe^{III}(C_2O_4^{2-})_3]$$

The decomposition of the intermediate would then explain the first-order decay of the observed transient.

Recently Cooper and DeGraff[5,6] made an extensive study on the photoreduction of $Fe(C_2O_4)_3^{3-}$, $Fe(C_2O_4)_2^{-}$, and $Fe(C_2O_4)^{+}$ by means of flash photolysis. They accept the revised mechanism of Parker as explanation for the photoreduction reaction but they believe that these reactions are very fast. The observed slower transients are explained as due to the decomposition of the Fe(II) oxalato complexes and the anation of $Fe(C_2O_4)_n(H_2O)_m^{3-2n}$.

Jamieson and Perone[7] on the other hand propose a Fe(III) intermediate as the primary product of the photolysis. Reduction would occur in a later bimolecular step

$$Fe(C_2O_4)_3^{3-} \xrightarrow{h\nu} [Fe(C_2O_4)_3^{3-}]^* \longrightarrow (C_2O_4)_2Fe\begin{matrix}O\text{—}C=O\\ \\ O\text{—}C=O\end{matrix}^{3-} \quad (A)$$

$$A \underset{k_{-1}}{\overset{k_1}{\rightleftharpoons}} B\ (?)$$

$$A + Fe(C_2O_4)_3^{3-} \xrightarrow{k} 2Fe(C_2O_4)_2^{2-} + 2CO_2 + C_2O_4^{2-}$$

$$B \xrightarrow{k_2} Fe(C_2O_4)_3^{3-}$$

Some of their experimental results are in conflict with other measurements, especially their observation that $FeOx_3^{3-}$ disappears in a second-order reaction. This is in contradiction with Parker and Hatchard's data.[4] Such discrepancies between the conclusions of different investigations clearly show that the problem of the reduction mechanism for $Fe(C_2O_4)_3^{3-}$ is not yet resolved.

The photolysis of $Co(C_2O_4)_3^{3-}$ has received, up to now, less attention. Copestake and Uri[8] concluded from their investigations that the photodecomposition follows the same pathway as $Fe(C_2O_4)_3^{3-}$, although the quantum yield is found to be much lower (0.73 as compared to 1.3 for $Fe(C_2O_4)_3^{3-}$). They proved the existence of an intermediate radical species which they presumed to be the $C_2O_4 \cdot^-$ species. No flash photolysis experiments have been done on $Co(C_2O_4)_3^{3-}$, apart from some fragmentary observations by Parker and Hatchard.[4] They supposed that the oxalate radical could eventually remain attached to a complex with a bivalent Co, or bound in a binuclear species. Dainton and Stranks[9] suggest such a complex plays a role in the charge transfer reactions between

Co(II) and Co(III) complexes. Several authors have studied the photolysis of $Co(C_2O_4)_3^{3-}$ in frozen samples in order to accumulate the reactive intermediate species. Shagisultanova and Posjnak[10,11] detected two radical species in their epr studies after uv irradiation of a solid $Co(C_2O_4)_3^{3-}$ matrix at 77°K. One of the signals was identified as belonging to the H· radical. The other belongs to an unknown radical. In the beginning of the photolysis the unknown radical is predominantly formed. Later its signal decreases as the H· radical signal increases. Their experiments indicate that the H· radicals are formed by the reaction

$$e^- + H^+ \longrightarrow H\cdot$$

The electrons are formed by the photoreduction of a radical species, formed subsequent to the photoreduction of $Co(C_2O_4)_3^{3-}$

$$Co(C_2O_4)_3^{3-} \xrightarrow{h\nu} R\cdot$$

$$R\cdot \xrightarrow{h\nu} R^+ + e^-$$

They conclude that R· is most probably not a free $C_2O_4\cdot^-$ species but rather an oxalate radical bound to the $Co(C_2O_4)_2^{2-}$ complex, similar to the radical proposed by Parker and Hatchard.[4] The occurrence of these two radical species H· and R· was confirmed by the experiments of Eaton and Suart.[12]

Experimental Section

(*a*) *Apparatus.* A flash-photolysis apparatus of the conventional type, inspired by the one developed by Parker and Hatchard,[4] has been constructed in the laboratory. As actinic light source two hydrogen-filled flash tubes were used. Two capacitors (20 μF each) could be charged to 10 kV. The flash duration was between 10 and 20 μsec. The reaction vessel was a fused quartz tube, length 20 cm and i.d. 1 cm, with optically flat windows sealed at each end.

Transmission was detected as a function of time, at constant wavelength. From these data absorbance values were calculated. As a detection light source a 450-W xenon lamp was used, fed by a current stabilized power supply. The detection system consisted of a Bausch & Lomb high-intensity monochromator and a RCA 1P28 photomultiplier tube. To improve the signal-to-noise ratio, only the first four dynodes were used. The others were electrically connected to the anode. The signals passed through an emitter follower (bandwidth 1 Mhz) and were recorded by means of an oscilloscope.

The experimental procedure followed is very similar to the one described by Parker and Hatchard.[4]

(*b*) *Preparation of the Solutions.* $K_3[Co(C_2O_4)_3]\cdot 3.5H_2O$ was prepared as described in the literature.[13] The molar extinction coefficients found were $\epsilon_{600\ nm}$ 162 and $\epsilon_{420\ nm}$ 219, in good agreement with the literature.[8,14] A cobalt analysis by atomic absorption spectrophotometry was likewise in agreement with the expected values.

Solutions were prepared by dissolving the 10^{-5} to 10^{-4} M $K_3[Co(C_2O_4)_3]\cdot 3.5H_2O$ in 3×10^{-3} M solutions of oxalic acid. The solutions were deaerated by bubbling with oxygen-free argon. All these manipulations were done with dimmed red light illumination.

Experimental Observations

In the experimental part as well as in the discussion two sets of data are to be clearly distinguished.

In the first set of experiments the initial concentration and the flash energy were chosen so as to convert with one flash discharge all the initially present $Co(C_2O_4)_3^{3-}$ into intermediate species, thus ruling out all reactions of the intermediate species with $Co(C_2O_4)_3^{3-}$. Such conditions will be referred to as "experiments with complete immediate conversion." In our experimental set up the lowest initial concentrations used (4×10^{-5} M) required a minimal flash energy of 320 J; for a concentration of 1.1×10^{-4} M 845 J was necessary to have complete immediate conversion.

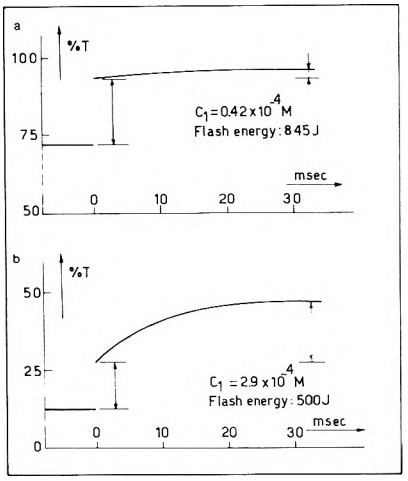

Figure 1. Transients at 600 nm for complete (a) and incomplete (b) immediate conversion of $Co(C_2O_4)_3^{3-}$.

In a subsequent series of experiments the kinetics were investigated when an important amount of initial reagent remained unreacted immediately after the flash, allowing the intermediate species to react with this excess $Co(C_2O_4)_3^{3-}$. Such conditions will be referred to as "experiments with incomplete immediate conversion."

(*1*) *Experiments with Complete Immediate Conversion.* The spectrum of $Co(C_2O_4)_3^{3-}$ shows three absorption bands with maxima at 254 (ϵ 21,400), 420 (ϵ 218), and 600 nm (ϵ 165). It was observed that the intermediate species produced by the flash pulse do not absorb at 600 nm. Indeed, when, *e.g.*, a 4.2×10^{-5} M solution is photolyzed with a flash of 845 J, the absorbance at 600 nm drops to zero within the time duration of the flash, and remains negligible throughout the longest observation times (see Figure 1a). This means that all the $Co(C_2O_4)_3^{3-}$ is immediately converted into intermediate species. The absorbance observed in the 320–550-nm region is, in this case, due only to the absorption of the intermediate species produced by the decomposition of the initial reagent.

Curve b of Figure 2 shows the spectrum observed at the end of the light burst when a 4.2×10^{-5} M $Co(C_2O_4)_3^{3-}$ solution is flashed with an energy of 845 J. The intersection around 390 nm is no isosbestic point; when either the energy of the flash is increased, or the initial concentration of the solution is decreased, within the limits of complete immediate conversion, the intersection point shifts. This means that the transient absorption signal is due to at least two intermediate species, whose concentration ratio depends on the initial concentration ratio of the solution and on the flash energy.

The decay of the transient signals observed in the wavelength region from 320 to 600 nm has been measured in order to establish their kinetic parameters.

(*2*) *Experiments with Incomplete Immediate Conversion.* In these experiments the transient absorbance sig-

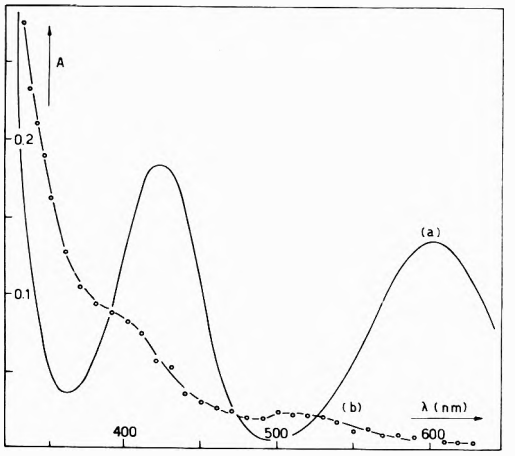

Figure 2. Absorption spectrum of a 4.2 × 10^{-5} *M* $Co(C_2O_4)_3^{3-}$ solution (a) before and (b) immediately after exposure to the flash (optical pathlength 20 cm).

nals result from the intermediate species as well as from the $Co(C_2O_4)_3^{3-}$ remaining immediately after the action of the flash.

Again, 600 nm was used as a specific monitoring wavelength for $Co(C_2O_4)_3^{3-}$. Figure 2 showed indeed that the intermediate species do not interfere at this wavelength. As can be seen from the comparison of Figure 1b and Figure 1a, the shape of the transmission signal changes drastically when the primary photodecomposition is not complete. Subsequent to the sudden drop in the $Co(C_2O_4)_3^{3-}$ concentration due to the decomposition by the flash, an appreciable amount is consumed in secondary reactions.

In order to investigate the kinetics of these secondary reactions, the absorbance transients have been recorded for initial $Co(C_2O_4)_3^{3-}$ concentrations varying from 1 to 3 × 10^{-4} *M*, using flash energies from 320 to 720 J.

The wavelength region from 320 to 600 nm was investigated. The transients at 600 nm were not only used to study the disappearance of $Co(C_2O_4)_3^{3-}$ but also to calculate the spectral changes due to the intermediate species in the region where their spectra overlap with the one of $Co(C_2O_4)_3^{3-}$. The absorbance due to $Co(C_2O_4)_3^{3-}$ was subtracted from the measured signal using the 600-nm data and the absortivity of $Co(C_2O_4)_3^{3-}$ at the wavelength under investigation.

Discussion of the Results

(A) Complete Immediate Conversion of $Co(C_2O_4)_3^{3-}$. *(1) Decay of the Intermediate Species.* The kinetic interpretation of the data of $Co(C_2O_4)_3^{3-}$ photolysis is facilitated by the fact that the final reaction products Co(II) and CO_2 do not absorb at the wavelengths under investigation. When all the $Co(C_2O_4)_3^{3-}$ is converted immediately during the flash, the transient spectrum can only be due to the intermediate reaction products. In conditions of complete immediate conversion, the decay of the transient absorbance signal at any chosen wavelength does not correspond to a simple first-order reaction. This is illustrated at 340 nm in Figure 3. The plot can be analyzed as composed of two first-order decays

$$A_t = A_{0,X}\, e^{-k_X t} + A_{0,Y}\, e^{-k_Y t}$$

where $A_{0,X}$ and $A_{0,Y}$ are the absorbance values of the intermediate species X and Y present at the end of the flash pulse (t = 0). This relation yields constant values for k_X and k_Y as can be seen in Table I, where some of the data

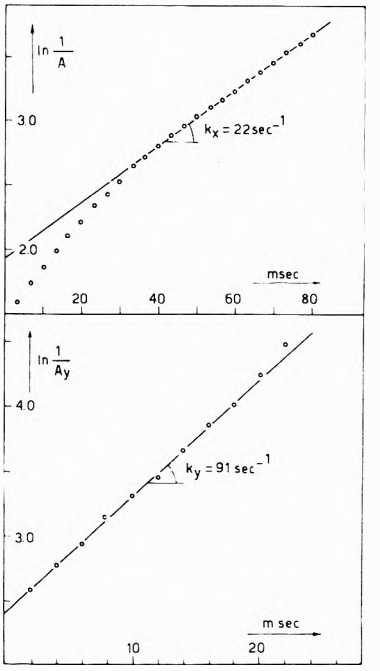

Figure 3. Rate constants for the decay of the intermediate species X (upper plot) and Y (lower plot).

TABLE I: Calculation of A_0 and k Values for the Intermediates X and Y in the Flash Photolysis of $Co(C_2O_4)_3^{3-}$[a]

Initial $Co(C_2O_4)_3^{3-}$ concn, *M*	Monitoring wavelength, nm	$A_{0,X}$	k_X, sec^{-1}	$A_{0,Y}$	k_Y, sec^{-1}
0.86 × 10^{-4}	330	0.230	20.0	0.238	85.3
	340	0.187	21.3	0.159	93.4
	350	0.127	20.0	0.144	90.0
	360	0.095	19.7	0.130	93.1
	370	0.070	20.0	0.135	99.1
0.71 × 10^{-4}	330	0.211	20.8	0.190	85.1
	340	0.148	18.6	0.152	75.2
	350	0.122	19.4	0.109	84.4
	360	0.081	20.0	0.089	82.5
	370	0.077	18.3	0.111	89.6
0.57 × 10^{-4}	330	0.173	20.0	0.145	73.4
	340	0.143	21.6	0.091	91.1
	350	0.103	18.3	0.079	86.0
	360	0.072	18.7	0.072	86.4
0.42 × 10^{-4}	330	0.171	23.5	0.080	94.8
	340	0.117	23.5	0.064	77.7
	350	0.090	20.4	0.051	87.0

[a] Flash energy = 845 J.

have been collected. The k_X and k_Y values thus obtained are independent of the monitoring wavelength and independent of the initial $Co(C_2O_4)_3^{3-}$ concentration. The average values obtained from some 40 experiments at different wavelengths between 320 and 600 nm and different initial concentrations of $Co(C_2O_4)_3^{3-}$ are k_X = 20 sec^{-1} and k_Y = 87 sec^{-1}. Standard deviations of the mean are σ_X = 1.6 and σ_Y = 5.4. This means that two species are formed upon photolysis of $Co(C_2O_4)_3^{3-}$, disappearing in two independent first-order reactions. It also shows that there are no other stable or reactive species formed that absorb between 320 and 600 nm.

Between 420 and 600 nm, $A_{0,X}$ becomes so small that it can be neglected as compared to $A_{0,Y}$. Consequently, the

TABLE II: Calculated Absorptivities and Initial Concentrations of the Intermediate Species X and Y for a Flash Energy of 845 J

			335 nm		340 nm		345 nm		355 nm	
$c_i \times 10^5$, M	$c_{0,X} \times 10^5$, M	$c_{0,Y} \times 10^5$, M	ϵ_X	ϵ_Y	ϵ_X	ϵ_Y	ϵ_X	ϵ_Y	ϵ_X	ϵ_Y
4.19	2.86	1.49	318	291	237	213	203	187	145	152
5.68	3.18	2.47	298	272	225	210			151	155
7.12	3.42	3.58	325	273			204	187	150	149
8.57	3.88	4.50	310	272	237	211			144	158
		Av values	313	277	233	211	204	187	148	154

ln $1/A$ *vs.* time plots give straight lines in the 420-600-nm region with a slope corresponding to k_Y. Previous experiments never outlined the presence of the two distinct intermediate species X and Y observed here. Intermediate X has probably not been detected in previous work since little attention has been paid to experimental conditions when all $Co(C_2O_4)_3^{3-}$ is suddenly and completely converted into intermediate species. As will be shown below the ratio $A_{0,X}/A_{0,Y}$ decreases sharply when the initial $Co(C_2O_4)_3^{3-}$ concentration is increased.

Parker and Hatchard[4] observed that their calculated first-order decay constants in the flash photodecomposition of $Fe(C_2O_4)_3^{3-}$ varied by a factor of 1.8 when the initial concentration varied by a factor of 20. This variation could well be due to the simultaneous decay of two species instead of the one proposed by these authors.

(2) *Absorptivities and Concentrations of the Intermediate Species.* When complete immediate conversion into intermediate species is achieved for a given flash energy and for a given initial concentration of $Co(C_2O_4)_3^{3-}$, such complete conversion will of course also be obtained when higher flash energies are used. A systematic investigation revealed however that, although the conversion is complete for such experiments the absorbance immediately after the flash is found to be a function of the flash energy. In fact the ratio $A_{0,X}/A_{0,Y}$ depends on the flash energy as well as on the initial reagent concentration. High light intensity or low initial $Co(C_2O_4)_3^{3-}$ concentrations favor the formation of species X at the expense of species Y. Although it is in general not possible to calculate the concentrations of two simultaneously present intermediate species from absorbance data obtained in flash work, this concentration dependence turns the present system into one of the fortunate cases in which this can actually be done.

For two experiments with identical flash energy but different initial concentrations $c_{i,1}$ and $c_{i,2}$ one has, provided the immediate conversion is complete

$$c_{i,1} = (c_{0,X})_1 + (c_{0,Y})_1 \tag{3}$$

where $(c_{0,X})_1$ and $(c_{0,Y})_1$ are the concentrations of the intermediate species X and Y at time $t = 0$ and the initial concentration $c_{i,1}$ considered.

For the concentration $c_{i,2}$ one can write

$$c_{i,2} = a(c_{0,X})_1 + b(c_{0,Y})_1 \tag{4}$$

where the factors a and b have different values, since the concentration dependence of the two intermediates species on c_i is different. If one of the intermediates had a binuclear structure the equations would have to be adapted in the proper way.

To calculate a and b the experimental values of $A_{0,X}$ and $A_{0,Y}$ are used. Indeed, one can write that at the concentrations $c_{i,1}$ and $c_{i,2}$

$$(A_{0,X})_1 = \epsilon_{X,\lambda}(c_{0,X})_1 l \tag{5}$$

$$(A_{0,X})_2 = \epsilon_{X,\lambda} a(c_{0,X})_1 l \tag{6}$$

where l is the pathlength of the cell, and $\epsilon_{X,\lambda}$ the extinction coefficient of species X at wavelength λ. $(A_{0,X})_1$ and $(A_{0,X})_2$ are the $A_{0,X}$ values corresponding to the initial concentrations $c_{i,1}$ and $c_{i,2}$. Dividing these, one obtains

$$a = (A_{0,X})_2/(A_{0,X})_1 \tag{7}$$

Similarly from the absorbance data for the species Y it follows that

$$b = (A_{0,Y})_2/(A_{0,Y})_1 \tag{8}$$

The concentration $c_{0,X}$ and $c_{0,Y}$ of the two intermediates for a given initial concentration of $Co(C_2O_4)_3^{3-}$ can thus be computed from expressions 3 and 4. From the corresponding A_0 values at different wavelengths $\epsilon_{X,\lambda}$ and $\epsilon_{Y,\lambda}$ are easily calculated. This procedure can be repeated for any set of absorbance values and should yield constant values for ϵ_X and ϵ_Y, if the assumptions made are correct. Such a set of calculations is collected in Table II, for a series of experiments with a flash energy of 845 J. Table II gives only part of the data. It has been extended to calculate the absorption spectra of the intermediate species. Figure 4 gives these spectra together with that of $Co(C_2O_4)_3^{3-}$.

The formation of species X is inhibited by the presence of large initial concentrations of $Co(C_2O_4)_3^{3-}$. High flash energies on the other hand, favor its formation. The dependence of the ratio $c_{0,Y}/c_{0,X}$ on the amount of initial reagent can be visualized in Figure 5, using the data of Table II. The following linear relationship is found: $c_{0,Y}/c_{0,X} = 1.39 \times 10^4 c_i$. This equation suggests that for high $Co(C_2O_4)_3^{3-}$ concentrations (10^{-3} M or higher) the concentrations of X will be neglibible as compared to Y.

(*B*) *Incomplete Immediate Conversion of* $Co(C_2O_4)_3^{3-}$. As already mentioned, $Co(C_2O_4)_3^{3-}$ concentration *vs.* time plots change considerably whenever, instead of having complete immediate conversion, a large excess of reagent is left immediately after the flash. This is shown in Figure 1b. In this case there is an important secondary consumption of $Co(C_2O_4)_3^{3-}$ at a rate comparable to that of the disappearance of the intermediate species.

In order to find out whether this secondary reaction of $Co(C_2O_4)_3^{3-}$ is one in which one of the two intermediate species X or Y is involved, the kinetics of these intermediates were investigated in conditions of incomplete immediate conversion.

(*1*) *Mass Balance of the System.* When, *e.g.*, a 2.9×10^{-4} M solution is photolyzed with a 845-J flash, one obtains the following results: initial $Co(C_2O_4)_3^{3-}$ concentration 2.9×10^{-4} M, amount decomposed by the flash 1.55×10^{-4} M, initial concentration of Y 1.37×10^{-4} M, $Co(C_2O_4)_3^{3-}$ decomposed by secondary reaction 1.07×10^{-4} M, $Co(C_2O_4)_3^{3-}$ remaining after the experiment 0.29×10^{-4} M. The concentration of $Co(C_2O_4)_3^{3-}$ was calculated from the absorbance data at 600 nm. The concentra-

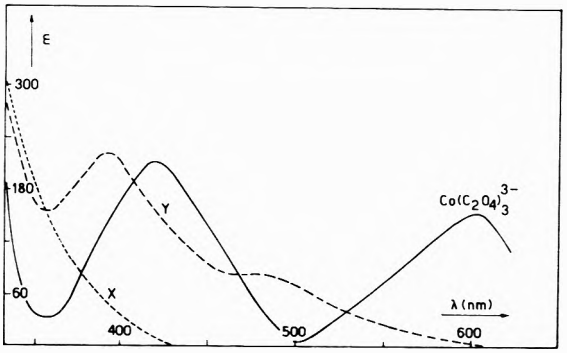

Figure 4. Spectrum of $Co(C_2O_4)_3^{3-}$, and of the two intermediate species.

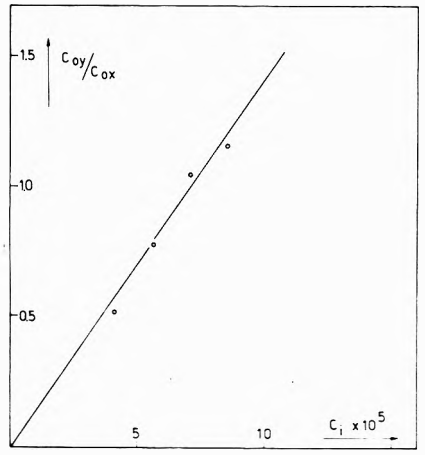

Figure 5. Ratio $C_{0,Y}/C_{0,X}$ as a function of the initial $Co(C_2O_4)_3^{3-}$ concentration for flash energy of 845 J.

tion of Y was obtained from the absorbance at 500 nm. Figure 4 shows indeed that at this wavelength Y is the only absorbing species.

It is clear that the concentration of X is low as compared to Y. Indeed, 88% of the $Co(C_2O_4)_3^{3-}$ decomposed by the flash is converted into Y. This sets an upper limit of 12% to the concentration of X and all eventual other intermediates formed due to the presence of excess $Co(C_2O_4)_3^{3-}$.

(2) *Kinetic Behavior of Species X and Y in the Presence of Excess* $Co(C_2O_4)_3^{3-}$. The influence of an excess $Co(C_2O_4)_3^{3-}$ on the kinetics of Y was investigated by measurements at 500 nm. The decay at Y under these circumstances remains strictly monomolecular with a rate constant of 80 sec^{-1}. The good fit with the k_Y value of 87 sec^{-1}, found from the fully independent complete conversion experiments, has to be emphasized. This proves indeed that the main pathway for the disappearance of Y is the same monomolecular reaction whether an excess $Co(C_2O_4)_3^{3-}$ is present or not. This conclusion is in line with Parker and Hatchard's observation that no bimolecular process should be observed in the flash photolysis of $Fe(C_2O_4)_3^{3-}$.[4]

It is however in obvious disagreement with the observation of Jamieson and Perone,[7] who did not observe a monomolecular decay of the main intermediate species in the photolysis of $Fe(C_2O_4)_3^{3-}$. The investigation of the kinetic behavior of X raises a problem. We have shown that for experiments with incomplete immediate conversion of $Co(C_2O_4)_3^{3-}$, X is present in rather low concentrations (12%). The combination of these low concentrations

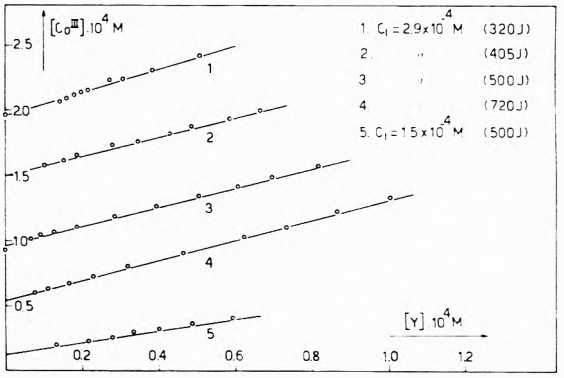

Figure 6. Concentration–concentration plots for $Co(C_2O_4)_3^{3-}$ and Y at various initial $Co(C_2O_4)_3^{3-}$ concentrations and flash energies.

with the absorptivities of X, which are comparable to those of Y and $Co(C_2O_4)_3^{3-}$, simultaneously present in much larger concentrations, rules out the possibility for a direct kinetic study of X.

In the subsequent analysis of the system it is presumed that the decay rate constant for X in conditions of incomplete immediate conversion is identical with the one found for complete immediate conversion. It will be shown that this assumption is correct.

(3) *Kinetics of the Secondary* $Co(C_2O_4)_3^{3-}$ *Consumption.* For the reason just mentioned a bimolecular reaction such as

$$Y + Co(C_2O_4)_3^{3-} \longrightarrow \text{products}$$

is very improbable.

Nevertheless, there exists a relation between the rate of disappearance of Y and the rate of secondary $Co(C_2O_4)_3^{3-}$ consumption. This relationship is shown in Figure 6, where for a number of initial $Co(C_2O_4)_3^{3-}$ concentrations and different flash energies the actual $Co(C_2O_4)_3^{3-}$ concentration is related to the corresponding concentration of the Y species in the same solution at various times after the flash. A linear relationship is found.

Its average slope is 0.9 except for the two experiments under conditions of near-complete immediate conversion. This means that for each species Y which disappears, $0.9Co(C_2O_4)_3^{3-}$ molecules are instantly reduced, independently of the eventual excess of $Co(C_2O_4)_3^{3-}$.

The reaction rate for the secondary conversion of $Co(C_2O_4)_3^{3-}$ can thus be written as

$$d[Co(C_2O_4)_3^{3-}]/dt = 0.9\, d[Y]/dt = 0.9\, k_Y[Y]$$

To demonstrate this in a different way, the change in absorbance at 600 nm (where only $Co(C_2O_4)_3^{3-}$ absorbs) due to this secondary conversion can be expressed as presented in Figure 7. A_t is the absorbance at time t and A_e is the final absorbance at $t = \infty$. Ln $1/(A_t - A_e)$ is a linear function of t, with a slope $q_{CoIII} = 75$ sec^{-1}. The absorbance due to $Co(C_2O_4)_3^{3-}$ at time t can be calculated from the equation

$$A_t = A_e + (A_0 - A_e)\, e^{-q_{CoIII}t}$$

A_0 being the absorbance of $Co(C_2O_4)_3^{3-}$ immediately after the flash. The kinetics of the observed secondary conversion of $Co(C_2O_4)_3^{3-}$ can only be explained by a scheme in which the intermediary species Y decomposes into an unobserved species Z. This would in turn react very quickly and almost exclusively with $Co(C_2O_4)_3^{3-}$

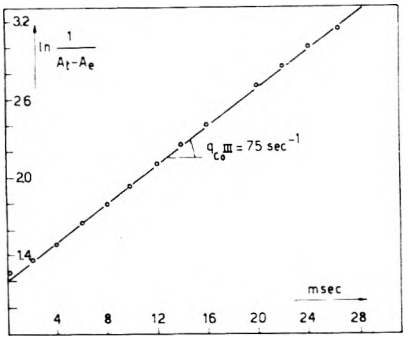

Figure 7. Calculation of the apparent rate constant for the reaction in which a secondary amount of $Co(C_2O_4)_3^{3-}$ is converted.

$$Y \xrightarrow{k_Y} Z + \text{products}$$

$$Z + Co(C_2O_4)_3^{3-} \longrightarrow Co^{II} + \text{products}$$

The last reaction must be very fast compared to the first. In this assumption Z should not be detectable spectroscopically since it should not accumulate. Even in experiments where a secondary conversion of $Co(C_2O_4)_3^{3-}$ is not possible, Z has not been detected. Two explanations are available for this: either the recombination reaction Z + Z → products is also fast, or, more probably, Z does not absorb in the investigated spectral region.

(4) Recalculation of the Transient Signal at Any Chosen Wavelength. If the conclusions resulting from the kinetic analysis are correct, it should be possible to recalculate any decay at any chosen wavelength using the absorptivities of the species $Co(C_2O_4)_3^{3-}$, X, and Y, the rate constants k_X and k_Y, the constant q_{CoIII}, and the concentrations of $Co(C_2O_4)_3^{3-}$, X, and Y immediately after flash. Such a test is most elucidative when applied to incomplete immediate conversion experiments, since in this case one has to account for the secondary reduction of $Co(C_2O_4)_3^{3-}$ as well as for the disappearance of possible intermediate species.

The absorbance A_t at a time t after the flash would then be

$$A_t = A_e + A_{0,X}e^{-k_X t} + A_{0,Y}e^{-k_Y t} + (A_{0,CoIII} - A_e)e^{-q_{CoIII}t}$$

All A terms refer to absorbances at the wavelength λ. The various symbols have the following significance: A_t is the overall absorbance at any time t, $t = 0$ at the end of the light emission by the flash; A_e is the final absorbance due to the remaining $Co(C_2O_4)_3^{3-}$ at the longest observation times; $A_{0,CoIII}$, $A_{0,X}$, and $A_{0,Y}$ are absorbances at time $t = 0$ due to respectively excess $Co(C_2O_4)_3^{3-}$ and the intermediates X and Y; q_{CoIII}, k_X, and k_Y are constants for the decay rates of the species referred to, the average values used are respectively 75, 20, and 87 sec^{-1}.

Figure 8 shows both the calculated and observed A_t values for a monitor wavelength of 340 nm, an initial $Co(C_2O_4)_3^{3-}$ concentration of 2.9×10^{-4} M and 845-J dissipated flash energy. The good fit between the two kinds of values speaks favorably of the interpretation brought forward. It does even more so, if one keeps in mind that the values of k_X, k_Y, ϵ_X, and ϵ_Y used are the averages from the complete immediate conversion experiments.

(5) Mechanism for the Photodecomposition of $Co(C_2O_4)_3^{3-}$. It is not possible to fit all these kinetic data into one of the mechanisms quoted in the Introduction. One should indeed account for the following observations.

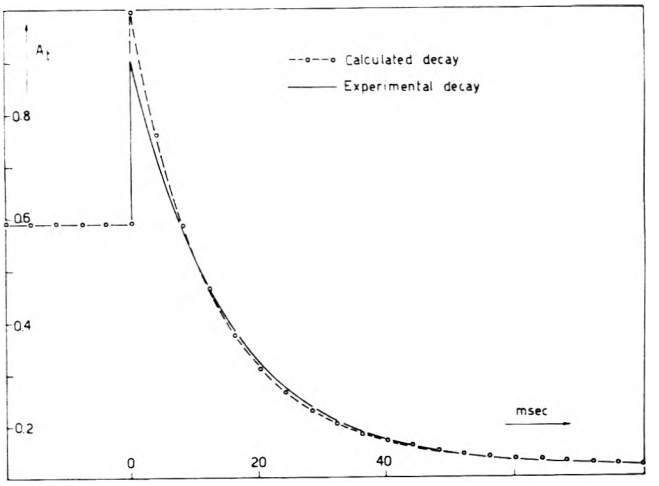

Figure 8. Comparison between a measured and a calculated transient signal at 340 nm.

(1) The $Co(C_2O_4)_3^{3-}$ decomposed during the flash is transformed into two reactive intermediate species, X and Y. Their relative concentrations depend on both the concentration of the initial cobalt complex and the flash energy used. In conditions of complete immediate conversion both species are present in comparable concentrations. When excess $Co(C_2O_4)_3^{3-}$ is available Y is the predominant form. (2) Both X and Y decay through a first-order process, no matter whether $Co(C_2O_4)_3^{3-}$ is present in excess or not. (3) When sufficient unreacted $Co(C_2O_4)_3^{3-}$ is left at the end of the flash, a second amount of $Co(C_2O_4)_3^{3-}$ is decomposed at a rate 0.9 times that of the decay of Y.

The first of these experimental observations can be explained by two types of mechanisms

$$Co(C_2O_4)_3^{3-} \xrightarrow{h\nu} [Co(C_2O_4)_3^{3-}]^* \longrightarrow \cdots \longrightarrow M$$

followed by

$$M \begin{cases} \longrightarrow X \\ + Co(C_2O_4)_3^{3-} \longrightarrow \cdots \longrightarrow Y \end{cases} \quad \text{(a)}$$

or

$$M \longrightarrow Y \xrightarrow{h\nu} X \quad \text{(b)}$$

Reaction a is to some extent similar to that proposed by Parker and Hatchard for the flash photolysis of $Fe(C_2O_4)_3^{3-}$.[4] Parker did not consider however the eventual formation of a second intermediary species corresponding to X.

In the case of $Co(C_2O_4)_3^{3-}$ the reaction product of M with $Co(C_2O_4)_3^{3-}$ could have a structure of the form

$$[Co^{II}(C_2O_4)_2\text{-}OCO\text{-}COO\text{-}Co^{III}(C_2O_4)_3]^{6-}$$

Although such a mechanism eventually could account for the data when all the $Co(C_2O_4)_3^{3-}$ is immediately converted by the flash, it cannot explain the secondary conversion of $Co(C_2O_4)_3^{3-}$.

The decomposition of this binuclear complex will indeed produce stable reaction products

$$[Co^{II}(C_2O_4)_2\text{-}OCO\text{-}COO\text{-}Co^{III}(C_2O_4)_3]^{6-} \longrightarrow 2Co(II) + 5C_2O_4^{2-} + 2CO_2$$

None of these reaction products can reduce another $Co(C_2O_4)_3^{3-}$ molecule. Reaction a is thus in conflict with the experimental observation that Y, when decomposing, produces a species that is so reactive toward $Co(C_2O_4)_3^{3-}$

that both the secondary conversion of $Co(C_2O_4)_3^{3-}$ and the decomposition of Y proceed at equal rates. Therefore reaction b is preferred. In this reaction the intermediate species Y is photochemically active.

The presence of an excess $Co(C_2O_4)_3^{3-}$ will inhibit the formation of X by its inner-filter effect. This scheme is in fact the same as the one witheld by Shagisultanova and Posjnak[10,11] (see Literature Survey) on the basis of a fully different kind of work.

Our spectroscopic data give no direct indication as to the indentity of Y and X. There are however a number of arguments which can be enlighting as to these identities. It is improbable that Y would have a structure such as the nonreduced species proposed by Jamieson and Perone[7] for $Fe(C_2O_4)_3^{3-}$ (see also Literature Survey). In our opinion such a nonreduced species should be very short lived. Indeed, a species with biradical character such as

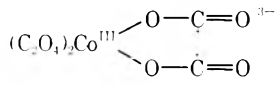

having both radical fragments linked in each others vicinity to the same metal atom, should show an outspoken tendency to recombine, thus yielding the initial reagent. Our complete immediate conversion experiments rule out such a back reaction.

Since our experiments also rule out the possibility of a binuclear species, and in view of the well-established ligand-to-metal charge transfer nature of the actinic light, it seems logical to propose that the primary photochemical act will be the transfer of an electron from the ligand to Co(III) leading to an intermediary species with the structure $[Co^{2+}\ (C_2O_4)_2C_2O_4\cdot^-]^{3-}$. Such a structure has already been proposed as intermediate in the photoreduction of $Fe(C_2O_4)_3^{3-}$.[4] This species would, upon irradiation, produce species X. It is much more difficult to propose a structure for X. The work of Shagisultanova and Posjnak[10,11] suggests that the reactive intermediate in the photolysis of $Co(C_2O_4)_3^{3-}$ undergoes a second photochemical reaction, producing a solvated electron. This leads us to propose the following reaction

$$[Co^{2+}(C_2O_4^{2-})_2(C_2O_4\cdot^-)]^{2-} \xrightarrow{h\nu} [Co^{2+}(C_2O_4^{2-})(C_2O_4\cdot^-)_2]^{2-} + e^-$$

The two monomolecular decomposition reactions of these intermediates will then be

$$X = [Co^{2+}(C_2O_4^{2-})(C_2O_4\cdot^-)_2]^{2-} \longrightarrow [Co^{2+}(C_2O_4^{2-})_2]^{2-} + 2CO_2$$

$$Y = [Co^{2+}(C_2O_4^{2-})_2C_2O_4\cdot^-]^{3-} \longrightarrow [Co^{2+}(C_2O_4^{2-})_2]^{2-} + C_2O_4\cdot^-$$

When no excess $Co(C_2O_4)_3^{3-}$ is present the oxalate radical (species Z) will disappear in a dismutation reaction with its own species. If however there is $Co(C_2O_4)_3^{3-}$ left after the flash photolysis there will be a very fast reduction of a second Co^{III}.

$$Co(C_2O_4)_3^{3-} + C_2O_4\cdot^- \longrightarrow Co(C_2O_4)_2^{2-} + 2CO_2$$

This reaction must be fast since $Co(C_2O_4)_3^{3-}$ disappears with the same rate as the decomposition of Y.

Conclusions

In conditions of incomplete immediate conversion, the reaction mechanism proposed by Copestake and Uri[8] is qualitatively in agreement with our results.

When very high light intensities are used or very low initial reagent concentrations, another intermediary species is observed. Its formation can only be explained by accepting that it results from the photolysis of the primary radical. This biphotonic process can be observed only when the $Co(C_2O_4)_3^{3-}$ concentration has become sufficiently low to avoid its inner-filter effect.

The complete reaction scheme is

$$Co(C_2O_4)_3^{3-} \xrightarrow{h\nu} \cdots \longrightarrow Y$$

$$Y \xrightarrow{h\nu} X$$

$$Y \longrightarrow Co^{2+} + C_2O_4\cdot^-$$

$$C_2O_4\cdot^- + Co(C_2O_4)_3^{3-} \xrightarrow{\text{(fast)}} Co(C_2O_4)_2^{2-} + 2CO_2 + C_2O_4^{2-}$$

$$X \longrightarrow \text{reaction products}$$

$$2C_2O_4\cdot^- \longrightarrow C_2O_4^{2-} + 2CO_2$$

There are sound arguments to accept that the structure of Y is $[Co^{2+}\ (C_2O_4^{2-})_2\ C_2O_4\cdot^-]^{3-}$. In line with this, the structure of X would be $[Co^{2+}\ (C_2O_4^{2-})\ (C_2O_4\cdot^-)_2]^{2-}$.

Acknowledgments. The authors gratefully thank the Belgian Fonds voor Kollektief Fundamenteel Onderzoek (F.K.F.O.) for substantial support. Two of us (L. C. and J. H.) are indebted to the Belgian Instituut voor Aanmoediging van het Wetenschappelijk Onderzoek in Nijverheid en Landbouw (I.W.O.N.L.) for a research grant.

References and Notes

(1) V. Balzani and V. Carassiti, "Photochemistry of Coordination Compounds," Academic Press, London, 1970, pp 138, 167–172, 221–224.
(2) C. A. Parker, *Proc. Roy. Soc., Ser. A*, **220**, 104 (1953).
(3) C. A. Parker, *Trans Faraday Soc.*, **50**, 1213 (1954).
(4) C. A. Parker and C. G. Hatchard, *J. Phys. Chem.*, **63**, 22 (1959).
(5) G. D. Cooper and B. A. Degraff, *J. Phys. Chem.*, **75**, 2897 (1971).
(6) G. D. Cooper and B. A. Degraff, *J. Phys. Chem.*, **76**, 2618 (1972).
(7) R. A. Jamieson and S. P. Perone, *J. Phys. Chem.*, **76**, 830 (1972).
(8) T. B. Copestake and N. Uri, *Proc. Roy. Soc., Ser. A*, **228**, 252 (1955).
(9) F. S. Dainton and D. R. Stranks, "Radioisotopes in Scientific Research," R. C. Exterman, Ed., Pergamon Press, New York, N. Y., 1958, pp 305–325.
(10) G. A. Shagisultanova, L. N. Neokladnova, and A. L. Posjnak, *Dokl. Akad. Nauk SSSR*, **162**, 1333 (1965).
(11) A. L. Posjnak and G. A. Shagisultanova, *Dokl. Akad. Nauk SSSR*, **173**, 612 (1967).
(12) D. R. Eaton and S. R. Suart, *J. Phys. Chem.*, **72**, 400 (1968).
(13) "Inorganic Synthesis," Vols. I–VI, McGraw-Hill, New York, N. Y., 1939–1960.
(14) S. T. Spees, Jr., and A. W. Adamson, *Inorg. Chem.*, **1**, 531 (1962).

Pulse Radiolysis of the Aqueous Ferro–Ferricyanide System. II. Reactions of Hydrogen Atoms and e_{aq}^- with Ferrocyanide and Ferricyanide Ions

Dov Zehavi and Joseph Rabani*

Department of Physical Chemistry, The Hebrew University, Jerusalem 91000, Israel *(Received November 27, 1973)*

Hydrogen atoms react with both ferro- and ferricyanide. The reaction with ferrocyanide, previously unknown, proceeds with a rate constant $k(H + Fe(CN)_6^{4-}) = 4 \times 10^7\ M^{-1}\ sec^{-1}$, independent of pH in the range 1–8. This reaction is followed by two consecutive processes, of which the first one is first order, while the second one is a reaction of an intermediate with ferrocyanide ions. Aquapentacyanoferrate(II) was identified as a final product. All the intermediates reacted with ferricyanide. The nature of the reaction products is discussed and the rates of the various processes measured as a function of pH are given. Hydrated electrons react only slowly, if at all, with ferrocyanide ions, $k(e_{aq}^- + Fe(CN)_6^{4-}) < 7.5 \times 10^4\ M^{-1}\ sec^{-1}$. Low yields of aquapentacyanoferrate(II) (~10%) are produced by reduction of ferricyanide ions by H atoms and e_{aq}^- at neutral pH.

Introduction

In the present manuscript we would like to present results which demonstrate a novel reaction of hydrogen atoms with ferrocyanide ions and to discuss the sources of $Fe(CN)_5H_2O^{3-}$ formation in irradiated ferro–ferricyanide aqueous solutions. The radiation chemistry of the ferro–ferricyanide system has been discussed in a previous paper,[1] and in the references cited therein.

Experimental Section

The experimental procedure has been previously described.[1]

Results

Ferrocyanide–Acid Solutions. General Features. When ferrocyanide solutions ($>10^{-3}$ *M*) are pulse irradiated, OH radicals react according to reaction 1 during the electron pulse. $Fe(CN)_6^{4-}$ and $Fe(CN)_6^{3-}$ include also the various protonated forms of ferrocyanide and ferricyanide, respectively.[1,2]

$$OH + Fe(CN)_6^{4-} \longrightarrow OH^- + Fe(CN)_6^{3-} \qquad (1)$$

In acidic solutions, the fast oxidation of ferrocyanide ions by OH radicals is followed by additional changes in the optical absorption in the range 400–600 nm. Three consecutive processes can be observed after the electron pulse. This is demonstrated in Figure 1 for 10^{-2} *M* ferrocyanide solutions at pH 1.5. Relatively fast formation of absorption is observed at 470 nm (process I). This is followed by decay of absorbance at 550 nm and a simultaneous formation of absorbance at 420 nm in the 10^1–10^2-μsec range (process II). Process II is followed by additional formation of absorbance at 420 nm, simultaneously with decay of absorbance at 480 nm (process III).

The kinetics of processes I, II, and III, and the spectra at the beginning and at the end of each process, depend on pH. At all acid pH values, processes I and III are first order in ferrocyanide, while process II does not depend on the ferrocyanide concentration. Addition of ferricyanide prior to pulse irradiation enhances processes II and III, and decreases the changes in absorbance in all three processes. A similar enhancement is observed upon increasing the pulse intensity. Saturation with N_2O (at pH >2) partially suppresses all three reactions.

The absorbance obtained at the end of process III decays partially (~30% at 480 nm) within a few seconds (experiments were carried out in the pH range 1.8–2.5). This is observed at wavelengths >440 nm (practically no change is observed at 420 nm), when [ferrocyanide] > 0.05 *M*. No systematic measurements were carried out for the investigation of this process (process IV).

The chemistry of the system can schematically be represented by the following equations

(process I)

$$H + \text{ferrocyanide} \longrightarrow X_I \qquad (2)$$

$$H + \text{ferricyanide} \longrightarrow H^+ + \text{ferrocyanide} \qquad (2')$$

(process II)

$$X_I \longrightarrow X_{II} \qquad (3)$$

$$X_I + \text{ferricyanide} \longrightarrow Y \qquad (3')$$

(process III)

$$X_{II} + \text{ferrocyanide} \longrightarrow X_{III} \qquad (4)$$

$$X_{II} + \text{ferricyanide} \longrightarrow Z \qquad (4')$$

Rate Constants. Rate constants were measured from plots of log $(D_i - D_t)$ *vs.* t (where D_i is the absorbance at the end of process i). These plots were linear for all three processes (I, II, and III). From such plots and Table I, the reaction rate constant $k_2 = (3.9 \pm 0.6) \times 10^7\ M^{-1}\ sec^{-1}$ could be calculated for the pH range 1.0–3.3. (At pH <1, k_2 decreased somewhat.) The apparent rate constants for processes II and III, k_{II} and k_{III}, could be obtained as well. The time separation between processes II and III varied according to the ferrocyanide concentration and the pH. In the cases where the separation was relatively poor, only the first part of process II and the last part of process III were analyzed. In such cases D_{II} values were chosen so that log $(D_t - D_{II})$ was over 50% linear with t. The reaction rate constants k_3 and k_4 which resulted were in agreement with those calculated from experiments in which there was a good time separation. The apparent rate constants k_{II} and k_{III}, obtained at various pH values and concentrations of ferrocyanide and ferricyanide, are presented in Table II (see paragraph at end of text regarding miniprint material).

TABLE I: Measurements of k_2 in Acidic Solutions[a]

$[K_4Fe(CN)_6]$, M	$10^2[H_2SO_4]$, M	pH[b]	$10^{-7}k_2$, M^{-1} sec^{-1}	10^3D[c]
0.02	0.5	3.3	3.5	41
0.02	1.0	2.8	3.4	41
0.02	1.5	2.4	3.9	39
0.02	2.0	2.1	3.9	37
0.02	3.0	1.8	3.8	43
0.02	5.0	1.5	3.4	44
0.02	10.0	1.2	3.9	45
0.02	20.0	1.0	4.1	45
0.02	50.0	0.7	2.8	44
0.05	1.5	3.0	4.3	60
0.05	1.5	3.0	3.4	123
0.05	2.5	2.5	4.1	59
0.05	4.0	2.0	4.3	58
0.05	7.5	1.6	4.0	60
0.05	7.5	1.6	3.6	120
0.05	15.0	1.3	3.7	65
0.10	8.5	1.9	4.1	55

[a] Each value represents an average of three–seven measurements in the range 480–550 nm. The results are corrected (<5%) for the competing reaction 2'.[3] [b] Measured. [c] At 420 nm, at the end of process I. These optical densities can be used for the estimation of the dose. The absorption is almost entirely due to reaction 1 (see Figure 1). Light path 12.2 cm.

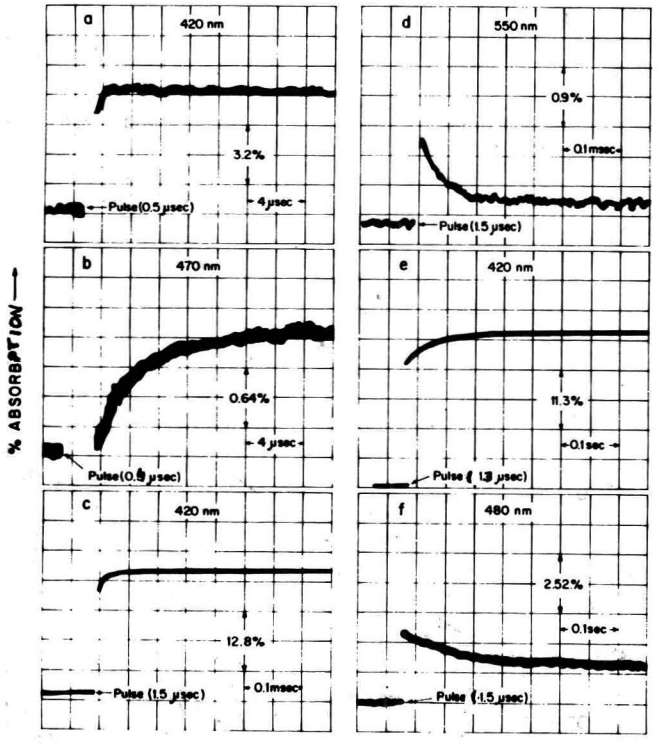

Figure 1. Oscilloscope traces of deaerated 10^{-2} M ferrocyanide solutions at pH 1.5.

The reaction rate constants k_3, $k_{3'}$, k_4, and $k_{4'}$ can be evaluated from Table II, using eq I and II.

$$k_{II} = k_3 + k_{3'}[\text{ferricyanide}] \quad \text{(I)}$$

$$k_{III} = k_4[\text{ferrocyanide}] + k_{4'}[\text{ferricyanide}] \quad \text{(II)}$$

In Figures 2 and 3 we demonstrate the dependence of k_{II} and k_{III} on [ferricyanide] according to eq I and II. The concentration of ferricyanide at each process was calculated with the aid of the appropriate reaction rate constants and yields, and using α values from Table II. From the slopes and intercepts of figures such as 2 and 3 it is possible to determine k_3, $k_{3'}$, k_4, and $k_{4'}$. Figures 4 and 5 summarize the effect of pH on these rate constants. The rate constants k_4 and $k_{4'}$ were determined only from experiments in which $\alpha < 0.8$.

TABLE II

The apparent reaction rate constants k_{II} and k_{III}[a]

[Ferricyanide][b] M	$[H_2SO_4]$ M	pH[c]	pulse intensity[d]	10^{-4} k_{II} sec^{-1}	α[e]	10^{-2} k_{III} sec^{-1}	$10^4(\epsilon_{II}-\epsilon_I)$[f]	$10^4(D_{III}-D_{II})$[f]
			0.01 M FERROCYANIDE					
	0.0025	3.5	6.0	0.22	0.29	4.0	68-16 (550)	666-785 (430)
2.0×10^{-5}	"		6.0	0.43	0.64	6.2	58-12 (550)	329-373 (440)
4.0×10^{-5}	"		6.0	0.65	0.76	8.0	47-8 (550)	248-271 (440)
-	0.005	2.9	11.3	0.43	0.22	1.7	58-1 (580)	1180-1390 (430)
1.0×10^{-4}	"		11.3	1.32	0.75	4.3	32-0 (580)	308-377 (430)
-	0.02	1.8	11.3	1.81	0.13	0.39	84-12 (550)	86-52 (500)
1.0×10^{-4}	"		11.3	4.04	0.61	0.58	28-2 (555)	269-306 (430)
-	0.04	1.5	11.3	2.80	0.11	0.14	(410-660) fig.6	(390-510) fig.6
1.0×10^{-4}	"		11.3	5.90	0.57	0.45	23-3 (555)	251-281 (430)
-	0.10	1.2	11.3	4.60	0.07	0.088	42-11 (550)	102-52 (480)
4.0×10^{-5}	"		6.0	5.70	0.25	0.11	28-11 (550)	304-335 (430)
-	0.30	0.8	11.3	5.98	0.04	0.064	17-6 (555)	153-69 (475)
2.0×10^{-4}	"		11.3	10.7	0.46	0.087	65-29 (470)	77-50 (475)
			0.02 M FERROCYANIDE					
2.0×10^{-5}	0.0025	3.8	6.3	0.81	0.70		51-5 (600)	
4.0×10^{-5}	"		6.3	1.24	0.81		44-3 (600)	
-	0.005	3.3	3.8	0.25	0.32	15.0	56-22 (550)	615-688 (420)
2.0×10^{-4}	"		14.8	4.74	0.96		23-2 (575)	
-	0.01	2.8	3.2	0.38	0.15		38-3 (550)	
4.0×10^{-5}	"		5.3	1.12	0.71	7.0	52-3 (600)	445-541 (430)
-	0.015	2.3	3.2	0.88	0.08		38-3 (550)	
2.5×10^{-4}	"		14.8	6.80	0.88		17-0 (575)	
			0.05 M FERROCYANIDE					
2.0×10^{-5}	0.005	3.7	6.7	1.46	0.92		64-5 (600)	
4.0×10^{-5}	"		6.7	2.47	0.95		58-5 (600)	
-	0.015	3.0	4.3	0.59	0.17	3.0	79-7 (550)	556-728 (420)
-	0.015	3.0	9.2	0.77	0.36		110-2 (600)	
2.5×10^{-4}	"		15.8	8.13	0.94	69.1	(525-575) fig.8	(490,500) fig.8
5.0×10^{-4}	"		15.8	16.1	0.97		20-1 (575)	
-	0.025	2.5	4.3	0.82	0.12		90-6 (550)	
5.0×10^{-4}	"		15.8	11.7	0.94	30.0	27-1 (575)	61-41 (490)
-	0.04	2.0	4.3	1.28	0.14		75-2 (550)	
1.0×10^{-3}	"		15.8	41.6	0.97	12.6	14-4 (550)	36-21 (490)
			0.10 M FERROCYANIDE					
-	0.025	3.0	3.8	0.95	0.16	49.3	55-0 (600)	88-130 (480)
-	"		9.0	1.25	0.36		112-7 (600)	
1.0×10^{-4}	"		11.6	6.25	0.87	185	87-2 (600)	337-306 (480)
5.0×10^{-4}	"		16.3	25.0	0.97		24-3 (575)	
-	0.05	2.4	9.4	1.43	0.08	39.4	168-14 (550)	148-195 (430)
-	"		15.0	1.92	0.31	41.0	(530-610) fig.7	(415-440) fig.7
5.0×10^{-5}	"		9.4	3.02	0.56	69.1	162-15 (550)	115-137 (430)
1.0×10^{-4}	"		9.4	4.74	0.72	84.0	108-16 (550)	99-122 (430)
1.0×10^{-4}	"		11.6	5.35	0.75	94.7	53-0 (600)	787-935 (440)
2.0×10^{-4}	"		9.4	8.58	0.85		96-14 (550)	
5.0×10^{-4}	"		16.3	18.1	0.93		51-1 (575)	
-	0.055	2.2	3.8	1.55	0.09	30.8	50-3 (600)	518-851 (420)
1.0×10^{-4}	"		11.6	5.62	0.75	63.3	93-0 (600)	787-944 (440)
-	0.085	1.9	3.8	3.16	0.04	18.8	70-4 (550)	508-910 (420)
1.0×10^{-4}	"		11.6	7.10	0.57	30.8	78-0 (600)	783-946 (440)

(a) Light path 12.2 cm. Each value in the table is an average of 3-7 determinations.

(b) Before pulsing.

(c) Measured.

(d) In units of micromolar ferricyanide which are produced by reaction 1. The values G_{OH} = 3.27, 3.40, 3.62 and 3.72 for 0.01, 0.02, 0.05 and 0.1 M ferrocyanide, respectively [4], were used for the calculations of [ferricyanide], whenever it was based on dosimetry.

(e) Defined as the fraction of X_I which reacts with ferricyanide in process II. It was calculated taking into account reaction 2' (see later in the text) and assuming G(H) = 3.73 for 0.01 M ferrocyanide and 3.75 for higher concentrations [4].

(f) The number in parenthesis is the wavelength at which the measurements were carried out.

Absorption Spectra. The absorption spectra of the products of processes I–III depend on the pH and on [ferrocyanide]. This is demonstrated in Figures 6–8. Corrections were carried out for the fraction of absorbance due to ferricyanide (see the previous section and Table II).

Ferrocyanide Neutral Solutions. Reactions of H Atoms. When neutral solutions of ferrocyanide saturated with N_2O are pulse irradiated, reaction 1 is followed by additional changes to absorbance. These changes are relatively small, and are observed only at relatively high ($\geq 10^{-2}$ M) ferrocyanide concentrations. Thus, using a solution of 10^{-2} M ferrocyanide, we observed a decrease in the absorbance at 420 nm, and an increase at wavelengths greater than 450 nm. Two processes could be observed. One of them was observed in the microsecond time range, and we attribute it to process I. The other process was found to be dependent on [ferricyanide] and to be independent of the ferrocyanide concentration. The absorption at the end

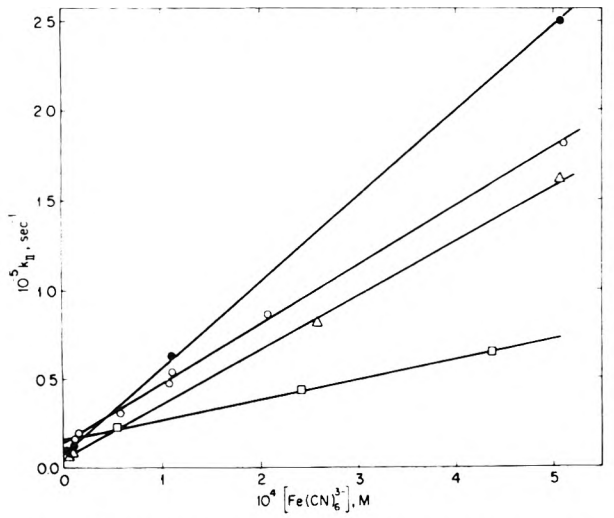

Figure 2. Effect of ferricyanide on process II (data from Table II): □, 0.01 *M* ferrocyanide, pH 3.5 [ferricyanide] and k_{II} are multiplied by 10 in the figure; △, 0.05 *M* ferrocyanide, pH 3.0; ●, 0.1 *M* ferrocyanide, pH 3.0; ○, 0.1 *M* ferrocyanide, pH 2.4.

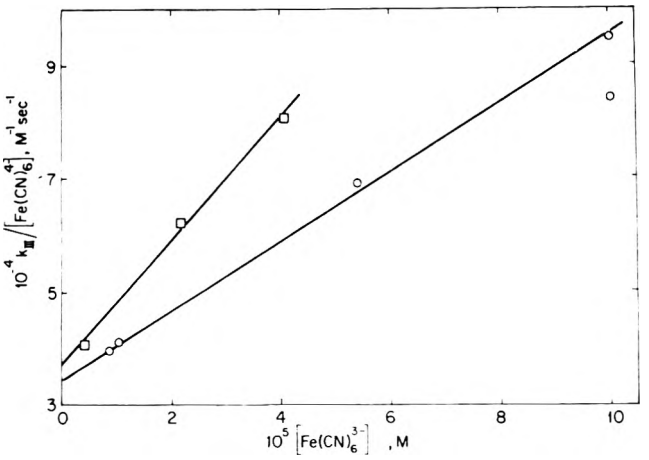

Figure 3. Effect of ferricyanide on process III (data from Table II): □, 0.01 *M* ferrocyanide, pH 3.5; ○ 0.1 *M* ferrocyanide, pH 2.4.

of the second process was found to be stable in the range 480–550 nm for at least 0.1 sec. The spectrum indicates that $Fe(CN)_5H_2O^{3-}$, known[5] as a stable irradiation product, was formed as a final product.[6,7] We attribute the second process to reaction 3′. The kinetic treatment yields $k_{3'} = (2 \pm 1) \times 10^9\ M^{-1}\ sec^{-1}$, which is in agreement with the results in acid solutions. Unlike the acid solutions (which will be discussed later) X_I in near neutral pH's produces an equal amount of aquapentacyanoferrate(II) (it was tested in 0.1 *M* ferrocyanide solutions).

For the determination of k_2, we carried out competition experiments for H atoms between ferrocyanide and 2-propanol. It can be shown that the hydrogen yield in such solutions is expected to follow eq III where $G(H_2)$ is the experi-

$$1/(G(H_2) - G_{H_2}) = (1/G_H)(1 + k_2[Fe(CN)_6^{4-}]/k_5[2\text{-propanol}]) \quad (III)$$

mental yield of H_2, G_{H_2} is the so called "molecular yield" of H_2, G_H is the radical yield of H atoms at neutral pH, and k_5 is the reaction rate constant for reaction 5. $G(H_2)$

$$H + CH_3CHOHCH_3 \longrightarrow H_2 + CH_3COHCH_3 \quad (5)$$

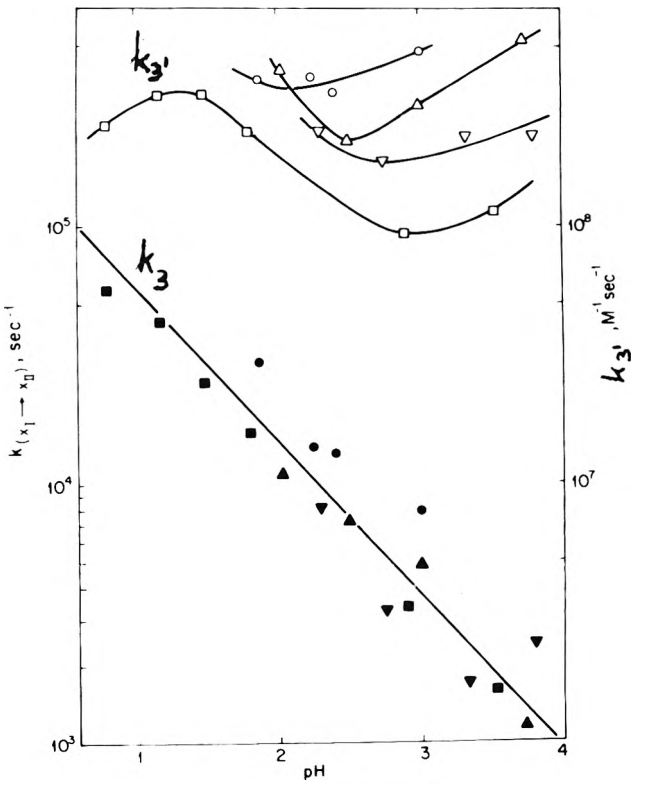

Figure 4. Dependence of k_3 and $k_{3'}$ on pH: ferrocyanide concentrations (*M*) □, ■, 0.01; △, ▲, 0.05; ▽, ▼, 0.02; ○, ●, 0.1.

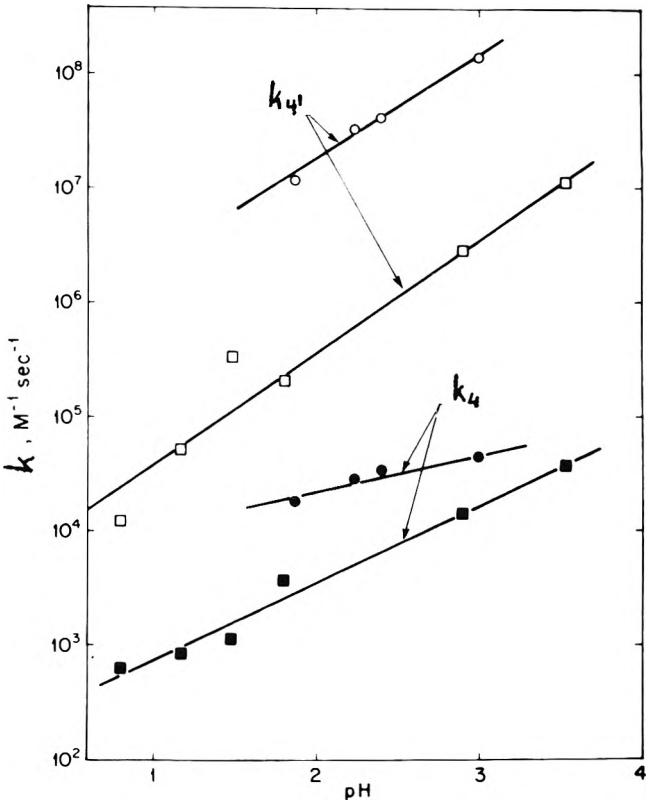

Figure 5. Dependence of k_4 and $k_{4'}$ on pH: □, ■, 0.01 *M* ferrocyanide; ○, ●, 0.1 *M* ferrocyanide.

$= G_{H_2} = 0.42 \pm 0.02$ was measured in the absence of 2-propanol over a wide range of ferrocyanide concentrations (10^{-3} to 0.5 *M*) in neutral solutions and in acid solutions

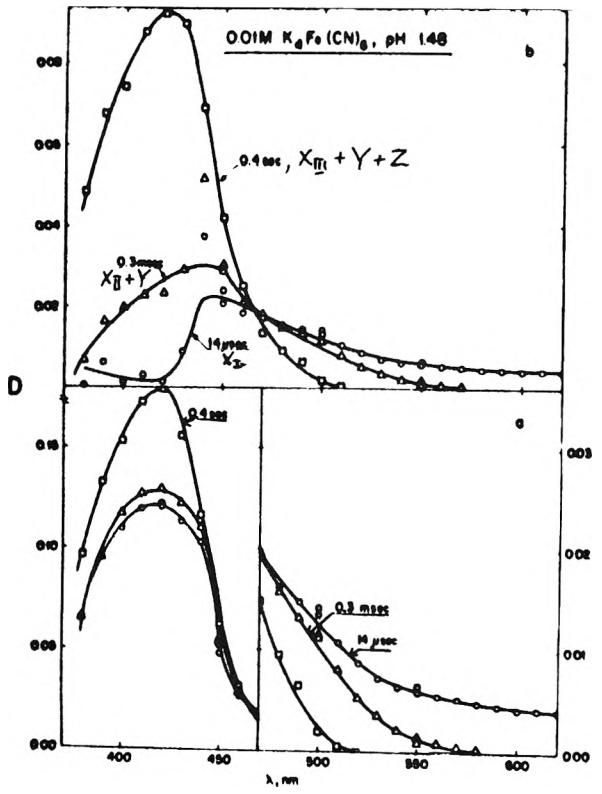

Figure 6. Spectra (processes I–III) for 0.01 *M* ferrocyanide solutions at pH 1.5: (a) optical absorptions at the end of each process; (b) optical absorptions corrected by subtraction of the ferricyanide absorbance (see Table II for the dose); (O) spectrum at the end of process I; (Δ) spectrum at the end of process II; (□) spectrum at the end of process III; $[X_I] = 8.9 \times 10^{-6}$, $[X_{II}] = 7.9 \times 10^{-6}$, $[X_{III}] = 6.3 \times 10^{-6}$, $[Y] = 1.0 \times 10^{-6}$, $[Z] = 1.6 \times 10^{-6}$ *M*.

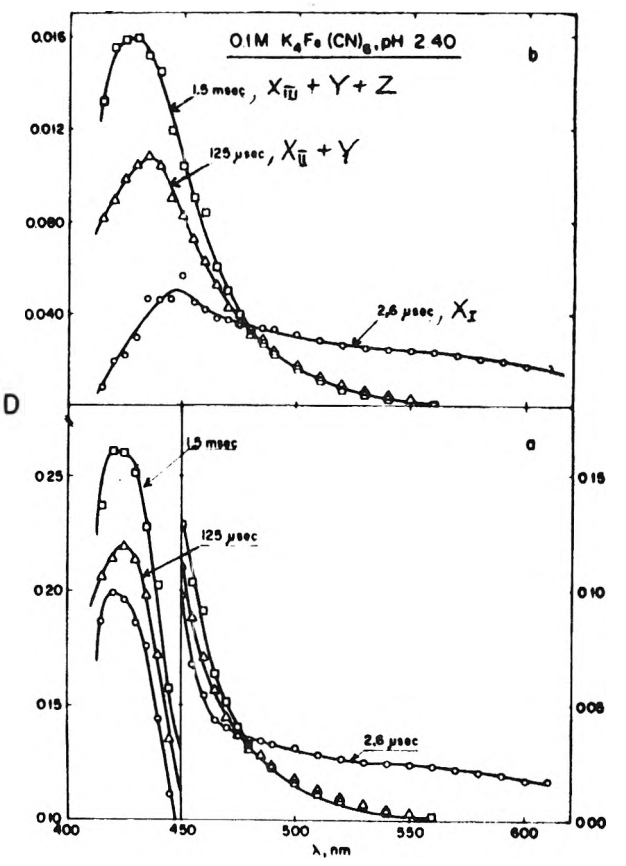

Figure 7. Spectra (processes I–III) for 0.1 *M* ferrocyanide solutions at pH 2.4. Process II is not well separated from process III. See Figure 6 and Table II for explanations: $[X_I] = 14.4 \times 10^{-6}$, $[X_{II}] = 9.9 \times 10^{-6}$, $[X_{III}] = 8.3 \times 10^{-6}$, $[Y] = 4.5 \times 10^{-6}$, $[Z] = 1.6 \times 10^{-6}$ *M*.

(5×10^{-2} *M* ferrocyanide in 0.15 *M* H_2SO_4). A plot of $1/(G(H_2) - G_{H_2})$ *vs.* $[Fe(CN)_6^{4-}]/[2\text{-propanol}]$ yielded a straight line as demonstrated in Figure 9. From Figure 9, $k_2 = (4.4 \pm 0.8) \times 10^7\ M^{-1}\ sec^{-1}$ can be obtained, based on $k_5 = 7.2 \times 10^7\ M^{-1}\ sec^{-1}$.[8] These competition experiments were carried out using a ^{137}Cs γ source, with a dose rate of about 2000 rads/min and a total dose up to 10^5 rads.

An upper limit, $100\ M^{-1}\ cm^{-1}$, for the extinction coefficient of X_I at 420 nm could be estimated from pulse radiolysis experiments.

Reaction with e_{aq}^-. Solutions of 0.2 *M* ferrocyanide and 0.5 *M* ethanol were argon saturated and pulse irradiated at high ionic strength (1 *M* Na_2SO_4). The addition of ethanol had the purpose of eliminating the ferricyanide formation by reaction 1. An upper limit, $k(e_{aq}^- + \text{ferrocyanide}) < 7 \times 10^4\ M^{-1}\ sec^{-1}$ could be estimated from the rate of decay of e_{aq}^- (followed at 580 nm). This is in agreement with the limit of $10^5\ M^{-1}\ sec^{-1}$ reported previously.[9]

Reactions of Ferricyanide Ions. Reaction with Hydrogen Atoms. The rate constant for the reaction has been determined previously[3] as $k = (6.5 \pm 0.5) \times 10^9\ M^{-1}\ sec^{-1}$ in acid (pH 2) solutions, where ferrocyanide was present as an OH scavenger. We determined this rate constant over a wide range of $HClO_4$ concentrations (pH 0.4–3.2) as $(5.5 \pm 0.4) \times 10^9\ M^{-1}\ sec^{-1}$. Corrections were carried out for the competing reaction 2 and recombination of H atoms. When we carried out such corrections for the previous results,[3] a value of $(6.0 \pm 0.8) \times 10^9$ was obtained. The mean value of all the results is $(5.8 \pm 0.6) \times 10^9\ M^{-1}\ sec^{-1}$.

Absorption measurements at 480 nm, where aquapentacyanoferrate(II) has optical absorption (ϵ 200 $M^{-1}\ cm^{-1}$[6,7] at pH 2), showed that not more than 2% of the H atoms reacted according to reaction 6 at pH 2 (10^{-2} *M* ethanol was added to eliminate OH radicals).

$$H + Fe(CN)_6^{3-} \xrightarrow{H_2O} Fe(CN)_5H_2O^{3-} + HCN \qquad (6)$$

In neutral solutions, about 10% of the H atoms reacted according to reaction 6. (N_2O and *tert*-butyl alcohol were present at sufficiently high concentrations to eliminate e_{aq}^- and OH.)

Reaction with e_{aq}^-. The reaction rate constant had been determined by Gordon, *et al.*[10] Dorfman and Matheson[11] have shown that if log *k* is plotted *vs.* $\mu^{1/2}/(1 + 2\mu^{1/2})$, a straight line is obtained with a slope = 3 when μ is low. At higher ionic strength ($\mu > 0.03$) the slope tends to the value of 2, as ferricyanide associates with K^+ or Na^+. We reexamined the reaction and evaluated the rate constant for $KFe(CN)_6^{2-}$ from a plot according to eq IV, which was used before.[1]

$$\frac{ak_{expt}}{[Fe(CN)_6^{3-}]} = k^0_{Fe(CN)_6^{3-}} + bk^0_{KFe(CN)_6^{2-}}\frac{[KFe(CN)_6^{2-}]}{[Fe(CN)_6^{3-}]} \qquad (IV)$$

where

$$a = 10^{-3.06\mu^{1/2}/(1+2\mu^{1/2})}$$

$$b = 10^{-1.02\mu^{1/2}/(1+2\mu^{1/2})}$$

k_{expt} is the experimental value, where k^0 is the rate con-

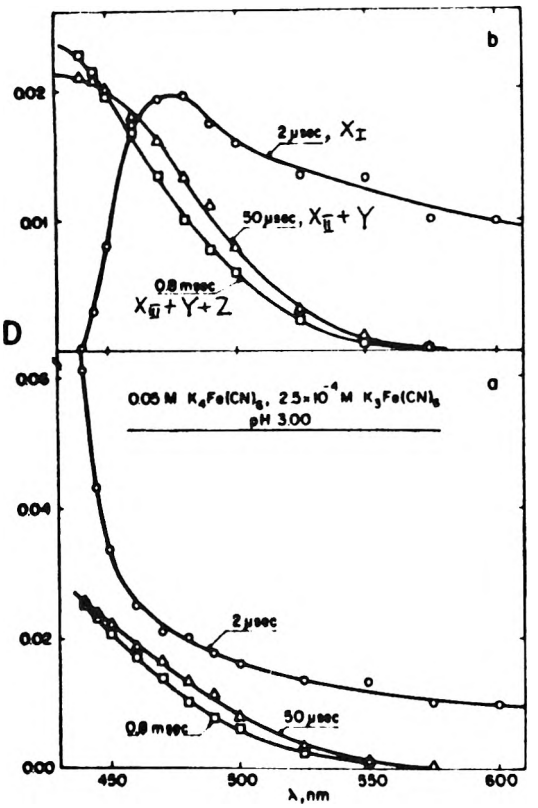

Figure 8. Spectra (processes I–III) for 0.05 *M* ferrocyanide solutions containing 2.5×10^{-4} *M* ferricyanide at pH 3.0. See Figure 6 and Table II for explanations: $[X_I] = 9.1 \times 10^{-6}$, $[X_{II}] = 0.6 \times 10^{-6}$, $[X_{III}] = 0.3 \times 10^{-6}$, $[Y] = 8.5 \times 10^{-6}$, $[Z] = 0.3 \times 10^{-6}$ *M*.

stant at $\mu = 0$. The rate constants k^0 obtained were 2.4×10^9 for $Fe(CN)_6^{3-}$ (in full agreement with 2.5×10^9 M^{-1} sec^{-1} [11]) and 2.7×10^9 M^{-1} sec^{-1} for $KFe(CN)_6^{2-}$.

Optical absorption measurements at 480–550 nm in deaerated neutral solutions of 10^{-4} *M* ferricyanide + 10^{-4} *M* ferrocyanide + 1 *M* ethanol and 5×10^{-4} *M* ferricyanide + 1 *M* 2-propanol were carried out. It was found that about 12% of the e_{aq}^- reacted according to reaction 7.

$$e_{aq}^- + Fe(CN)_6^{3-} \xrightarrow{H_2O} Fe(CN)_5H_2O^{2-} + CN^- \qquad (7)$$

Discussion

Reduction of Ferricyanide Ions by H and e_{aq}^-. The reaction of H atoms with ferricyanide may well involve an addition of the H to the ligand, followed by electron transfer. Halpern[12] suggested a general mechanism for reduction by H atoms

$$Fe^{3+}X^- + H \longrightarrow [Fe^{3+} \cdots X^- \cdots H] \longrightarrow Fe^{2+}XH \qquad (8)$$

$$Fe^{2+}XH + H_2O \longrightarrow Fe^{2+}X^- + H_3O^+ \qquad (9)$$

$$Fe^{2+}XH + H_2O \longrightarrow Fe^{2+}H_2O + HX \qquad (9')$$

This mechanism is in good agreement with our results, assuming reaction 8 is rate determining. As the Fe–CN bond is strong, reaction 9 is more important as compared to (9'). In acid solutions, the association of the intermediate $Fe^{2+}XH$ with H_3O^+ would probably strengthen the Fe–CN bond, as is the case in ferrocyanide,[13] thus preventing reaction 9' almost completely. This is in agreement with the negligible yield of aquapentacyanoferrate(II) in acid solutions.

The reaction of e_{aq}^- with ferricyanide is a diffusion-controlled electron transfer reaction.[14] As for many complexes,[14] there might be tunneling of the electron from the water to a d orbital of the metal. In such a reaction an excited state, $Fe(CN)_6^{4-}$*, may be formed as an intermediate,[14] which by monomolecular dissociation will form to some extent the aquapentacyanoferrate(II) complex.

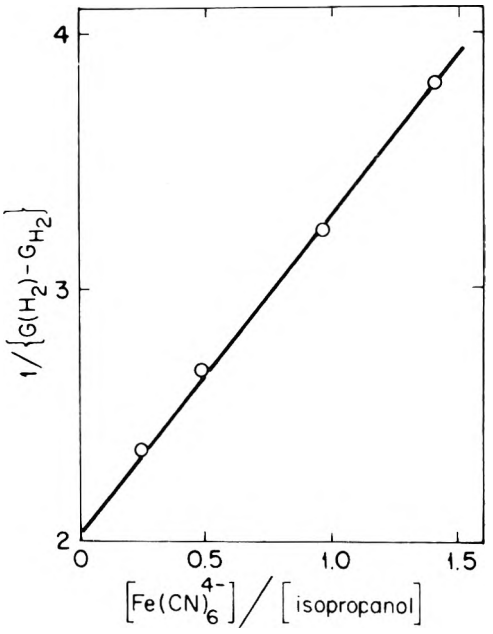

Figure 9. Competition between ferrocyanide (0.1 *M*) and 2-propanol for H atoms.

Reaction of H Atoms with Ferrocyanide Ions. The results presented in the previous sections show that H atoms react with ferrocyanide (reaction 2). There are reasons to propose that Fe(I) complexes are formed as a consequence of this reaction. Such a complex has been proposed previously in the electrolytic reduction of ferrocyanide, in the presence of excess of cyanide ions.[15] The reaction of H atoms with ferrocyanide, with the subsequent formation of aquapentacyanoferrate(II), has also been proposed.[16]

It might be argued that H atoms oxidize ferrocyanide, either *via* the H_2^+ mechanism[17] or *via* hydride formation.[18] However, in such a case reaction 2 is expected to be enhanced by H^+, contrary to our observations. Moreover, material balance would require that H_2 and some form of ferricyanide would be produced. This is again in disagreement with the data. (a) No ferricyanide was obtained after the termination of reaction 1. (b) No absorption which could be attributed to $Fe(CN)_5H_2O^{2-}$ was observed at 565 nm, which is the peak absorption of this Fe(III) complex.[19] (c) The hydrogen yield in the absence of organic scavengers and ferricyanide was identical with the so-called "molecular yield." Moreover, the product of reaction 2 reacts with ferricyanide ions, in agreement with the assumption that it is a reduction product. Another possibility that might be argued, is the addition of H atom to the –C≡N bond and subsequent oxidation of the ligand. Such reactions possibly take place when H atoms or OH radicals react with free CN^- (with rate constants of about 3×10^9 M^{-1} sec^{-1} [20]). However, product analysis showed that CN^- is formed in an equivalent yield to the aquapentacyanoferrate(II) complex,[5] ruling out significant amounts of oxidation products.

We propose that X_I is identical with $Fe(CN)_6H^{4-}$, so that reaction 2 is in fact reaction 10

$$H + Fe^{II}(CN)_6^{4-} \longrightarrow Fe(CN)_6H^{4-} \quad (10)$$

Reactions 3 and 3′ become 11 and 11′, respectively

$$Fe(CN)_6H^{4-} \longrightarrow Fe^{I}(CN)_5^{4-} + HCN \quad (11)$$

$$Fe(CN)_6H^{4-} + Fe^{III}(CN)_6^{3-} \longrightarrow \begin{cases} 2Fe^{II}(CN)_6^{4-} + H^+ \\ \text{or} \\ Fe^{II}(CN)_5^{3-} + Fe^{II}(CN)_6^{4-} + HCN \end{cases} \quad (11')$$

Reactions 4 and 4′ become 12 and 12′, respectively

$$Fe^{I}(CN)_5^{4-} + Fe^{II}(CN)_6^{4-} \longrightarrow Fe^{II}(CN)_5^{3-} + Fe^{I}(CN)_6^{5-} \quad (12)$$

$$Fe^{I}(CN)_5^{4-} + Fe^{III}(CN)_6^{3-} \longrightarrow Fe^{II}(CN)_5^{3-} + Fe^{II}(CN)_6^{4-} \quad (12')$$

Reactions 10 and 11 can be explained in a way which is schematically similar to the ferricyanide reduction (reactions 8 and 9). The H atom adds to the ligand CN^- (reaction 10) producing the radical $(NC)_5Fe-\dot{C}=NH$. We assume that the bond Fe–CNH is weak (in comparison with the Fe–C≡N bond in the normal complexes) and it breaks according to reaction 11. Aquapentacyanoferrate(II) is produced in reactions 11′, 12, and 12′, as it is reasonable to assume that $Fe^{II}(CN)_5^{3-}$ becomes very quickly hydrated.

All the reaction rate constants are expected to be pH dependent, due to possible protonation of the reactants. As the reactions 11, 11′, 12, and 12′ are between charged species, ionic strength effects are also expected. The rate of reaction 11 is linearly dependent of $[H^+]$. It is perhaps due to a catalytic effect on the breakage of the Fe–CNH bond.

We do not know the fate of $Fe^{I}(CN)_6^{5-}$ formed in reaction 12. It is probably oxidized by ferricyanide or H_2O_2 to yield ferrocyanide ions, within a few seconds or even later. Due to light instability and photolysis, we were unable to investigate this possibility.

Process IV, observed at high ferrocyanide concentrations, may be the equilibrium which was proposed by Emschwiller[7,21]

$$Fe(CN)_6^{4-} + Fe(CN)_5H_2O^{3-} \rightleftharpoons (NC)_5Fe(CN)Fe(CN)_5^{7-} + H_2O \quad (13)$$

It might be argued that H_2O_2, formed as a radiation product ($G \sim 0.7$), can react with the various Fe(I) complexes. Changing the pulse intensity (and hence $[H_2O_2]$) at various $Fe(CN)_6^{4-}$ and $Fe(CN)_6^{3-}$ concentrations gave no evidence for such reactions as being important under our conditions.

Spectra in Acid pH. According to the mechanism proposed, the spectra in Figures 6–8 must be assigned to aquapentacyanoferrate(II) which is formed *via* reactions 11′, 12, and 12′, along with other products. Optical absorbance is indeed produced in the range where the aquapentacyanoferrate(II) is known to absorb. However, a quantitative examination shows that the aquapentacyanoferrate(II) is not the only absorbing product. Other products may have $\epsilon < 300\ M^{-1}\ cm^{-1}$ in the same range. Since the absorption of aquapentacyanoferrate(II) is known at the various pH values,[6,7] it is possible to estimate the extinction coefficients of the radiation products from Figures 6–8.

Acknowledgment. The authors are indebted to Mr. Y. Ogdan for careful linear operation, and to Drs. M. S. Matheson and D. Meyerstein for useful discussions.

Miniprint Material Available. Full-sized photocopies of the miniprinted material from this paper only or microfiche (105 × 148 mm, 24× reduction, negatives) containing all of the miniprinted and supplementary material for the papers in this issue may be obtained from the Journals Department, American Chemical Society, 1155 16th St., N.W., Washington, D. C. 20036. Remit check or money order for $3.00 for photocopy or $2.00 for microfiche, referring to code number JPC-74-1368.

References and Notes

(1) D. Zehavi and J. Rabani, *J. Phys. Chem.*, **76**, 3703 (1972).
(2) (a) J. Jordan and G. J. Ewing, *Inorg. Chem.*, **1**, 587 (1962); (b) G. I. H. Hanania, D. H. Irvine, W. A. Eaton, and P. George, *J. Phys. Chem.*, **71**, 2022 (1967).
(3) J. Rabani and D. Meyerstein, *J. Phys. Chem.*, **72**, 1599 (1968).
(4) D. Zehavi and J. Rabani, to be submitted for publication.
(5) (a) E. Masri and M. Haissinsky, *J. Chim. Phys.*, **60**, 397 (1963); (b) M. Haissinsky, A. M. Koulkès, and E. Masri, *J. Chim. Phys.*, **63** 1129 (1966).
(6) M. Shirom and G. Stein, *J. Chem. Phys.*, **55**, 3379 (1971).
(7) G. Emschwiller, *Colloq. Int. Centre Nat. Rech. Sci.*, **191**, 307 (1970).
(8) (a) P. Neta, G. R. Holdren, and R. H. Schuler, *J. Phys. Chem.*, **75**, 449 (1971); (b) P. Neta, R. W. Fessenden, and R. H. Schuler, *ibid.*, **75**, 1654 (1971).
(9) M. Anbar, *Chem. Commun.*, 416 (1966).
(10) S. Gordon, E. J. Hart, M. S. Matheson, J. Rabani, and J. K. Thomas, *J. Amer. Chem. Soc.*, **85**, 1375 (1963).
(11) L. M. Dorfman and M. S. Matheson, *Progr. React. Kinet.*, **3**, 237 (1965).
(12) J. Halpern, *Discuss. Faraday Soc.*, **29**, 252 (1960).
(13) N. K. Hamer and L. E. Orgel, *Nature (London)*, **190**, 439 (1961).
(14) E. J. Hart and M. Anbar, "The Hydrated Electron," Wiley-Interscience, New York, N. Y., 1970.
(15) W. D. Treadwell and D. Huber, *Helv. Chim. Acta*, **26**, 10 (1943).
(16) G. Navon and G. Stein, *J. Phys. Chem.*, **70**, 3630 (1966).
(17) G. Czapski, J. Jortner, and G. Stein, *J. Phys. Chem.*, **65**, 950 (1961).
(18) G. Czapski and J. Jortner, *Nature (London)*, **188**, 50 (1960).
(19) M. Haissinsky and R. Julien, *J. Chim. Phys.*, **57**, 666 (1960).
(20) M. Anbar and P. Neta, *Int. J. Appl. Radiat. Isotopes*, **18**, 493 (1967).
(21) G. Emschwiller, *C. R. Acad. Sci.*, **268**, 692 (1969).

Dynamic and Static Quenching of the Tris(2,2′-dipyridyl)ruthenium(II) Phosphorescence by Anionic Coordination Compounds in Various Solvents[1]

F. Bolletta,* M. Maestri, L. Moggi, and V. Balzani

Istituto Chimico "G. Ciamician" dell'Università, 40126 Bologna, Italy *(Received December 20, 1973)*

The quenching of the $Ru(dipy)_3^{2+}$ phosphorescence intensity and lifetime by $Mo(CN)_8^{4-}$, $IrCl_6^{3-}$, and $PtCl_4^{2-}$ has been investigated in different solvents. For most of the systems examined, the intensity and lifetime are quenched in parallel, showing that only a dynamic quenching of the $Ru(dipy)_3^{2+}$ emitting state takes place. However, for two systems (namely, $Ru(dipy)_3^{2+}$-$Mo(CN)_8^{4-}$ in water and $Ru(dipy)_3^{2+}$-$PtCl_4^{2-}$ in *N,N*-dimethylformamide) the phosphorescence intensity is quenched more than the phosphorescence lifetime, showing that both dynamic and static quenching processes take place. This seems to be the first example of both dynamic and static quenching between inert, saturated coordination compounds. From the luminescence measurements, the values 3×10^2 and 1×10^3 M^{-1} are obtained for the ion-pairing equilibrium constants of $Ru(dipy)_3^{2+}$-$Mo(CN)_8^{4-}$ in water and $Ru(dipy)_3^{2+}$-$PtCl_4^{2-}$ in DMF. These values are in fair agreement with the theoretical values calculated by the Fuoss equation. For each of the systems examined, the bimolecular rate constant of the dynamic quenching is in fair agreement with the calculated diffusion rate constant.

Introduction

The study of the quenching processes between coordination compounds has recently attracted much attention. The following features seem to emerge from the body of the available results: (i) the quenching can occur by electronic energy transfer mechanisms, as is evidence by the sensitized emission[2-5] and the sensitized photoreaction[3,6-10] of the acceptor complexes; (ii) the quenching efficiency in the collision encounter is strongly affected by the nature of the ligands and the geometry of the acceptor complex;[5] (iii) the ionic charge may also play some role in the quenching efficiency,[11] but its real effect is difficult to examine because a change in the ionic charge is always accompanied by a change of other factors (*e.g.*, the nature of the ligands);[5] (iv) in agreement with the theoretical expectations, the ionic strength affects the quenching constants when both the excited state and the quencher are charged species;[5] (v) no clear evidence has thus far been reported for the participation of static quenching processes.[12]

We are continuing our systematic investigations with the aim of elucidating the various aspects of the quenching processes between coordination compounds. We wish to report here the results obtained on the quenching of the $Ru(dipy)_3^{2+}$ phosphorescence intensity and lifetime by some anionic coordination compounds in various solvents. For some of our systems, we found that the lifetime quenching did not parallel the intensity quenching, and we believe that such systems represent the first examples of both dynamic and static quenching processes in the field of coordination compounds. The equilibrium constant for the ion-pairing between two coordinatively saturated coordination compounds was obtained by luminescence measurements only. This unusual technique proves to be very sensitive and will certainly provide a new and important means for determining association and ion-pairing constants.

Experimental Section

Materials. Tris(2,2′-dipyridyl)ruthenium(II) chloride tetrahydrate, $[Ru(dipy)_3]Cl_2 \cdot 4H_2O$, was prepared and purified by Burstall's method.[15] Potassium octacyanomolybdate(IV) dihydrate, $K_4[Mo(CN)_8] \cdot 2H_2O$, was prepared by the method described by Furman and Miller.[16] Potassium tetrachloroplatinate(II), $K_2[PtCl_4]$, was prepared and purified according to the procedure given by Fernelius.[17] Fluka potassium hexachloroiridate(III), $K_3[IrCl_6]$, was used without further purification. *N,N*-Dimethylformamide (DMF) Baker analyzed and *N*-methylformamide (MF) Merck-Schuchard for synthesis were used. All of the other chemicals used were of reagent grade.

Apparatus. The absorption spectra were recorded with an Optica CF4 NI spectrophotometer. The emission intensity and the phosphorescence spectra were measured with a Perkin-Elmer MPF-3 spectrofluorimeter. The lifetime measurements were carried out with the apparatus described by Hutton, *et al.*[18]

Procedures. All the experiments were carried out at room temperature (~22°) in air-equilibrated solutions, unless otherwise noted. When necessary, deaeration was carried out by bubbling purified N_2 for 40 min. The general procedure was as follows. Stock solutions of $Ru(dipy)_3^{2+}$, of the various quenchers, and of KCl and NH_4Cl were prepared by dissolving weighed amounts of each salt in the selected medium. By appropriate mixing and dilution of these stock solutions, solutions were obtained which contained 1×10^{-4} *M* $Ru(dipy)_3^{2+}$ and the appropriate quencher concentration at the desired ionic strength. These solutions were stable in the dark for periods much longer than those needed for our experiments. Exposure to the light beam of the spectrofluorimeter was reduced to a few seconds in order to avoid sensitized reactions of the quenchers.[19] For the intensity measurements the excitation was carried out at 450 nm and the emission was measured at 620 nm. For our conditions, the quencher absorption was always negligible at both the excitation and emission wavelengths. The intensity data taken before and after the lifetime measurements were unchanged within the experimental error. The reproducibility of the intensity values was ±2%. For the lifetime measurements, excitation was performed at 487 nm and the decay of the luminescence emission was monitored on the beam

emerging from cut-off filters which absorbed practically all light of λ <600 nm. The semilogarithmic plots (log I *vs.* time) obtained from the oscilloscope traces were linear as expected for a first-order decay. The reproducibility was ±5% for lifetimes longer than 0.15 μsec, and ±10% for shorter lifetimes.

Results

The absorption (λ >300 nm) and emission spectra of $Ru(dipy)_3^{2+}$ in DMF and MF were practically identical with those recorded in aqueous solutions (λ_{max}^{abs} 452 nm, ϵ_{max} 1.4×10^4, λ_{max}^{em} ~610 nm). The relative emission intensity of the complex at 610 nm was found to decrease in going from water to MF or DMF. No change was found in both the absorption and emission spectra when the ionic strength of the solution was changed (up to 0.1). Moreover, absorption measurements showed that the spectra (λ >300 nm) of solutions containing 1×10^{-4} *M* $Ru(dipy)_3^{2+}$ and various amounts of the quenchers (up to the maximum concentrations used in our quenching experiments) were equal to the sum of the individual donor and quencher spectra within the experimental error, except for the $Ru(dipy)_3^{2+}$–$PtCl_4^{2-}$ system in DMF. For this system, a slight increase in absorbance (~5%) was observed at ~480 and 370 nm, *i.e.*, where the $Ru(dipy)_3^{2+}$ absorption is lower. Although such a behavior clearly shows that an ion pair is formed, the effect was too small to allow the evaluation of the association constant. The lifetime (τ_T^0) of the $Ru(dipy)_3^{2+}$ phosphorescence emission in water was found to be 0.40 and 0.63 μsec in air-equilibrated and deaerated solutions, respectively, in agreement with previously reported values.[6,14] In air-equilibrated DMF and MF solutions, τ_T^0 was found to be 0.32 and 0.31 μsec, respectively. The τ_T^0 values were not affected by changing the ionic strength of the solution (up to 0.1).

The lifetime and intensity Stern–Volmer plots for the quenching of the $Ru(dipy)_3^{2+}$ phosphorescence by $Mo(CN)_8^{4-}$, $IrCl_6^{3-}$, and $PtCl_4^{2-}$ at constant ionic strength in the various solvents are shown in Figures 1–3. Low solubilities prevented experiments in DMF for the $Ru(dipy)_3^{2+}$–$Mo(CN)_8^{4-}$ and $Ru(dipy)_3^{2+}$–$IrCl_6^{3-}$ systems. For the $Ru(dipy)_3^{2+}$–$PtCl_4^{2-}$ system in aqueous solution, only quenching of the intensity emission could be measured because the apparatus for lifetime measurements was no longer available. However, a parallel quenching of lifetime and intensity for this specific system has already been reported by Demas and Adamson.[6]

Discussion

The experimental data (Figures 1–3) show that the lifetime and intensity of the $Ru(dipy)_3^{2+}$ phosphorescence are quenched in parallel (within the experimental error) for the following systems: $Ru(dipy)_3^{2+}$–$Mo(CN)_8^{4-}$ in MF, $Ru(dipy)_3^{2+}$–$IrCl_6^{3-}$ in H_2O and MF, and $Ru(dipy)_3^{2+}$–$PtCl_4^{2-}$ in H_2O and MF. On the contrary, for the two remaining systems (namely, $Ru(dipy)_3^{2+}$–$Mo(CN)_8^{4-}$ in H_2O and $Ru(dipy)_3^{2+}$–$PtCl_4^{2-}$ in DMF) the intensity quenching clearly exhibits a different behavior than the lifetime quenching.

The reaction scheme of Figure 4 will be used in discussing the results. By means of the usual kinetic treatment, the following equations can be obtained for the lifetime and intensity quenching of the $Ru(dipy)_3^{2+}$ phosphorescence emission[21]

$$\tau_T^0/\tau_T = (1 + k_q\tau_T^0[A]) \quad (1)$$

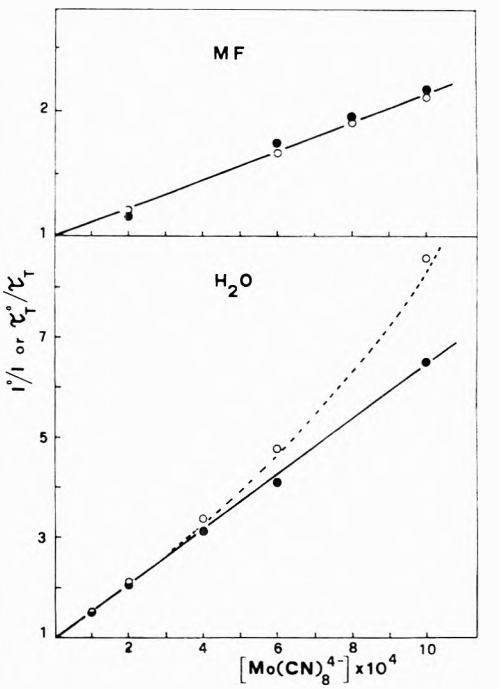

Figure 1. Intensity (○) and lifetime (●) quenching of the $Ru(dipy)_3^{2+}$ phosphorescence by $Mo(CN)_8^{4-}$ in MF and deaerated H_2O solutions. Ionic strength = 1.04×10^{-2}. The dotted curve represents the intensity quenching calculated on the basis of eq 4 (see text).

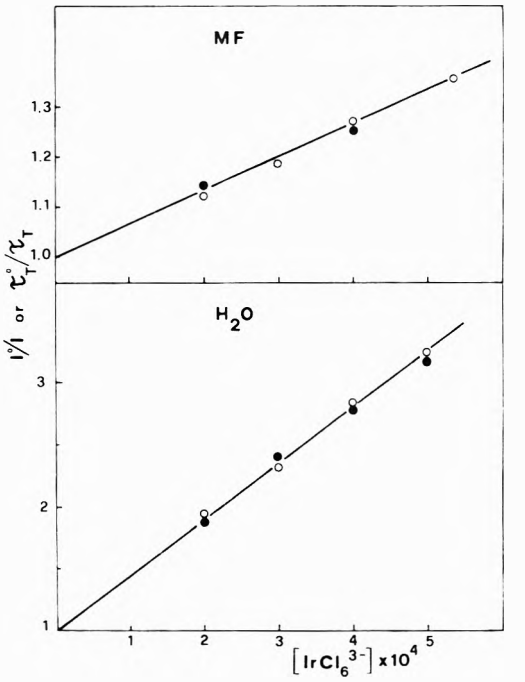

Figure 2. Intensity (○) and lifetime (●) quenching of the $Ru(dipy)_3^{2+}$ phosphorescence by $IrCl_6^{3-}$ in MF and H_2O. Ionic strength = 3.6×10^{-3}.

$$I^0/I = (1 + k_q\tau_T^0[A])(1 + k_s\tau_S^0[A])(1 + K_{ip}[A]) \quad (2)$$

Equation 1 shows that the lifetime quenching is only due to the dynamic quenching of the emitting state. Equation 2 shows that the intensity quenching, besides being due to the dynamic quenching of the emitting state, may also contain a contribution from the dynamic quenching of the singlet excited state and from the static quenching in the ion pairs. If one or both of these last two quenching pro-

TABLE I: Experimental and Calculated Parameters for the Dynamic and Static Quenching of the $Ru(dipy)_3^{2+}$ Phosphorescence by Anionic Complexes

Quencher	Quenching rate constants, $k_8 \times 10^{-9}$, M^{-1} sec^{-1} (Diffusion rate constants, $k_d \times 10^{-9}$, M^{-1} sec^{-1})[a]			Ion-pairing constants, $K_{ip} \times 10^{-2}$, M^{-1} (Theoretical values $K_{ip} \times 10^{-2}$, M^{-1})[b]		
	MF	H_2O	DMF	MF	H_2O	DMF
$Mo(CN)_8^{4-}$	4 ± 1 (6.6)	9 ± 2 (8.9)		≤0.5 (0.2)	3 ± 1 (1.8)	
$IrCl_6^{3-}$	2 ± 1 (6.9)	12 ± 3 (15.0)		≤0.5 (0.1)	≤0.5 (0.9)	
$PtCl_4^{2-}$	0.8 ± 0.2 (6.2)	10 ± 2 (16.4)	15 ± 4 (17.2)	≤0.5 (0.1)		10 ± 5 (4.0)

[a] Calculated using the Brønsted–Debye equations[24] at the experimental (see Figures 1–3) ionic strength, with an encounter radius of 5 Å for each complex. The viscosity and dielectric constants were 1.65 cP and 182.4 for MF, 0.89 cP and 78.30 for H_2O, and 0.79 cP and 36.7 for DMF, respectively. [b] Calculated by the Fuoss equation[25] using the same parameters as in footnote *a*.

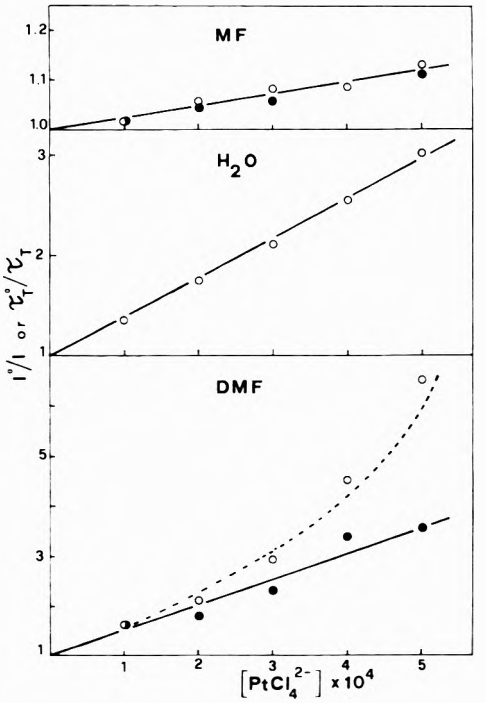

Figure 3. Intensity (○) and lifetime (●) quenching of the $Ru(dipy)_3^{2+}$ phosphorescence by $PtCl_4^{2-}$ in MF, H_2O, and DMF. Ionic strength = 1.8×10^{-3}. The dotted curve represents the intensity quenching calculated on the basis of eq 4 (see text).

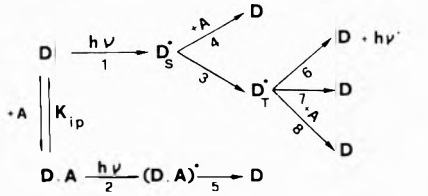

Figure 4. Schematic mechanism showing the possible quenching paths for the $Ru(dipy)_3^{2+}$ phosphorescence. *D*, D_S^*, and D_T^* are the ground state, the lowest excited singlet state, and the lowest excited triplet state of $Ru(dipy)_3^{2+}$, respectively; A is the quencher; K_{ip} is the ion-pair association constant.

cesses are negligible, eq 2 reduces as follows: (a) when [DA] ≪ [D], K_{ip}[A] is much lower than 1, so that one obtains

$$I^0/I = (1 + k_8\tau_T^0[A])(1 + k_4\tau_S^0[A]) \quad (3)$$

(b) when k_4[A] ≪ k_3, $k_4\tau_S^0$[A] is much lower than 1, so that one obtains

$$I^0/I = (1 + k_8\tau_T^0[A])(1 + K_{ip}[A]) \quad (4)$$

(c) when both the conditions a and b apply, one obtains

$$I^0/I = (1 + k_8\tau_T^0[A]) \quad (5)$$

It follows that whenever the lifetime and intensity are quenched in parallel, only the dynamic quenching of the emitting state takes place (compare eq 1 and 5). In the case of $Ru(dipy)_3^{2+}$–$Mo(CN)_8^{4-}$ in H_2O and of $Ru(dipy)_3^{2+}$–$PtCl_4^{2-}$ in DMF, on the contrary, some contribution to the intensity quenching from either static quenching (eq 4) or dynamic quenching of the singlet excited state (eq 3) or both (eq 2) must be present. Under our experimental conditions, however, the dynamic quenching of the singlet excited state can be excluded, since k_4[A] ≤ 10^7 sec^{-1} (k_4 ≤ 10^{10} M^{-1} sec^{-1}, [A] ≤ $10^{-3}M$) whereas k_3 is higher than 5×10^{10} sec^{-1}.[22,23] It follows that the difference between lifetime and intensity quenching can only be due to a static mechanism (eq 4).

It is evident that static quenching might also occur in the other systems at higher quencher concentrations. Unfortunately, there are severe limitations connected with solubility reasons and with the competition in the light absorption between the donor and the acceptor. It should also be noted that higher quencher concentrations would imply higher ionic strength values, which would depress both k_8 and K_{ip}, thus vanishing the effect of the increased quenching concentration.

From the experimental Stern–Volmer plots of the emission lifetime, the k_8 values (see eq 1) reported in Table I were obtained. Plots of $(I^0/I)/(\tau^0/\tau)$ *vs.* [A] (see eq 4 and 1) were used for obtaining the K_{ip}'s (or their upper limiting values) which are also reported in Table I.

Because of the inaccuracy of the experimental constants and the drastic assumptions of the theoretical equations used for obtaining the calculated diffusion-controlled rate constants[24,26] and the ion pairing constants,[25,27] only the "gross" features of the data reported in Table I can be discussed. As far as the dynamic part of the quenching process is concerned, we observe that there is a fair agreement between the experimental and the calculated rate constants, and that the experimental rate constant change with changing the solvent in the same way as the calculated values do (*i.e.*, they increase with decreasing viscosity and dielectric constant of the solvent). This indicates that in our systems there is no factor (see Introduction) which limits the quenching efficiency during the collision encounter. A possible exception to this behavior could be that of $PtCl_4^{2-}$ in MF, where the experimental and calculated values differ by a factor of about 8. It should be noted, however, that the differences between the experimental and calculated values are higher in MF than in H_2O for the two other complexes also, which may mean that the theoretical equation for the diffusion rate and/or its "correction" for the ionic strength lose part of their va-

lidity for a solvent like MF, which has a high viscosity and a very high dielectric constant (see Table I).

As far as the ion-pairing constants are concerned, there is again a fair agreement between the theoretical values and those obtained from our experimental results. We can also see that, as expected, the ion pairing is favored by decreasing the dielectric constant of the solvent. To best of our knowledge our results represent the first case in which the ion pairing of coordinatively saturated compounds of transition metal ions has been measured by means of the luminescence technique. Ion pairing between coordination compounds has previously been shown for the $Co(en)_3^{3+}$-$Fe(CN)_6^{4-}$ system by means of polarimetric measurements,[28,29] and for the $Co(NH_3)_5H_2O^{3+}$-CrO_4^{2-} system by means of pH and spectrophotometric measurements.[30] We believe that the technique used in this paper, although not general because it requires a luminescent complex, can make an important contribution to the study of equilibria involving transition metal complexes in solution.

Acknowledgment. This work was supported in part by the National Research Council of Italy.

References and Notes

(1) Presented in part at the VII International Conference of Photochemistry, Jerusalem, Israel, Aug 28–Sept 4, 1973.
(2) S. N. Chen and G. B. Porter, *J. Amer. Chem. Soc.*, **92**, 3196 (1970).
(3) N. Sabbatini and V. Balzani, *J. Amer. Chem. Soc.*, **94**, 7587 (1972); N. Sabbatini, M. A. Scandola, and V. Carassiti, *J. Phys. Chem.*, **77**, 1307 (1973).
(4) N. Sabbatini, M. A. Scandola, and V. Balzani, *J. Phys. Chem.*, **78**, 541 (1974).
(5) F. Bolletta, M. Maestri, L. Moggi, and V. Balzani, *J. Amer. Chem. Soc.*, **95**, 7864 (1973).
(6) J. N. Demas and A. W. Adamson, *J. Amer. Chem. Soc.*, **93**, 1800 (1971).
(7) P. Natarjan and J. F. Endicott, *J. Phys. Chem.*, **77**, 971 (1973); *J. Amer. Chem. Soc.*, **95**, 2470 (1973).
(8) P. Natarjan and J. F. Endicott, private communication.
(9) R. Matsushima, *Chem. Lett.*, 115 (1973).
(10) J. N. Demas and W. A. Adamson, *J. Amer. Chem. Soc.*, **95**, 5159 (1973).
(11) J. N. Demas, Proceedings of the XIV International Conference on Coordination Chemistry, Toronto, Canada, June 22–28, 1972, p 166.
(12) The evidence reported by Fujita and Kobayashi[13] in favor of a static quenching seems to be incorrect.[10,14]
(13) J. Fujita and H. Kobayashi, *Ber. Bunsenges. Phys. Chem.*, **76**, 115 (1972).
(14) F. Bolletta, M. Maestri, and L. Moggi, *J. Phys. Chem.*, **77**, 861 (1973).
(15) F. H. Burstall, *J. Chem. Soc.*, 173 (1936).
(16) N. H. Furman and C. O. Miller, *Inorg. Syn.*, **3**, 160 (1950).
(17) W. C. Fernelius, *Inorg. Syn.*, **8**, 240 (1963).
(18) A. Hutton, G. Giro, S. Dellonte, and A. Breccia, *Int. J. Radiat. Phys. Chem.*, **5**, 387 (1973).
(19) For the sensitization of $PtCl_4^{2-}$ by $Ru(dipy)_3^{2+}$, see ref 6. A photosensitized reaction also takes place in the cases of $Mo(CN)_8^{4-}$.[20]
(20) Unpublished results from our laboratory.
(21) In these equations, A] represents the "free" quencher concentration. Under our experimental conditions, the ion-pair concentration is negligible or small enough to render the "free" quencher concentration practically equal to the total quencher concentration. Therefore, the total quencher concentration has been used in the plots of Figures 1–3. Note also that a more general formulation for eq 2 should contain βK_{ip} instead of K_{ip}, where $\beta = \epsilon_{DA}/\epsilon_D$. In our conditions, however, β was practically equal to unity (see previous sections).
(22) F. E. Lytle and D. M. Hercules, *J. Amer. Chem. Soc.*, **91**, 253 (1969).
(23) A lifetime lower than 10^{-10} sec for the lowest excited singlet state of $Ru(dipy)_3^{2+}$ can also be evaluated from the absorption intensity and lack of fluorescence.
(24) See, for example, A. D. Pethybridge and J. E. Prue, *Progr. Inorg. Chem.*, **17**, 327 (1972).
(25) R. M. Fuoss, *J. Amer. Chem. Soc.*, **80**, 5059 (1958).
(26) M. Eigen, W. Kruse, G. Maass, and L. De Maeyer, *Progr. React. Kinet.*, **2**, 285 (1964).
(27) R. A. Robinson and R. H. Stokes, "Electrolyte Solutions," 2nd ed, Butterworths, London, 1959.
(28) R. Larsson, *Acta Chem. Scand.*, **21**, 257 (1967).
(29) For the $Co(en)_3^{3+}$-$Fe(CN)_6^{4-}$ system, both 1:1 and 1:2 outer-sphere complexes are present.[28] Since the association of $Ru(dipy)_3^{2+}$ with one quencher molecule is sufficient to quench the emission, our K_{ip} represent the first association constant. The possibility that outer-sphere complexes of different stoichiometry may be formed in the case of the $Ru(dipy)_3^{2+}$-$Mo(CN)_8^{4-}$ system is under investigation in our laboratory.
(30) J. M. Sullivan and J. E. French, *Inorg. Chem.*, **3**, 832 (1964).

Thermodynamics of the Reactions $(NH_3)_n \cdot SO_2(s) \rightleftharpoons nNH_3(g) + SO_2(g)$[1]

Ronald Landreth, Rosa G. de Pena, and Julian Heicklen*

Departments of Chemistry and Metrology and Center for Air Environment Studies, The Pennsylvania State University, University Park, Pennsylvania 16802 *(Received October 29, 1973; Revised Manuscript Received April 17, 1974)*

Publication costs assisted by the Environmental Protection Agency

Anhydrous SO_2 and NH_3 were allowed to react to form their solid adducts. Equilibrium vapor pressures for each gas were measured at 5, 15, 24.5, 35, and 45°. The reaction is $NH_3 \cdot SO_2(s) \rightleftharpoons NH_3(g) + SO_2(g)$ with $\ln K(atm^2) = \Delta S/r - \Delta H/RT$ where K is the equilibrium constant, ΔS = 15.3 cal/mol °K, and ΔH = 9.5 kcal/mol to within ±10% uncertaiy. The equilibrium was unaffected by the presence of excess O_2 or N_2. With excess NH_3 at the lowest two temperatures, there was thermodynamic evidence for the production of the $(NH_3)_2 \cdot SO_2$ adduct. For the reaction $(NH_3)_2 \cdot SO_2(s) \rightleftharpoons 2NH_3(g) + SO_2(g)$ the thermodynamic functions are crudely estimated to be $\Delta S \sim 82$ cal/mol °K and $\Delta H \sim 23$ kcal/mol with at least ±20% uncertainty.

Introduction

The anhydrous reaction between NH_3 and SO_2 has been known for a very long time, and the history of this reaction has been reviewed by Scott, *et al.*[2] Above 10°, the reaction between NH_3 and SO_2 produces a 1:1 adduct which is a yellow solid. Below 10° an additional white solid is produced which is the adduct of two molecules of NH_3 and one molecule of SO_2. Both reactions are reversible, and as the pressure is reduced, the solids sublime to form NH_3 and SO_2.

Neither the chemical structures nor the thermodynamics of the adducts are precisely known. Scott, *et al.*,[2] measured the vapor pressure of the solids between −10 and −70°. From their data they estimated the enthalpy of sublimation to be ~1 and ~15 kcal/mol, respectively, for the 1:1 and 2:1 adducts.

McLaren, *et al.*,[3] report a heat of reaction of −30 kcal/mol for anhydrous NH_3 with SO_2 both in the presence and absence of O_2. They did not specify their temperature range and it is not known whether this value refers to the 1:1 or 2:1 adduct. Friend, *et al.*,[4] worked at very low pressures and found no evidence for solid formation in the absence of ultraviolet radiation.

In this paper we have examined the reaction in the temperature range 5-45° and at partial pressures very much larger than those employed by Friend, *et al.*[4] We show, from thermodynamic arguments, that the solid is the 1:1 adduct in this temperature range, except with excess NH_3 at the lowest two temperatures. Furthermore, ΔH and ΔS are determined to be 9.5 kcal/mol and 15.3 cal/mol °K, respectively, for the reaction

$$NH_3 \cdot SO_2(s) \rightleftharpoons NH_3(g) + SO_2(g)$$

Experimental Section

The reaction was carried out in a 2.7-l. cylindrical cell 137 cm long and 5 cm in diameter. The cell was capped at each end by a 2-mm thick quartz window to allow passage of ultraviolet light. Inside and along the length of the cell was a small tube with holes every 10 cm through which the gases entered to allow thorough mixing of the gases. Temperature variation was accomplished by changing the temperature of a constant temperature water bath around the cell.

Particle formation was determined by light scattering. The light from a Hanovia Utility 30620 ultraviolet quartz lamp was passed through a Jarrell-Ash 82-410 monochromator set at 3660 Å and through the cell. The light was detected by a RCA 935 phototube and the signal sent through a General Radio Co. 1432-M resistance box to a Texas Instruments Inc. 1-mV recorder.

SO_2, NH_3, and O_2 gases were from the Matheson Co., and N_2 gas was from Phillip Wolf and Sons Inc. Before use, the N_2 was passed through a trap packed with glass wool at −196° to remove water and impurities. The same was done with O_2 at −98°. Both SO_2 and NH_3 were twice purified by distillation from −98 to −196°. The gases were handled in a mercury- and grease-free vacuum line containing Teflon stopcocks with Viton "O" rings. The vacuum line was connected to the reaction cell and the pressure could be reduced to 1×10^{-4} Torr.

The gases were introduced into the reaction cell as follows. For experiments with SO_2 and NH_3 only, one gas was added to the cell and the pressure read on a National Research Corp. 820 alphatron vacuum gauge. The alphatron gauge had been calibrated by an oil monometer for each gas. After having closed off the cell and frozen down the excess gas, the second gas was added in increments until light attenuation was noticed on the recorder. At 5° light attenuation was not seen on the recorder because the particles settled on the wall. Particle formation was determined visually. For runs with O_2 or N_2 present, one reactant was placed in the cell, and the other reactant diluted in N_2 or O_2 was then added.

Results

Anhydrous SO_2 and NH_3 gases were mixed, and a yellow solid was produced instantly if the gas pressures were sufficiently large. The reaction was completely reversible; when the gas pressures were reduced sufficiently, the solid disappeared. When one of the reactants was diluted in O_2 or N_2, there was about a 30-sec delay before particle production, if particles were produced at all. In these experiments, we waited 5-10 min after each addition to be sure that particles either were or were not produced.

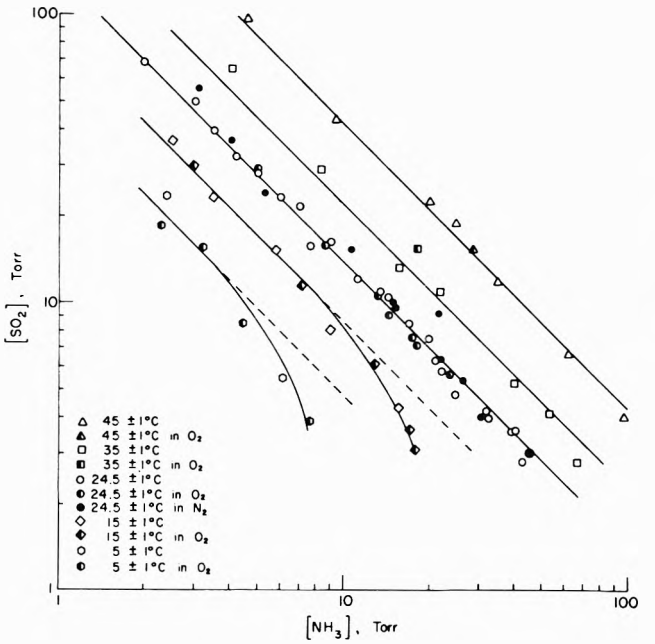

Figure 1. Log–log plots of the vapor pressures of SO_2 and NH_3 in equilibrium with their solid product at 5, 15, 24.5, 35, and 45°.

Experiments were done in which the lower pressure reactant was placed in the reaction vessel and then the other reactant, either alone or diluted in N_2 or O_2, was added. Several additions of the second reactant were made until the solid was produced. The point at which solid appeared was taken as the equilibrium condition. For some runs, the total pressure was then reduced by 10% and the solid disappeared. When O_2 or N_2 was used as a diluent, the ratio of its pressure to the reactant pressure was varied between 2.45 and 12.1.

The pressures of the gases could be ascertained to within 5% accuracy for pressures <100 Torr and 7–10% accuracy for pressures >100 Torr. To be sure that the reaction was not photochemically induced by the monitoring lamp (SO_2 absorbs weakly at 3660 Å), runs were done with the lamp off while the mixture was equilibrating. The lamp was then turned on just to take the measurement. The results were the same as with continuous exposure.

The equilibrium conditions, *i.e.*, the pressure limits at which solid is just formed, are shown graphically in log–log plots in Figure 1 at five temperatures between 5 and 45°. As the temperature is raised the data points lie successively higher. The results in the presence of diluent gases are identical with those with no diluent added in agreement with McLaren, *et al.*[3] The plots of SO_2 pressure *vs.* NH_3 pressure at the three highest temperatures are linear and can be fitted with a slope of −1.00. At the two lower temperatures, the data points are fitted with a line of slope −1.00 in excess SO_2. However, in excess NH_3, deviations occur and the data points lie below the linear extension of the results in excess SO_2.

Discussion

The equilibrium of interest is the heterogeneous one

$$n\mathrm{NH_3 \cdot SO_2(s)} \rightleftharpoons \mathrm{SO_2(g)} + n\mathrm{NH_3(g)}$$

where n is either one or two. The equilibrium expression for the reaction is

$$K = [\mathrm{SO_2}][\mathrm{NH_3}]^n$$

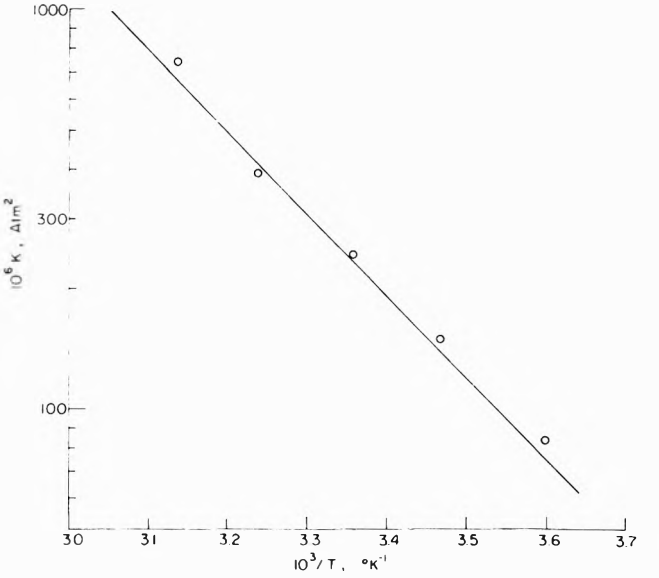

Figure 2. Semilog plot of the equilibrium constant K *vs.* the reciprocal temperature for the reaction $NH_3 \cdot SO_2(s) \rightleftharpoons NH_3(g) + SO_2(g)$.

TABLE I: Equilibrium Constants for the Reaction $NH_3 \cdot SO_2(s) \rightleftharpoons NH_3(g) + SO_2(g)$[a]

Temp, °C	K, Torr²	10^6K, atm²
45 ± 1	425	736
35 ± 1	223	386
24.5 ± 1	140	243
15 ± 1	86	149
5 ± 1	48	83

[a] Ln $K(\mathrm{atm^2}) = \Delta S/R - \Delta H/RT$, ΔS = 15.3 cal/mol °K, ΔH = 9.5 kcal/mol.

where K is the equilibrium constant at each temperature. Consequently, a log–log plot of the equilibrium pressure of SO_2 *vs.* that for NH_3 should be linear with a slope of $-n$. The plots in Figure 1 clearly show that n = 1 for the three higher temperatures under all conditions and for the lower two temperatures in excess SO_2. The equilibrium constants are the products of the equilibrium reactant gas pressures, and they are listed in Table I. They range from 48 Torr² at 5° to 425 Torr² at 45°.

The equilibrium constant, K, is related to the entropy, ΔS, and enthalpy, ΔH, of reaction through the well-known expression

$$\ln K(\mathrm{atm^2}) = \Delta S/R - \Delta H/RT$$

where T is the absolute temperature. Figure 2 is a semilog plot of K *vs.* $1/T$. The plot is linear. From the slope ΔH is found to be 9.5 kcal/mol, and from the intercept ΔS is found to be 15.3 cal/mol °K. These values have a ±10% uncertainty.

The falloff from linearity in Figure 1 for runs with excess NH_3 at the two lowest temperatures indicate production of the adduct of two NH_3 molecules with one SO_2 molecule. Thus the slope becomes steeper and approaches two. From the very limited data the equilibrium constants are estimated to be 225 Torr³ (0.51×10^{-6} atm³) at 5° and 1030 Torr³ (2.34×10^{-6} atm³) at 15° for the reaction

$$(\mathrm{NH_3})_2 \cdot \mathrm{SO_2(s)} \rightleftharpoons 2\mathrm{NH_3(g)} + \mathrm{SO_2(g)}$$

Thus $\Delta S \sim 82$ cal/mol °K and $\Delta H \sim 23$ kcal/mol, with at least a ±20% uncertainty.

It should be noted that our values for ΔH for both reactions are greater than those reported by Scott, *et al.*,[2] but lower than the value of 30 kcal/mol reported by McLaren, *et al.*[4] If the value of McLaren, *et al.*, refers to the 2:1 adduct, it and our value may agree to within the large experimental uncertainty.

Acknowledgment. The authors wish to thank Drs. K. Olszyna and M. Luria for their help. This work was supported by the Environmental Protection Agency through Grant No. 800874, for which we are grateful.

References and Notes

(1) CAES report No. 320-73
(2) W. D. Scott, D. Lamb, and D. Duffy, *J. Atm. Sci.*, **26**, 727 (1969).
(3) E. McLaren, A. J. Yencha, and J. Kushnir, I.J.G.G. Symposium on Trace Gases, Germany, April 2-5, 1973.
(4) J. P. Friend, R. Leifer, and M. Trichon, *J. Atm. Sci.*, **30**, 465 (1973).

Conductance Measurements of Alkali Metal Trifluoroacetates in Propylene Carbonate

Murray L. Jansen[1] and Howard L. Yeager*

Department of Chemistry, The University of Calgary, Calgary, Alberta, Canada *(Received February 6, 1974)*

Publication costs assisted by the National Research Council of Canada

Precise conductance measurements are reported for the alkali metal trifluoroacetates, tetrapropylammonium chloride, and tetrabutylammonium nitrate in propylene carbonate. Lithium trifluoroacetate is extensively associated, with the formation of ion aggregates at higher concentrations. The degree of association for the trifluoroacetates decreases with increasing size of the alkali metal ion. Single ion mobilities are reported for chloride, nitrate, and trifluoroacetate ions in propylene carbonate.

Introduction

Conductance measurements for a variety of alkali metal and tetraalkylammonium halides and perchlorates in propylene carbonate (PC) have been reported.[2] All salts were found to be essentially unassociated in this solvent of moderately high dielectric constant (64.92 at 25°).[3] Single ion mobilities were derived and discussed in terms of the ion solvating ability of PC.

We have extended this work to study the conductance behavior of the alkali metal trifluoroacetates. Wu and Friedman[4] have measured the heats of solution of these salts in PC. Results indicated that the lithium salt is extensively associated, and the formation of ion pair dimers was suggested. Conductance measurements indicated that the lithium and sodium trifluoroacetates are associated, but no equilibrium constants were calculated.[4] Precise conductance measurements are reported here for these salts, in order to accurately evaluate the influence this more strongly basic anion has on association processes in PC. Association trends are discussed in terms of the relative sizes of the alkali metal ions.

In addition, conductance measurements are reported for tetrapropylammonium chloride and tetrabutylammonium nitrate in order to estimate single ion mobilities for the respective anions. Trends for anion mobilities in PC are discussed.

Experimental Section

The purification of PC has been described previously.[2] Tetra-*n*-propylammonium chloride (Eastman Kodak) was precipitated three times from acetone with ether and dried under vacuum at 150° for 40 hr. Analysis by silver nitrate titration: 99.7%. Tetra-*n*-butylammonium nitrate was prepared by metathesis from tetra-*n*-butylammonium chloride (Eastman Kodak) and silver nitrate (Engelhard Industries Ltd.) in an ethanol–water mixture. The filtrate remaining after removal of silver chloride was evaporated to yield the crude product. The salt was recrystallized three times from ethyl acetate and dried under vacuum at 85° for 72 hr. *Anal.* Calcd: C, 63.12; H, 11.92. Found: C, 63.15; H, 11.70.

Lithium trifluoroacetate was prepared from recrystallized and dried lithium bromide (Research Organic/Inorganic Chemical Corp.) and dried silver trifluoroacetate (Eastman Kodak) in ether. The filtrate remaining after removal of the silver bromide was reduced in volume, and the precipitated salt was dried under vacuum at 60° for 36 hr, and then at 100° for 72 hr. Analysis by cation exchange and acid titration: 99.2%. Sodium, potassium, rubidium, and cesium trifluoroacetates were prepared by adding equivalent amounts of trifluoroacetic acid (Eastman Kodak) to aqueous solutions of the corresponding carbonates, followed by careful reduction in the volume of the solutions to initiate crystallization. Sodium trifluoroacetate was recrystallized three times from a 6:1 dioxane–methanol mixture and then dried under vacuum at 80° for 24 hr and at 125° for 48 hr. Analysis by cation exchange and acid titration: 99.8%. Potassium trifluoroacetate was recrystallized from dioxane and ethanol and dried under vacuum at 130° for 72 hr: analysis 100.0%. Rubidium trifluoroacetate was recrystallized twice from a 1:1 dioxane–ethanol mixture and dried under vacuum at 70° for 1 week: analysis 100.5%. Cesium trifluoroacetate was recrystallized twice from ethyl acetate and dried under vacuum at 60° for 12 hr: analysis 100.3%. The purification of the alkali metal trifluoroacetates proved to be a formi-

TABLE I: Conductance Parameters for 1:1 Electrolytes in PC at 25°

Salt	Λ_0	K_A	J_2	$\sigma\Lambda$
$NaCF_3CO_2$	27.2 ± 1.4	189 ± 58	9318 ± 5340	0.5
	27.2 ± 1.2	189 ± 50	9373 ± 4581	0.6
KCF_3CO_2	29.04 ± 0.009	42.3 ± 0.2	912 ± 37	0.006
	29.04 ± 0.008	42.5 ± 0.2	897 ± 32	0.006
$RbCF_3CO_2$	29.57 ± 0.003	26.7 ± 0.1	419 ± 10	0.001
$CsCF_3CO_2$	30.21 ± 0.002	18.1 ± 0.04	278 ± 7	0.001
Pr_4NCl	28.74 ± 0.004	2.0 ± 0.1	163 ± 33	0.002
	28.70 ± 0.007	2.1 ± 0.2	151 ± 54	0.004
Bu_4NNO_3	29.42 ± 0.003	1.9 ± 0.1	257 ± 20	0.002
	29.39 ± 0.002	1.9 ± 0.1	262 ± 13	0.001

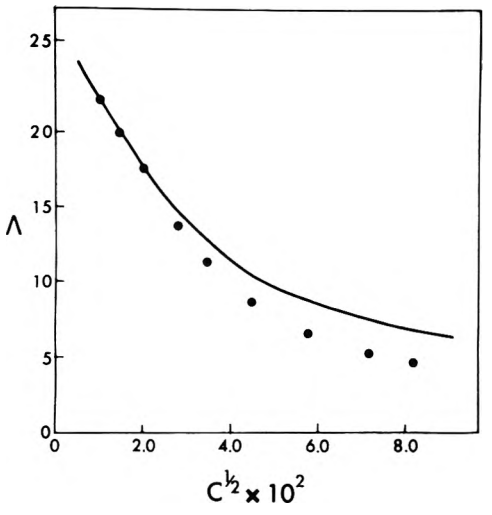

Figure 1. Equivalent conductance *vs.* the square root of molar concentration for lithium trifluoroacetate in PC at 25°. The line shows calculated values assuming Λ_0 = 26.4 and K_A = 1900.

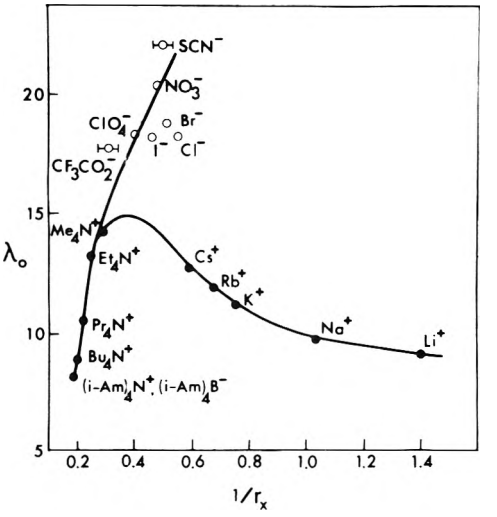

Figure 2. Single ion conductivities in PC *vs.* the reciprocal of estimated crystallographic radii. Lines representing cation and anion trends have no theoretical significance.

dable task; temperatures of drying were found to be a critical factor.[4,5]

The apparatus and procedure used to make the conductance measurements and to measure electrolyte solution densities and viscosities have been described previously.[2] All salt transfers were performed in a glovebox under N_2 atmosphere.

Results

The measured equivalent conductances and corresponding electrolyte concentrations together with solution density and salt viscosity coefficients appear in the microfilm version of this volume of the journal.[6] For all salts except lithium trifluoroacetate, the conductance data were analyzed by the Fuoss-Hsia equation[7,8]

$$\Lambda = \Lambda_0 - S(c\gamma)^{1/2} + Ec\gamma \log c\gamma + (J_1 - B\Lambda_0)c\gamma - J_2(c\gamma)^{3/2} - K_A c\gamma\Lambda f_\pm^2 \quad (1)$$

where the ion pair association constant is given by

$$K_A = (1 - \gamma)/\gamma^2 c f_\pm^2 \quad (2)$$

In eq 1, $S = 0.30464\Lambda_0 + 23.597$, and $E = 0.93398\Lambda_0 - 10.595$. Values of 64.92[3] and 2.513 cP[2] for the dielectric constant and viscosity of PC at 25° were used to calculate the coefficients. In the calculation of J_1 and $f_\pm$, the ion size parameter was set equal to the sum of estimated ionic radii. A computer least-squares program was used to evaluate the adjustable parameters Λ_0, K_A, and J_2. These values with their standard deviations are listed in Table I, along with the standard deviations of fit, $\sigma\Lambda$.

Attempts to analyze the conductance data for lithium trifluoroacetate by eq 1 were unsuccessful. Results indicated that the association behavior of this salt is more complex than ion pairing. A plot of Λ *vs.* $c^{1/2}$ is shown in Figure 1. Also shown is a plot calculated using eq 1, assuming that Λ_0 = 26.4 and K_A = 1900. These values were obtained by a graphical application of the Fuoss-Onsager conductance equation,[9] using only the data for the more dilute solutions. Although the two lines are coincident to a concentration of about 4×10^{-4} *M*, the experimental plot shows marked negative deviation at higher concentrations. We attribute this to the formation of higher ionic aggregates.

Two conductance equations which treat the formation of ion triples in addition to ion pairs were applied to the data. The Kraus equation[10] assumes that both cationic and anionic triple species form, and the Wooster equation[11] assumes that only one kind of triple ion is present. Of the two treatments, the Wooster equation was found to provide a better fit of the data, although even with this equation deviations became large at higher concentrations. A conductance function which assumes the formation of only ion pairs and ion pair dimers was derived and applied to the data, but the fit was poor. We conclude that lithium trifluoroacetate forms a variety of ion aggregate species in PC. Although it was not possible to evaluate all equilibrium constants for these processes, the value of 1900 for the ion pair formation constant is estimated to have an uncertainty of about 30%. The large standard deviation in the least-squares analysis of sodium trifluoroacetate data may indicate a slight amount of ion aggre-

gation as well. Kohlrausch differences calculated from Λ_0 values for alkali metal perchlorates[2] and the corresponding trifluoroacetates differ by about 0.3 units in the worst case.

Discussion

The alkali metal trifluoroacetates show a significant degree of ion pairing, in contrast to the corresponding perchlorates which were found to be unassociated.[2] Lithium chloride and bromide were found to be associated in PC, with K_A values of 557 and 19, respectively.[12] These results indicate that size and distribution of charge on the anion strongly influences association behavior in PC. Presumably the halide salts are associated due to small anion size, whereas the trifluoroacetates ion pair due to the localized charge on the oxygen atoms. In addition, the geometry of the carboxylate group would be expected to yield an ion of enhanced stability, particularly for smaller alkali metal ions. This may help to explain the trend of decreasing association from the lithium to the cesium salts.

This trend in association behavior is opposite to that found for the alkali metal perchlorates in acetonitrile,[13] which shows increasing association with increasing size. This was attributed to the lower ion solvation energies and consequent increased stability of ion pairs for larger cations. In contrast, the trend in association constants for alkali metal trifluoroacetates in PC indicates that ion–ion interactions predominate in determining the stability of ion pairs, and changes in cation–solvent interactions are relatively unimportant. This trend in association constants is the same as those found for a variety of alkali metal carboxylate salts in ethyl methyl ketone.[14] It appears that lithium ion derives greater stabilization from the carboxylate oxygens than could a larger cation such as cesium ion.

Values of single ion mobilities for chloride, nitrate, and trifluoroacetate ions, 18.26, 20.42 and 17.87, respectively, were calculated from Λ_0 values listed in Table I and cation mobilities listed in ref 2. The potassium salt was used to estimate the value for trifluoroacetate, for this salt was found to have the highest purity. These single ion mobilities, along with those of other ions in PC,[2] are plotted *vs.* the reciprocal of estimated crystallographic radii in Figure 2.

The higher anion mobilities have been discussed in terms of the ability of PC to solvate cations more strongly than anions.[2] Of the anion mobilities reported here, even the relatively large trifluoroacetate ion is found to have enhanced mobility over cations of corresponding size. The surprisingly large mobilities of the nitrate and thiocyanate ions might be ascribed to their nonspherical shapes and charge distributions, which could give rise to mechanisms of ion migration which are different from more spherical anions.

Bromide is found to be the most mobile of the halide ions. In some dipolar aprotic solvents the mobilities of the halide ions decrease regularly with increasing ion size, although the reverse trend also occurs.[15] Bromide ion is the most mobile halide ion in acetone.[16] The observed maximum in halide ion mobility in PC could be a combination of two effects. A decrease in the anion size increases the mobility (normal Stokes law behavior), while an increase in anion–solvent interaction lowers the mobility.

Acknowledgments. Financial support by the National Research Council of Canada and the University of Calgary is gratefully acknowledged.

Supplementary Material Available. Equivalent conductance data will appear following these pages in the microfilm edition of this volume of the journal. Photocopies of the supplementary material from this paper only or microfiche (105 × 148 mm, 24× reduction, negatives) containing all of the supplementary material for the papers in this issue may be obtained from the Journals Department, American Chemical Society, 1155 16th St., N.W., Washington, D. C. 20036. Remit check or money order for $3.00 for photocopy or $2.00 for microfiche, referring to code number JPC-74-1380.

References and Notes

(1) From the Ph.D. Thesis of M. L. Jansen, The University of Calgary, 1973.
(2) M. L. Jansen and H. L. Yeager, *J. Phys. Chem.*, **77**, 3089 (1973).
(3) R. Payne and I. E. Theodorou, *J. Phys. Chem.*, **76**, 2892 (1972).
(4) Y.-C. Wu and H. L. Friedman, *J. Phys. Chem.* **70**, 501 (1966).
(5) M. J. Baillie, D. H. Brown, K. C. Moss, and D. W. A. Sharp, *J. Chem. Soc. A*, 3110 (1968).
(6) See paragraph at end of text regarding supplementary material.
(7) R. M. Fuoss and K.-L. Hsia, *Proc. Nat. Acad. Sci. U. S.*, **59**, 1550 (1967).
(8) R. Fernandez-Prini, *Trans. Faraday Soc.*, **65**, 3311 (1969).
(9) R. M. Fuoss and F. Accascina, "Electrolytic Conductance," Interscience, New York, N. Y., 1959.
(10) C. A. Kraus, *J. Amer. Chem. Soc.*, **55**, 2387 (1933).
(11) C. B. Wooster, *J. Amer. Chem. Soc.*, **59**, 377 (1937).
(12) L. M. Mukherjee and D. P. Boden, *J. Phys. Chem.*, **73**, 3965 (1969).
(13) R. L. Kay, B. J. Hales, and G. P. Cunningham, *J. Phys. Chem.*, **71**, 3925 (1967).
(14) S. Crisp, S. R. C. Hughes, and D. H. Price, *J. Chem. Soc. A*, 603 (1968).
(15) B. Kratochvil and H. L. Yeager in "Topics in Current Chemistry," Vol. 27, Springer-Verlag, New York, N. Y., 1972.
(16) M. B. Reynolds and C. A. Kraus, *J. Amer. Chem. Soc.*, **70**, 1709 (1948).

Derivation of the Justice Conductance Equation

Raymond M. Fuoss

Sterling Chemistry Laboratory, Yale University, New Haven, Connecticut 06520 *(Received October 15, 1973)*

Publication costs assisted by the Office of Saline Waters

It is shown that the Justice conductance equation is not a "modification" of the Fuoss-Hsia equation, because it does not describe the behavior of the primitive model (rigid charged spheres in a continuum) used by Fuoss and Hsia. Instead, it is derivable from a model in which the ions are point charges surrounded by impenetrable spheres of radius equal to half the Bjerrum radius $q = \epsilon^2/2DkT$, which is 28 Å at a dielectric constant of 10. Alternatively, the model could be charged spheres of diameter a, surrounded by rigid shells of thickness $(q - a)/2$. It is also shown that the Justice equation does not in general give a unique solution for the parameters which appear as coefficients of the c and $c^{3/2}$ terms of the conductance function, and that, when a unique solution is obtained, the corresponding distance parameter does not always equal q.

Since 1968, the following equation[1-4]

$$\Lambda = \gamma[\Lambda_0 - Sc^{1/2}\gamma^{1/2} + Ec\gamma \log c\gamma + c\gamma J_1(R) - c^{3/2}\gamma^{3/2}J_{3/2}(R)] \quad (1)$$

with R set equal to the Bjerrum distance

$$q = \epsilon^2/2DkT \quad (2)$$

has been used to analyze a number of sets of conductance data. (Here Λ = equivalent conductance, γ = conducting fraction of the stoichiometric concentration c. R is the distance parameter, and the other symbols have their familiar meanings.) The equation has been referred to as "the Justice modification of the Fuoss-Onsager equation," "the Justice version of the Fuoss-Hsia equation," "the Justice-Fuoss equation," *etc.* It is the purpose of this communication to show first that eq 1 does *not* describe the theoretical behavior of the primitive model (charged rigid spheres of diameter a in a continuum) used by Fuoss. It is therefore suggested that eq 1 be called "the Justice equation." Furthermore, it will then be shown that the Justice equation describes the properties of a model in which the ions are represented by charged spheres surrounded by rigid impenetrable shells of thickness $(q - a)/2$. For $D = 40$ and $\mathring{a} = 4.0$, this would correspond to a layer $(280/40 - 4.0)/2 = 1.5$ Å which could conceivably represent a tight solvation sheath around both anions and cations. But for $D > 40$, the average shell would be less than one solvent molecule thick, while for $D < 40$, q rapidly increases; at $D = 10$, $(q - a)/2$ is 12 Å. In the writer's opinion, this model is physically unrealistic and therefore useless in the interpretation of conductance data. Finally, it is shown that the Justice equation does not in general lead to a unique evaluation of the parameters of the conductance equation and that, when it does, the distance parameter R does not always equal the Bjerrum radius. In solvents of high dielectric constant, $R > q$ and for lower dielectric constants, $R < q$; in the intermediate range, of course, $R \approx q$.

We begin with a brief review of the relevant conductance functions. Their derivation began with the integration[5] of the Onsager-Fuoss equation[6] of continuity and the Poisson equation, subject to the boundary conditions for the primitive model. The Poisson equation for the potentials is of second order. The equation of continuity relates the pairwise distribution function[5,6]

$$f_{ji} = n_j n_i \exp\left(-\sum_i \epsilon_i \psi_j / kT\right) \quad (3)$$

to the potentials and likewise is of second order. (Here n_j is the average concentration of ions of species j, *i.e.*, the total number of j ions divided by the total volume of the solution. The exponential function is the Boltzmann factor, which relates local concentrations to average concentrations, in which ϵ_i is the charge on an ion of species i located at a distance r_{ji} from a reference ion of species j where the potential is ψ_j, and kT is a measure of thermal energy.) Consequently four boundary conditions are necessary in order to evaluate the four constants of integration which necessarily appear in the mathematical development. Three of these are electrostatic

$$\psi_j'(\infty) = 0 \quad (4)$$

$$\psi_j'(a - 0) = \psi_j'(a + 0) \quad (5)$$

$$(d\psi_j'/dr)_{a-0} = (d\psi_j'/dr)_{a+0} \quad (6)$$

where ψ_j' is the perturbation potential due to the asymmetry which the external field X generates in the ionic potential, *i.e.*, the relaxation field. The fourth boundary condition[7]

$$[(f_{ji}\mathbf{v}_{ji} - f_{ij}\mathbf{v}_{ij})\cdot\mathbf{r}]_{r=a} = 0 \quad (7)$$

is the mathematical statement of the fact that the *radial components of the relative velocities* of two ions become zero when they come into contact, or to put it more colloquially, rigid spheres (ions) move freely (except for viscous drag) in a continuum until they bump into something solid, such as another ion.

In eq 7, $\mathbf{v}_{ji}$ represents the velocity in a continuum of a sphere with charge ϵ_i at a distance r_{ji} from the reference sphere with charge ϵ_j; it is the vector sum of the velocity of the model ion with respect to the continuum in the element of volume which contains it plus the velocity of the element of volume with respect to a stationary observer (the electrodes). It should be emphasized that $\mathbf{v}_{ji}$ is the velocity of a rigid sphere in a continuum. The experimentally observable quantity $\langle v_i \rangle = \lambda_i X/300F$ (equivalent conductance times field strength in volts over the Faraday

equivalent) is the average value of the components of motion in the field direction which the field superimposes on the Brownian motion of the ions, averaged over a time which is many orders of magnitude greater than the duration of a single Brownian jump. It is $\mathbf{v}_{ji}$ which is the object of our theoretical treatment; in the final comparison of theory and experiment, we equate $\langle \mathbf{v}_i \rangle$ with $|\mathbf{v}_{ji}|$ and thereby test both model and theory. Model and theory are absolutely inseparable.

Evaluation of the relaxation field ΔX by the above integrations and use of the 1932 electrophoratic velocity led to a rather complicated function which, for very low concentrations ($\kappa a < 0.15$), could be reduced to the linearized form

$$\Lambda = \Lambda_0 - Sc^{1/2} + Ec \log c + Jc \qquad (8)$$

Electronic computers were not generally available in 1955; the above simplification was a necessary practicality. It was realized that terms of higher order than those linear in concentration were present in $\Lambda(c)$; in fact, it was found that the semiempirical equation[8,9]

$$\Lambda = \Lambda_0 - Sc^{1/2} + Ec \log c + Jc + J_2c^{3/2} \qquad (9)$$

reproduced within about 0.01Λ unit the conductance of the alkali halides in water up to about 0.1 N, while (8) became useless above $c \approx 0.01$ N. It seemed worthwhile, therefore, to repeat the 1955–1957 calculations to a higher degree of approximation: in effect, with retention of terms of order $c^{3/2}$. This was completed[10] in 1967, giving

$$\Lambda = (\Lambda_0 - \Delta\Lambda_e)(1 + \Delta X/X) \qquad (10)$$

where $\Delta X/X$ is an explicit function of concentration, DT product, viscosity, and a, the distance parameter which appears in boundary condition (7). Combining eq 10, which gives the conductance of free ions, with the equation of mass action, gives the Fuoss-Hsia equation

$$\Lambda = \gamma(\Lambda_0 - \Delta\Lambda_e)(1 + \Delta X/X) \qquad (11)$$

(in which $c\gamma$, of course, is used for the ionic concentration in the electrophoresis and relaxation terms). It should be emphasized at this point that eq 11 derives from the same model as the 1955 equation, using the same boundary conditions in the integration of the same differential equations. The only difference between the 1955 equation and eq 11 is in mathematical detail.

In 1968, Justice[1] proposed that the Fuoss-Onsager equation, in the form which retained some[11,12] of the terms of order $c^{3/2}$, be combined with the equation for association as defined by Bjerrum,[13] *with replacement of the distance parameter a by the Bjerrum radius* $q = \beta/2$. Later,[4,14] a linearized form of the Fuoss-Hsia equation (which contains the $c^{3/2}$ terms which were omitted or missing from the 1957 equation) replaced the 1968 proposal. This was in principle an improvement, possibly partially negated by the replacement of explicit functions by the first few terms of their power series. For example, approximating $f(x) = 1/(1 + x)$ by $(1 - x + x^2)$ is numerically out by 2.5% for $x = 0.3$. These details are trivialities; the significant point is that the Justice equation is obtained by simply writing q everywhere in the Fuoss-Hsia equation where a appeared. However consistency between theory and model then requires that q also replace a everywhere in the mathematical development leading to the Fuoss-Hsia equation, specifically in the fourth boundary condition, eq 7. This would call for zero relative radial component of velocity at a distance $r = q$ from the center of the reference ion; this occurs for the primitive model only for the trivial case when, by coincidence, $a = q$. That is, in general, $a \neq q$, and if (7) is satisfied at $r = a$, it obviously cannot *also* apply to $r = q$ ($>a$); hence the Justice equation is not derivable from the primitive model by the Fuoss-Onsager method of derivation.

It is, however, easy to construct a model which will lead to the Justice equation by the Fuoss-Onsager treatment: surround the ions by concentric rigid impenetrable spheres of radius $q/2$, and assume that these spheres move with the velocity of the ions at their centers. (Alternative equivalent models would be point charges at the centers of rigid spheres of the same dielectric constant as the solvent, or rigid charged spheres with total integrated charge equal to $\pm\epsilon$, or other variations on the theme). Such a model satisfies all four boundary conditions and clearly it is routine to derive the Justice equation: one simply replaces a's by q's everywhere. The implication of the model is that the ion firmly binds a shell of solvent of thickness $(q - a)/2$, so that the relative velocities of the encapsulated ions become zero on contact at center-to-center distance $r = q$, by the fourth boundary condition. For dioxane–water mixtures[2] covering the range $69.90 \leq$ wt % dioxane ≤ 82.82, $19.32 \leq D \leq 10.19$, the Bjerrum radius covers the range $14.50 \leq 10^8 q \leq 27.49$. These are the mixtures in which Justice, Bury, and Treiner[2] measured the conductance of cesium bromide. In order to conform to the model from which the Justice equation can be derived, the cesium and the bromide ions would have to carry rigidly held water shells which would prevent center-to-center distances less than 14.5–27.5 au between the ions counted as pairs. The model appears to be completely unrealistic.

The Justice equation has, however, been fitted to some hundreds[4] of sets of conductance data, within a standard deviation in Λ that ranges[15] from 0.004 to 0.2%; usually the fit is within 0.05%. Examination of the process of calculation of the three parameters Λ_0, K_A, and $J_{3/2}$ leads to three conclusions: (1) the form of the equation (and also of the Fuoss-Hsia equation) guarantees a good fit; (2) if eq 1 is treated as a three parameter equation $\Lambda(c; \Lambda_0, K_A, R)$, a wide range of R values can often be found which give the same good fit to the data; and (3), if we tentatively accept the model of ions centered in icebergs, and let R instead of $J_{3/2}$ be the third parameter [*i.e.*, $\Lambda = \Lambda(c; \Lambda_0, K_A, R)$, where the *same* distance parameter is used in *both* coefficients J_1 and $J_{3/2}$], it is found that $R > q$ in solvents of high dielectric constant (50–100), that $R < q$ in solvents of lower dielectric constant (10–30), and that R does not differ greatly from q in the intermediate range. Regarding (1), we make the additional comment: if a given theoretical equation does *not* fit the data within the experimental tolerance, we may with complete confidence assert that either the theory or the model on which it is based (or both) cannot be correct. Unfortunately the converse does not hold. It would be possible to find an infinite set of three-parameter functions which would fit within a given tolerance a set of say six–ten Λ–c points covering a 10:1 range in concentration. In other words, "goodness of fit" is an invalid criterion against which to test the credibility of any equation.

The reason why the Justice equation (or the Fuoss-Hsia equation, or in fact any three-parameter equation which includes the theoretically predictable $Sc^{1/2}$ and Ec log c

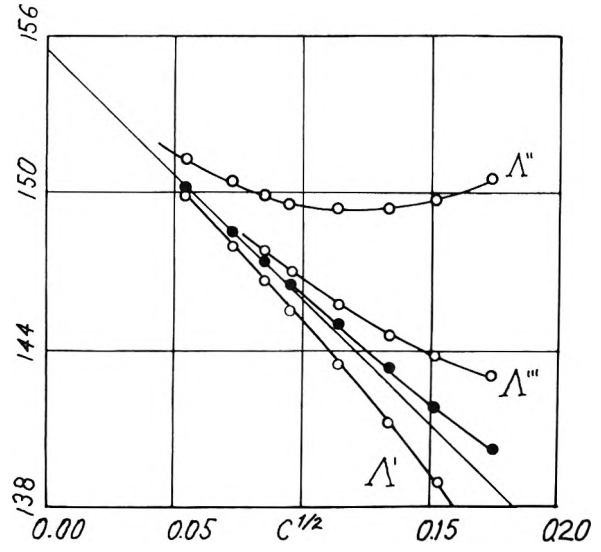

Figure 1. Conductance functions for cesium bromide in water at 25°: solid circles, Λ (obsd).

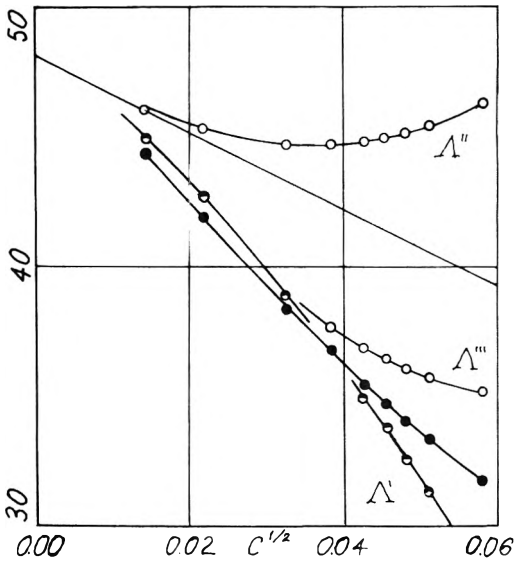

Figure 2. Conductance functions for cesium bromide in water–dioxane, 30–70 by weight: solid circles, Λ (obsd).

terms) fits the data so well is shown graphically in Figures 1 and 2. By substitution of γ from the mass action equation

$$1 - \gamma = K_A c\gamma^2 f^2 \tag{12}$$

eq 1 becomes

$$\Lambda = \Lambda_0 - Sc^{1/2}\gamma^{1/2} + Ec\gamma \log c\gamma + c\gamma J_1(R) - (c\gamma)^{3/2}J_{3/2}(R) - K_A c\gamma f^2 \Lambda \tag{13}$$

Now define three quantities Λ', Λ'', and Λ''' as follows

$$\Lambda' = \Lambda_0 - Sc^{1/2}\gamma^{1/2} + Ec\gamma \log c\gamma \tag{14}$$

$$\Lambda'' = \Lambda' + c\gamma J_1(R) \tag{15}$$

$$\Lambda''' = \Lambda'' - K_A c\gamma f^2 \Lambda \tag{16}$$

Figure 1 shows Λ (obsd), Λ', Λ'', and Λ''' for cesium bromide in water[2] and Figure 2 the same functions for cesium bromide in a water–dioxane mixture[2] containing 70% dioxane (D = 19.32). The limiting tangent with slope S is the straight line. Λ' is the theoretically predictable part of the conductance (given Λ_0); the *difference* between Λ (obsd) and Λ', which clearly is much smaller than Λ (obsd), is that part of the observed conductance which must serve to evaluate J_1, $J_{3/2}$, and K_A. If we add the J_1 term to Λ, we get Λ'', which now lies above Λ (obsd), and above by an amount which depends entirely on what value of R is used to compute the coefficient $J_1(R)$. In the Justice method of computation, R is usually set equal to q. Now in order to get back down to Λ(obsd), two terms are subtracted, the ion pair term (giving Λ''') and the $J_{3/2}$ term. The first is of leading order c and the second of order $c^{3/2}$, so that

$$\Delta\Lambda''' = \Lambda(\text{obsd}) - \Lambda''' = -Ac - Bc^{3/2} + \text{higher terms} \tag{17}$$

This termwise breakdown of $\Lambda(c)$ shows that what actually is done to evaluate K_A and $J_{3/2}$ is in effect to put the best straight line through the function

$$F(c) = \Delta\Lambda'''/c \tag{18}$$

where $F(c)$ is determined by the value of the J_1 term. Since [Λ(obsd) − Λ'''] is usually less than a tenth of Λ(obsd), a fit to (17) within 0.5% thus appears as a 0.05% fit to Λ(obsd). As a matter of fact, however, the observable being fitted is not [Λ(obsd) − Λ''']; it is $\Delta\Lambda' = [\Lambda(\text{obsd}) - \Lambda']$, a difference which is even smaller, as can be seen in Figures 1 and 2. To reduce the goodness-of-fit argument to its essentials, we have

$$\Delta\Lambda' = +J_1 \text{ term} - (J_{3/2} \text{ and } K_A) \text{ terms} \tag{19}$$

and one is merely compensating an arbitrarily chosen positive J_1 term by the sum of two negative ones. With two degrees of freedom, it is not surprising that the equation fits the data, especially when we recall that only a fair fit to $\Delta\Lambda'$ corresponds to at least a ten times better fit to Λ(obsd).

Let us now consider what happens if other values than $R = q$ are used to evaluate J_1. A computer program was written to answer the following: given a set of data points (c_j, Λ_j; j = 1, . . . ,n) and a sequence of values of R, find the values of Λ_0, $J_{3/2}$, and K_A which best fit the data to eq 13. The results of such a calculation are shown in Figure 3 for cesium bromide in a water–tetrahydrofurane mixture[2] containing 50% THF (D = 40.0). The abscissa is R/q, the ratio of the input R to the Bjerrum radius; calculations were made for R values equal to two thirds the Bjerrum radius up to twice as large. Over this wide range, σ, the standard deviation expressed as percentage of the limiting conductance

$$\sigma = (100/\Lambda_0)\,\Sigma[\Lambda(\text{obsd}) - \Lambda(\text{calcd})]^2/(n-2)\}^{1/2} \tag{21}$$

was practically constant, equal to 0.015–0.016%. Plotted are the values of $J_{3/2}$ and $K_A\Lambda_0$ delivered by the computer, and the values of $J_1(R)$, calculated[14] from the *input* values of R. As R increases, all three coefficients increase, and in such a way that the sum of the corresponding terms of eq 13 matches the experimental $\Delta\Lambda'$–c curve so well that σ has the "excellent" value of 0.015%, regardless of the value chosen for the center-to-center distance of a pair of ions in the Justice model, where *radial component of velocity* must vanish at $r = R$. If R is set equal to q, we can indeed find values of $J_{3/2}$ and K_A which fit these data to 0.015%, but so will $2q/3$ or $2q$, or anything between. Put in different terms, what results is not a unique solu-

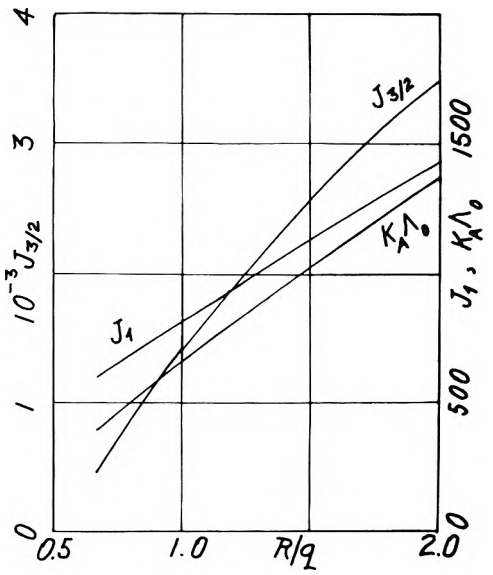

Figure 3. Parameters of eq 1 for cesium bromide in tetrahydrofurane–water, 50–50 by weight.

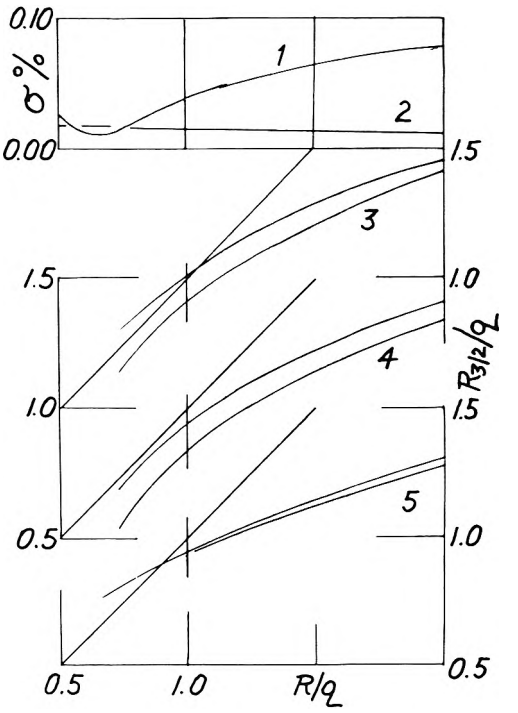

Figure 4. Curve 1 shows the standard deviation of eq 21 for CsBr in 70% dioxane. Curve 2 shows the same for CsBr in water. Curves 3 shows the dependence on R (input)/q of R/q calculated from $J_{3/2} \pm \Delta J_{3/2}$ for CsBr in water; ordinate scale, upper right. Curves 4 is the same for CsBr n 50% THF; ordinate scale, left center. Curves 5 is the same for CsBr in 70% dioxane; ordinate scale, lower right.

tion for the parameters $J_{3/2}$ and K_A, but a band of solutions. To quote Evans,[16] "what is worrisome is that what one gets out as K_A is essentially what was put in as q."

Finally, it can be shown that the value of R calculated from the output value of $J_{3/2}$ in general does *not* equal the value of R which was used to compute J_1, although it is nearly equal to the input R when the latter is not greatly different from q. The abscissae in Figure 4 are also the ratios R (input)/q (Bjerrum). The ordinates are the ratios to q of the R's calculated from the output values of $J_{3/2}$. Results for cesium bromide in water, 50% THF, and 70% dioxane are shown. If R (input) = R (output), *i.e.*, if the same distance parameter gave the values of J_1 and $J_{3/2}$ required to fit the data, the plot would be a 45° line. The bands shown correspond to the R's calculated from $J_{3/2} \pm \Delta J_{3/2}$ where $\Delta J_{3/2}$ is the uncertainty in $J_{3/2}$ corresponding to the standard deviation σ, defined by (21). It will be seen that $R(J_{3/2})$ equals $R(J_1)$ for $2q/3 < R < q$ for CsBr in water, that $R(J_{3/2}) < R(J_1)$ for the THF system, and that the (rather narrow) band of $R(J_{3/2})$ values crosses the 45° line for the dioxane system, R (input) being equal to R (output) for $R = 0.90q$. Furthermore, in solvents of lower and higher dielectric constants, the insensitivity of σ to the choice of input R disappears, as shown by the plots at the top of Figure 4. For water, $\sigma = 0.011\%$ for $R = 2q$ and gradually increases to 0.017% at $R = 2q/3$, showing that here there is a better fit for r greater than the Bjerrum distance. As already mentioned, σ for the THF system is practically independent of the distance parameter. For the dioxane system (where $q = 14.50$ Å), a distinct minimum in the $\sigma - R/q$ plot appears at about $0.6q = 8.7$ Å. These examples show that, if the same distance parameter is used in both J_1 and $J_{3/2}$, the value which gives the best fit will in general not equal q, while, if $J_1(R)$ be set equal to $J_1(q)$, the coefficient $J_{3/2}$ then leads to a value of R not in general equal to q.

Acknowledgment. This work was supported by a grant from the Office of Saline Water, U. S. Department of the Interior, under Contract No. 14-01-0001-1308.

References and Notes

(1) J. C. Justice, *J. Chim. Phys.*, **65**, 353 (1968).
(2) J. C. Justice, R. Bury, and C. Treiner, *J. Chim. Phys.*, **65**, 1708 (1968).
(3) M. C. Justice, R. Bury, and J. C. Justice, *Electrochim. Aca*, **16**, 687 (1971).
(4) J. C. Justice, *Electrochim. Acta*, **16**, 701 (197[illegible]).
(5) R. M. Fuoss and L. Onsager, *J. Phys. Chem.*, **61**, 668 (1957); *Proc. Nat. Acad. Sci. U. S.*, **41**, 274, 1010 (1955).
(6) L. Onsager and R. M. Fuoss, *J. Phys. Chem.*, **36**, 2689 (1932).
(7) Reference 5, eq 3.4.
(8) K. L. Hsia and R. M. Fuoss, *J. Amer. Chem. Soc.*, **90**, 3055 (1968).
(9) Y. C. Chiu and R. M. Fuoss, *J. Phys. Chem.*, **72**, 4123 (1968).
(10) R. M. Fuoss and K. L. Hsia, *Proc. Nat. Acad. Sci. U. S.*, **57**, 1550 (1967); correction, *ibid.*, **58**, 1818 (1967).
(11) R. M. Fuoss, *J. Chim. Phys.*, **66**, 1191 (1969).
(12) J. C. Justice, *J. Chim. Phys.*, **66**, 1193 (1969).
(13) N. Bjerrum, *Kgl. Dan. Vidensk. Selsk.*, **7**, No. 6 (1926).
(14) R. Fernandez-Prini, *Trans. Faraday Soc.*, **65**, 3311 (1969).
(15) Reference 4, Table VII.
(16) M. A. Matesich, J. Knoefel, H. Feldman, and D. F. Evans, *J. Phys. Chem.*, **77**, 366 (1973).

Interfacial and Micellar Properties of Bolaform Electrolytes

F. M. Menger*[1] and Simeon Wrenn[2]

Department of Chemistry, Emory University, Atlanta, Georgia 30322 *(Received February 20, 1974)*

Publication costs assisted by the National Science Foundation

Critical micelle concentrations, molecular areas, coareas, and standard free energies of adsorption at an air-water interface have been determined for a series of bolaform electrolytes ($R_3N^+-(CH_2)_n-^+NR_3$ where R = methyl or *n*-butyl and *n* = 4, 8, and 12). The parameters are compared with those of mono-quaternary ammonium salts, $CH_3(CH_2)_{11}{}^+NR_3$. It is found that the C_{12} bolaform electrolytes (but not the C_4 and C_8 homologs) form vertical loops or "wickets" at the air-water interface.

Introduction

Organic molecules possessing two positive or negative sites separated by relatively great distances have been euphoniously designated "bolaform electrolytes."[3] This paper concerns itself with dicationic bolaforms of the general structure

$$R_3\overset{+}{N}-(CH_2)_n-\overset{+}{N}R_3$$
$$R = Me,\ n\text{-}Bu$$
$$n = 4,\ 8,\ 12$$

We will represent the various bolaforms as C_4Me_6, C_8Bu_6, etc., depending on the chain length and alkyl group on the nitrogen. A simple surfactant such as dodecyltrimethylammonium ion will be abbreviated $C_{12}Me_3$.

Bolaform electrolytes have not received all the attention they deserve. The compounds can display physiological activity,[4] bind to polymers,[5,6] associate in water,[7] and form crystalline clathrates.[8] Additional references can be found in a few recent articles.[9-11] Our interest in bolaforms stems from our previous work with amphiphilic substances,[12,13] and from the obvious resemblance of bolaforms to the pairs of lipid molecules which comprise biological membranes.[14] We have collected surface tension and kinetic data with the objective of learning more about the interfacial and micellar properties of the homologous series of bolaform electrolytes. Critical micelle concentrations, molecular areas, coareas, and standard free energies of adsorption have been determined. We also focused on the interesting question of whether or not bolaform electrolytes form "wickets" at the air-water interface.

Experimental Section

Preparation of Compounds. The preparation of octane-1,8-bis(trimethylammonium) dibromide (C_8Me_6) typifies the procedure used for all the bolaforms. 1,8-Dibromooctane (25.10 g, 0.092 mol) and anhydrous trimethylamine (30.0 g, 0.51 mol) in 25 ml of absolute ethanol were boiled under reflux for 47 hr. The material obtained after removal of the solvent with a rotary evaporator was crystallized from ethanol–ether. The crystals were then dried in a vacuum desiccator at ambient temperature and 1-mm pressure for 12 hr to give 33.70 g (94%) of the desired product, mp 298–300° dec (lit.[15] >280°). Since the ir spectrum showed the presence of water, the compound was dried again at 2 mm and 110°. Elemental analysis and melting point data are given in Table I. Bolaforms were routinely tested for the presence of primary and secondary amines.[16]

Surface Tension Measurements. Surface tensions were obtained with a Fisher Model 21 Tensiomat (employing the de Nouy ring method) after calibration of the torsion wire. A freshly prepared aqueous bolaform solution was poured into a clean 50-ml beaker with a mean diameter of 39–40 mm. Apparent surface tensions were measured a minimum of 10 times by manual control of the dial. The platinum–iridium ring was then removed, rinsed with distilled water, flamed, dipped while hot into dilute HCl, rinsed with distilled water, and flamed a second time in preparation for the next measurement. Since the experiments were carried out at ambient temperature, the room temperature was recorded immediately after the last surface tension reading for each solution. The dew point and barometric pressure were also noted.

Apparent surface tensions were multiplied by a correction factor F, calculated from eq 1 as supplied with the

$$F = 0.7250 + \sqrt{\frac{0.01452P}{S^2(D-d)} + 0.04534 - 1.679r/R} \quad (1)$$

tensiometer, in order to secure absolute surface tensions. R, r, and S are the radius of the ring, the radius of the wire of the ring, and the circumference of the ring (all in cm), respectively; P is the apparent surface tension reading in dyn/cm; D and d are the densities of the aqueous solution and the air above the interface in g/cm^3. The value of R/r was furnished with the ring when it was purchased. The density of the moist air in g/cm^3 was calculated from eq 2 where T is the absolute temperature, B is

$$d = 0.0012929(273.13/T)[(B - 0.3783e)/760] \quad (2)$$

the barometric pressure in mm, and e is the vapor pressure of the moisture in the air in mm.[17] Correction factors obtained *via* eq 1 agreed to better than 0.2% with those obtained by Harkins and Jordan.[18] Likewise, the absolute surface tension of pure water agreed to within 0.2% of the literature value.[19]

Kinetics. The kinetic methods were very similar to those in a previous publication.[12]

Results

Surface area calculations were based upon the Gibbs adsorption equation for a 2:1 electrolyte with no added

TABLE I: Melting Point and Analytical Data for the Bolaform Electrolytes

Bolaform[f]	Mp, °C	Lit. mp, °C	Calcd, % C	Calcd, % H	Calcd, % N	Found, % C	Found, % H	Found, % N
C_4Me_6	348–349	320[a]	35.95	7.84	8.38	35.66	8.15	8.36
C_4Bu_6	155–156		57.33	10.65	4.78	57.52	10.67	4.82
C_8Me_6	298–300	>280[b]	43.09	8.78	7.18	42.96	8.93	6.91
C_8Bu_6	122–123	123–125[c]	59.80	10.98	4.36	59.96	11.09	4.16
$C_{12}Me_6$	229.5–230	228.5–230.5[d]	48.44	9.48	6.28	48.21	9.68	6.09
$C_{12}Bu_6$	*e*		61.87	11.25	4.01	61.69	11.20	4.17

[a] E. J. Gabbay, *Biochemistry*, **5**, 3036 (1966). [b] Reference 15. [c] Reference 8. [d] R. B. Barlow and A. Zoller, *Brit. J. Pharmacol.*, **23**, 131 (1964). [e] This compound is a viscous pale yellow oil which did not crystallize upon cooling in a Dry Ice–acetone bath or after sitting in a refrigerator for several months. [f] All bolaforms are dibromide salts.

salt[20]

$$\Gamma = \frac{-1}{3RT}\frac{d\gamma}{d \ln C} \quad (3)$$

where γ, C, and Γ denote surface tension in dyn/cm, bulk concentration in molarity, and surface excess in mol/cm^2, respectively. Equation 4 (where N = Avogadro's number)

$$A = 10^{16}/\Gamma N \quad (4)$$

gives the surface area in Å^2 per molecule. Two methods were used to secure the surface areas. First, the rectilinear midportions of γ *vs.* log C plots[21] were selected visually. The slopes of these lines, obtained by a least-squares treatment, were inserted into eq 3 to obtain Γ and hence A. In the second method, we fitted γ *vs.* ln C data to a second-order polynomial of the form $\gamma = A_1 + A_2 \ln C + A_3 (\ln C)^2$ utilizing either a Marquardt[22] or Hartley[23] algorithm. The values of the first derivatives of γ with respect to ln C at appropriate values of C were then substituted into the Gibbs isotherm. The coefficients of the nonlinear regression are listed in Table II for seven surfactants.

The surface pressure (π in dyn/cm) at a given bolaform electrolyte concentration was obtained from the difference between the surface tension of pure water and that of the solution. At low surfactant concentrations, surface activity coefficients equal unity, and π is linearly related to C. This is seen in Figure 1 for $C_{12}Me_3$ and $C_{12}Me_6$. If C is small, the standard free energy of adsorption in kcal/mol of a surfactant at an air–water interface is given by eq 5 (where α is the slope of the π *vs.* C plot at low C).[24,25]

$$\Delta G^\circ_{A\text{-}W} = -RT \ln \left(\frac{d\pi}{dC}\right)_{C=0} = -RT \ln \alpha \quad (5)$$

Surface tension data, treated as described above, led to the following conclusions concerning interfacial and micellar properties of bolaform electrolytes in aqueous solutions in the absence of added salts.[26]

(1) C_4Me_6 shows no surface activity or indication of micellization over the concentration range studied (0.005–0.100 *M*). In contrast, C_4Bu_6 displays surface activity (*e.g.*, γ = 57.5 at 0.100 *M* and 24° compared with γ = 72.1 for pure water at 24°). The cmc of C_4Bu_6, if one exists, must exceed the highest concentration studied (0.505 *M*).

(2) C_8Me_6 exhibits surface activity (*e.g.*, γ = 63.4 at 0.100 *M* and 22°),[27] but its cmc, if one exists, must be greater than 0.504 *M*. The same holds true for C_8Bu_6 for which γ = 53.7 at 0.100 *M* and 24.5°. Comparison of C_4Bu_6 with C_8Bu_6 shows that the latter is somewhat more surface active, which is consistent with the generalization that for a given head group the surface adsorption increases (and the cmc decreases) with increasing chain length.

(3) Both $C_{12}Me_6$ and $C_{12}Bu_6$ form micelles as evidenced by sigmoidal γ *vs.* log C plots of the type first observed by Milner.[28] Such a plot for $C_{12}Bu_6$ is shown in Figure 2 along with that for $C_{12}Bu_3$. Although the curve for $C_{12}Bu_3$ is seen to have a sharp transition at its cmc, this is not the case for the bolaform electrolyte. The wide micellization range for $C_{12}Bu_6$ may mean, if the "mass action" theory of micelle formation[29] is correct, that the aggregation number of the micelle is small. We estimate that the cmc values for $C_{12}Me_6$ and $C_{12}Bu_6$ are 0.02–0.03 and 0.002–0.004 *M*, respectively. Addition of NaCl or Na_2SO_4 to maintain an ionic strength of 1.0 lowers the cmc of $C_{12}Me_6$ by a factor of 3–4. The absence of a minimum at the cmc in Figure 2 is a good indication of bolaform purity.[30]

TABLE II: Calculated Coefficients of the Second-Order Non-Linear Regression Equation Fitted to the Experimental Data[a]

Surfactant	Coefficients A_1	Coefficients A_2	Coefficients A_3
C_4Bu_6	42.85	−7.975	−0.5776
C_8Me_6	42.32	−12.65	−1.371
C_8Bu_6	41.05	−6.449	−0.3437
$C_{12}Me_6$	−71.50	−35.73	−2.268
$C_{12}Bu_6$	−57.82	−22.95	−1.036
$C_{12}Me_3$	−81.13	−36.29	−2.161
$C_{12}Bu_3$	−85.02	−26.69	−1.144

[a] Surface tensions may be calculated at various surfactant concentrations with an accuracy of ±2% using the equation $\gamma = A_1 + A_2 \ln C + A_3 (\ln C)^2$.

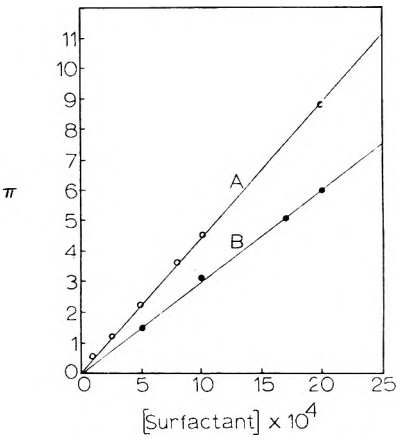

Figure 1. Plots of surface pressure (π, dyn/cm) *vs.* concentration of (A) $C_{12}Me_3$ and (B) $C_{12}Me_6$ in the ideal region.

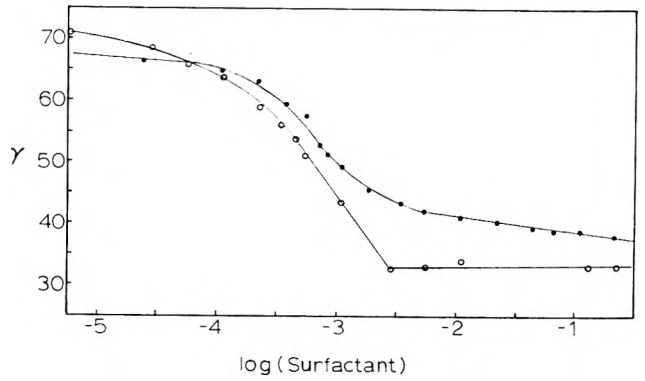

Figure 2. Plots of surface tension (γ, dyn/cm) *vs.* log of the concentration of $C_{12}Bu_3$ (○) and $C_{12}Bu_6$ (●).

TABLE III: Surface Areas and Standard Free Energies of Adsorption for Mono and Bis Quaternary Ammonium Salts

Surfactant[a]	Area, Å²/molecule[b]	$\Delta G°_{A-W}$, kcal/mol
C_4Bu_6	216	−3.53
C_8Me_6	151	−2.38
C_8Bu_6	258	−4.46
$C_{12}Me_6$	107	−4.72
$C_{12}Bu_6$	146	−6.68
$C_{12}Me_3$	55	−4.95
$C_{12}Bu_3$	73	−6.95

[a] All salts have bromide counterions. [b] Estimated uncertainty = ±5%.

(4) Molecular areas at the air-water interface are presented in Table III. These surface areas were calculated using the rectilinear portion of γ *vs.* log C plots. In this region of "saturation adsorption,"[31] the area per molecule is practically independent of bulk concentration and surface pressure. For our purposes it is unnecessary to attach physical significance to the area parameter; we simply regard the areas as measures of the relative degree of interfacial surface occupied by adsorbed surfactants. $C_{12}Me_3$ has a surface area of 55 Å²/molecule which is consistent with the value of 61 Å²/molecule for $C_{14}Me_3$ obtained by other workers.[32] Importantly, comparison of the C_{12} compounds in Table III shows that the bolaforms have twice the surface area as their "one-headed" counterparts.

(5) Standard free energies of adsorption, listed in Table III, were calculated by inserting the slopes of π *vs.* C plots (Figure 1) into eq 5.[33] The free energy of adsorption per methylene for the bis(trimethyl)ammonium derivatives is found to be −0.59 kcal/mol in good agreement with a literature value of −0.60 kcal/mol obtained with another system.[34] One-fourth the difference in free energies between $C_{12}Bu_6$ and C_8Bu_6 gives a $\Delta G°_{A-W}$ per methylene = −0.56 kcal/mol for the bis(tributyl)ammonium bolaforms.

Discussion

Bis(tributyl)ammonium bolaforms are more surface active than their bis(trimethyl)ammonium homologs. For example, C_4Me_6 exhibits no surface activity, whereas 0.100 M C_4Bu_6 lowers the surface tension of water by about 15 dyn/cm. From Table III it is evident that both C_8Bu_6 and $C_{12}Bu_6$ have more favorable free energies of adsorption (by 2 kcal/mol) than the corresponding methylated bolaforms.

Compelling evidence exists that $C_{12}Me_6$ and $C_{12}Bu_6$ assume "wicket-like" conformations (Figure 3) at the air-water interface. Thus, the $C_{12}Me_6$ and $C_{12}Bu_6$ have surface areas which are, respectively, twice those of $C_{12}Me_3$ and $C_{12}Bu_3$ (Table III). Under the relatively high pressures where the surface areas were determined, C_4Bu_6, C_8Me_6, and C_8Bu_6 have *larger* molecular areas than any member of the C_{12} series (Table III). Therefore, C_4 and C_8 compounds seem to resist vertical looping, prefering instead to lie horizontally on the water surface in a gaseous soluble film. Resistance of C_4Bu_6 to buckling is not surprising in view of the well-known preference of butane to assume the anti conformation rather than the eclipsed conformation. Pressure-area curves[26] support the "wicket" hypothesis. For example, although C_8Me_6 and $C_{12}Me_6$ have similar areas at low pressures (π < 5 dyn/cm), C_8Me_6 gives a more expanded monolayer (*i.e.*, a greater area for a given value of π) at π > 10 dyn/cm.

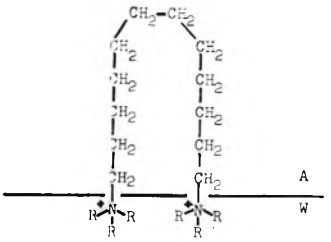

Figure 3. Schematic representation of the orientation of $C_{12}Me_6$ and $C_{12}Bu_6$ dibromides at an air–water interface with high surface pressure.

The coareas, A_0, of the bolaform electrolytes are also relevant to the question of molecular configuration at the air-water interface. Coareas are calculated from the slopes of πA *vs.* π plots which, according to the Amagat equation (eq 6),[35] are linear for many films at higher values of π.

$$\pi A = \pi A_0 + \text{constant} \qquad (6)$$

The parameter is useful in that it approximates the cross-sectional areas of the interfacial molecules. Hence, A_0 is smaller than the surface area A which incorporates both the molecular area and the area of the solvation layers.[31] On the other hand, A_0 sometimes exceeds the true molecular area owing to thermal effects. The coarea of $C_{12}Me_3$, 31 Å²/molecule, is consistent with the area of 28 Å²/molecule determined with the aid of molecular models and with the assumption that the dodecyl chain is aligned perpendicular to the interface. The coarea of $C_{12}Me_6$ is 58 Å²/molecule, in agreement with the theoretical value of 54 Å²/molecule obtained by assuming a "wicket" configuration. If C_8Me_6 lies horizontally at the interface with no arching, the expected area is roughly 102 Å²/molecule; the experimental value is 87 Å²/molecule.

The remainder of this discussion will be devoted to the micellar properties of bolaform electrolytes. As we pointed out in the Results section, $C_{12}Me_6$ and $C_{12}Bu_6$ (but not the C_4 and C_8 compounds) form micelles. Since Pearson[36] feels that $C_{10}Me_6$ is not micellar in the usual sense of the word, bolaforms of the type C_nMe_6 do not form micelles at less than 0.1 M unless $n \geq 12$. $C_{12}Me_6$ has a cmc of 0.02–0.03 M, as determined by surface tension measurements, which is surprisingly close to the cmc of 0.012 M for $C_{12}Me_3$. Owing to the fact that cmc determinations often depend upon the experimental method,[37] we also measured the cmc of $C_{12}Me_6$ by the spectral shift technique[38] using the absorbance of Orange II at 500 nm and 25.0°. The cmc obtained in this way falls within the range of 0.04–0.05 M. $C_{12}Bu_6$ is endowed with a cmc many fold smaller than that of $C_{12}Me_6$; this probably reflects a more

favorable entropy of micellization for the larger head group.[39] Standard free energies of micellization[40] for $C_{12}Me_6$ and $C_{12}Bu_6$ favor formation of the latter by 1.2 kcal/mol.

Adsorption onto or into micelles often perturbs the reaction rates of organic molecules.[41,42] Analysis of the rate data using the equations of Menger and Portnoy[12] allows the evaluation of substrate-micelle association constants as well as the reaction rate of adsorbed material. We have applied this kinetic method to bolaform systems. C_4Me_6 was found to have a negligible effect on the hydrolysis rate of *p*-nitrophenyl dodecanoate at pH 12.00 and 25.0° (*e.g.*, the rate increases 10% upon addition of 0.100 *M* C_4Me_6). On the other hand, 0.100 *M* $C_{12}Me_6$ enhances the rate of ester hydrolysis 28-fold. A log k_{obsd} *vs.* [$C_{12}Me_6$] plot is sigmoidal with a flex point near 0.04 *M*. Since this concentration corresponds to the cmc determined from surface tension and spectral data, the rate increases must be micellar in origin. Unfortunately, the transition at the cmc is not sufficiently sharp to permit an accurate evaluation of ester-micelle association constants. Experiments with *p*-nitrophenyl octanoate in $C_{12}Me_6$ solutions show that 0.08 *M* bis quaternary ammonium salt increases the hydrolysis rate only twofold; the effect of $C_{12}Me_3$ is much larger.[12] It appears then that either $C_{12}Me_3$ binds hydrophobic substrates more efficiently than does $C_{12}Me_6$ or else the $C_{12}Me_3$ micelle has a higher concentration of catalyst (*i.e.*, hydroxide ion) at its surface where hydrolysis of bound ester takes place.

One of the main conclusions of this paper is that C_{12} bolaform electrolytes fold at the air-water interface. At present it is not known whether a bolaform molecule is also folded within a micelle or whether it extends linearly across the entire width of the micelle. Characterization of the size, shape, and molecular weight of bolaform micelles would remove this uncertainty.

Acknowledgment. This work has been supported in part by grants from the National Science Foundation and National Institutes of Health.

References and Notes

(1) Recipient of a Camille and Henry Dreyfus Foundation Teacher-Scholar Grant and a National Institutes of Health Research Career Development Award.
(2) Participant in the Emory University Medicinal Chemistry Program supported by the National Institutes of Health (Grant No. GM01970).
(3) O. V. Brody and R. M. Fuoss, *J. Phys. Chem.*, **60**, 156 (1956).
(4) C_6Me_6 is an antihypertensive. P. G. Stecher, Ed., "The Merck Index," 8th ed, Merck and Co., Rahway, N. J., 1968, p 528.
(5) H. Morawetz and A. Y. Kandanian, *J. Phys. Chem.*, **70**, 2995 (1966).
(6) S. Ehrenpreis and M. G. Kellock, *Biochim. Biophys. Acta*, **45**, 525 (1960).
(7) R. M. Fuoss and V. F. H. Chu, *J. Amer. Chem. Soc.*, **73**, 949 (1951).
(8) T. L. Broadwater and D. F. Evans, *J. Phys. Chem.*, **73**, 164 (1969).
(9) O. D. Bonner and S. Kim, *J. Phys. Chem.*, **73**, 1367 (1969).
(10) S. Lindenbaum, *J. Phys. Chem.*, **73**, 4334 (1969).
(11) G. L. Collins and J. Smid, *J. Amer. Chem. Soc.*, **95**, 1503 (1973).
(12) F. M. Menger and C. E. Portnoy, *J. Amer. Chem. Soc.*, **89**, 4698 (1967).
(13) F. M. Menger and M. J. McCreery, *J. Amer. Chem. Soc.*, **96**, 121 (1974).
(14) W. D. Stein, "The Movement of Molecules across Cell Membranes," Academic Press, New York, N. Y., 1967.
(15) R. B. Barlow and H. R. Ing, *Brit. J. Pharmacol.*, **3**, 298 (1948).
(16) F. Feigl, "Qualitative Analysis by Spot Tests," Elsevier, New York, N. Y., 1946.
(17) "Handbook of Chemistry and Physics," R. C. Weast, Ed., 50th ed, Chemical Rubber Publishing Co., Cleveland, Ohio, 1969, p F-9.
(18) W. D. Harkins and H. F. Jordan, *J. Amer. Chem. Soc.*, **52**, 1751 (1930).
(19) J. J. Jasper, *J. Phys. Chem. Ref. Data*, **1**, 841 (1972).
(20) J. T. Davies and E. K. Rideal, "Interfacial Phenomena," Academic Press, New York, N. Y., 1961, p 196.
(21) A typical plot of this type is shown in L. I. Osipow, "Surface Chemistry," Reinhold, New York, N. Y., 1962, p 127.
(22) D. W. Marquardt, *J. Soc. Indust. App. Math.*, **11**, 431 (1968).
(23) H. O. Hartley, *Technometrics*, **3**, 269 (1961).
(24) N. D. Weiner and G. Zografi, *J. Pharm. Sci.*, **54**, 436 (1965).
(25) J. Betts and B. Pethica, *Proc. 2nd Int. Congr. Surface Activity*, **1**, 152 (1957).
(26) For the sake of brevity, many results are summarized only in sentence form. For detailed tabular and graphical data, see the Ph.D. Thesis of S. Wrenn entitled "Interfacial and Micellar Properties of Bolaform Electrolytes" (Part I).
(27) Since the surface tension of water changes only 0.15 dyn cm^{-1} deg^{-1} near room temperature, the 3° temperature range over which the data were collected is not serious.
(28) S. R. Milner, *Phil. Mag.*, **13**, 96 (1907).
(29) D. J. Shaw, "Introduction to Colloid and Surface Chemistry," Butterworths, London, 1966, p 69.
(30) L. Shedlovsky, J. Ross, and C. W. Jakob, *J. Colloid Sci.*, **4**, 25 (1949).
(31) F. V. Vader, *Trans. Faraday Soc.*, **56**, 1067 (1960).
(32) R. L. Venable and R. V. Nauman, *J. Phys. Chem.*, **68**, 3498 (1964).
(33) D. W. Blois and J. Swarbrick, *J. Colloid Interface Sci.*, **36**, 226 (1971).
(34) I. Langmuir, *J. Amer. Chem. Soc.*, **39**, 1848 (1917).
(35) A. E. Alexander and A. M. Posner, *Nature (London)*, **166**, 432 (1950); R. K. Schofield and E. K. Rideal, *Proc. Roy. Soc., Ser. A*, **109**, 57 (1925).
(36) J. T. Pearson, *J. Colloid Interface Sci.*, **37**, 509 (1971).
(37) P. Mukerjee, *J. Phys. Chem.*, **66**, 1375 (1962).
(38) M. L. Corrin, H. B. Klevens, and W. D. Harkins, *J. Chem. Phys.*, **14**, 480 (1946).
(39) S. Lindenbaum and G. E. Boyd, *J. Phys. Chem.*, **68**, 911 (1964).
(40) For a discussion of electrical energies and free energies of micellization, see ref 26.
(41) E. H. Cordes and R. B. Dunlap, *Accounts Chem. Res.*, **2**, 329 (1969).
(42) E. J. Fendler and J. H. Fendler, *Advan. Phys. Org. Chem.*, **8**, 271 (1970).

Decay Kinetics of Sorbed Methyl Radicals Generated by Photodecomposition and Radiolysis of Methyl Halides on Silica Gel[1]

G. R. Joppien and J. E. Willard*

Department of Chemistry, University of Wisconsin, Madison, Wisconsin 53706 *(Received February 7, 1974)*

Publication costs assisted by U. S. Atomic Energy Commission

The decay kinetics of adsorbed CH_3 radicals produced by γ-irradiation at 77°K of silica gel containing adsorbed methyl halides indicate the presence of several types of trapping sites. The decay rates are all first order with respect to the initial concentration and the predominant decay processes have activation energies of 3–6 kcal/mol. The relative yields of the more rapidly decaying populations decrease with increase in the temperature (25, 460, and 600°) at which the gel is evacuated prior to irradiation at 77°K. The nature of this decrease suggests correlation with the changing ratio of geminal to vicinal to isolated hydroxyl groups on the surface. γ-Irradiation at 300°K of silica gel containing CH_3I produced no observed CH_3 but photolysis of the sorbed CH_3I at either 300 or 77°K yielded stable radicals.

Introduction

γ-Irradiation at 77°K of silica gel containing adsorbed methyl halides produces surface stabilized methyl radicals, the yields and chemical reactions of which have been investigated.[2,3] These decay on warming and are unobservable at room temperature.[4] Surface stabilized CH_3 are also formed by photolysis of methyl halides on silica gel[5-8] or porous Vycor glass,[9-11] and a portion of these are stable at room temperature.[6,8,9a] Their decay on porous glass has been briefly studied.[9,10] The present work has investigated the usefulness of studies of decay kinetics of sorbed radicals as a source of information about the properties of surfaces and has sought answers to the following questions. (1) Are the radicals stabilized by caging in pores[9] of the gel, or by binding to surface sites? (2) Are CH_3 radicals on silica gel held with a continuum of trapping energies, with identical energies, or in a few homogeneous groups of different energy? (3) Are the radical decay kinetics correlated with the conformations of hydroxyl groups on the gel surface? (4) Are CH_3 radicals produced from CH_3I by γ-irradiation and by photolysis bound to the surface in the same way?

Experimental Section

Materials. Davison Chemical Co. Grade 950 60–200 mesh silica gel with a stated BET surface area of 700 m^2 g^{-1} was heated in air at 200° for 2 hr prior to sample preparation, to remove organic impurities. It was then pumped on for 24 hr on the vacuum line at either room temperature, 460, or 600°, during which time the pressure dropped to 10^{-5} Torr. The desired sorbate was then introduced by condensation of a metered volume of the vapor and the sample was sealed off. All samples were thoroughly mixed by shaking and were stored at room temperature for several hours prior to irradiation to allow random surface distribution of the sorbates. CH_3Cl and CH_3Br were used as received from the Matheson Chemical Co. Gas chromatographic tests showed that the purity of each was greater than 99.5%. Aldrich CH_3I (purity greater than 99.9% by gas chromatography) was stored over silver powder.

In this work the concentrations of adsorbed compounds are expressed as mole fractions, using 60 as the molecular weight of silica gel. The 6×10^{-3} mole fraction of CH_3Cl, typically used, was equivalent to 1.7% of a monolayer coverage assuming 20 $Å^2$ as the space occupied by one CH_3Cl molecule.

Irradiations. Samples for γ and uv irradiation and esr examination were prepared in 3-mm i.d. Suprasil tubes as previously described.[2] For uv irradiations the samples were held in the finger of a liquid nitrogen esr dewar which was surrounded by a 12-mm i.d. Vycor tube to remove 185-nm radiation and inserted in the center of a quartz spiral low-pressure mercury lamp which delivered about 10^{16} photons sec^{-1} of 254-nm radiation to the sensitive region of the sample.[12] or were exposed to unfiltered collimated light from a quartz jacketed AH-4 lamp.

Decay Measurements. Esr measurements were made in the X-band with a Varian V-4500 spectrometer with a V-4531 cavity, using 100-kHz field modulation, and microwave power levels of 0.25–8 mW. For temperatures of 129°K and above, where spectral resolution did not increase with temperature, relative radical concentrations during decay were assumed to be proportional to the peak heights of their esr spectra (after correction for the change in esr sensitivity with temperature). Desired temperatures in the range 129–262°K were maintained within ±0.5°K using a Varian variable temperature device. During decay the whole CH_3 radical spectrum was recorded repeatedly in time intervals of 2.5 or 5 min.

Results

Decay of γ-Produced CH_3 as a Function of Dose, Temperature, and Pretreatment of the Gel. Curves for the decay at 129°K of CH_3 radicals produced by γ-irradiation at 77°K of silica gel containing adsorbed CH_3Cl are shown in Figure 1 for different γ doses. Zero time on this decay plot is the start of warm-up of the sample to the desired decay temperature following reading of the initial radical concentration at 77–78°K with the esr sample tube in the variable temperature device. Rapid warm-up was achieved by briefly stopping the cold nitrogen flow. Samples stored under liquid nitrogen for 14 days did not show any radical decay.

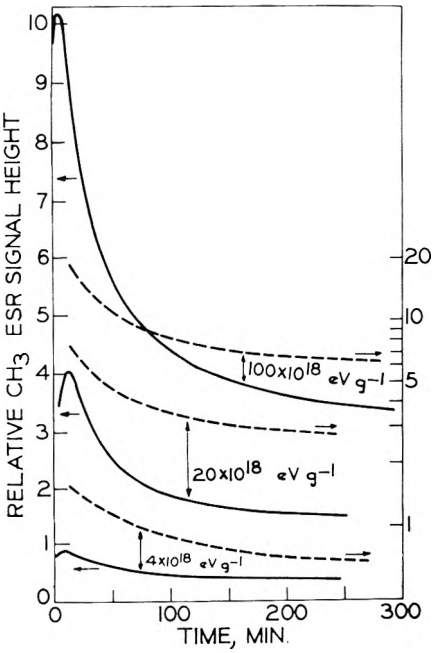

Figure 1. Decay of CH_3 on silica gel at 129°K following production with different radiation doses. Solid lines with left-hand scale show linear plots. Dashed lines with right-hand scale show logarithmic plots: gel treatment, 2 hr in air at 200°, 24 hr at 460° with a final pressure of 10^{-5} Torr, sorption of 6×10^{-3} mole fraction of CH_3Cl; γ-irradiation at 77°K. Esr measurements made at a power of 8 mW.

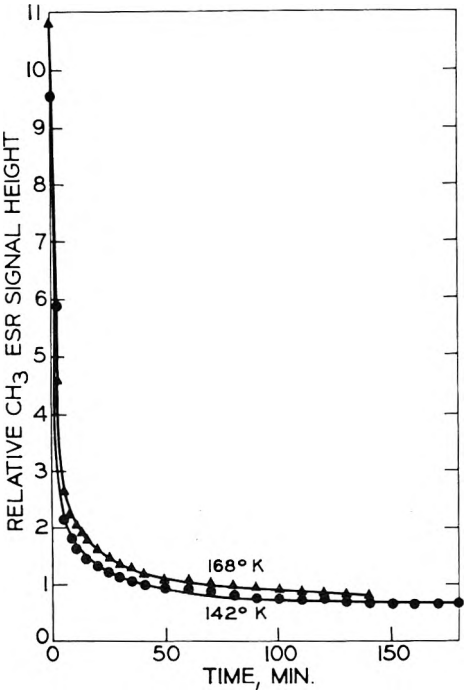

Figure 2. Effect of temperature on decay of CH_3 on silica gel evacuated at room temperature: gel treatment, 2 hr in air at 200°, 24 hr at 25° at $<10^{-4}$ Torr, sorption of 6×10^{-3} mole fraction of CH_3I, γ-irradiation at 77°K, γ-dose 16×10^{18} eV g^{-1}. Esr power 8 mW.

As noted earlier,[2] the increase in radical concentration with dose is less than proportional to dose. The initial rise shown by the solid lines of Figure 1 results from a narrowing and heightening of the lines of the CH_3 esr spectrum as it becomes better resolved on warming to 129°K. This

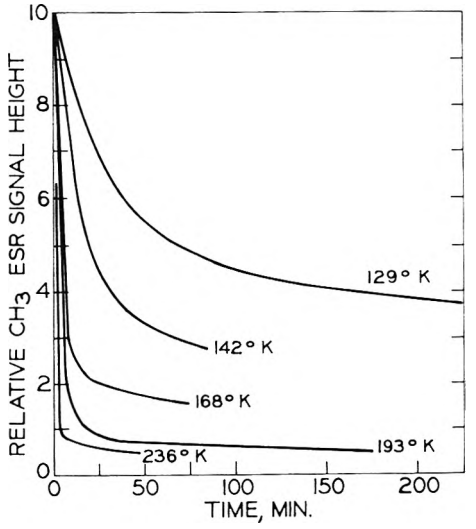

Figure 3. Effect of temperature on decay of CH_3 on silica gel evacuated at 460°. Gel treatment and esr power same as for Figure 1: γ-irradiation at 77°K, γ-dose 20×10^{18} eV g^{-1}.

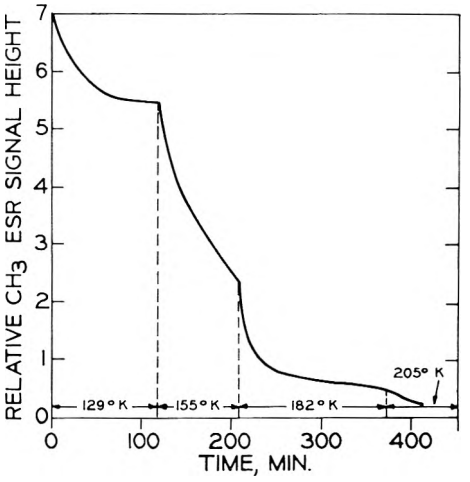

Figure 4. Effect of temperature on decay of CH_3 on silica gel evacuated at 600°: gel treatment, 2 hr in air at 200°, 24 hr at 600° at 10^{-4} to 10^{-5} Torr, sorption of 6×10^{-3} mole fraction of CH_3Br, γ-irradiation at 77°K, γ dose 16×10^{18} eV g^{-1}. Esr power 2 mW.

change is reversible on cooling the sample to 77°K. It would be larger if the esr sensitivity did not decrease with rise in temperature. In all subsequent decay plots zero time has been taken as the maximum of this rise. Very few radicals disappear during the short warm-up period.

The effect of temperature on the rate of decay of CH_3 produced on silica gel by γ-irradiation is shown in Figures 2-4 for gel pretreated by evacuation at 25, 460, and 600°, respectively. In each case, as in Figure 1, there is an initial relatively rapid decay followed by progressively slower decay which approaches a plateau. The fraction of the total CH_3 population which undergoes initial rapid decay at a given temperature decreases with increasing temperature used during the preparatory evacuation of the gel. For example, for decay at 129° this fraction is *ca.* 50% on gel pretreated at 460° (Figure 3) and *ca.* 20% for gel pretreated at 600° (Figure 4). The data for the two experiments done with evacuation at room temperature (Figure 2) suggest that most of the CH_3 radicals on the gel are sorbed on similar sites with a relatively low activation energy for the decay process, since the decay curves at 142

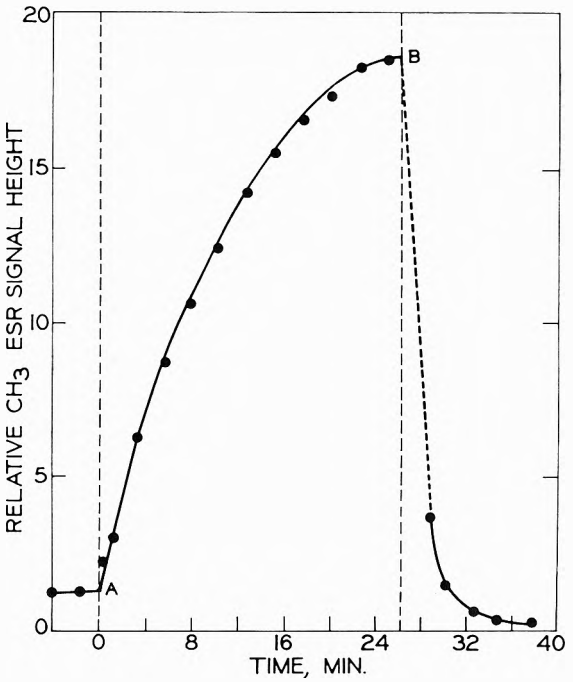

Figure 5. Growth of CH_3 concentration during photolysis of CH_3I on silica gel at 77°K, and decay in dark at room temperature. Gel contained 6×10^{-3} mole fraction of CH_3I, sorbed after 24 hr evacuation at 460° and 10^{-3} Torr. A γ dose of 6×10^{19} eV g^{-1} at 77°K prior to illumination produced the CH_3 concentration shown by the horizontal line preceding zero on the time scale. At A the sample was exposed at 77°K in the esr cavity to the light of the AH-4 lamp. At B the illumination was stopped and the sample warmed to room temperature.

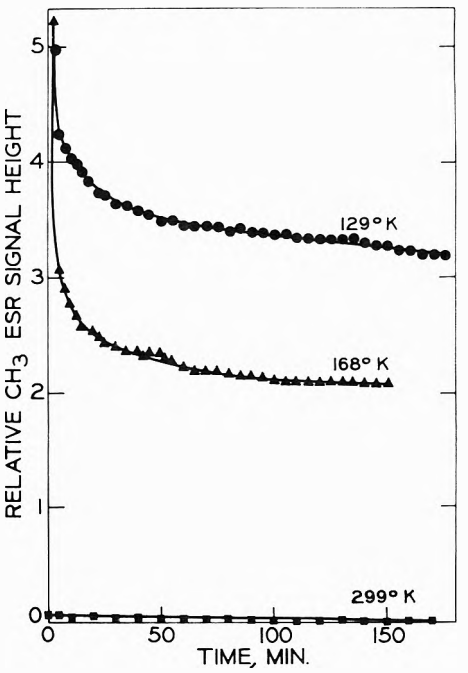

Figure 6. Effect of temperature on decay of CH_3 radicals formed by 5-min photolysis of CH_3I on silica gel at 77°K using the spiral lamp. Gel treatment and esr power same as for Figures 1 and 3.

and 168°K are nearly superimposable, whereas those on the gels pretreated by evacuation at higher temperatures show evidence for three or more differently sorbed populations.

CH_3 Radicals Produced by Photolysis of Methyl Halides on Silica Gel at 77 and 300°K. When silica gel, prepared by evacuation at 460° and containing 6×10^{-3} mole fraction of CH_3I, is exposed at 77°K in the esr cavity to the unfiltered light of a quartz-jacketed AH-4 medium-pressure mercury arc, the four-line spectrum of CH_3 radicals grows. On warming to room temperature following illumination, it decays rapidly to about 1% of its peak intensity, at which point the remaining radicals decay relatively slowly (Figure 5). Similar samples exposed for 5 min at 77°K in the low-pressure spiral mercury lamp with Vycor filter contained 30-fold higher CH_3 concentrations than produced by a 1.6×10^{19} eV g^{-1} dose.

The sorbed CH_3 radicals produced by photolysis at 77°K differ from those produced by γ-irradiation in at least three ways. (1) The four well-defined lines of the CH_3 esr spectrum are accompanied by only six very weak satellite lines, whereas the spectra of γ-irradiated samples have a complex satellite structure of over 16 lines (which is greatly reduced on warming to 110°K or above and reappears on returning to 77°K). (2) The fractions of the radicals which decay rapidly on heating to 129 or 168°K appear to be smaller than in the case of the γ-irradiated samples (Figures 6 and 3). (3) About 1% of the radicals produced photolytically at 77°K remain at 300°K and decay relatively slowly ($t_{1/2}$ = *ca.* 100 min).

Photolysis at 300°K of CH_3I sorbed on silica gel produces CH_3 radicals in about the same yield and with about the same decay characteristics as those which remain after photolysis for the same time at 77°K and warming the sample to 300°K. In contrast a γ dose of 7.6 $\times 10^{20}$ eV g^{-1} on silica gel pretreated by evacuation at 460° and containing 6×10^{-3} mole fraction of CH_3Cl gave no detectable CH_3 esr signal.

For radicals produced by photolysis at 299°K using gel evacuated at 460°, the decrease in initial concentration in 10 min at 299, 318, 338, 362, and 374°K is approximately 15, 20, 68, 78, and 88%, respectively. At 299 and 318°K, 30 and 13% of the radicals, respectively, are still present at 500 min. The decay kinetics are complex.

Discussion

Implications of Decay Curves of γ-Irradiated Samples. The curvature of the semilogarithmic plots of Figure 1 indicates that the CH_3 radical decay on the γ-irradiated silica gel is not a single first-order process and plots of 1/(esr signal height) *vs.* time show curvature at the start, indicating that the decay is not a single second-order process. When the curves of Figure 1 are normalized with respect to the concentration at 200 min they superimpose throughout (with minor deviations at short times), indicating that the fractional rate of decay per unit time is independent of the initial concentration, although it is a function of the fraction decayed. Such a decay pattern may result from the presence of a limited number of differently stabilized populations of CH_3 radicals, each of which decays by a pure first-order process with a different decay constant, or from a continuum of stabilized states resulting in a continuum of decay probabilities. Figures 3 and 4 show that at successively higher temperatures new plateaus of very slow decay are approached, suggesting discrete populations with different activation energies for decay. Although the available data do not define these plateaus perfectly, it is of interest to approximate a resolution of the separate processes which they imply. The most reproducible way of achieving this resolution which

TABLE I: Tentative Resolution of Different Populations of CH_3 Radicals on Silica Gel by Studies of Decay Rates at Different Temperatures[a]

T of decay, °K ± 0.5	Dose, eV g^{-1} × 10^{-18}	Decay populations I k_1 min^{-1}	I %	II k_2 min^{-1}	II %	III k_3 min^{-1}	III %	IV %
129	4	0.022	48	———		52% ———		
	20	0.036	50	———		50% ———		
	100	0.035	53	———		47% ———		
142	20	0.092	56	———		44% ———		
168	4	0.63	45	0.15	33	← ———	22% →	
	20	0.63	52	0.16	26	———	23% →	
	141	0.60	52	0.19	22	———	25% →	
193	20	[b] ———	88% →			0.065	7	7
236	8	[b] ———	74% ———				19	7

[a] Silica gel heated in air at 200°, evacuated 24 hr at 460°, γ-irradiated at 77°K with 6 × 10^{-3} mole fraction of adsorbed CH_3Cl. [b] Too fast to measure.

we have found employs plots of 1/(esr signal height) *vs.* time. These show initial curvature terminating in an effectively straight line on the time scales covered. After extrapolation of the straight line to zero time, the time dependence of the relatively rapidly decaying population is evaluated from the difference between the extrapolated line and the curved portion of the plot. When the logarithms of this difference in concentration are plotted for the data at 129 and 142°K, straight lines are obtained. At 168°K the log [CH_3] *vs.* t plot can be resolved into two first-order components. The data for 193 and 236°K indicate two additional components (Table I). The activation energy derived for component I from the values of k_1 in Table I is 3 kcal mol^{-1} and the values estimated for components II and III, with the aid of additional data, are 5 and 6 kcal mol^{-1}. Component IV disappears below room temperature but the rate as a function of temperature was not determined.

Conclusions

The results of this exploratory investigation show that the fractional rates of decay of methyl radicals on silica gel vary with time, temperature, pretreatment of the surface, and method of formation of the radicals. The variation with time (Figure 1) indicates that the radicals are sorbed in more than one way with respect to the forces which control decay. The approach to different plateaus of decay at successively higher temperatures suggests that there are a few discrete populations, and the somewhat arbitrary but plausible analysis of Table I indicates four such populations.

The difference in the distribution of decaying fractions between the gels prepared by evacuation at 25, 460, and 600° (Figures 2, 3, and 4) suggests strongly that the number and distribution of the hydroxyl groups relative to siloxane bonds on the gel surface determines the relative proportions of the different decaying populations. For gel dried at 100° in air Peri and Hensley[13] obtained evidence that all of the hydroxyl groups are paired, 81% being geminal and 19% vicinal. We have obtained 73–79% of CH_3 radicals in population I, 11–14% in II, and 10–14% in the remainder for samples heated at 200° in air and evacuated for 24 hr at 10^{-5} Torr. Estimates[13] for gels pretreated in air at 500 and 600° indicate about 50% of the hydroxyls to be geminately paired, 35% vicinal, and 15% single. For gel evacuated at 460°, we find *ca.* 50% of the radicals decaying as population I, 30% II, 15% III, and 5% IV.

The greater stability of CH_3 radicals from photolysis of CH_3I on silica gel than of radicals produced by radiolysis indicates that the ease of decay is influenced by (a) the energy with which the CH_3 is born as a determining factor in how it is adsorbed or (b) the nature of its dissociation partner (I or I$^-$); or (c) the specific nature of the site on which the CH_3I is absorbed.[14]

The above findings suggest the speculation that the relatively rapidly decaying first 50% of the radicals sorbed on the "460° gel" (population I) may be associated with adsorption in conjunction with geminal hydroxyl groups

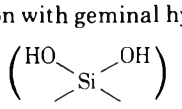

that population II may depend on the presence of vicinal hydroxyl groups

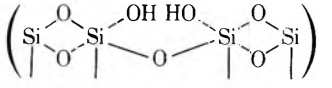

population III on isolated hydroxyl groups, and population IV on adsorption on other active sites on the surface or stabilization by caging effects in pores. The larger (and apparently faster) rapidly decaying component at 142 and 168°K on gel evacuated at 25° (Figure 2) as compared to gel evacuated at 460° (Figure 3) may be due to the larger number of geminal hydroxyl groups on the surface, or possibly to the effect of adsorbed layers of water.

The independence of fractional decay rates of the radicals on the concentration requires that the rate-determining step in the decay be either (1) combination with a predestined partner (most probably the geminate X or X$^-$), (2) abstraction of a hydrogen atom from a hydroxyl group (which would be expected to have an activation energy too high for the fast decays observed unless tunneling occurs), or (3) the act of desorption, following which it inevitably combines with another CH_3 or an X, X$^-$, or X_2, regardless of their concentration, without being readsorbed. Whichever mechanism or mechanisms prevail the radicals must be sorbed in several distinctly different types of trapping sites from which the reaction occurs with significantly different activation energies.

References and Notes

(1) This work has been supported in part by the U. S. Atomic Energy Commission under Contract No. AT(11-1)-1715, by the W. F. Vilas Trust of the University of Wisconsin, and by the Deutsche Forschungsgemeinschaft.
(2) G. R. Joppien and J. E. Willard, *J. Phys. Chem.*, **76**, 3185 (1972).
(3) N. H. Sagert, J. A. Reid, and R. W. Robinson, *Can. J. Chem.*, **48**, 17 (1970).
(4) P. K. Wong and J. E. Willard, *J. Phys. Chem.*, **72**, 2623 (1968).
(5) V. B. Kazanskii and G. B. Pariiski, Sixth International Symposium on Free Radicals, Cambridge, England, July, 1963.
(6) G. B. Garbutt and H. D. Gesser, *Can. J. Chem.*, **48**, 2685 (1970).
(7) S. Kubota, M. Masamoto, and T. Isobe, *Bull. Chem. Soc. Jap.*, **44**, 2684 (1971).
(8) B. Wiseall, private communication.
(9) (a) J. Turkevich and Y. Fujita, *Science*, **152**, 1619 (1966); (b) P. Svejda, *J. Phys. Chem.*, **76**, 3690 (1972).
(10) M. Fujimoto, H. D. Gesser, B. Garbutt, and A. Cohen, *Science*, **154**, 381 (1966).
(11) M. Fujimoto, H. D. Gesser, B. Garbutt, and M. Shimizu, *Science*, **156**, 1105 (1967).
(12) L. C. Glasgow, Ph.D. Thesis, University of Wisconsin, Madison, Wisc., 1970.
(13) J. B. Peri and A. L. Hensley, Jr., *J. Phys. Chem.*, **72**, 2926 (1968).
(14) Photochemical dissociation is random, whereas excitons, holes, or electrons produced inside the gel by ionizing radiation may be released at preferred surface sites.

Photoconductivity of Trinitrofluorenone in Tetrahydrofuran

R. W. Bigelow

Rochester Corporate Research Center, Xerox Corporation, Webster, New York 14580 (Received November 12, 1973)

Publication costs assisted by Xerox Corporation

Weak new absorption bands, not present in either parent compound, were observed when 2,4,7-trinitro-9-fluorenone (TNF) was dissolved in tetrahydrofuran (THF). These new bands appear at ~4700, 5100, and 6500 Å and are attributed to the formation of a donor–acceptor complex between the two molecules. A Benesi–Hildebrand analysis of a 5.0×10^{-3} M solution showed the extinction coefficient of the complex to be ~10 M^{-1} cm^{-1} at 4700 Å and the equilibrium constant to be ~0.06 M^{-1}. Under monochromatic irradiation, the solution exhibited photoconductivity that closely paralleled the photoresponse curve of a TNF single crystal. No photoconductivity was observed in the absorption bands of the donor–acceptor complex. The saturation photocurrent was found to be proportional to the applied potential, the square root of the incident photon flux, and TNF concentration. The photocurrent decayed by second-order kinetics when the light was terminated while initial irradiation produced a hyperbolic tangential growth curve in the photocurrent. A bimolecular recombination mechanism is proposed which explains the dynamic and static behavior of the photoproduced charge carriers. The steady-state photocurrent is then expressed in terms of Ohm's law which exhibits the appropriate dependence on applied voltage, light flux, and TNF concentration. Upon uv irradiation or prolonged standing the solution undergoes an irreversible color change from a pale yellow to a reddish-orange with a simultaneous decrease in photoconductivity.

Introduction

2,4,7-Trinitro-9-fluorenone (TNF) is widely used as an electron acceptor to form solid state donor–acceptor complexes with aromatic polynuclear hydrocarbons which exhibit new optical absorption bands in the visible spectral region characteristic of the complex.[1,2] Of current interest is the donor–acceptor complex formed between electron acceptors such as TNF and molecules of a carbazole base, particularly the photoconductive polymer, poly(N-vinylcarbazole) (PVK).[3-13] Although TNF and PVK are separately photoconductive, correlations between electrical and optical properties have shown that with the formation of a complex between the two molecules in the solid state the photoconductivity is significantly enhanced and extended to the spectral region of absorption of the donor–acceptor complex.

Tetrahydrofuran (THF) is a liquid of the cyclic ether variety. It has been used as a solvent in the investigation of the spectroscopic properties of the donor–acceptor complex between TNF and PVK in solution[11] and to solvent cast this complex onto appropriate substrates.[6-10] THF has been found to behave as an electron donor itself, forming complexes with the electron acceptors tetracyanoethylene, maleic anhydride, and pyromellitic dianhydride.[14-17] Each of these donor–acceptor complexes of THF were found to exhibit esr signals and photoconductivity when irradiated in the region of absorption of the complex. This was interpreted as a photoinduced ionic dissociation of the complex by complete charge transfer from donor to acceptor.

Solution photoconductivity of organic materials not involving charge-transfer complexes have been observed for pyranthrene in benzene and was attributed to a single-photon process involving interaction between the electrode and an absorbed pyranthrene layer.[18] Bimolecular ionization of the triplet state accounted for photoconduction of anthracene, naphthalene, phenanthrene, and pyrene in solvents of appropriate dielectric constant.[19] Flash photoconductivity of rubrene in benzene was shown to be limited by diffusion of excited rubrene molecules to the anode.[20]

A general observation that has been reported when using cyclic ethers as a solvent or as an electron donor in these type measurements is the irreversible degradation of the system after prolonged standing or continuous ultraviolet irradiation.[15-17] In general, the total amount of photoproducts produced in these cases in the time taken to do any electrical measurements is negligible. The explicit identification of the products have only been accomplished in a few cases.[15] Identification of the photoproduct observed in this work is underway and will be presented in a subsequent report.

Experimental Section

Eastman Kodak 2,4,7-trinitro-9-fluorenone and Burdick and Jackson tetrahydrofuran were used in these measurements. The tetrahydrofuran was bottled under a nitrogen atmosphere and contained no stabilizers. Both chemicals were used without further purification. Spectroscopic measurements were made with a Cary 14 recording spectrophotometer. The sample compartment in which the photoconductivity measurements were made consisted of parallel nesa plates with a variable separation controlled by a micrometer screw drive. The sample was held in place by the surface tension of the liquid. A potential was applied between the plates using a 412B Fluke power supply. The steady-state light intensity dependence and the dynamic behavior of the photocurrent was monitored using a Keithley 610BR electrometer and recorded on a Hewlett-Packard 7100B strip chart recorder. The light source consisted of an Osram 1000-W xenon arc lamp filtered through a Leiss double quartz prism monochrometer

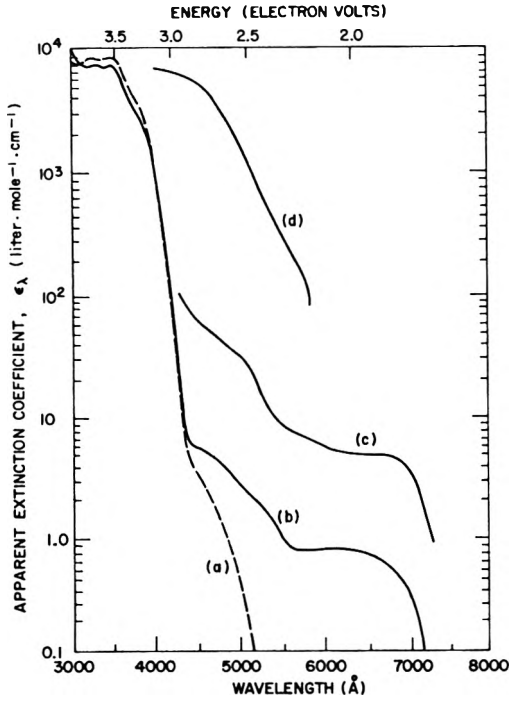

Figure 1. Apparent extinction coefficient of TNF *vs.* wavelength: (a) TNF in dichloromethane, (b) initial absorption of TNF in THF, (c) TNF–THF after 0.5 hr standing; and (d) TNF–THF after 2 hr uv irradiation.

operating with all slits at maximum extension. The light intensity was measured with an SDG-100A calibrated photodiode and was varied using calibrated Oriel neutral density filters. Maximum photon fluxes were in the range of $\sim 10^{12}$–10^{13} photons sec^{-1} cm^{-2}. Quantum gain curves were measured by placing a 150-Hz chopper in the light beam while monitoring the photocurrent output through a resistor into a PAR Model 122 lock-in amplifier.

Results

The optical absorption spectra of TNF in THF solution show three new weak bands, Figure 1, at 4700 (~2.63 eV), 5100 (~2.45 eV), and ~6500 Å (~1.90 eV). These bands are not present in the parent compound absorption. Variance of the donor concentration (THF) obeyed the standard Benesi-Hildebrand equation,[21] Figure 2, yielding an extinction coefficient of $\sim 10\ M^{-1}$ cm^{-1} and an equilibrium constant of $\sim 6.0 \times 10^{-2}\ M^{-1}$ at 4700 Å. Using these values for a $5.0 \times 10^{-3}\ M$ TNF solution the extinction coefficient as a function of wavelength was calculated for the donor-acceptor complex, Figure 3.

The photocurrents in this system exhibited two distinct types of behavior depending on the light level and the applied voltage. Upon exposure to lower photon fluxes and applied voltages the photocurrent increased to a steady-state value. However, upon raising the photon flux and applied potential past a certain level the photocurrent initially increased until it reached a maximum where it then decayed to a steady-state value. This investigation was confined to the study of those photocurrents produced by the lower levels of incident light and potential.

The quantum gain of the system, defined as the number of electronic charges measured as photocurrent per photon absorbed, shows the peak efficiency to be near 4200 Å. No photoconductivity was observed at wavelengths longer than 4500 Å, Figure 4. The quantum gain approaches

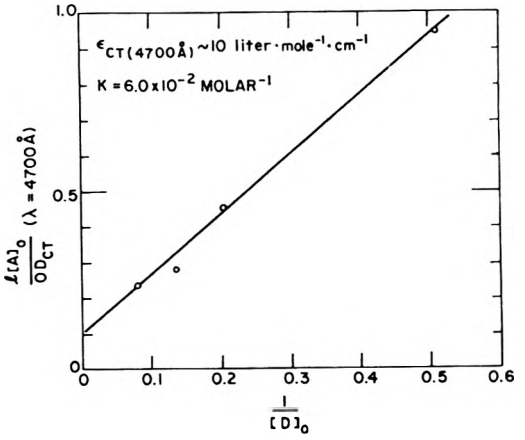

Figure 2. Benesi-Hildebrand plot considering a 1:1 donor-acceptor complex between TNF and THF. $l/[A]_0/OD(4700\ Å)$ is plotted against $1/[D]_0$ where l is the optical path length (10 cm), $[A]_0$ is the total concentration of TNF molecules, OD is the optical density, and $[D]_0$ is the total concentration of THF molecules.

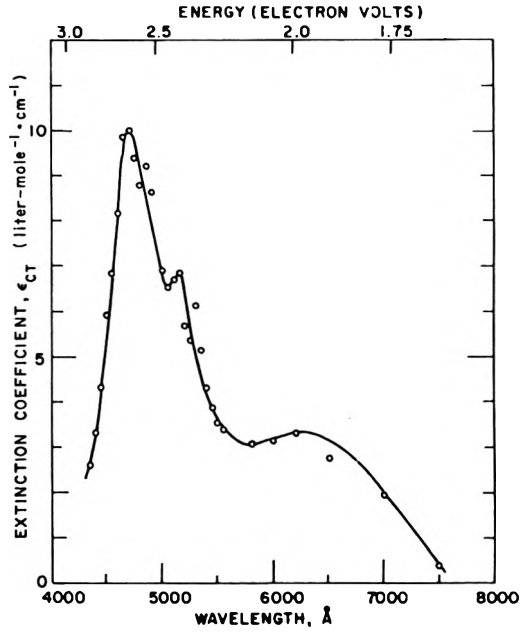

Figure 3. Extinction coefficient *vs.* wavelength for the TNF–THF complex based on the results shown in Figure 2.

unity as the TNF concentration is decreased. When the system was exposed to light the photocurrent increased proportional to the hyperbolic tangent of the time, Figure 5. Upon termination of the light, the photocurrent decreased according to a second-order rate equation, Figure 6. The steady-state photocurrent was found to be proportional to the square root of the light intensity, and the square root of the TNF concentration, Figure 7. Current *vs.* voltage curves show the photocurrent increases linearly with voltage while the dark current varies approximately as the square of the voltage, Figure 8. The photocurrent, as used in this report, is the current in the light minus the dark current.

Discussion

Analysis of the absorption bands in the visible spectral region conform to a Benesi-Hildebrand equation for a 1:1 electron donor-acceptor complex in equilibrium with the

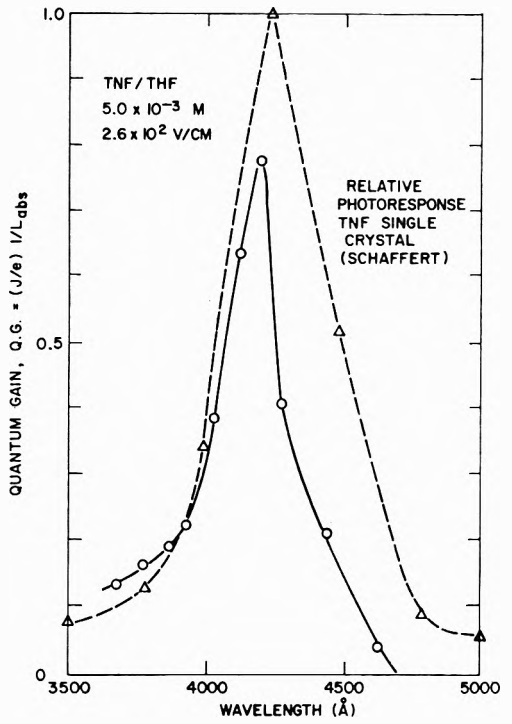

Figure 4. Quantum gain *vs.* wavelength for a 5.0 × 10^{-3} *M* solution of TNF in THF. The applied potential was 10 V across 3.81 × 10^{-2} cm. This is compared with the relative photoresponse for a TNF single crystal.[9]

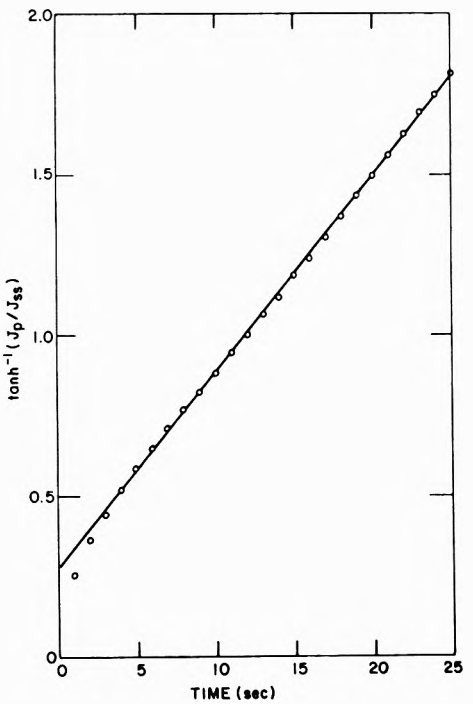

Figure 5. The growth of the photocurrent for a 5.0 × 10^{-3} *M* solution of TNF in THF. $\tanh^{-1}$ (J_p/J_{pss}) is plotted against time. The potential was 2.0 V across 3.81 × 10^{-2} cm. The incident wavelength was 4000 Å.

free molecules. The expression for the equilibrium constant is given by

$$K = [DA]/[D][A]$$

where [DA], [D], and [A] are the concentrations of complexed molecules, free donors, and free acceptors, respec-

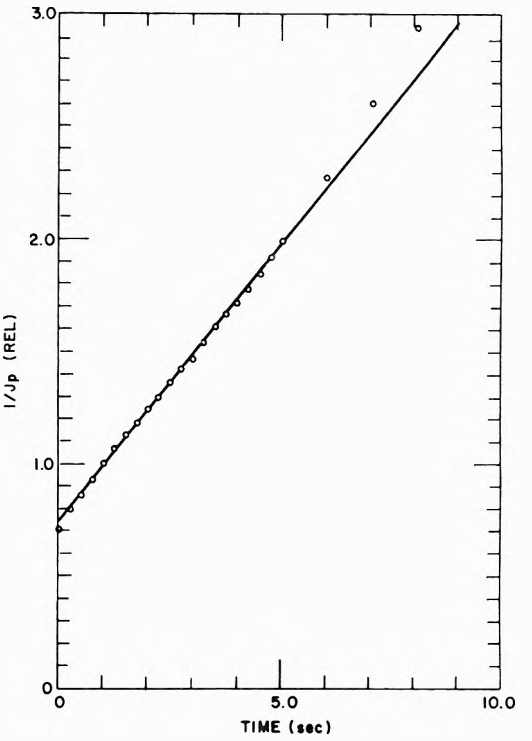

Figure 6. Decay of the photocurrent for a 5.0 × 10^{-3} *M* solution of TNF in THF. The reciprocal of the relative photocurrent is plotted against time. The potential was 2.0 V across 3.81 × 10^{-2} cm.

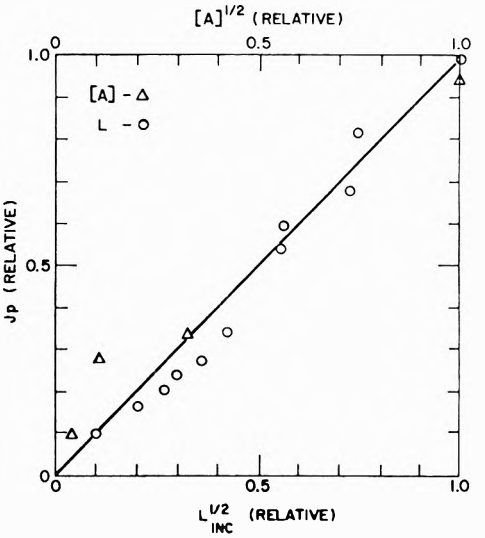

Figure 7. Steady-state photocurrent dependence on light intensity and TNF concentration. The relative photocurrent is plotted against the square root of the relative light intensity (λ 4000 Å) for a 5.0 × 10^{-3} *M* solution of TNF in THF (bottom) and the relative value of the square root of the TNF concentration (top). The concentration of TNF was varied from 10^{-4} to 5.0 × 10^{-2} *M*. The potential was 10 V across 3.81 × 10^{-2} cm.

tively. For the condition [D] ≫ $[A]_0$, where $[A]_0$ is the total concentration of acceptor molecules, and using the above value for the equilibrium constant gives [DA] ~ $0.423[A]_0$. Calculating [DA] directly from its absorbance in a 5.0 × 10^{-3} *M* solution using the above extinction coefficient at λ 4700 Å gives [DA] ~ 1.27 × 10^{-3} *M*. These values are in approximate agreement and show that the TNF molecules are between ~25–50% complexed. The extinction coefficients calculated for the TNF:THF complex are several orders of magnitude smaller than

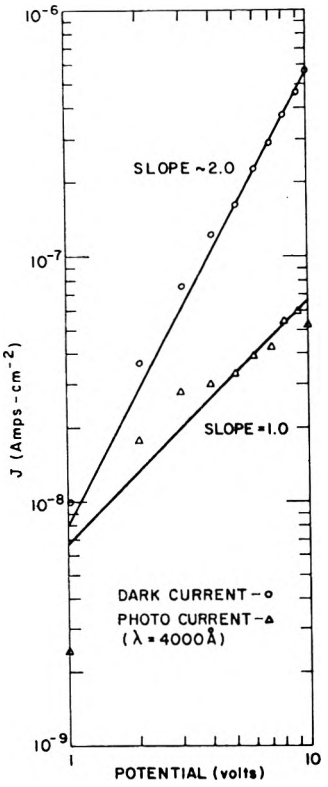

Figure 8. Current-voltage dependence for dark and photocurrent (λ 4000 Å). Log (voltage) is plotted against log (current) for a 5.0 × 10^{-3} *M* solution of TNF in THF. The potential was varied from 1 to 10 V across 3.81 × 10^{-2} cm.

those normally reported for donor-acceptor complexes, inferring that these are very weak interactions. On the basis of the preceding results the following mechanism is proposed to explain the generation and the behavior of the photocurrents studied. No charge carriers are formed by irradiation within the charge-transfer band. Therefore the photoconduction process does not directly proceed by dissociation of the complex upon excitation to form positive and negative ions. By incorporating the light chopper and lock-in amplifier the instrumentation in this experiment is capable of detecting photocurrents of approximately 10^{-12} A in the presence of much larger dark currents. This means that, if photoconductivity does exist in the donor-acceptor absorption region, it would be seen if the quantum gain is 0.02 or greater. No photoconductivity was observed above a wavelength of 4500 Å above which the donor-acceptor absorption appears. The quantum gain *vs.* wavelength curve of Figure 4 is identical in structure with the photoresponse curve for a TNF single crystal.[9] It is thereby assumed that the complex does not contribute to the process of photoconduction. The current-voltage curves are different for the dark and the light and it was observed that addition of TNF to THF had no effect on the magnitude of the dark current or its current-voltage characteristic. This suggests that the charge carriers in the dark and in the light are different and that the photocurrent is totally dependent on the TNF concentration. Thus, in the first step of the process the TNF molecules initially absorb light creating a molecular excited state, this process being proportional to L, the amount of light absorbed

$$A + h\nu \xrightarrow{L} A^* \tag{1}$$

This excited state can then relax back to the ground state with a rate constant k_1

$$A^* \xrightarrow{k_1} A + \text{energy} \tag{2}$$

An excited TNF molecule can react with a neutral solvent molecule (THF) to give positive and negative charge carriers, this process occurring with a rate constant k_2

$$A^* + B \xrightarrow{k_2} A^- + B^+ \tag{3}$$

These ions can recombine by a second-order mechanism to give the neutral molecules, this reaction proceeding with a rate constant k_3

$$A^- + B^+ \xrightarrow{k_3} A + B \tag{4}$$

This formulation does not distinguish between excited singlet or triplet state mechanisms as both would give identical gross dependencies differing only by a combination of rate constants.

The kinetic equations corresponding to the above mechanism and leading to the parameter dependencies studied in this work parallel those presented in ref 17, differing only in definition of rate constants. These equations are discussed in the Appendix.

The proposed mechanism gives for the photoconductive steady-state concentration of charge carriers

$$n_{ss} = \left[\frac{k_2}{k_3(k_1 + k_2)}\right]^{1/2} L^{1/2} \tag{5}$$

where n is the concentration of both negative, $[A^-]$, and positive, $[B^+]$, charge carriers. The increase in photocurrent when the sample is initially illuminated is

$$n(t) = n_{ss} \tanh [(k_3 \alpha L)^{1/2} t] \tag{6}$$

where $\alpha = k_2/(k_1 + k_2)$. The time dependence of the photocurrent decay when the light is switched off is given by

$$\frac{1}{n(t)} = \frac{1}{n_{ss}} + k_3 t \tag{7}$$

The quantum gain, defined previously, is calculated from the relationship

$$QG = \left(\frac{J}{2e}\right)\frac{1}{L_{abs}} \tag{8}$$

The quantum gain is then related to the TNF concentration and incident light intensity by (see Appendix)

$$QG \propto \frac{1}{L_{inc}^{1/2}[A]^{1/2}} \tag{9}$$

Substituting the value for n_{ss} given in eq 5 into the Ohm's law expression for the concentration of charge carriers gives for the photocurrent

$$J_p = e\mu\left[\frac{k_2}{k_3(k_1 + k_2)}\right]^{1/2} \xi L^{1/2} \tag{10}$$

Equation 10 accounts for the steady-state photocurrent dependence of the three variables investigated, the applied voltage, photon flux, and TNF concentration. Although TNF and THF interact to form a weak charge-transfer complex and under the influence of light to form charge carriers it is unlikely that this influences the resulting charge-transfer complex of PVK:TNF when solvent cast from THF. The possibility of the THF reacting with TNF is essentially eliminated by use of amber flasks which filter out the uv light initiating the photoreaction. Mort and Emerald[22] have obtained similar mobility data

for holes and electrons in a PVK–TNF system cast from a toluene–cyclohexanone mixture as those obtained by Gill[8] casting the complex from THF. It was observed in this investigation that the TNF–toluene visible absorption spectra closely resembled that of TNF–dichloromethane shown in Figure 2 which shows no complexing.

Analysis of the photocurrents in the TNF–THF system show that the low field and photon flux region to which this investigation was confined was adequately described by an Ohm's law behavior with a bimolecular recombination mechanism for charge carriers. The quantum gains calculated here are unusually large in comparison to other systems reported in the literature, particularly for solid arrangements. It is likely that in approaching the higher field and photon flux region a transition occurs from the bulk limited mechanism to one dependent on carrier neutralization at the electrodes. The decrease in photocurrent at the higher field and photon flux condition can not be accounted for with the mechanism proposed for the observations made in this experiment.

Acknowledgments. The author wishes to acknowledge J. Sharp who suggested the problem. Special thanks are due to D. Blossey and A. Monahan for many helpful discussions and J. Mort, R. Emerald, and A. Lakatos for helpful comments.

Appendix

The rate of change with time of the concentration of excited states [A*] is from eq 1–3

$$d[A^*]/dt = L - (k_1 + k_2)[A^*] \quad (A1)$$

The equation governing the formation of charge carriers is from eq 3–4

$$dn/dt = k_2[A^*] - k_3n^2 \quad (A2)$$

Under steady-state conditions where $d[A^*]/dt$ and dn/dt are zero equating the right-hand sides of eq A1 and A2 yields eq 5. When the light is terminated the concentration of excited states goes to zero. Integrating eq A2 under this condition yields eq 7. The solution of eq A1 for the increase of [A*] when the light is switched on is the sum of two terms, one being an exponential. When $t \gg k_1 + k_2$ this exponential term approaches zero. Under this condition eq A2 becomes

$$dn/dt + k_3n^2 - \alpha L = 0 \quad (A3)$$

Integration of eq A3 gives eq 6.

Quantum gain calculations were made with the following approximations considered. For a liquid $I_{abs} = [1 - \exp(-2.303\epsilon_\lambda Ad)]$. To obtain a quantum gain *vs.* TNF concentration dependence at λ 4000 Å and $d = 3.81 \times 10^{-2}$ cm the TNF concentration was varied from 5.0×10^{-2} to 10^{-4} *M*. Expanding the exponential in a Taylor's series and retaining terms linear in concentration shows $1 - \exp(2.303\epsilon_\lambda[A]d) = 2.303\epsilon_\lambda[A]d$ and the amount of light absorbed becomes $I_{abs} = 2.303I_{inc}\epsilon_\lambda[A]d$. Substituting the value for I_{abs} into eq 8 yields

$$QG = \frac{J_p}{4.6eI_{inc}\epsilon_\lambda[A]d} \quad (A4)$$

Substituting the expression for the steady-state concentration of charge carriers, n_{ss}, from eq 5 into eq A4 for J_p gives the quantum gain dependence in eq 9.

References and Notes

(1) M. Orchin and E. Woolfolk, *J. Amer. Chem. Soc.*, **68**, 1727 (1946).
(2) Polysciences Data Sheet No. 106. This publication lists 65 references of TNF complexing with aromatic polynuclear hydrocarbons.
(3) J. Sharp, *J. Phys. Chem.*, **70**, 584 (1966).
(4) E. Ong and M. Sambhi, *J. Phys. Chem.*, **76**, 2102 (1972).
(5) M. Lardon, E. Lel-Doller, and J. Weigl, *Mol. Cryst.*, **2**, 241 (1967).
(6) H. Hoegl, G. Barchietto, and D. Tar, *Photochem. Photobiol.*, **16**, 335 (1972).
(7) G. Weiser, *J. Appl. Phys.*, **43**, 5028 (1972).
(8) W. Gill, *J. Appl. Phys.*, **43**, 5033 (1972).
(9) R. Schaffert, *IBM J. Res. Develop.*, **115**, 75 (1971).
(10) P. Melz, *J. Chem. Phys.*, **57**, 1694 (1972).
(11) G. Weiser and H. Seki, *IBM J. Res. Develop.*, **16**, 598 (1972).
(12) D. Williams, M. Abkowitz, and G. Pfister, *J. Amer. Chem. Soc.*, **94**, 7970 (1972).
(13) H. Meier, W. Albrecht, and V. Tschirwitz, *Photochem. Photobiol.*, **16**, 353 (1972).
(14) R. Vars, L. Tripp, and L. Pickett, *J. Phys. Chem.*, **66**, 1754 (1962).
(15) A. Ledwith and M. Sambhi, *J. Chem. Soc. B*, 670 (1966).
(16) R. Ward, *J. Chem. Phys.*, **38**, 852 (1963).
(17) D. Ilten and M. Calvin, *J. Chem. Phys.*, **42**, 3760 (1965).
(18) A. Prock and R. Zahradnik, *J. Chem. Phys.*, **49**, 3204 (1968).
(19) L. Gary, K. DeGroot, and R. Jarnagin, *J. Chem. Phys.*, **49**, 1577 (1968).
(20) R. Romanets, A. Prock, and R. Zahradik, *J. Chem. Phys.*, **53**, 4093 (1970).
(21) J. B. Birks, "Photophysics of Aromatic Molecules," Wiley-Interscience, London, 1970.
(22) J. Mort and R. Emerald, *J. Appl Phys.*, submitted for publication.

Studies in Linear Dichroism. XI.[1] Determination of the Polarization of Electronic Transitions in Coronene and Penta- and Hexahelicene

Amnon Yogev, Leon Margulies, Batia Strasberger, and Yehuda Mazur*

Department of Organic Chemistry, The Weizmann Institute of Science, Rehovot, Israel *(Received August 10, 1973; Revised Manuscript Received April 1, 1974)*

A method for the interpretation of linear dichroic spectra of disk-like molecules is discussed. The absorption spectra of coronene and penta- and hexahelicene are resolved into in- and out-of-plane polarizations and compared with previously reported data and with theoretical predictions.

Helicenes have attracted considerable attention in the last decade,[2-4] due to the unique helical arrangement of their aromatic rings.

Measurements of absorption, excitation, and CD spectra and of emission polarization were reported for both penta- and hexahelicene. The resulting polarizations and rotational strength data were used to determine the chirality of the molecules and then correlated with the molecular handedness as established by X-ray data.

We shall discuss the determination of the polarization spectra of penta- and hexahelicenes using linear dichroic measurements and compare the results with the relative polarization directions previously reported.

We have used a previously described technique to incorporate compounds into stretched polyethylene films to establish the dichroic ratios, d_0, for two orthogonal polarizations, one being the direction of film stretching.[5] The measurements were performed using the novel, highly accurate technique recently described by us, involving the use of both polarized and nonpolarized light (the PNP method).[1,6]

We have previously shown[5] that in an assembly of molecules possessing axial symmetry, the dichroic ratio, d_0, may be expressed as a function of only two parameters α and f, where α is the angle between the transition moment vector and the orientational axis[7] of the molecules, and f is related to the orientation of such an assembly. The latter parameter is conveniently expressed as a fraction of oriented molecules; therefore the fraction of randomly distributed molecules is equal to $1 - f$.

The relation between the dichroic ratio, d_0, and the two parameters α and f is given in eq 1[5]

$$d_0 = \frac{f \cos^2 \alpha + \frac{1}{3}(1 - f)}{\frac{1}{2}f \sin^2 \alpha + \frac{1}{3}(1 - f)} \quad (1)$$

Furthermore we have shown[5] that an assembly of elongated molecules incorporated in a stretched polyethylene film has a preferential orientation; their longitudinal axes of inertia[7] are in the direction of stretching. Since the helicenes do not possess a longitudinal axis of inertia, they will orient themselves in the stretched films preferentially with their planes parallel to the stretching direction. The dichroic ratio of such assembly will also be represented by eq 1 where f will now describe the fraction of the molecules having their planes in the stretching direction. The preferred orientations of disk and of elongated molecules, and the random distribution of spherical molecules are shown schematically in Figure 1.

It follows that transitions polarized perpendicularly to the plane of the disk-like molecules will absorb preferentially light polarized perpendicularly to the direction of stretching (Figure 1). Were the molecules all oriented, the dichroic ratio would have the limiting value of zero. However, were only a fraction f of the molecules oriented, the dichroic ratio, d_0, would be a function of f only. Its value may be obtained from eq 1 by substituting α by 90°, and is given in eq 2.

$$d_0 = \frac{f \cos^2 90° + \frac{1}{3}(1 - f)}{\frac{1}{2}f \sin^2 90° + \frac{1}{3}(1 - f)} = \frac{\frac{1}{3}(1 - f)}{\frac{1}{2}f + \frac{1}{3}(1 - f)} = \frac{2(1 - f)}{f + 2} \quad (2)$$

As f varies between 0 and 1, it follows from eq 2 that $0 \leq d_0 \leq 1$.

To find the dichroic ratio for a transition polarized in the plane of the disk-like molecules, we use the following reasoning.

The absorption of light polarized in the direction of stretching (z axis) by a single oriented molecule would be represented by eq 3 while that of light polarized in the orthogonal direction (y axis) by eq 4

$$\epsilon_{iz} = |\vec{E}_z|^2 |\vec{M}|^2 \cos^2 \phi_i \quad (3)$$

$$\epsilon_{iy} = |\vec{E}_y|^2 |\vec{M}|^2 \sin^2 \phi_i \cos^2 \psi_i \quad (4)$$

where M is the transition moment vector in the plane of the molecule, E_z and E_y the electric vectors of the incident light and the angles ϕ_i and ψ_i are defined according to Figure 2.

In an assembly of molecules oriented with their plane parallel to the stretching direction, the transition moment vector M will be randomly distributed within this plane.

It follows that the corresponding absorptions of an assembly consisting of N such molecules (Figure 1) will be given by

$$\epsilon_z = \sum_i \epsilon_{iz} = \frac{4}{\pi^2} N |\vec{M}|^2 |\vec{E}_z|^2 \int_0^{\pi/2} \int_0^{\pi/2} \cos^2 \phi_i \, d\phi \, d\psi = \frac{1}{2} N |\vec{M}|^2 |\vec{E}_z|^2 \quad (5)$$

$$\epsilon_y = \sum_i \epsilon_{iy} = \frac{4}{\pi^2} N |\vec{M}|^2 |\vec{E}_y|^2 \int_0^{\pi/2} \int_0^{\pi/2} \sin^2 \phi_i \cos^2 \psi_i \, d\phi \, d\psi = \frac{1}{4} N |\vec{M}|^2 |\vec{E}_y|^2 \quad (6)$$

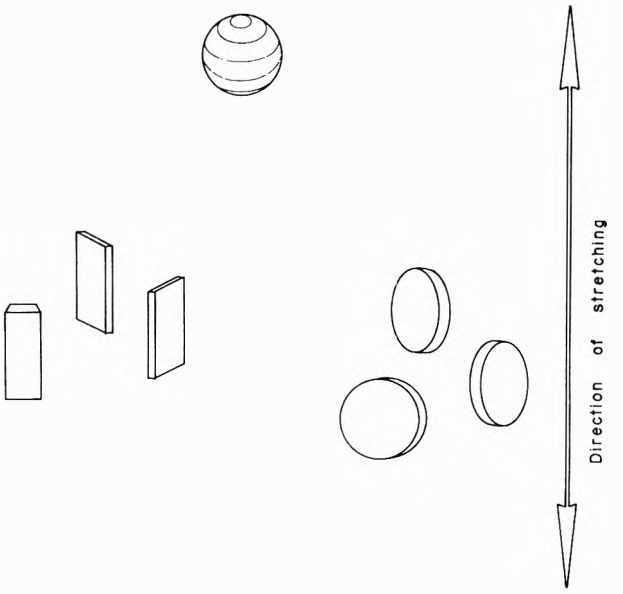

Figure 1. Schematical representation of the preferred orientation of elongated and disk molecules, and of random distribution of the spherical molecules.

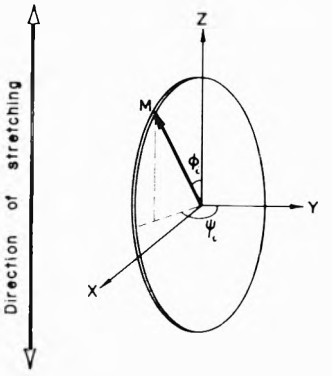

Figure 2.

Since $|\vec{E}_z|^2 = |\vec{E}_y|^2$, the dichroic ratio for the "in-plane" transitions of such an assembly of oriented disk-like molecules will have the value of

$$d_0 = \epsilon_z/\epsilon_y = 2$$

When only a fraction f of these molecules is oriented, the absorption coefficients for the two orthogonal polarizations are given by the following equation

$$\epsilon_z = \frac{1}{2} fN|\vec{M}|^2|\vec{E}|^2 + \frac{1}{3}(1 - f)N|\vec{M}|^2|\vec{E}|^2 \qquad (7)$$

$$\epsilon_y = \frac{1}{4} fN|\vec{M}|^2|\vec{E}|^2 + \frac{1}{3}(1 - f)N|\vec{M}|^2|\vec{E}|^2 \qquad (8)$$

and the dichroic ratio d_0 by

$$d_0 = \frac{\epsilon_z}{\epsilon_y} = \frac{\frac{1}{2}f + \frac{1}{3}(1 - f)}{\frac{1}{4}f + \frac{1}{3}(1 - f)} = \frac{2f + 4}{4 - f} \qquad (9)$$

Comparison of eq 1 and 9 reveals that eq 1 can be used for in-plane transitions of disk molecules if an effective value of 45° is used for α. Thus, these transitions may be regarded as being located at an angle of 45° with the stretching direction. This value comes from averaging over the random orientations in the plane, so it is not a fixed angle but rather an effective value.[8]

When the transition moment vector is located out of the plane of the disk molecule, forming an angle β with the plane of molecule, its in-plane component will also make an averaged effective angle of 45° with the direction of stretching, as shown in Figure 3. It is apparent from this figure that the "out-of-plane" angle β is related to the angle α between the transition moment and the direction of stretching, by[9]

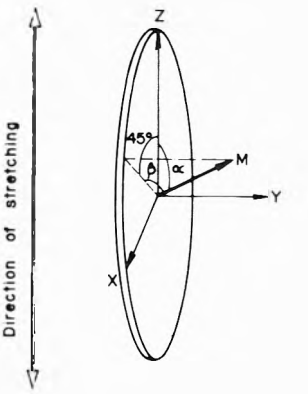

Figure 3.

$$\cos^2 \beta = \cos^2 \alpha/\cos^2 45° = 2 \cos^2 \alpha \qquad (10)$$

Thus the determination of dichroic ratios of disk-like molecules easily distinguishes between in- and out-of-plane (not necessarily perpendicular) transitions; all in-plane transitions will show constant dichroic ratios, their numerical value depending only on the degree of orientation of the molecules ($2 \leq d_0 \leq 1$). The dichroic ratios of out-of-plane transitions will be invariably smaller than the in-plane transitions, and thus are easily recognized.

In this treatment we have dealt with disk-like molecules having a unique direction of their transition moment. In a perfect disk a transition moment does not have a unique direction in the plane, but has an equal magnitude in any direction.

For degenerate in-plane transitions eq 3 and 4 describing the absorption by a single molecule of light polarized in two orthogonal directions must be replaced by eq 3′ and 4′, respectively.

$$\epsilon_{iz} = |\vec{E}_z|^2|\vec{M}|^2 \qquad (3')$$

$$\epsilon_{iy} = |\vec{E}_y|^2|\vec{M}|^2 \cos^2 \psi_i \qquad (4')$$

Thus for an assembly consisting of N molecules oriented with their plane parallel to the stretching direction, the corresponding absorptions for each orthogonal polarization will be given by eq 5′ and 6′

$$\epsilon_z = \sum_i \epsilon_{iz} = N|\vec{M}|^2|\vec{E}_z|^2 \qquad (5')$$

$$\epsilon_y = \sum_i \epsilon_{iy} = \frac{2}{\pi} N|\vec{M}|^2|\vec{E}_y|^2 \int_0^{\pi/2} \cos^2 \psi_i \, d\psi = \frac{1}{2} N|\vec{M}|^2|\vec{E}_y|^2 \qquad (6')$$

The dichroic ratio for in-plane degenerate transitions in oriented disk-like molecules will be

$$d_0 = \epsilon_z/\epsilon_y = 2$$

as in the case of single transition in such molecules.

The corresponding absorptions for the degenerate transition in partially oriented molecules will be now modified and given by

$$\epsilon_z = fN|\vec{M}|^2|\vec{E}|^2 + \frac{2}{3}(1 - f)N|\vec{M}|^2|\vec{E}|^2 \qquad (7')$$

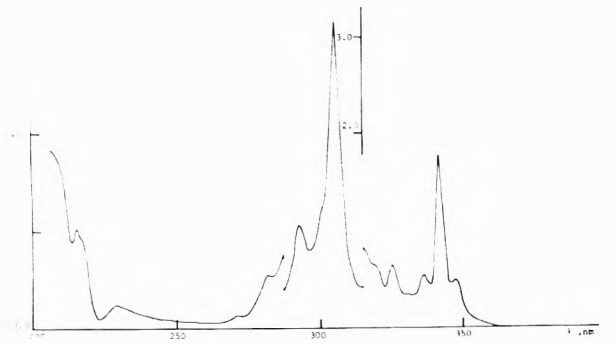

Figure 4. Uv spectrum of coronene in polyethylene.

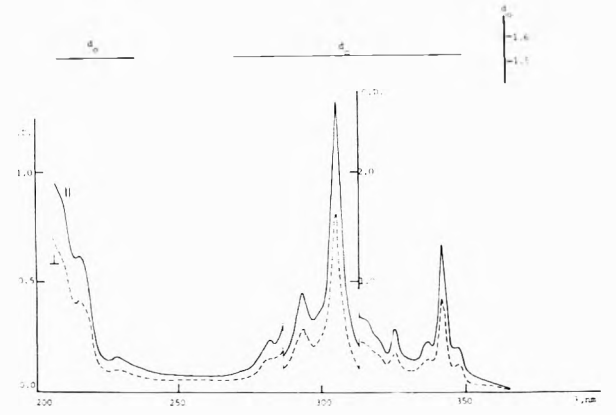

Figure 5. LD spectrum of coronene: lower part, (——) the curve of optical densities obtained by light polarized in the direction of stretching; (– – –) the curve obtained by light polarized perpendicular to the direction of stretching; upper part, the plot of the dichroic ratios d_0 vs. λ.

and

$$\epsilon_v = \frac{1}{2} fN|\vec{M}|^2|\vec{E}|^2 + \frac{2}{3}(1 - f)N|\vec{M}|^2|\vec{E}|^2 \qquad (8')$$

However, the resulting equation for the dichroic ratio will be the same as in the case of disk-like molecules possessing an unique transition (eq 9).

Coronene

We have chosen coronene as a representative perfect disk molecule. This molecule belongs to point group D_{6h} and therefore transitions both in-plane and perpendicular to the molecular plane are allowed.

The uv and LD spectra of coronene (Figures 4 and 5) show that the dichroic ratio over the entire spectrum of coronene has a constant value which is greater than unity (d_0 = 1.53). Thus all the measured transitions in this molecule are polarized in plane only.

Substitution of the value of the dichroic ratio (d_0 = 1.53) into eq 9 results in f = 0.60. Thus according to our hypothetical distribution model, 60% of the coronene molecules are oriented with their planes parallel to the direction of the film stretching.

Pentahelicene

The uv and LD spectra of pentahelicene are shown in Figures 6 and 7. It is evident from this figure that its dichroic ratio, unlike that of coronene, is not constant; it varies along the spectrum. We can however distinguish four regions in the uv spectrum exhibiting a constant dichroic ratio. These are I at 345–290 nm with d_0 = 1.33, II at 270–250 nm with d_0 = 1.48, III at 230–225 nm with d_0 = 1.26, and IV at <210 nm with d_0 = 1.48. We assume that there is no overlap of transitions of different polarization in each of these regions.

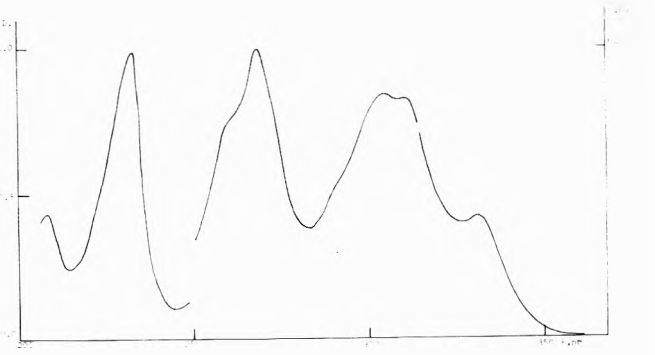

Figure 6. Uv spectrum of pentahelicene in polyethylene.

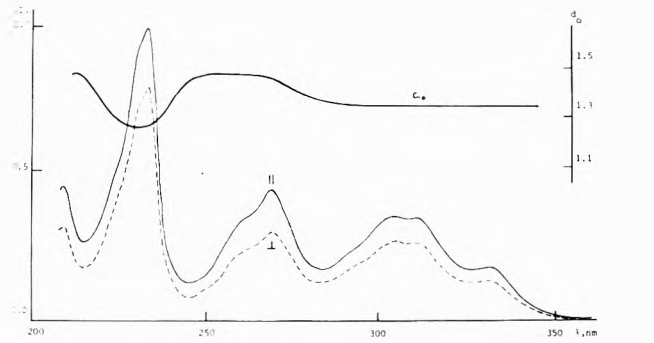

Figure 7. LD spectrum of pentahelicene: lower part, (——) the curve of optical densities obtained by light polarized in the direction of stretching; (– – –) the curve obtained by light polarized perpendicular to the direction of stretching; upper part, the plot of the dichroic ratios d_0 vs. λ.

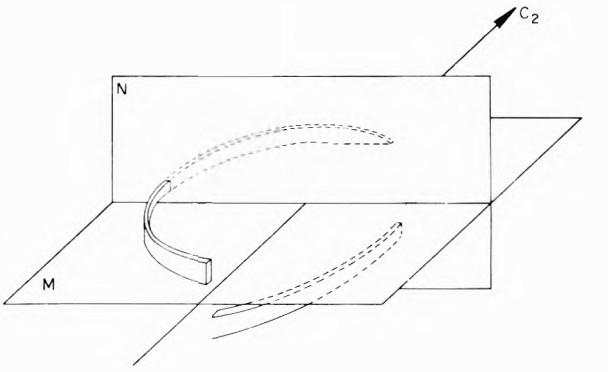

Figure 8. Schematical representation of an helicene molecule: C_2, the twofold symmetry axis (A type symmetry); N, plane perpendicular to the symmetry axis (B type symmetry); M, the best plane of the molecule.

The following analysis is based on the assumption that pentahelicene may be treated as a disk-like molecule oriented with its best plane (M in Figure 8) parallel to the stretching direction.

Accordingly, the regions with highest dichroic ratio, namely II and IV, are composed of in-plane transitions, and those with smaller dichroic ratios, regions I and III, of out-of-plane transitions.[10]

Using the value of d_0 = 1.48 for the in-plane transition and eq 9, we have calculated f to be equal to 0.55. This value is further used to estimate the angles α and β (eq 1

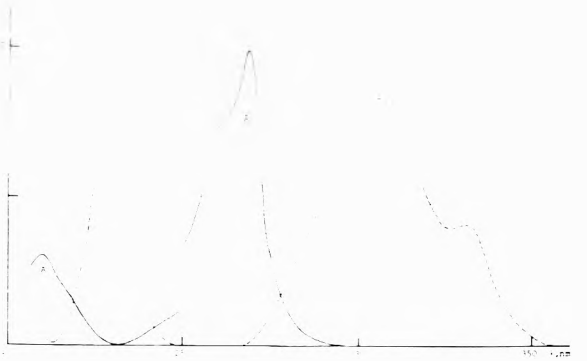

Figure 9. Resolved spectrum of pentahelicene: (——) the in-plane component; (- - -) the out-of-plane component.

TABLE I: Out-of-Plane Angle (Direction of Polarization), Sign of the Rotational Strengths R,[a] and Symmetry Assignments of the Uv Transitions in Pentahelicene

Spectral region (nm)	λ_{max}, nm	This work: Out-of-plane angle (β), deg	This work: Sym-metry[c]	Literature[b]: Sign of R[d]	Literature[b]: Sym-metry[c]
	392			+	A
I (345–290)	328	19	B	−	B
	306	19	B	−	B
II (270–250)	268	0	A	+	A
III (230–225)	230	22	B	−	
IV (<210)	209	0	A	+	

[a] As reported in the literature. [b] Reference 2a. [c] Point group C_2. [d] For the (−) isomer (left-handed M configuration).

and 10). We have thus obtained for the region I $\alpha = 48°$, $\beta = 19°$ and for the region III $\alpha = 49°$, $\beta = 22°$.

In order to resolve the entire spectrum of pentahelicene into its in-plane and out-of-plane components we have taken into consideration that the parts of the spectrum which do not show constant d_0 value are composed of two overlapping transitions. Equation 1 was extended to include extinction coefficients (ϵ_1 and ϵ_2) and the angles (α_1 and α_2) of each of the two overlapping transitions. It will now have the following form

$$d_0 = \frac{\epsilon_1[f\cos^2\alpha_1 + \tfrac{1}{3}(1-f)] + \epsilon_2[f\cos^2\alpha_2 + \tfrac{1}{3}(1-f)]}{\epsilon_1[\tfrac{1}{2}f\sin^2\alpha_1 + \tfrac{1}{3}(1-f)] + \epsilon_2[\tfrac{1}{2}f\sin^2\alpha_2 + \tfrac{1}{3}(1-f)]} \quad (11)$$

Since at any wavelength the total absorption coefficient will be given by

$$\epsilon = \epsilon_1 + \epsilon_2 \quad (12)$$

both ϵ_1 and ϵ_2 may be calculated using eq 11 and 12.

Using these two equations we have resolved the entire spectrum of pentahelicene, as shown in Figure 9.

In Table I we have listed the transitions of pentahelicene according to the wavelength of maximum absorption. Thus region I contains two out-of-plane transitions while region III one out-of-plane transition.

Pentahelicene belongs to point group C_2 and its absorption spectrum consists therefore of transitions which are allowed either along the twofold symmetry axis (A type symmetry) or in a plane perpendicular to this axis (B type symmetry, Figure 8). Obviously the above-defined out-of-plane transitions are of symmetry B, while the in-plane transitions may he of either symmetry. Our LD measurements are unable to distinguish between the latter two possibilities.

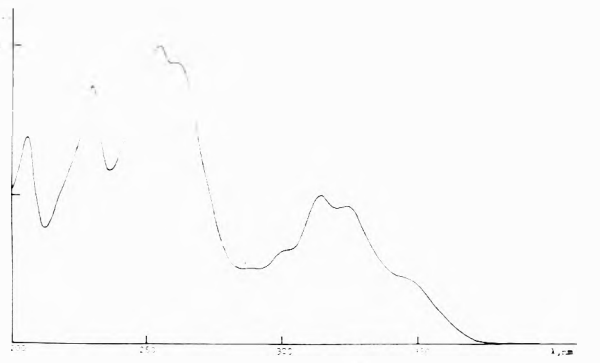

Figure 10. Uv spectrum of hexahelicene in polyethylene.

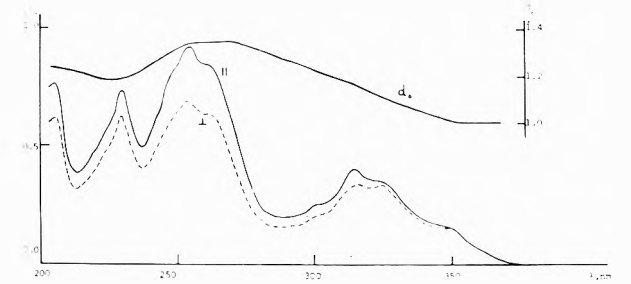

Figure 11. LD spectrum of hexahelicene: lower part, (——) the curve of optical densities obtained by light polarized in the direction of stretching; (- - -) the curve obtained by light polarized perpendicular to the direction of stretching; upper part, the plot of the dichroic ratios d_0 vs. λ.

However, additional information about the symmetries of the in-plane transitions may be obtained by correlation of the LD and CD spectra of pentahelicene. The sign of the CD peaks[2a] in (−)pentahelicene (left-handed M configuration) corresponding to the individual absorptions are given in Table I. It appears that all out-of-plane and in-plane transitions show negative and positive rotational strengths, respectively. Considering Wagniere's[11] suggestion that the transitions of symmetry B in the left-handed M configuration show negative CD peaks and those of symmetry A, positive CD peaks, we may deduce that the in-plane transitions are all of A symmetry.

Table I compares our results with the relative polarization directions previously obtained from emission experiments.[2a] The direction of polarization of three transitions are in accord with the previous estimates. However, we have not analyzed the longest wavelength transition which according to calculations should have A symmetry. On the other hand, the two shortest wavelength transitions have not previously been dealt with.

Hexahelicene

Another example of a disk-like molecule is hexahelicene. Its uv and LD spectra are shown in Figures 10 and 11. There is a distinct similarity between the uv spectrum of this compound and that of pentahelicene. However, as seen from the plot of its dichroic ratio, d_0, *vs.* wavelength, the transitions in hexahelicene are much more overlapped than those of pentahelicene.

We have also divided the spectrum of hexahelicene into four regions, corresponding to those of pentahelicene. These are I at 370–290 nm, II at 280–240 nm, III at 240–220 nm, and IV at <210 nm. However, unlike the case of pentahelicene, only region II and the longer wavelength

TABLE II: Out-of-Plane Angle (Direction of Polarization), Sign of the Rotational Strengths R,[a] and Symmetry Assignments of the Uv Transitions in Hexahelicene

Spectral region (nm)	λ_{max}, nm	This work		Literature			
		Out-of-plane angle (β), deg	Symmetry[b]	Sign of R[c]	Symmetry[b] Weigang[d]	Wagniere[e]	Mason[f]
	411			−	B	B	B
I (370–290)	347	30	B	+	A	A	A
	325	30	B	+		B	B
	315	0	A	(+)	B		B
II (280–240)	255	0	A	−	A	A	A
III(240–220)	230	(30)	B	+			
IV (<210)	205	0	A	−			

[a] As reported in the literature. [b] Point group C_2. [c] For the (+) isomer (right-handed P configuration), ref 2b, 3a, and 3b. [d] Reference 3a. [e] Reference 3c. [f] Reference 2b.

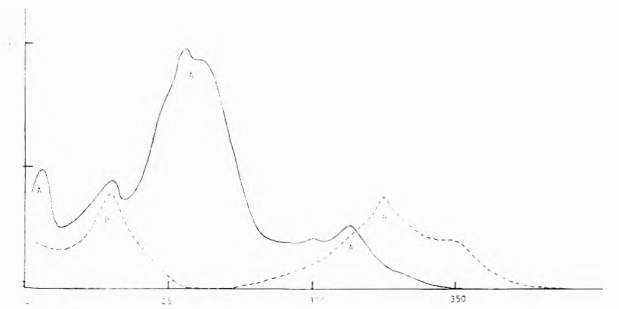

Figure 12. Resolved spectrum of hexahelicene: (——) the in-plane component; (- - -) the "out-of-plane" component

part of region I show a constant dichroic ratio. The dichroic ratio of region II has the highest value in the spectrum, thus representing an in-plane transition. It may also be assumed that the longer wavelength part of region I is polarized out-of-plane, since its dichroic ratio has a smaller value.

Using the value of the dichroic ratio of the in-plane transition $d_0 = 1.35$ and eq 9, we have calculated $f = 0.42$. The out of plane angle β for the longer wavelength part of region I was calculated from eq 10, giving a value of 30° ($\alpha = 55°$).

Unlike the corresponding part of the spectrum of pentahelicene the shorter wavelength part of region I of hexahelicene does not show a constant dichroic ratio and thus does not represent a pure transition. We assume this part of the spectrum to be caused by overlap of the above out-of-plane transition with a new in-plane transition.

Thus region I of the hexahelicene spectrum is composed of three transitions, the two of longest wavelength being out-of-plane and the third in-plane (Figure 12). Further support for this assignment may be obtained by comparison with the CD spectrum, reported by Weigang.[3b] Calculation of the anisotropy factor $\Delta\epsilon/\epsilon$ dividing the $\Delta\epsilon$ of the CD with the corresponding ϵ values of the resolved curve of the out-of-plane transitions results in a constant factor throughout region I of the spectrum. This constant value indicates also that only the out-of-plane transition in this region is optically active.

We have also resolved the shorter wavelength part of the spectrum (regions III and IV) assuming that the out-of-plane transitions have the same direction of polarization as in the region I ($\beta = 30°$). The resulting spectrum shows (Figure 12) that region III contains two transitions of different polarization, while region IV is purely in-plane polarized. Our assumption, however, that the out-of-plane angle β is 30° is apt to be erroneous. However, any other assumption about this angle will always lead to an out-of-plane polarization and the existence of an in-plane component is questionable.

Since hexahelicene belongs to the C_2 point group, its transitions as in pentahelicene are either of A or B type symmetry. It follows that here also the out-of-plane transitions are of B symmetry. In order to distinguish between the A and B symmetries of the in-plane transitions of hexahelicene, we correlate them with the published CD value of (+)hexahelicene (right-handed P configuration).[2b,3a,3b]

It may be seen from Table II that all the B symmetry transitions show negative rotational peaks, which are in accord with Wagniere's[11] postulate. On the other hand, the in-plane transitions show positive rotational peaks except for a transition at 315 nm which is optically inactive) and thus might be of symmetry A.

No complete agreement exists between our results and those previously reported (Table II) on the direction of polarization and the corresponding symmetries of transitions.

According to Mason[2a] there are three transitions in region I of the hexahelicene spectrum, one of A and two of B symmetry, but whose sequence was different than the one found by us. Wagniere[3c] and Weigang[3a] divide this region into two separate transitions only, the one at longer wavelength being of A symmetry. However, there is disagreement on the wavelength of maximum absorption between the two assignments.

In conclusion it may be noted that the comparison of the values of the fraction of orientation of coronene and penta- and hexahelicene (0.60, 0.55, and 0.42, respectively) indicates a gradual change of their shape arising from distortion from planarity. The values of the out-of-plane angles in the corresponding transitions of penta- and hexahelicene (*e.g.*, $\beta = 19$ and 30°, respectively) also point in the same direction.

References and Notes

(1) For Part X in this series see A. Yogev, J. Sagiv, and Y. Mazur, *Rev. Sci. Instrum.*, **45**, 386 (1974).

(2) (a) A. Brown, C. M. Kemp, and S. F. Mason, *J. Chem. Soc. A*, 751 (1971); (b) W. S. Brickell, A. Brown, C. M. Kemp, and S. F. Mason, *ibid.*, 756 (1971).

(3) (a) O. E. Weigang, Jr., J. A. Turner, and P. A. Trouard, *J. Chem. Phys.*, **45**, 1126 (1966); (b) O. E. Weigang, Jr., and P. A. Trouard Dodson, *ibid.*, **49**, 4248 (1968); (c) G. Wagniere, *Proc. Jerusalem Symp. 3rd*, 127 (1970).

(4) D. A. Lightner, D. T. Hefelfinger, T. W. Powers, G. W. Frank, and K. N. Trueblood, *J. Amer. Chem. Soc.*, **94**, 3492 (1972).

(5) (a) A. Yogev, L. Margulies, D. Amar, and Y. Mazur, *J. Amer. Chem. Soc.*, **91**, 4558 (1969); (b) A. Yogev, J. Riboid, J. Marero, and Y. Mazur, *ibid.*, **91**, 4559 (1969); (c) A. Yogev, L. Margulies, and Y. Mazur, *ibid.*, **92**, 6059 (1970); (d) A. Yogev, L. Margulies,

and Y. Mazur, *Ibid.*, **93**, 249 (1971); (e) A. Yogev, L. Margulies, and Y. Mazur, *Chem. Phys. Lett.*, **8**, 157 (1971); (f) A. Yogev, J. Sagiv, and Y. Mazur, *Chem. Commun.*, 411 (1972).
(6) A. Yogev, J. Sagiv, L. Margulies, and Y. Mazur, *Chem. Phys. Lett.*, **23**, 178 (1973).
(7) It appears from previous measurements that this orientational axis is identical with the longitudinal axis of inertia, however, we have not proved this generalization rigorously.
(8) We are indebted to the referees for their comments on this matter.
(9) Similar relations were derived by Norden [*Chem. Script.*, **1**, 145 (1971)] for the interpretation of the linear dichroic spectra of certain triarylmethane dyes.
(10) The "in-plane" transitions are those polarized in the best plane of the molecule (which includes the twofold symmetry axis) whereas the "out-of-plane" transitions are those polarized out of this plane.
(11) G. Wagniere and W. Hug, *Tetrahedron Lett.*, **55**, 4765 (1970).

Infrared Optical Constants of Aqueous Solutions of Electrolytes. Acids and Bases[1]

Paul Rhine, Dudley Williams,*

Department of Physics, Kansas State University, Manhattan, Kansas 66506

G. Michael Hale, and Marvin R. Querry

Department of Physics, University of Missouri, Kansas City, Missouri 64110 *(Received January 7, 1974)*

Publication costs assisted by Kansas State University and the University of Missouri—KC

The normal-incidence spectral reflectances of aqueous solutions of HCl, NaOH, and KOH have been measured in the spectral range 350–5000 cm^{-1}. From the measured values of reflectance we have used a Kramers–Kronig phase-shift analysis to obtain values of the real n and imaginary k parts of the refractive indices of the solutions. The spectral reflectance and the refractive index n of the solutions in the 5000–4000-cm^{-1} region and in other spectral regions that are remote from characteristic water bands increase monotonically with concentration. Plots of absorption index k for HCl as a function of concentration indicate (1) a gradual decrease in the peak height and frequency of the 3400-cm^{-1} water band, (2) strong general absorption in the 3200–2000-cm^{-1} region, (3) an apparent shift of the ν_2 water band toward high frequencies, (4) the appearance of a new band near 1100 cm^{-1}, and (5) shifts of the libration water band to lower frequencies. Plots of k for NaOH as a function of concentration reveal (1) a reduction of the k peak for water near 3400 cm^{-1}, (2) the appearance of strong additional absorption near 2800 cm^{-1} along with strong general absorption in the 3000–1700-cm^{-1} region, and (3) shifts in the position of the librational water band. The observed effects are discussed qualitatively.

Introduction

In an earlier paper[2] we have given the results of a study of near-normal-incidence spectral reflectance of aqueous solutions of alkali halides in the 350–5000-cm^{-1} region of the infrared. By applying the Kramers–Kronig (KK) theorem for phase-shift analysis, we obtained values of the real n and imaginary k parts of the complex refractive index $\tilde{N} = n + ik$ for the spectral region covered in our measurements of reflectance.

In the present paper we report a similar study of solutions of the strong acid HCl and two strong bases, NaOH and KOH. None of the alkali or halide ions involved in our earlier studies had characteristic bands in the infrared. In the present study, the OH^- ion was expected to exhibit a characteristic vibrational band; the hydrogen ions are presumably strongly attached to one or more water molecules in such a way that new characteristic bands could result.

Experimental Section

The experimental arrangements employed in the reflectance measurements were similar in all details to those described in our previous paper; similar methods of carrying out the KK analysis were also employed. The uncertainties δn in n amount to ±1% of the plotted values over most of the range but increase to as much as ±3% in the 500–350-cm^{-1} region. The uncertainty δk is approximately ±0.03 over most of the range but may increase to ±0.05 at 350 cm^{-1}.

Results

Our results are presented graphically in Figures 1–6. The upper panel in each figure gives measured spectral reflectance R at near-normal incidence; the center panel gives the values of the refractive index n as given by the KK analysis; the bottom panel gives the values of the absorption index k. In each panel, for purposes of comparison, we indicate the corresponding values for water by a light continuous curve.

A. Hydrochloric Acid. The spectrum in the 5000–2500-cm^{-1} region is dominated by a strong absorption band, which appears in the vicinity of 3400 cm^{-1} in the spectrum of water at 27°. Figure 1 gives our results for HCl at the concentrations indicated in the legend. The values of R and n for the solutions in the 5000–3800-cm^{-1} range are greater than the values of water; the difference between

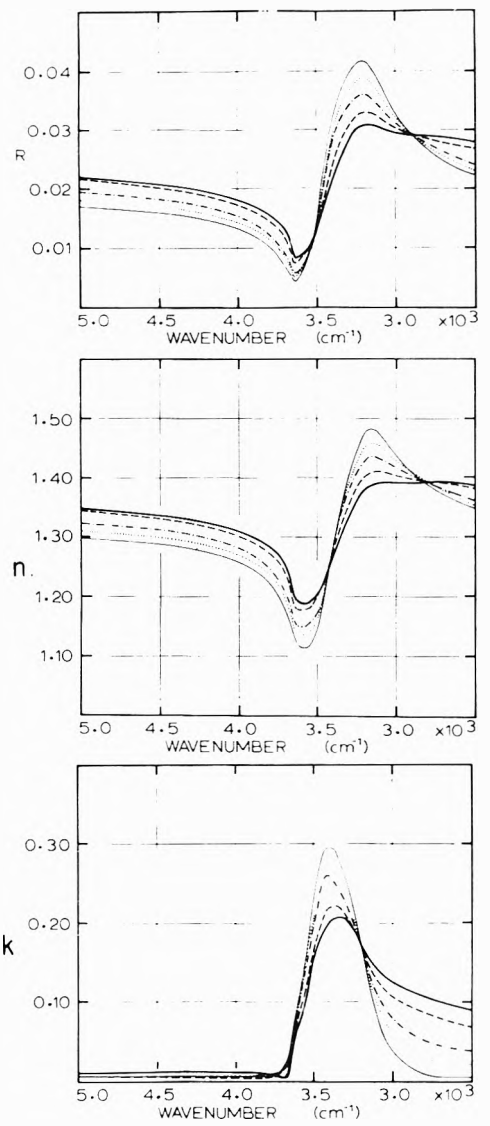

Figure 1. Reflectivity, refractive index, and absorption index curves for HCl solutions: 12 *M*, heavy continuous; 8 *M*, dashed; 4 *M*, dash-dot-dash; 2 *M*, dotted; water, light continuous.

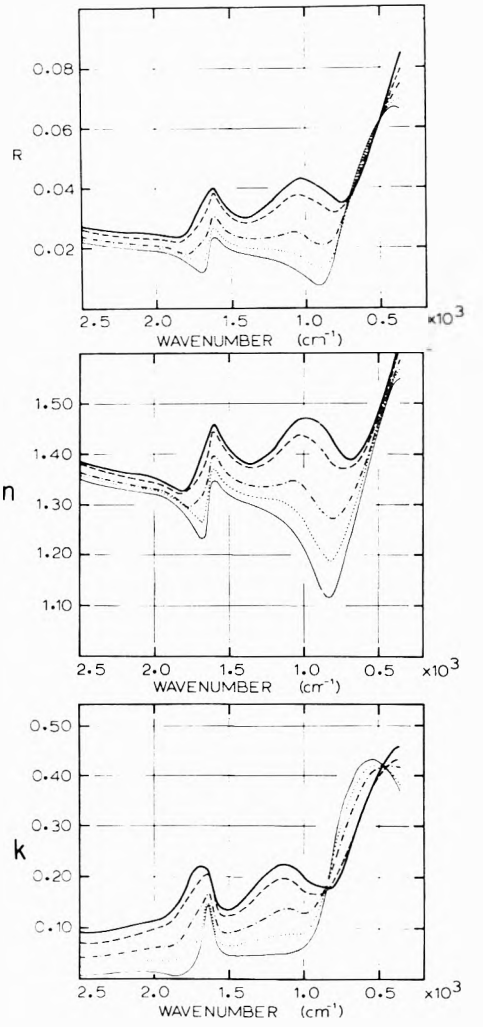

Figure 2. Reflectivity, refractive index, and absorption index curves for HCl solutions: 12 *M*, heavy continuous; 8 *M*, dashed; 4 *M*, dash-dot; 2 *M*, dotted; water, light continuous.

the curves for the solutions and the curve for water increases monotonically with increasing concentration. In the vicinity of the resonance feature near 3400 cm^{-1} the R and n curves cross and the resonance feature becomes less sharp with increasing concentration. In view of our uncertainty $\delta k = 0.03$, the values of the absorption index are not measurably different from zero in the 5000–3800-cm^{-1} range. The absorption peak at 3400 cm^{-1} in pure water shifts to noticeably lower frequencies with increasing concentration of HCl; the peak value of k becomes progressively lower with increasing concentration. Although the k peak appears to increase in width at half-height, this effect may be due to the greatly increased absorption in the low-frequency wing of the band. General absorption occurs in the region between 3200 and 2500 cm^{-1} and increases with increasing concentration; there is no evidence of a separate peak in k associated with the general absorption.

The spectra of HCl solutions in the 2500–350-cm^{-1} region are shown in Figure 2. The spectral reflectance of all solutions is higher than that of water for all regions except the 700–500-cm^{-1} range, where all the measured reflectance curves nearly coincide; the same is true for the n curves. In both R and n curves, the resonance features in the vicinity of the 1640-cm^{-1} water band apparently become broader and shift to higher frequency. An additional resonance feature not present in the spectrum of pure water produces a broad n maximum near 1000 cm^{-1} in the 8 and 12 *M* solutions.

The absorption characteristics of the solutions are shown by the plots of k in the bottom panel. All solutions exhibit stronger absorption than water in the 2500–1800-cm^{-1} region; the absorption in this region is general and is not characterized by clearly discernible peaks. The k peak appearing at 1640 cm^{-1} in the spectrum of pure water appears to increase in height, to broaden, and to shift to higher frequencies with increasing concentration. At the highest HCl concentrations a new broad band having no counterpart in the water spectrum appears in the vicinity of 1100 cm^{-1}. The librational band with maximum k near 600 cm^{-1} in the water spectrum shifts to progressively lower frequencies with increasing HCl concentration.

B. Sodium and Potassium Hydroxide. The results obtained for NaOH and KOH in the 5000–2500-cm^{-1} region

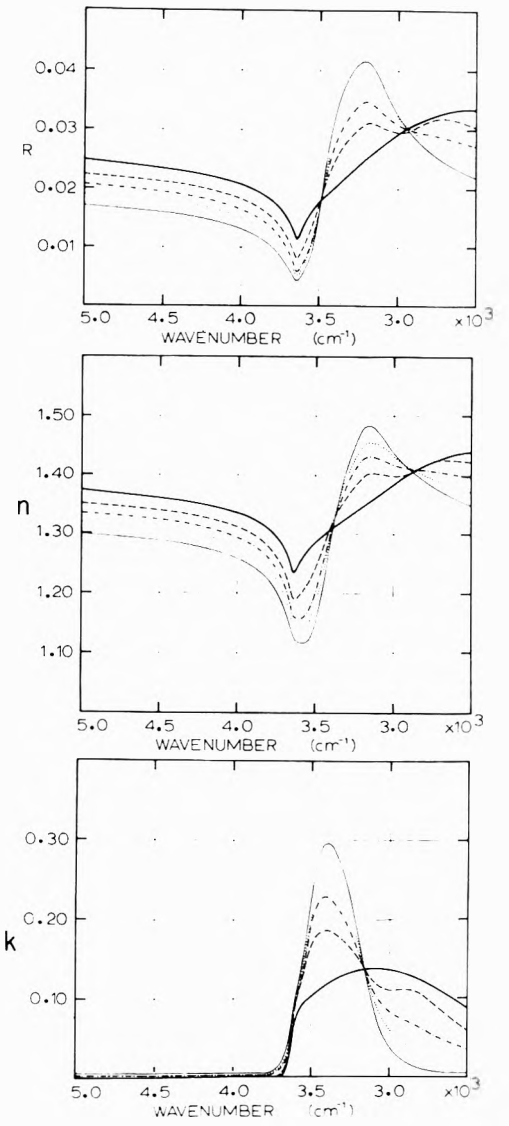

Figure 3. Reflectivity, refractive index, and absorption index curves for NaOH solutions: 16 *M*, heavy continuous; 8 *M*, dashed; 4 *M*, dash-dot-dash; 2 *M*, dotted; water, light continuous.

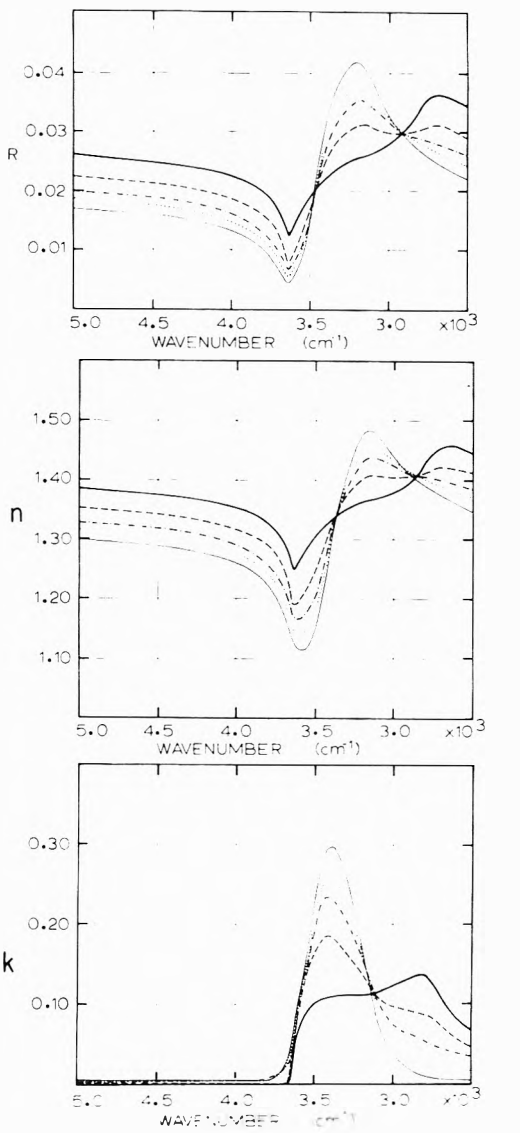

Figure 4. Reflectivity, refractive index, and absorption index curves for KOH solutions: 16 *M*, heavy continuous; 8 *M* dashed; 4 *M*, dash-dot-dash; 2 *M*, dotted; water, light continuous.

are shown in Figures 3 and 4, respectively. In spectral regions remote from absorption bands, the values of R and n are slightly larger for KOH than for NaOH; in other respects the contours of the R and n curves for the solutions are similar for corresponding concentrations. In the vicinity of the 3400-cm^{-1} water band, the dispersion features in the R and n curves for the 2 and 4 M solutions become progressively less pronounced with increasing concentration. The curves for the 8 M solutions for both hydroxides show clearly an additional small dispersion feature near 3000 cm^{-1}; further evidence of this feature appears in the n and R curves for the 16 M solution of KOH but is less apparent in the corresponding curves for NaOH.

The plots of the absorption index k in the bottom panels of Figures 3 and 4 indicate a progressive reduction of peak height of the 3400-cm^{-1} water band along with a progressive broadening of the band toward lower frequencies with increasing concentration. For the 8 M solutions, there is some evidence of a second incompletely resolved band near 2800 cm^{-1}. In the 16 M solution of KOH, there is clear evidence of a peak near 2800 cm^{-1}, where the value of k is greater than that of k at 3400 cm^{-1}. In the k curve for 16 M NaOH, a single broad region of absorption replaces the two peaks appearing at 3400 and 2800 cm^{-1} in the spectrum of the 8 M solution.

The results obtained in the 2500–350-cm^{-1} region for NaOH and KOH are shown in Figures 5 and 6, respectively. In most of this spectral region, values of R and n become progressively greater with increasing concentration; however, in the 600–400-cm^{-1} region, the R and n curves for the 16 M solutions cross the corresponding curves for lower concentrations and attain lower values at 400 cm^{-1}. In the vicinity of the 1640-cm^{-1} water band all R and n curves for the hydroxide solutions exhibit dispersion features. However, for the 8 and 16 M solutions there is some evidence of a narrower additional dispersion feature near 1500 cm^{-1}; this narrow feature is clearly separated from the 1640-cm^{-1} water band in the NaOH solutions but is barely resolved in the KOH solutions. Except for the 16 M solutions, the major dispersion feature near 600 cm^{-1} shifts to progressively lower frequencies with increasing concentration; for the 16 M solution the maxima in R and n appear at considerably higher frequencies than for the less concentrated solutions.

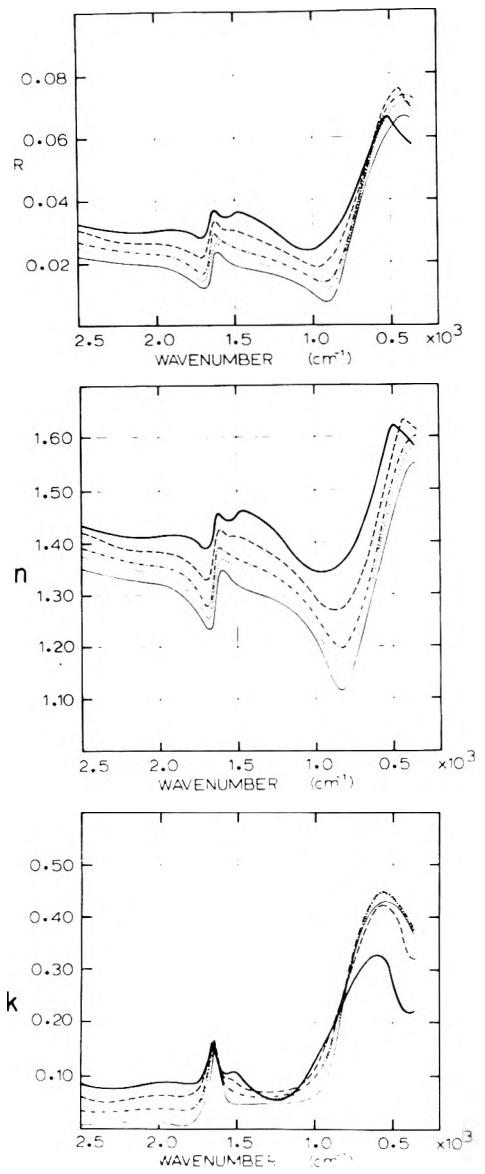

Figure 5. Reflectivity, refractive index, and absorption index curves for NaOH: 16 *M*, heavy continuous; 8 *M*, dashed; 4 *M*, dash-dot-dash; 2 *M*, dotted; water, light continuous.

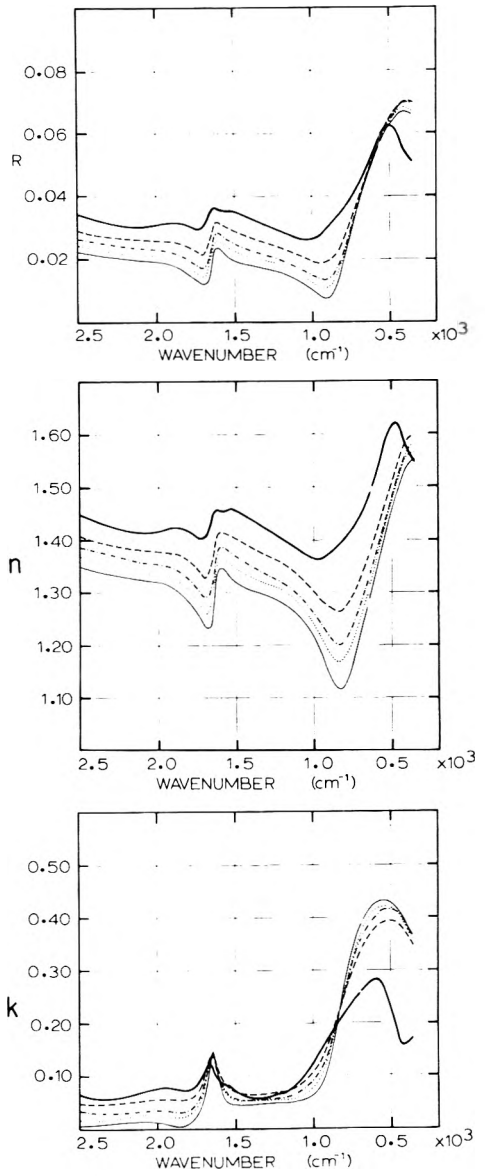

Figure 6. Reflectivity, refractive index, and absorption index curves for KOH: 16 *M*, heavy continuous; 8 *M*, dashed; 4 *M*, dash-dot-dash; 2 *M*, dotted; water, light continuous.

The absorption indices k for the hydroxides are plotted in the bottom panels of Figures 5 and 6. In the entire spectral region between 3400 and 1640 cm^{-1} the values of k for all solutions are much greater than the corresponding k values for water; for the more concentrated hydroxide solutions the absorption indices k at all frequencies in the interband region maintain values that are nearly half the value of k at the center of the 1640-cm^{-1} band in pure water. The value of k at 1640 cm^{-1} remains constant in all solutions within our limits of uncertainty $\delta k = 0.03$; there is some evidence of a splitting of the band at higher concentrations. The values of k for the 2 and 4 M solutions in the vicinity of the 600-cm^{-1} water band are also within the limits of uncertainty equal to the k value for pure water. There is a small progressive shift of the 600-cm^{-1} band to lower frequencies in the 2, 4, and 8 M KOH solutions but little change in band position for the corresponding NaOH solutions; this band becomes narrower, has a smaller maximum value of k, and shifts noticeably to higher frequencies in the 16 M solutions.

Discussion of Results

The major portion of the new information regarding solutions obtainable from the present reflectance studies is connected with the quantitative measurements of the refractive indices n and the absorption indices k. Many earlier measurements of transmission spectra of acids and bases have provided only qualitative values of Lambert absorption coefficients $\alpha(\nu)$, since the published curves were labeled "absorption" or "transmission" with no numbers on the ordinate scales: in view of the difficulties[3] involved in preparing uniform absorption layers of well-measured thickness, these earlier transmission studies could not have been expected to yield quantitative results. However, many of the features shown in the $k(\nu)$ *vs.* ν plots of Figures 1–6 have been noted in earlier studies. No earlier studies have provided values of the refractive index $n(\nu)$ for comparison with the present work.

A. Hydrochloric Acid. In a beautiful piece of work Falk and Giguere[4] have investigated the transmission spectra of aqueous solutions of five mineral acids with the purpose

of identifying spectral features characteristic of the H_3O^+ ion; these authors also reviewed earlier work on the subject. Falk and Giguere observed increased absorption associated with broad bands with maxima at 1205, 1750, and 2900 cm^{-1}, which they attributed to the H_3O^+ ion, and report that the lifetime of this ion in aqueous solution is longer than 10^{-13} sec. These band positions are in close agreement with the positions of H_3O^+ bands reported in earlier infrared studies of crystalline hydrates of strong acids[5-7] and in related Raman studies.[8,9]

In view of these results and other structural information, the observed spectrum has been interpreted[7] in terms of a pyramidal form of H_3O^+, which is isoelectronic with NH_3; the incompletely resolved ν_1 and ν_3 fundamentals are associated with the broad band near 2900 cm^{-1}, the ν_4 fundamental with the band near 1205 cm^{-1}, and the ν_2 fundamental with the band near 1750 cm^{-1}. However, Pavia and Giguere[10] have shown that the spectrum of perchloric acid dihydrate gives evidence of the ion $H_5O_2^+$. Gilbert and Sheppard[11] have recently obtained infrared spectra of crystalline mono- and higher hydrates of HCl and HBr; the higher hydrates exhibit features not clearly attributable to H_3O^+; in particular, in the di- and trihydrates there is evidence for the $H_5O_2^+$ ion. In the spectrum of the $H_5O_2^+$ ion, the existence of which is supported by X-ray diffraction measurements,[12,13] bands corresponding to ν_2 and ν_4 in H_3O^+ in the monohydrate spectrum are split into sharp components in the dihydrate and broaden in the trihydrate; the ν_1 and ν_3 bands in H_3O^+ coalesce into a single somewhat narrower band in the di- and trihydrate spectra.

The broad regions of absorption shown in our plots of k for HCl shown in Figures 1 and 2 doubtless include contributions from both H_3O^+ and $H_5O_2^+$ ions. However, attempts to divide the integrals $\int k(\nu)\,d\nu$ or $\int \alpha(\nu)\,d\nu$ between the two forms of hydrated H^+ ions would at present represent mere speculation; however, evaluation of these integrals in restricted spectral intervals for various HCl concentrations might be used in testing various possible future theories.

We have also compared the reflection spectra of HCl with HBr. Although HBr solutions have higher reflectivity as a result of stronger Br^- bands in the ultraviolet,[2] the general shape of the two reflectance curves exhibit marked similarity. Similarities in the spectra of HCl and HBr crystal hydrates were also noted by Gilbert and Sheppard.[11]

The observed shift of the libration band of the solutions in the 600-cm^{-1} region to lower frequencies with increasing HCl concentration confirms the results obtained in the earlier transmission study of Draegert and Williams.[14]

B. Sodium and Potassium Hydroxide. Although there has been little discussion of the nature of the hydration of the OH^- ion, the general absorption of the hydroxides in the region between the 3400- and 1640-cm^{-1} water bands is nearly as intense as the corresponding HCl absorption, which we have attributed to the H_3O^+ and $H_5O_2^+$ ions. The absorption spectrum of crystalline NaOH is characterized by a sharp band at 3637 cm^{-1} attributed to the OH^- ion;[15] a similar band at 3600 cm^{-1} occurs in the spectrum of KOH.[16-18] Jones[19] has reported an extremely sharp OH^- band at 3678 cm^{-1} in crystalline LiOH; in the hydrated crystal $LiOH{\cdot}H_2O$ Jones found a somewhat broadened OH^- band at 3574 cm^{-1} and an extremely broad, intense band with a maximum at 2850 cm^{-1}, which he attributed to the overlapping ν_1 and ν_3 bands of the strongly hydrogen-bonded water molecule of crystallization. The frequency of the band due to the water of crystallization is even lower than that of the H_2O molecule in ice. In a Raman study of KOH solutions Busing and Hornig[20] report a band with a sharp peak near 3600 cm^{-1} with an accompanying broad band extending to frequencies as low as 2200 cm^{-1}; these authors attribute the sharp peak to OH^- and the broad band to three overlapping unresolved bands associated with molecules of the solvent.

Although there is no evidence of a resolved sharp OH^- band in the bottom panels of Figures 3 and 4, the absorption index curves rise abruptly near 3700 cm^{-1}; this abrupt rise may correspond to the sharp band noted by Busing and Hornig in their Raman study. However, if a sharp OH^- band is present in the infrared, its intensity is small as compared with the broader bands at lower frequencies. It would appear from Figures 3 and 4 that there are two such bands with frequencies in the vicinity of 3400 and 2800 cm^{-1}, respectively; it is tempting to attribute the former to the normally hydrogen-bonded molecules of liquid water and the latter to water molecules strongly hydrogen-bonded to OH^- ions. If this interpretation involving two types of differently hydrogen-bonded molecules is correct, it might also account for the apparent splitting of the band at 1640 cm^{-1} associated with the ν_2 bending fundamental of the H_2O molecule in liquid water; this splitting is particularly pronounced in the 16 M solution curves in Figures 5 and 6.

We note that in the $k(\nu)$ *vs.* ν curves for the 16 M hydroxide solutions there is an apparent shift of the librational maximum to higher frequencies and a marked narrowing of the band. The curves for the other less concentrated solutions are in general agreement with the earlier work of Draegert and Williams,[14] whose study was limited to hydroxide solutions with concentrations of 12 M and less and was hampered by the lack of suitable absorption cell windows.

We note that the influence of Na^+ and K^+ ions on the water structure is nearly negligible as compared with the influence of the OH^- ions, which are capable of forming hydrogen bonds with water molecules. In the case of acids, the influence of Cl^- and Br^- ions on the water structure is similarly small as compared with the hydrogen ions that are responsible for the hydrates H_3O^+ and $H_5O_2^+$, or possibly even higher hydrates.

The structure of the crystal monohydrate $LiOH{\cdot}H_2O$ has been determined by Pepinsky[21] on the basis of X-ray diffraction measurements; his results indicate that the distance between the oxygen of the H_2O unit and the oxygen of the nearest OH^- unit is 2.68 Å as compared with the 2.76 Å O–O distance in ice. This short distance implies strong hydrogen bonds $H_2O\cdots OH^-$; thus, it seems probable that the broad band with maximum near 2850 cm^{-1} in the spectrum of the monohydrate crystal is indeed due to strongly hydrogen-bonded H_2O molecules. The increasingly strong absorption noted in this region in the present study would seem to indicate increasingly great numbers of strong $H_2O\cdots OH^-$ hydrogen bonds as the concentration increases. In the case of the 16 M concentration, there are no longer sufficient numbers of water molecules to approximate a normal water structure; this paucity of solvent molecules results in the marked decrease in $k(\nu)$ in the 3400-cm^{-1} region and also near 600 cm^{-1}, where stronger bonds to OH^- units could also account for the apparent increase in the frequency of the li-

bration band of water. If this interpretation is correct, the lack of significant decrease of $k(\nu)$ near 1640 cm^{-1} together with the apparent splitting of the ν_2 peak would indicate greater transition probabilities for the more strongly bonded H_2O units than for the H_2O units in liquid water; this would be in contrast to the situation in ice, for which peak $k(\nu)$ values in this region are somewhat smaller[22] than for liquid water.

As for the mean lifetimes of the local environment of hydrogen-bonded $H_2O\cdots OH^-$ units, the reasonably well-defined bands observed in the present study and in earlier Raman studies indicate that local lattice structures exist for times long compared with 10^{-13} sec. However, the fact that single proton resonances[23] are observed in nmr studies of concentrated solutions of strong bases indicates that the mean lifetimes of local lattice structures are short compared with 10^{-7} sec.

In closing, we note that many of our interpretations of the observed spectra in the 2500–300-cm^{-1} region can be tested by extending studies of crystalline $LiOH\cdot H_2O$ into the far infrared and that more detailed information regarding band shapes can probably be obtained by ATR studies of solutions.

We also note that Zundel and his associates[24,25] have recently discussed the properties of $H_5O_2^+$ ions. Their theoretical work dealing with the hydrogen bonds involved may provide an interpretation of some of the continuous general absorption that we have observed in the spectra of acids and bases in the present study.

Acknowledgment. It is a pleasure to acknowledge helpful discussions with Professors C. H. Moser, R. M. Hammaker, K. F. Purcell, and B. Curnutte.

References and Notes

(1) Supported in part at Kansas State University by the Office of Naval Research and at the University of Missouri, Kansas City, by the National Science Foundation.
(2) P. Rhine, D. Williams, G. M. Hale, and M. R. Querry, *J. Phys. Chem.*, **78**, 238 (1974).
(3) (a) A. N. Rusk, M. R. Querry, and D. Williams, *J. Opt. Soc. Amer.*, **61**, 895 (1971); (b) C. W. Robertson and D. Williams, *ibid.*, **61**, 1316 (1971).
(4) M. Falk and P. A. Giguere, *Can. J. Chem.*, **35** 1195 (1957).
(5) D. E. Bethell and N. J. Sheppard, *J. Chim. Phys.*, **50**, C72 (1953).
(6) C. C. Ferriso and D. F. Horning, *J. Amer. Chem. Soc.*, **75**, 4113 (1953).
(7) C. C. Ferriso and D. F. Hornig, *J. Chem. Phys.*, **23**, 1464 (1959).
(8) J. T. Mullhaupt and D. F. Hornig, *J. Chem. Phys.*, **24**, 169 (1956).
(9) R. C. Taylor and G. L. Vidale, *J. Amer. Chem. Soc.*, **78**, 5999 (1956).
(10) A. C. Pavia and P. A. Giguere, *J. Chem. Phys.*, **52**, 3551 (1970).
(11) A. S. Gilbert and N. Sheppard, *Chem. Commun.*, 337 (1971).
(12) J. O. Lundgren and I. Olovsson, *Acta Crystallogr.*, **23**, 966 (1967).
(13) J. O. Lundgren and I. Olovsson, *Acta Crystallogr.*, **23**, 971 (1967).
(14) D. A. Draegert and D. Williams, *J. Opt. Soc. Amer.*, **48**, 401 (1968).
(15) W. R. Busing, *J. Chem. Phys.*, **23**, 933 (1955).
(16) J. A. Ibers, J. Kumamoto, and R. G. Snyder, *J. Chem. Phys.*, **33**, 1164 (1960).
(17) R. G. Snyder, J. Kumamoto, and J. A. Ibers, *J. Chem. Phys.*, **33**, 1171 (1960).
(18) R. A. Buchanan, *J. Chem. Phys.*, **31**, 870 (1959).
(19) L. H. Jones, *J. Chem. Phys.*, **22**, 217 (1954).
(20) W. R. Busing and D. F. Hornig, *J. Phys. Chem.*, **65**, 284 (1961).
(21) R. Pepinsky, *Z. Kristallogr., Abt. A*, **102**, 119 (1940).
(22) J. Schaaf and D. Williams, *J. Opt. Soc. Amer.*, **63**, 726 (1973).
(23) H. S. Gutowsky and A. Saika, *J. Chem. Phys.*, **21**, 1688 (1953).
(24) R. Lindemann and G. Zundel, *J. Chem. Soc., Faraday Trans. 2*, **68**, 979 (1972).
(25) R. Janoschek, E. G. Wiedemann, and G. Zundel, *J. Chem. Soc., Faraday Trans. 2*, **69**, 505 (1973).

Hyperfine Models for Piperidine Nitroxides

C. C. Whisnant, S. Ferguson, and D. B. Chesnut*

P. M. Gross Chemical Laboratory, Duke University, Durham, North Carolina 27706 *(Received March 7, 1974)*

Publication costs assisted by the National Science Foundation

Esr spectra for the piperidine nitroxides 2,2,6,6-tetramethylpiperidine-*N*-oxyl (TEMPO) and 2,2,6,6-tetramethylpiperidine-*N*-oxyl-4-ol (TEMPOL) in benzene have been obtained in which the proton hyperfine structure is partially resolved. Comparisons to spectra calculated for coupling constants inferred from prior nmr investigations confirm the proper hyperfine models for these two species. For TEMPO the magnetic nonequivalence of the axial and equatorial substituents at each position of the piperidine ring is averaged. This is not the case for TEMPOL, and INDO calculations indicate that the coupling constant of larger absolute magnitude at each position is associated with the equatorial substituent. Using the appropriate models the proton hyperfine envelope line widths are calculated as a function of the individual line width. The magnitude of the corrections necessary to obtain the true line width from the envelope width is greater for TEMPO and TEMPOL than for previously studied radicals of this type.

Introduction

Nitroxide radicals with adjacent tetramethyl substitution have been the chief source of spin labels for many biological and physical applications.[1] In particular, the piperidine nitroxide derivative 2,2,6,6-tetramethylpiperidine-*N*-oxyl (TEMPO) and the hydroxyl compound (the 4-ol compound, TEMPOL) have been used extensively since they are small and compact molecules giving rise to a minimum of perturbation to the system which they probe. Although less emphasis is currently placed on the

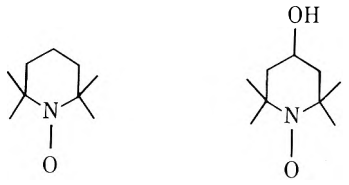

TEMPO TEMPOL

measurement of rotational correlation times from the spectra of such species because of the many complicating features now known,[2] often these times can be obtained through careful measurement. Furthermore, it is still of basic importance to understand the origin of the observed line widths in the relatively simple spectra of such species. One typically observes simply the three-line nitrogen hyperfine esr spectra, but it has been well established now that a major contributor to the overall width of such lines is the usually unresolved proton hyperfine structure. Poggi and Johnson[2] have pointed out that hyperfine structure significantly affects line widths and rotational activation energies and that in order to accurately determine these quantities the widths of the individual components for each major line in the nitroxide spectra must be determined by simulation of the spectra *via* computers. Jolicoeur and Friedman[3] in the introduction to their paper concerning the effects of hydrophobic interactions on dynamics in aqueous solutions give a good example of the effect of unresolved hyperfine structure on what one would otherwise take to be the intrinsic nitrogen hyperfine line width. Since the measurement of the line width is the chief ingredient in the equations which determine the rotational correlation time, it is clear that an accurate determination of this parameter must be had.

Obviously, in order to provide for corrections such as unresolved hyperfine structure one needs to know the correct model for the hyperfine coupling in the nitroxide species involved. Recent work in this laboratory has been concerned with the hydroxy derivative of the piperidine nitroxide (TEMPOL) in both model membrane systems[4] and in ion-exchange resins.[5] Hints of extra-nitrogen hyperfine structure in certain ion-exchange resins have lead us to be concerned with the underlying nature of the structure involved. Briere, *et al.*,[6] have studied a variety of simple nitroxide species by observing the contact shift of the protons in concentrated radical solutions. Previously, Kreilick[7] carried out similar measurements as well and reported some partially resolved esr spectra for the piperidine-based nitroxides. These two studies give the same coupling constants for the radical TEMPO but result in somewhat different conclusions for the TEMPOL species. Briere, *et al.*, were able to differentiate between not only the axial and equatorial methyl groups in the piperidine system but also, in a number of cases, the different β-methylene protons as well while Kreilick's investigation indicated that axial and equatorial substituents at these positions were not different in their coupling constants.

We have obtained resolved esr spectra of both TEMPO and TEMPOL in degassed benzene and by match of the experimentally observed and computer-simulated spectra have confirmed the coupling constants for TEMPO and have established that the coupling constants of Briere, *et al.*, are a suitable model for the proton hyperfine interaction in this radical. In addition, by calculating spectra for component line widths where no resolution is seen one is also able to illustrate for TEMPO and TEMPOL the correction that must be made to the *apparent* line width in order to calculate the true line width that should be used in the calculation of correlation times.

Experimental Section

TEMPO and TEMPOL were prepared according to the procedure of Briere, Lemaire, and Rassat[8] and solutions approximately 1×10^{-4} and 5×10^{-4} *M*, respectively, in benzene were degassed on a vacuum line by the freeze–pump–thaw technique. After sufficient degassing the samples were frozen and the tubes sealed off under reduced pressure. By refrigeration when not in use such samples appear to be indefinitely stable. Measurements were made at room temperature or slightly below on a standard 12-in. Varian V-4502-15 X-band spectrometer. Since effects of saturation on the proton hyperfine structure were readily apparent power levels were kept below 1.00 mW; the intrinsically narrow line widths require minimum modulation applitude (approximately 0.04 G) in order to avoid modulation broadening.

The proton hyperfine envelope for a single nitrogen component (*i.e.*, one of the three major nitrogen hyperfine splittings) was simulated with a double-precision Fortran program for summing derivatives of lorentzian lines. The calculations were carried out on the Triangle Universities Computation Center's IBM 370/165. A *single* line width ($\Delta H_{pp} = 2/\sqrt{3}T_2$, the derivative peak-to-peak width) was employed and the program also determined and listed the positions of the extrema of the total spectrum. The goodness of fit between calculated and observed spectra was taken to be measured by

$$R = \sum_{i}^{N} |A_i^{\text{obsd}} - A_i^{\text{calcd}}| / \sum_{i}^{N} A_i^{\text{obsd}} \qquad (1)$$

where the A_i represent the amplitudes at selected abscissas on the positive half of the derivative spectrum. Extrema of the spectra were used for resolved spectra while multiples of the observed envelope width were employed in cases where the proton hyperfine structure was unresolved. Typically four (for unresolved spectra) or six (for resolved spectra) such points were used (the value of N). R as defined in eq 1 may be viewed as an average relative error where a weighting factor proportional to A_i^{obsd} is used.

Results and Discussion

General Results. The coupling constants as reported by Briere, *et al.*, and by Kreilick are given in Table I along with other data. These are the coupling constants employed in the spectral simulation of a single envelope (one of the nitrogen hyperfine triplets) in which it was assumed that each component line of the envelope could be represented by a single line width. Lorentzian line shapes were assumed and the comparison of a calculated spectrum for a given line width with the experimentally observed spectrum was made by calculating the previously defined quantity R. Figures 1 and 2 show the $m = 0$ envelope for the best fit to the experimental data for both the Briere and Kreilick models. Figure 3 illustrates how the quantity R varies with ΔH_{pp} in the case of the TEMPOL radical over the range of significant resolution and qualitative fit. The curves in Figure 3 clearly indicate the Briere model to be correct in terms of a significantly lower value of R

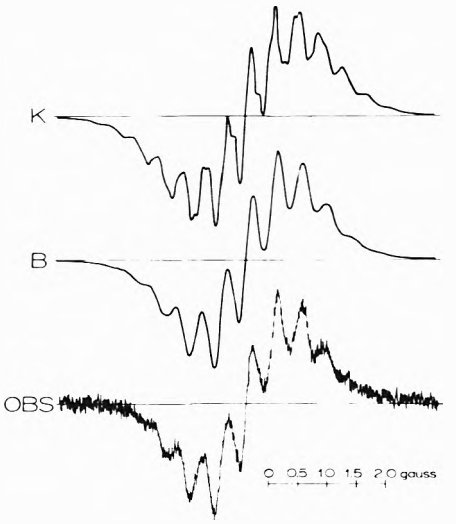

Figure 1. Best-fit derivative curves for TEMPOL according to the Kreilick (K) and Briere (B) models and the experimental spectrum (OBS) for the $m = 0$ envelope of the 5×10^{-4} M radical in degassed benzene at room temperature.

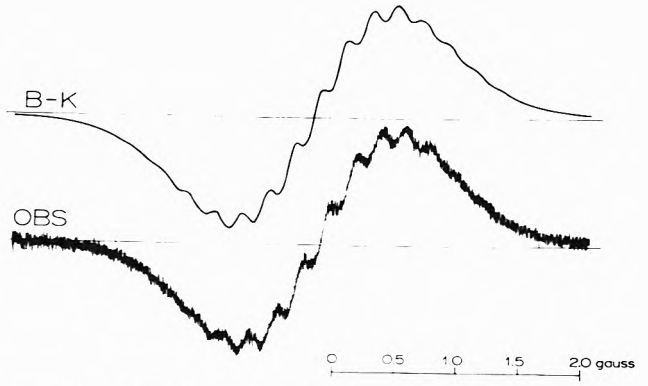

Figure 2. Best-fit curve for TEMPO according to the Briere–Kreilick model (B–K) and the experimental spectrum (OBS) for the $m = 0$ envelope of the 1×10^{-4} M radical in degassed benzene at +8°.

and this judgment is confirmed by an examination of Figure 1 which illustrates the very good agreement between the best fit Briere model and the observed spectrum and, conversely, the poor qualitative fit of the best fit Kreilick model. These results clearly confirm Briere's experimental measurement of two different methyl proton splittings as well as confirming their assignment of different coupling constants for axial and equatorial proton species at the β- and γ-methylene positions in the piperidine ring. Both Briere and Kreilick have identical models for TEMPO and the best fit model spectrum is shown to agree well with that which is observed as seen in Figure 2. For the $m = 0$ components the minimum value of R was 0.060 for TEMPOL and 0.013 for TEMPO.

Because of the small hyperfine coupling constants involved in these two species the observed spectrum is quite sensitive to experimental and instrument conditions. As mentioned before, very low modulation amplitudes are needed to avoid modulation broadening; in the present study one can easily detect effects of modulation broadening with modulation amplitudes greater than 0.04 G. Power values lower than 1 mW were normally employed in order to avoid power saturation broadening and to obtain maximum resolution. In fact, the use of the power

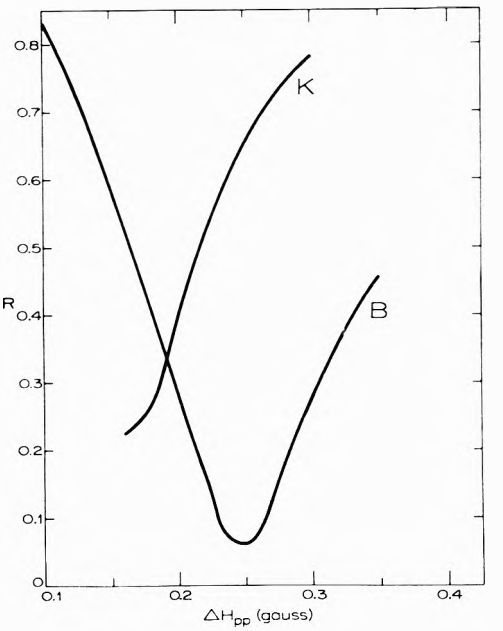

Figure 3. Variation of the goodness-of-fit parameter R as a function of the line width ΔH_{pp} for the Kreilick (K) and Briere (B) models. The data plotted are for comparison with the experimental $m = 0$ envelope and only extend over that region of fit where qualitative agreement is possible.

saturation technique can be used as a further confirmation of the model assignment here in that one can artificially and experimentally create a spectrum whose component line widths are significantly broader and thus obtain a spectrum which requires analysis in terms of a different line width parameter. This is possible since power saturation affects the line width but not the line shape of an individual component. The TEMPOL species was not sufficiently power saturated at high powers to achieve a completely unresolved line but it was possible to do so in the case of TEMPO. An envelope (the $m = 0$ envelope) with essentially no structure was obtained and was fit to the theoretical Briere model using a line width parameter, ΔH_{pp}, of approximately 0.34 G and yielding an R value of approximately 0.007. This adds further confirmation to the analysis. The very small value of R obtained in the power saturated spectra is, however, in part due to the relative insensitivity of the spectra to the line width parameter in this range of resolution.

Although the variation of coupling constants with temperature may be small,[7] the variation is sufficient in the present cases to significantly affect the degree of resolution. Although good resolution was obtained for TEMPOL at room temperature, such was not the case for TEMPO. Indeed, no structure could be seen at room temperature whereas significant structure was observed at 8°.

The absence of structure in the present cases of undegassed samples (oxygen broadening present) is not unexpected in a system such as this where the hyperfine coupling constant differences are very small. In such cases a very small amount of paramagnetic species will cause exchange broadening and remove superhyperfine structure. However, even for the degassed samples in benzene, concentration effects were evident. While a 5×10^{-4} M TEMPOL solution was adequate for analysis, significant enhancement of the resolution for TEMPO was obtained in reducing the concentration by a factor of five to 1×10^{-4} M. A significant point is raised here with regard to

such exchange broadening. The optimum resolved TEMPO spectrum gave a best fit for a ΔH_{pp} of 0.20 G, R = 0.013, while the optimum fit to the exchange broadened 5×10^{-4} M solution yields a line width approximately 0.63 G at an R value of 0.021. This latter result should be compared to the power saturated (and therefore line shape unaffected spectrum) where a line width of 0.34 G gave rise to a R factor of approximately 0.007. The significant increase of the R value for the 5×10^{-4} M TEMPO solution (triple that of the power saturated unresolved spectrum) indicates that the model is considerably less applicable in the exchange broadened case. This is to be expected since the effects of exchange are not only to distort the line shapes but also to cause significant shifts of the lines resulting in effectively different hyperfine couplings. This is a serious complication in the attempt to properly analyze line widths of such spectra. A similar problem is going to arise in the case of exchange broadening by oxygen. In particular, spin label studies of systems of biological interest often involve the use of aqueous solutions that can obviously not be degassed without harmful effects to the system under study. One fortunate factor here is that, for the radicals in the present study at least, the effects of oxygen are less in aqueous solutions than in solutions of benzene; that is, the simple act of bubbling nitrogen through the solution results in very little improvement in the nitroxide envelope width for radicals in aqueous solution but causes the initially broader lines in benzene to approach the narrower but still unresolved width in water.

Spectra with resolution are sufficiently easy to analyze in terms of choice of model because of the great sensitivity of the simulated spectrum. However, when the lines are sufficiently broad to remove resolution a single envelope is observed and the model fit becomes less sensitive. Furthermore, single unresolved envelopes have often been interpreted in terms of single nitrogen hyperfine lines. When such widths are used to calculate correlation times errors will be made. Figure 4 shows the variation of the observed peak to peak line width of an unresolved envelope as a function of the true line widths of the component lines making up the envelope. In any correlation time analysis it is the true ΔH_{pp} that should be employed and not the line width of the observed width of the envelope. One can see from the figure that significant corrections must be made to the observed width to obtain the true line width and also that in this region of relatively low resolution different models and different radicals become less sensitive to the true line width employed. Figure 5 shows a set of spectra for increasingly larger intrinsic line widths. One can see that the detailed resolution vanishes quickly as the true single line width becomes comparable to the average hyperfine coupling constant. At this point the shape of the envelope is very nearly gaussian. Furthermore, as the envelope width increases to the point of showing no superhyperfine structure, a line is observed which is neither lorentzian nor gaussian. Accordingly, analyses of unresolved lines which assume a specific line shape will be in error. This is particularly important when one is comparing line widths of two of the three nitrogen envelopes since the broadening effects in each envelope will differ from one to another resulting in different effective line shape parameters. All in all, as shown by others before, the analysis of line widths and correlation time is in systems like this is difficult and must be undertaken with great care.

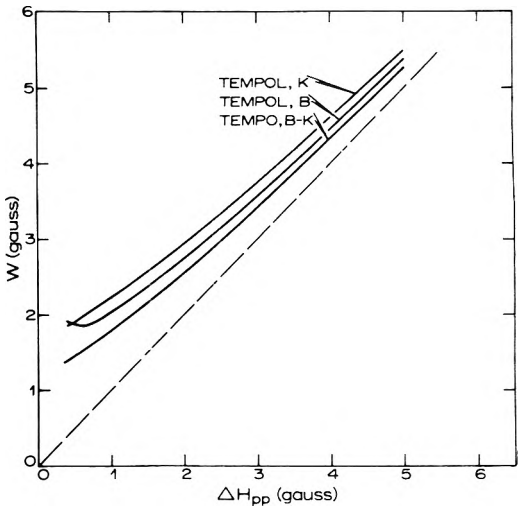

Figure 4. The peak-to-peak envelope width W as a function of the true single line width ΔH_{pp} for the Briere (B) and Kreilick (K) models for TEMPO and TEMPOL in the region of no individual line resolution. Comparison of the calculated curves to the dashed 45° line illustrates the nonlinear nature of W as a function of ΔH_{pp}.

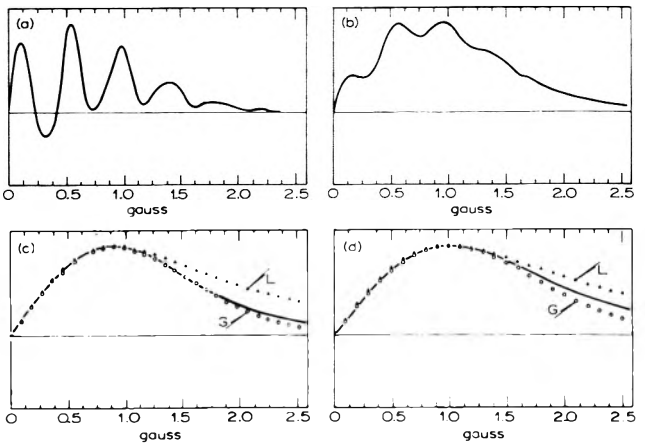

Figure 5. Calculated spectra for a single hyperfine envelope (one m value) of TEMPOL for single line ΔH_{pp} values of 0.15 (a), 0.35 (b), 0.60 (c), and 1.00 G (d). Lorentzian (L) and gaussian (G) curves are superimposed on the latter two spectra for comparison.

Envelope Asymmetry. The degree of fit of the calculated and observed spectra was done by assuming a line width for each proton species *independent* of the proton quantum number. Although the experimentally observed envelopes show some definite asymmetry, averages of low-field and high-field portions were used to compare to the calculated spectra. The line width asymmetry in nitroxide spectra is normally quite evident and is, of course, used to determine the rotational correlation time of the radical species. This asymmetry arises from the correlated anisotropy of the g and hyperfine tensors and leads to a line width dependence on the nuclear quantum number(s). To attempt to analyze the proton superhyperfine structure in this way in the present case would be very complicated since, for the case of TEMPOL, for example, five different coupling constants and group quantum numbers as high as 3 (for the equivalent methyl group protons) are involved. One might expect the effect to be small since the dipolar contribution to the hyperfine tensor while large and significant for the nitrogen nucleus (near the majority

TABLE I: Observed and Calculated Hyperfine Coupling Constants (in Gauss) for TEMPOL and TEMPO[a]

Species	TEMPOL			TEMPO		
	a^{obsd-K}	a^{obsd-B}	a^{calcd}	a^{obsd-K}	a^{obsd-B}	$a^{calcd\,b}$
γ-OH			−0.01			
γ-H(ax)	+0.09	+0.07	+0.02	+0.18	+0.18	+0.08
γ-H(eq)			+0.14			
β-CH_2(ax)	−0.29	−0.31	−0.17	−0.39	−0.39	−0.55
β-CH_2(eq)	−0.29	−0.48	−0.92			
α-CH_3(ax)	−0.43	−0.02	−0.11	−0.22	−0.23	−0.24
α-CH_3(eq)	−0.43	−0.45	−0.37			
N		15.3[c]	+8.59		15.3[c]	8.59

[a] The observed values are denoted as K and B for the data of Kreilick (ref 7) and Briere, *et al.* (ref 6). [b] Average of axial and equatorial values for TEMPOL. [c] One-half the measured splitting of the ±1 nitrogen lines, this work, in benzene.

of the spin density) might well be expected to be small for the protons spatially removed from the nitrogen. This argument, however, while attractive may not be valid since the observed effects themselves are small. Experimentally one *does* measure spectral parameters (amplitudes of peaks and valleys of the envelope derivatives) that differ in a statistical sense from the low-field portion to the high field portion from the experimental error in the corresponding measurements in a given half of the hyperfine envelope. These differences tend to be larger in the central portion of the envelopes but fall within experimental error at the outer portions for the spectra exhibiting good resolution. For spectra where individual proton lines are unobserved (low resolution) the differences are not statistically significant. These effects do not affect our model comparisons and would not contribute in a significant way to a calculation of "mean" rotational correlation times that ignores them. However, they are real and might well be explored in a more general and detailed study of the theory of line widths and rotational correlation times.

INDO Calculations. Since the previous nmr (and, for that matter, the present esr analysis) cannot experimentally distinguish between the equatorial and axial α-methyl and β-methylene protons in TEMPOL we carried out INDO calculations[9] to see if the theory gave a fit sufficiently good to allow an assignment of the coupling constants. The results are contained in Table I for calculations using the crystal structure data of Lajzerowicz-Bonneteau[10] with the molecule in the chair conformation and with the γ-OH group occupying the equatorial position. Presumably, this conformation is also the dominant one in solution although some effects from the axial OH conformer or the intermediate skew structure might come in. Calculations using the axial conformer showed relatively little change (<0.01 G) in the calculated coupling constants for axial or equatorial species; the γ proton can occupy an equatorial position only in the axial conformer. The reported values for the methyl protons represent simple averages of 12 discrete proton orientation and are meant to simulate the rotation of the methyl groups. There is a sizeable variation with angle, the variation being +0.27 to −0.43 G for the axial methyl species and −0.04 to −0.89 G for the equatorial methyl protons. Calculations of this type are sometimes sensitive to precise molecular geometry and without a careful and complete analysis of the various molecular geometric parameters we would not claim the reported values to be the best possible. However, the general agreement of magnitude (and sign) does indicate that the α-methyl and β-methylene protons occupying equatorial positions have larger coupling constants then those occupying axial positions. Including the γ-methylene proton one can further generalize by saying that equatorial species have coupling constants of larger absolute magnitude. Our incomplete calculations do not allow us to comment on what sort of conformer interconversion averaging takes place experimentally in solution or whether it is incomplete or rapid between species of differing thermodynamic stability. The calculated nitrogen coupling constant is also included in the table and does not show particularly good agreement with that measured experimentally by esr.

Although no calculations were explicitly carried out for TEMPO one would well expect the results to be essentially identical with those for TEMPOL with the possible exception of the γ-methylene proton. For TEMPO, equatorial and axial conformations are identical and the fact that a rapid interconversion is occurring is shown by the presence of single α-methyl and β-methylene coupling constants both in Briere's and Kreilick's data. Table I shows that a simple average of the axial and equatorial coupling constants for each proton type yields values in reasonable agreement with the experimental ones.

Summary

Unresolved proton hyperfine interaction significantly affects the line widths and line shapes of the principal lines in esr spectra of nitroxide radicals. The purposes of the present study were (a) to establish the correct models for proton hyperfine interaction in the piperidine nitroxides 2,2,6,6-tetramethylpiperidine-*N*-oxyl (TEMPO) and 2,2,6,6-tetramethylpiperidine-*N*-oxyl-4-ol (TEMPOL) and (b) to illustrate the magnitude of appropriate line width corrections for these radicals in benzene.

Esr spectra for these radicals in benzene have been obtained in which the proton hyperfine structure is partially resolved. Comparison of these spectra to spectra simulated using various models of the proton hyperfine coupling have confirmed the magnitude assignment of Briere, *et al.*[6] For TEMPO the magnetic nonequivalence of the axial and equatorial substituents at each position of the piperidine ring is effectively averaged. This is not the case for TEMPOL, and INDO calculations indicate that at each ring position the coupling constant of larger absolute magnitude is associated with the equatorial substituent.

Using the appropriate models for the proton hyperfine interaction observed envelope line widths have been calculated as a function of the true individual line width and are reported in graphical form. The magnitude of the correction needed to obtain the true width from the apparent one is greater for TEMPO and TEMPOL than for previously studied radicals. The effect of intrinsic proton line

width on the line shape of the overall envelope has also been illustrated.

Acknowledgments. This work was supported in part by the National Science Foundation Grant No. GP-22546. We are indebted to Duke University for partial funding of the computer calculations and to L. B. Gilman and J. M. Ciskowski for aid in sample preparation.

References and Notes

(1) Good reviews are to be found in (a) C. L. Hamilton and H. M. McConnell, "Structural Chemistry and Molecular Biology," A. Rich and N. Davidson, Ed., W. H. Freeman, San Francisco, Calif., 1968, p 115; (b) H. M. McConnell and B. G. McFarland, *Quart. Rev. Biophys.*, **3**, 91 (1970); (c) S. Schreier-Muccillo and I. C. P. Smith, "Progress in Surface and Membrane Science," J. F. Danielli, Ed., Academic Press, New York, N. Y., in press.
(2) G. Poggi and C. S. Johnson, Jr., *J. Magn. Resonance*, **3**, 436 (1970).
(3) C. Jolicoeur and H. L. Friedman, *Ber. Bunsenges. Phys. Chem.*, **75**, 248 (1971).
(4) K. Mukai, C. M. Lang, and D. B. Chesnut, *Chem. Phys. Lipids*, **9**, 196 (1972).
(5) D. B. Chesnut and J. F. Hower, *J. Phys. Chem.*, **75**, 907 (1971).
(6) R. Briere, H. Lemaire, A. Rassat, P. Rey, and A. Rousseau, *Bull. Soc. Chim. Fr.*, **12**, 4470 (1967).
(7) R. W. Kreilick, *J. Chem. Phys.*, **46**, 4260 (1967).
(8) R. Briere, H. Lemaire, and A. Rassat, *Bull. Soc. Chim. Fr.*, **11**, 3273 (1965).
(9) P. A. Dobosh, Program 141, Quantum Chemistry Program Exchange, Indiana University, 1968.
(10) P. J. Lajzerowicz-Bonneteau, *Acta Crystallogr., Sect. B*, **24**, 196 (1968).

Potential Function Model of Weak and Strong Hydrogen Bonds

J. N. Spencer,* George J. Casey, Jr., John Buckfelder, and H. D. Schreiber

Lebanon Valley College, Annville, Pennsylvania 17003 *(Received December 27, 1973)*

Publication costs assisted by Lebanon Valley College

The Lippincott-Schroeder empirical potential function model of the hydrogen bond has been used to calculate the bond energies of the strongly hydrogen-bonded bihalide ions HX_2^- and the bond properties of the weakly hydrogen bonded CHY (Y = O, S, N) systems. For experimental X-H-X bihalide internuclear distances, the bond energies for HF_2^-, HCl_2^-, HBr_2^-, and HI_2^- were calculated to be −32.5, −16.8, −21.7, and −13.8 kcal mol^{-1}, respectively. The influence of geometric parameters on CHY bonds is discussed. CHO and CHN bonds are calculated to be comparable in strength and have comparable frequency shifts. CHS bonds are stronger than CHO or CHN bonds with larger frequency shifts.

Introduction

Hydrogen bonding in the bihalide ions, HX_2^- (X = F, Cl, Br, I) and in systems of the type C-H···Y (Y = O, S, N)[2] has been well established. However, the bond energies and the influence of geometric relations on these bonds are not well known. Several theoretical studies on these systems have been made but no treatment by the Lippincott-Schroeder empirical potential function model of the hydrogen bond[3,4] (hereafter designated PFM) has been attempted. This model has been shown to allow calculations which provide excellent agreement with experimental hydrogen bond properties.[3-7] Correspondingly, the PFM has been used to calculate some of the properties of the less well-known weakly hydrogen-bonded systems CHY and to provide empirical calculations for the bond energies of the strongly hydrogen-bonded bihalide ions. The methods of calculation used in this study have been previously described.[5]

Bihalide Ions

Thermodynamic,[8-13] X-ray,[14] ir[15-21] and Raman,[21] neutron[21-23] diffraction, and nmr[24,25] investigations of the bihalides have been reported, but no direct experimental determination of the energy of the hydrogen bond in these systems has been made. Accordingly, The PFM has been used to calculate empirical bond energies for the HX_2^- ions. The parameters used for the calculations are given in Table I.

HF_2^-. Prior to the work of Williams and Schneemeyer[22] it had been thought[15,23,26] that the HF_2^- ion was a linear, symmetric ion with the F-H-F distance equal to 2.26 Å and the H-F distance equal to 1.13 Å, however these workers have shown that the F-H-F structure is probably asymmetric. The enthalpy of formation of this hydrogen bond has been variously reported to range from −27 to −50 kcal mol^{-1}.[9,14,27] The generally accepted bond enthalpy of −37 kcal mol^{-1} was established by Harrell and McDaniel[12] by measuring the temperature dependence of the vapor pressure for the reaction between *n*-alkylammonium salts and HF.

Murthy, Bhat, and Rao[28] have used molecular orbital calculations to calculate the F-H-F distance to be 2.2 Å with an H-F distance of 1.1 Å. The bond energy calculated was −300 kcal. Extended Hückel calculations by these same authors gave an F-H-F distance of 2.4 Å and a bond energy of −39 kcal. Noble and Kortzeborn[29] using LCAO-MO-SCF studies calculated the F-H-F distance as 2.25 Å, HF as 1.11 Å, and the bond energy as −40 kcal. Schuster[30] calculated F-H-F as 2.25 Å, HF as 1.125 Å, and the bond energy as −106 kcal from CNDO *ab initio* methods.

TABLE I: Primary Parameters Used for the Lippincott–Schroeder Empirical Potential Function Model of the Hydrogen Bond[a]

Bihalide	$k \times 10^{-5}$, dyn cm^{-1}	$r_e = r_e^*$, Å	D_e, kcal	ω_e, cm^{-1}
HF_2^-	9.654	0.9168	135.1	4138.33
HCl_2^-	5.160	1.2746	102.1	2989.74
HBr_2^-	4.117	1.413	86.47	2649.67
HI_2^-	3.142	1.604	70.47	2309.50

[a] All data taken from ref 36 except for HF_2^- which was taken from "JANAF Thermochemical Tables," The Dow Chemical Co., Midland, Mich., 1963.

For a F-H-F distance of 2.26 Å, a bond energy of −32.5 kcal mol^{-1} and H-F distance of 1.10 Å is calculated from the PFM. A frequency shift of 1564 cm^{-1} is obtained from the model which is in poor agreement with reported shifts of approximately 2690 cm^{-1} [9,15,26] for the hydrogen stretching motion.

The reported F-F distance in the cyclic hexamer, $(HF)_6$, is 2.53 Å.[31] If the F-H-F bond is considered to be linear, a bond energy of −7.16 kcal mol^{-1} of HF bonds is calculated from the PFM (Table II). This is in good agreement with the reported bond enthalpies of −6.67[32] and −6.80 kcal mol^{-1}.[33] However, Janzen and Bartell[31] suggest that some ring protons migrate off the F-F ring axis. If this migration occurs, the F-H-F bond will no longer be linear. For an H-F-F angle of about 10°, the energy calculated from the PFM is −6.28 kcal mol^{-1} of HF bonds. Thus it appears that if migration of the proton does occur, the migration is such as to give an H-F-F angle not greatly exceeding 10°. The dependence of the bond energy on angle is about the same for all the bihalide ions, *i.e.*, an angle of about 10° for a given X-X distance reduces the bond energy by about 1 kcal. The agreement of the bond energies calculated from the PFM with the accepted bond enthalpies for HF_2^- and $(HF)_6$, which have quite different F-H-F distances, indicates that the relation between bond energy and internuclear distance is adequately described by the PFM. Because the F-F distance in HF_2^- is well known, the PFM must give reasonable agreement with accepted bond energies if any degree of reliance is to be placed in the model for the calculation of bond energies for the other bihalide ions whose geometry is less well known.

Table II lists some of the results of the calculations of the PFM for hydrogen bonded F-H-F systems.

TABLE II: Hydrogen Bond Properties of F–H–F Systems as Calculated from the Potential Function Model

F-H-F, Å	H-F, Å	−E, kcal	Frequency shift, cm^{-1}
2.15	1.068	52.76	536
2.20	1.087	43.69	994
2.25	1.101	34.60	1472
2.30	1.104	25.91	1933
2.35	1.083	18.68	2148
2.40	1.045	13.91	1867
2.45	1.012	10.69	1462
2.50	0.988	8.28	1128
2.55	0.971	6.41	873
2.60	0.959	4.96	678

TABLE III: Hydrogen Bond Properties of HCl_2^- as Calculated from the Potential Function Model

Cl-H-Cl, Å	H-Cl, Å	−E, kcal	Frequency shift, cm^{-1}
3.00	1.483	32.47	727
3.05	1.496	26.57	1319
3.10	1.499	20.85	1511
3.15	1.482	15.80	1511
3.20	1.444	12.05	1424
3.25	1.405	9.43	1173

HCl_2^-

Waddington[16] and McDaniel and Vallee[11] report that HCl_2^- is linear and centrosymmetric like HF_2^-. Evans and Lo[17] also report from studies on crystals that the HCl_2^- ion is linear but that the symmetry of the ion depends upon the nature of the cation in the crystal structure. Evans and Lo consider the HCl_2^- crystalline salts to be of two types. Type I salts are linear and unsymmetric and type II salts are linear and centrosymmetric; the type II salts have the stronger hydrogen bond. In addition to the difference in hydrogen bond energy for type I and type II salts there is also a difference in the asymmetric hydrogen stretching frequency, the type II salt having the greater frequency shift. Nibler and Pimentel[34] have evidence that the type II salt is unsymmetrical but they could not resolve the symmetry of the type I structure.

Schroeder and Ibers[14] used X-ray diffraction to determine the Cl-Cl distance in HCl_2^- to be 3.14 ± 0.02 Å. The bond energy calculated from the PFM for this internuclear distance is −16.8 kcal mol^{-1}. The uncertainty of ±0.02 Å in the internuclear distance gives a corresponding uncertainty of about 2 kcal in the calculated bond energy. The reported bond enthalpies range from −8.3 to −14.2 kcal mol^{-1}.[11] A frequency shift of 1510 cm^{-1} was calculated as compared to the reported frequency shift of 1439 cm^{-1} [11,17] for a type I salt. The agreement between the calculated and experimental frequency shift is no doubt fortuitous and no distinction between type I and II salts seems possible from the PFM. The PFM does indicate that the difference between type I and II salts must lie in the difference in the Cl-Cl distance in the two salts; *i.e.*, if the Cl-Cl distance is the same in both types of salts, the predicted bond energies and frequency shifts would be identical. For linear ions, the only parameter necessary for calculation of bond energy from the PFM is the X-H-X distance, therefore any asymmetry in the structure enters into the calculations only in as far as the asymmetry affects the internuclear X-X distance.

Table III reproduces some of the results of the calculations of the PFM for HCl_2^-.

HBr_2^-

McDaniel and Vallee[11] established an apparent lower limit of −12.8 kcal mol^{-1} for the bond enthalpy of the HBr_2^- ion by measuring the heats of reaction for various $(n\text{-alkyl})_4N^+HBr_2^-$ salts. Evans and Lo[18,19] argue for the existence of type I and type II HBr_2^- salts corresponding to HCl_2^-. Schroeder and Ibers[14] report the Br-Br distance in HBr_2^- as 3.35 ± 0.02 Å as obtained from X-ray work. From this internuclear distance, a hydrogen bond energy of −21.7 kcal mol^{-1} is calculated from the PFM. This large discrepancy with the suggested limiting bond enthalpy of −12.8 kcal mol^{-1} is somewhat surprising, especially when the agreement between calculated and estimated bond energies and enthalpies for HF_2^- and HCl_2^- is considered. If this internuclear distance is correct, the bond enthalpy estimates may be low. An additional value for the Br-Br distance may be estimated from

TABLE IV: Hydrogen Bond Properties of HBr_2^- as Calculated from the Potential Function Model

Br-H-Br, Å	H-Br, Å	$-E$, kcal	Frequency shift, cm^{-1}
3.25	1.613	31.49	412
3.30	1.630	26.59	661
3.35	1.642	21.67	922
3.40	1.644	16.94	1175
3.45	1.624	12.80	1329
3.50	1.584	9.76	1239
3.55	1.545	7.63	1019
3.60	1.515	6.02	811

TABLE V: Hydrogen Bond Properties of HI_2^- as Calculated from the Potential Function Model

I-H-I, Å	H-I, Å	$-E$, kcal	Frequency shift, cm^{-1}
3.65	1.812	25.47	340
3.70	1.830	21.52	552
3.75	1.842	17.59	774
3.80	1.843	13.78	993
3.85	1.825	10.40	1140
3.90	1.786	7.88	1086

Nibler and Pimentel[34] who have calculated the H-Br distance in HBr_2^- to be 1.73 Å. If the ion is assumed to be linear and symmetric the Br-Br distance would be 3.46 Å giving a PFM calculation of the bond energy to be −12.2 kcal mol^{-1}. If the estimated bond enthalpies are considered to be nearly correct, the Br-Br distance must be close to that as calculated from the work of Nibler and Pimentel, however, because of the qualitative nature of the latter estimate for the Br-Br distance it seems possible that the PFM is in error in this instance. A frequency shift of 1329 cm^{-1} is calculated from the PFM, which is somewhat higher than the experimental value of 1230 cm^{-1} [18] for a type I salt.

Table IV lists the results of the calculations of the PFM for HBr_2^-.

HI_2^-

The estimated bond enthalpies for HI_2^- range from −7.3 to −12.4 kcal mol^{-1}.[1] McDaniel and Vallee,[11] who report the lower limit of −12.4 kcal mol^{-1} for the hydrogen bond enthalpy in HI_2^-, find a frequency shift of 660 cm^{-1}. Reddy, Knox, and Robin[35] found that the I-H-I distance in the inclusion compound $HI_3 \cdot 2C_6H_5CONH_2$ to be 3.80 Å from X-ray work. No report of type I or type II salts for HI_2^- was discovered in the literature. For an I-H-I distance of 3.80 Å, a hydrogen bond energy of −13.8 kcal mol^{-1} is calculated from the PFM. The HI distance given by Nibler and Pimentel[34] for HI_2^- is 1.93 Å. If HI_2^- is assumed to be linear and symmetric, the I-I distance would be 3.86 Å giving a calculated bond energy of −10.0 kcal mol^{-1}. The frequency shift is calculated to he 993 cm^{-1} for an I-I distance of 3.80 Å.

Table V lists the results of the calculations of the PFM for HI_2^-. A summary of the calculated bond energies for the bihalide ions is given in Table VI. The results of the calculations given in these tables also show the relation between the bond energies and internuclear distance for the hydrogen bond in the bihalides.

C-H···Y

The PFM of the hydrogen bond does not usually take into consideration the nature of the parent molecule which supplies the species participating in the hydrogen bond, *i.e.*, attention is focused solely on the atoms X-H···Y that form the hydrogen bond. However, in the case of the C-H···Y hydrogen bond, the PFM parameters for the CH bond will depend somewhat on the nature of the parent molecule insofar as the hybridization of the carbon atom affects the CH bond properties. For example, the hydrogen bonding ability of a CH group decreases with changes in the hybridization of carbon in the order C(sp)-H > $C(sp^2)$-H > $C(sp^3)$-H, and increases with the number of adjacent electron-withdrawing substituents. Agreement between calculated and experimental C-H···Y bond properties was slightly better when acetylene parameters were used instead of ethylene or methane parameters. Correspondingly, the CH bond parameters given in Table VII for general use in the PFM were taken from acetylene. However, for calculations from the PFM for a specific bond, better agreement with experiment is found when the parameters are taken from a molecule with the same hybricization as the molecule participating in the bond. The geometric parameters needed in the calculations are defined in Figure 1, and the parameters used for C-H···Y systems in general are given in Table VII. To account for changes in translational and rotational degrees of freedom on dissociation of the hydrogen bond Lippincott and Schroeder[3] have used a correction of $\frac{3}{2}RT$. Thus to convert intermolecular hydrogen bond energies to enthalpies, the energies reported in this work must be made more negative by $\frac{3}{2}RT$.

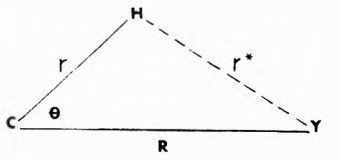

Figure 1. Geometry and symbols used for the description of the CHY hydrogen bond.

TABLE VI: Calculated and Estimated Bond Energies and Enthalpies for the Bihalide Ions, HX_2^-

Bihalide	X-H-X, Å	Calcd $-E$, kcal mol^{-1}	Lower limit for $-\Delta H$, kcal mol^{-1}	Range[e] for $-\Delta H$, kcal mol^{-1}
HF_2^-	2.26[f]	32.5	37[d]	27–58
HCl_2^-	3.14 ± 0.02[g]	16.8	14.2[c]	8.3–14.2
	3.14[a]			
HBr_2^-	3.35 ± 0.02[g]	21.7	12.8[c]	9.4–12.8
	3.46[a]	12.2		
HI_2^-	3.80[b]	13.8	12.4[c]	7.3–12.4
	3.86[a]	10.0		

[a] Calculated from the equation given by Nibler and Pimentel (ref 34) assuming a linear symmetric ion. [b] I-I distance from ref 35. [c] Reference 11. [d] Reference 12. [e] Reference 1. [f] Reference 26. [g] Reference 14.

C-H···O

The existence of C-H···O hydrogen bonds has been confirmed by the association of proton-donating CH groups with suitable strong oxygen-containing bases in solution.[2,37-40] The C-H···O bond enthalpy is reported to range from −1.6 to −3.6 kcal mol^{-1} for bond formation in solution.[41] Brand, *et al.*,[42] however, have shown that considerable discrepancy exists among ΔH values determined by various methods.

Studies on the crystalline state[43-46] have apparently confirmed the existence of C-H···O hydrogen bonds in solids. Much of the evidence for these hydrogen bonds is based upon crystallographically observed short C-H···O

TABLE VII: Parameters and Constants for C-H···Y Systems

	D_0, kcal[a]	$k_0 \times 10^{-5}$, dyn cm^{-1} [b]	r_0, Å[a]	D_0*, kcal	k_0* $\times 10^{-5}$, dyn cm^{-1}	r_0*, Å	ω_0, cm^{-1} [b]	$b \times 10^{-4}$, cm^{-1} [c]
CHO	103	5.85	1.058	118[e]	7.76[e]	0.97[e]	3372	4.8
CHS	103	5.85	1.058	91.5[d]	4.14[d]	1.334[d]	3372	4.8
CHN	103	5.85	1.058	101[a]	6.35[b]	1.025[a]	3372	4.8

[a] G. Herzberg, "Electronic Structure of Polyatomic Molecules," Van Nostrand, Princeton, N. J., 1967. [b] G. Herzberg, "Infrared and Raman Spectra," Van Nostrand, New York, N. Y., 1945. [c] Reference 5. [d] Reference 6.

intermolecular contacts.[47] Pimentel and McClellan[1] and Donohue[48] view this evidence with skepticism and believe the short contacts are no real proof for association of CH groups with oxygen atoms via hydrogen bonds in crystals. Although Sim[49] believes that there are indisputable cases of C-H···O hydrogen bonds in crystals, he argues that short C-H···O crystallographic contacts *per se* cannot be indiscriminately assigned as due to hydrogen bonds. In order to prove the existence of C-H···O hydrogen bonds in crystal structures, not only must there be a relatively short contact but there also must be evidence for an attractive association which specifically involves the hydrogen atom. Thus it must be possible to relate the geometry of the molecule and crystal to the properties of CH···O systems.

The applicability of the PFM to C-H···O hydrogen bonds was first tested by using compounds for which the geometric parameters and CH stretching frequency shifts (difference between the unassociated CH stretching frequency in solution or vapor and the associated frequency in the solid state) have been experimentally determined. Calabrese, McPhail, and Sim[43] have determined the structure of propargyl 2-bromo-3-nitrobenzoate from X-ray techniques and have determined the CH frequency shift for the compound. The intermolecular C-H···O bond distance (R) was found to be 3.39 Å with a hydrogen bond angle (θ) of about 17°, while the frequency shift was reported as 47 cm^{-1}. When this bond distance and angle are used in the PFM, a frequency shift of 27 cm^{-1} and a CHO bond energy of −0.2 kcal mol^{-1} are calculated. No experimental determination of the bond energy was reported.

Ferguson and Islam[44] found the C-H···O bond distance to be 3.21 Å and the hydrogen bond angle θ to be 12.2° in the X-ray study of crystalline *o*-chlorobenzoylacetylene. The CH stretch frequency shift was found to be 69 cm^{-1}. When this bond distance and angle are used in the PFM, a frequency shift of 84 cm^{-1} and a bond energy of −0.4 kcal mol^{-1} is calculated. Although the geometric parameters are not known, it is interesting to note that a frequency shift upon crystallization of 73 cm^{-1} has been reported for the similar compound benzoylacetylene.[39]

Calabrese, McPhail, and Sim[50] found the geometric parameters R and θ to be somewhat the same for the C-H···O intermolecular hydrogen bonds in propargyl 2-bromo-3-nitrobenzoate (R = 3.39 Å, θ = 17°) and triethylprop-2-nylammonium *p*-bromobenzenesulfonate (R = 3.36 Å, θ = 18°), but that the CH frequency shift for the two compounds differed considerably being 47 and 113 cm^{-1}, respectively. They concluded that there was no simple relation between geometric factors and the frequency shift. The PFM predicts just the opposite, *i.e.*, for a given set of geometric parameters, the frequency should be fixed. According to the PFM the benzenesulfonate should only have a frequency shift of about 3 cm^{-1} greater than the nitrobenzoate. The only noticeable chemical differences between these two compounds are that (1) in the C-H···O association in propargyl 2-bromo-3-nitrobenzoate crystals, the oxygen is bonded to a carbon atom while in the triethylprop-2-nylammonium *p*-bromobenzenesulfonate the oxygen of the acceptor group is attached to a sulfur atom, and (2) that the -benzenesulfonate crystal is composed of ionic entities unlike the molecular -nitrobenzoate units. Thus, if the CH stretch is perturbed by sulfur, a larger frequency shift might be expected on the basis of the PFM calculations on C-H···S systems (see later section); or the strongly ionic characteristics of the C-H···O attraction in the -benzenesulfonate system could result in a larger frequency shift than predicted by the PFM. In either case, these factors could possibly explain the unusually large frequency shift found for triethylprop-2-nylammonium *p*-bromobenzenesulfonate.

TABLE VIII: Calculated Energies and Frequency Shifts as a Function of R and θ

	R, Å	θ, deg	$\Delta\nu$, cm^{-1}	$-E$, kcal	θ, deg	$\Delta\nu$, cm^{-1}	$-E$, kcal
CHO	3.20[a]	0	106	0.53	20	60	0.31
	3.25		82	0.40		47	0.23
	3.30		63	0.30		36	0.18
	3.35		49	0.23		28	0.13
	3.45		29	0.13		16	0.08
CHS	3.50[a]	0	182	1.40	20	113	0.90
	3.55		147	1.10		91	0.71
	3.60		118	0.87		73	0.55
	3.65		95	0.68		59	0.43
	3.75		61	0.41		38	0.26
CHN	3.25[a]	0	93	0.46	20	53	0.27
	3.30		72	0.35		41	0.20
	3.35		56	0.26		32	0.15
	3.40		43	0.20		24	0.11
	3.50		25	0.11		14	0.06

[a] van der Waals radius.

The intermolecular C-H···O bonds in crystalline structures are generally of lengths in the range of 3.2 to 3.35 Å (R) and are typically bent with an angle (θ) of about 10 to 25°.[47] The frequency shifts and energies calculated from the PFM for such bonds as a function of the hydrogen bond length and angle are given in Table VIII.

According to Sutor[47] intramolecular C-H···O bonds exist in crystals with bond lengths (R) in the range from 2.7 to 3.2 Å and with an angle (θ) of about 50°. Although the bond length would be very favorable for hydrogen bond formation, the angle necessitated by steric considerations would severely strain and weaken the projected bond. The energies and frequency shifts calculated from the PFM for an angle of 50° range from −0.39 kcal mol^{-1} and 48 cm^{-1} for a bond distance of 2.7 Å to −0.03 kcal mol^{-1} and 4 cm^{-1} for a bond distance of 3.2 Å. Often *o*-nitrobenzaldehyde is offered as a classic possibility for an intramolecular C-H···O hydrogen bond between the aldehyde CH and the nitro oxygen. However, with a C-H···O bond length of 2.70 Å and bond angle of 62° in crystalline *o*-nitrobenzaldehyde, doubts have been expressed as to whether this is an actual hydrogen

bond.[48,49,51] Calculations from the PFM indicate that such a bond may exist but that it will be very weak.

For intermolecular C-H···O bonds due to association in solution, linear bonds are expected. In general, the bond lengths seem to be slightly larger than the sum of the van der Waal's radii. The experimental frequency shift for the haloforms in dimethyl sulfoxide solution range from 28 to 50 cm^{-1}.[2] For the van der Waals radius of 3.2 Å, the frequency shift is calculated to be 106 cm^{-1} from the PFM, and for a bond distance of 3.5 Å a frequency shift of 22 cm^{-1} is calculated. For $BrCH_2C{\equiv}CH$ in 1,2-dimethoxyethane, the experimental frequency shift is 64 cm^{-1},[52] while in dimethyl sulfoxide the frequency shift is 102 cm^{-1}.[2] The larger frequency shift in dimethyl sulfoxide would be interpreted by the PFM as being due to a shorter C-H···O bond length (3.2 Å) than in 1,2-dimethoxyethane (3.3 Å). Both 1,2-dimethoxyethane and dimethyl sulfoxide would be expected to form strong hydrogen bonds with concomitant shortening of the bond length. In general, for acetylenes in solution, the frequency shift is about 50 to 60 cm^{-1}. The energies calculated for these bonds may be found in Table VIII and are in fair agreement with the energy calculated from molecular orbital considerations, −0.61 kcal mol^{-1}.[53]

Evidence has recently been presented on the possibility of C-H···O hydrogen bonds in polypeptides, such as in polyproline, collagen, and polyglycine.[54-57] For the helical polyglycine II structure, Krimm, *et al.*,[56,57] have confirmed the existence of a C-H···O hydrogen bond integral to the inherent structure of the molecule by infrared studies which have shown a CH stretching frequency shift of 45 cm^{-1} due to the hydrogen bond formation. The distance of closest approach (*i.e.*, R) for this molecule has been estimated to be about 3.1 to 3.2 Å,[54-56] but no estimate of the angle θ has been given. Poland and Scheraga[58] have estimated the bond energy of the C-H···O hydrogen bond for this molecule to be −0.93 kcal mol^{-1} on the basis of their own potential function model. If the geometrical parameters for the C-H···O system in polyglycine II are taken to be R = 3.2 Å and θ = 20°, a frequency shift of 60 cm^{-1} is predicted from the PFM in good agreement with the experimental value, while likewise the PFM indicates a bond energy of −0.3 kcal mol^{-1} in fair agreement with the calculation of Poland and Scheraga. Although the C-H···O hydrogen bond is relatively weak, it may be important in the structural formulations of some complicated biochemical molecules such as proteins which involve polypeptide units.

C-H···N

C-H···N hydrogen bonds have not been extensively investigated. The bond, as calculated by the PFM, is roughly as strong as the C-H···O bond with comparable frequency shifts, as shown by Table VIII.

The applicability of the PFM to C-H···N hydrogen-bonded systems can be tested by utilizing the well-known crystallographic and spectroscopic properties of the two compounds, hydrogen cyanide (HCN) and cyanoacetylene (HC≡C-CN). In their respective crystal structures, both molecules are joined into linear chains by C-H···N hydrogen bonds. For the self-association of crystalline hydrogen cyanide a C-H···N bond length (R) of 3.18 Å[59] is reported, and the CH stretching frequency is found to decrease by 180 cm^{-1} [60] on passing from the vapor to crystalline state. Within the experimental error of the crystallographic measurements, this bond may be taken to be linear. A frequency shift of 115 cm^{-1} and a bond energy of −0.6 kcal mol^{-1} are calculated from the PFM for this bond length. Crystalline cyanoacetylene is reported to be connected by linear C-H···N hydrogen bonds of length 3.27 Å,[61] while the corresponding CH frequency shift was experimentally determined to be 125 cm^{-1}.[62] A frequency shift of 85 cm^{-1} and an energy of about −0.4 kcal mol^{-1} are calculated from the PFM for this bond.

A C-H···N bond enthalpy of −2.09 kcal mol^{-1} [63,64] for the association between chloroform and pyridine in CCl_4 solution has been reported. The frequency shift for this system is 53 cm^{-1},[63] giving a bond energy calculated from the PFM of −0.2 kcal mol^{-1}. Typically, frequency shifts have been reported in the range 23 to 113 cm^{-1} for C-H···N bonds in solution, while enthalpies of formation for similar bonds have ranged from −1 to −4 kcal mol^{-1}.[38,52,64-66] These experimental factors would roughly correspond to C-H···N bond distances ranging from 3.20 to 3.50 Å for association in solution according to the PFM. From nmr proton shifts for C-H···N association in solution, Berkeley and Hanna[67] have calculated the C-H···N hydrogen bond distance to vary from about 3.5 to 3.8 Å.

C-H···S

It is interesting to note that C-H···S hydrogen bonds are predicted to be two to three times stronger than C-H···O or C-H···N bonds with correspondingly larger frequency shifts for customary bond distances (Table VIII). Even though the C-H···S bond is calculated to be stronger than other accepted C-H···Y bonds, the literature does not show any evidence for the existence of this hydrogen bond. Donor-acceptor studies between proton-donating CH groups and organic sulfides should indicate fairly strong hydrogen bond associations according to the PFM. Of special interest is the possible importance of C-H···S links in biochemical systems similar to the previously reported C-H···O bonds in polypeptides. These links may be quite important in determining the stereochemistry of biopolymers.

Note Added in Proof. It has been brought to our attention that the existence of CHS hydrogen bonds has been reported in the literature.[68-70] The reported bond enthalpies fall in the 1-2 kcal range.

Acknowledgment. Support for this work was provided by Research Corporation through the Cottrell College Science Grants program.

References and Notes

(1) G. C. Pimentel and A. L. McClellan, *Annu. Rev. Phys. Chem.*, **22**, 347 (1971).
(2) A. Allerhand and P. Von Ragué Schleyer, *J. Amer. Chem. Soc.*, **85**, 1715 (1963).
(3) E. R. Lippincott and R. Schroeder, *J. Chem. Phys.*, **23**, 1099 (1955).
(4) E. R. Lippincott and R. Schroeder, *J. Phys. Chem.*, **61**, 921 (1957).
(5) E. A. Robinson, H. D. Schreiber, and J. N. Spencer, *Spectrochim. Acta*, **28**, 397 (1971).
(6) H. D. Schreiber, W. R. Snyder, and J. N. Spencer, *Spectrochim. Acta, Part A*, **29**, 1225 (1973).
(7) E. A. Robinson, H. D. Schreiber, and J. N. Spencer, *J. Phys. Chem.*, **75**, 2219 (1971).
(8) S. S. Chang and E. F. Westrum, Jr., *J. Chem. Phys.*, **36**, 2571 (1962).
(9) E. F. Westrum and K. S. Pitzer, *J. Amer. Chem. Soc.*, **71**, 1940 (1949).
(10) E. F. Westrum and K. S. Pitzer, *J. Chem. Phys.*, **15**, 526 (1947).
(11) D. H. McDaniel and R. E. Vallée, *Inorg. Chem.*, **2**, 996 (1963).
(12) S. A. Harrell and D. H. McDaniel, *J. Amer. Chem. Soc.*, **86**, 4487 (1964).
(13) J. A. Salthouse and T. C. Waddington, *J. Chem. Soc.*, 4664 (1964).
(14) L. W. Schroeder and J. A. Ibers, *Inorg. Chem.*, **7**, 594 (1968).

(15) G. L. Cote and H. W. Thompson, *Proc. Roy. Soc., Ser. A*, **210**, 206 (1951).
(16) T. C. Waddington, *J. Chem. Soc.*, 1708 (1958).
(17) J. C. Evans and G. Y-S Lo, *J. Phys. Chem.*, **70**, 11 (1966).
(18) J. C. Evans and G. Y-S Lo, *J. Phys. Chem.*, **71**, 3942 (1967).
(19) J. C. Evans and G. Y-S Lo, *J. Phys. Chem.*, **73**, 448 (1969).
(20) L. W. Schroeder, *J. Chem. Phys.*, **52**, 1972 (1970).
(21) J. J. Rush, L. W. Schroeder, and A. J. Melveger, *J. Chem. Phys.*, **56**, 2793 (1972).
(22) J. M. Williams and L. F. Schneemeyer, *J. Amer. Chem. Soc.*, **95**, 5780 (1973).
(23) J. A. Ibers, *J. Chem. Phys.*, **40**, 402 (1964).
(24) J. C. Evans and G. Y-S Lo, *J. Phys. Chem.*, **70**, 2702 (1966).
(25) J. C. Evans and G. Y-S Lo, *J. Phys. Chem.*, **71**, 3697 (1967).
(26) B. L. McGaw and J. A. Ibers, *J. Chem. Phys.*, **39**, 2677 (1963).
(27) J. A. A. Ketelaar, *Recl. Trav. Chim. Pays-Bas*, **60**, 523 (1941).
(28) A. S. N. Murthy, S. N. Bhat, and C. N. R. Rao, *J. Chem. Soc. A*, 1251 (1970).
(29) P. N. Noble and R. N. Kortzeborn, *J. Chem. Phys.*, **52**, 5375 (1970).
(30) P. Schuster, *Theor. Chim. Acta*, **19**, 212 (1970).
(31) J. Janzen and L. S. Bartell, *J. Chem. Phys.*, **50**, 3611 (1969).
(32) J. H. Simons and J. H. Hildebrand, *J. Amer. Chem. Soc.*, **46**, 2183 (1924).
(33) R. W. Long, J. H. Hildebrand, and W. E. Morrell, *J. Amer. Chem. Soc.*, **65**, 182 (1943).
(34) J. W. Nibler and G. C. Pimentel, *J. Chem. Phys.*, **47**, 710 (1967).
(35) J. M. Reddy, K. Knox, and M. B. Robin, *J. Chem. Phys.*, **40**, 1082 (1964).
(36) G. Hertzberg, "Molecular Spectra and Molecular Structure I," in "Spectra of Diatomic Molecules," 2nd ed, D. Van Nostrand, Princeton, N. J., 1950.
(37) C. J. Cresswell and A. L. Allred, *J. Amer. Chem. Soc.*, **85**, 1723 (1963).
(38) A. S. N. Murthy and C. N. R. Rao, *Appl. Spectrosc. Rev.*, **2**, 69 (1968).
(39) J. C. D. Brand, G. Eglinton, and J. F. Morman, *J. Chem. Soc.*, 2526 (1960).
(40) T. S. Pang and S. Ng, *Spectrochim. Acta, Sect. A*, **29**, 207 (1973).
(41) S. Singh, A. S. N. Murthy, and C. N. R. Rao, *Trans. Faraday Soc.*, **62**, 1056 (1966).
(42) J. C. D. Brand, G. Eglinton, and J. Tyrrell, *J. Chem. Soc.*, 5914 (1965).
(43) J. C. Calabrese, A. T. McPhail, and G. A. Sim, *J. Chem. Soc. B*, 1235 (1966).
(44) G. Ferguson and K. M. S. Islam, *J. Chem. Soc. B*, 593 (1966).
(45) G. Ferguson and J. Tyrell, *Chem. Commun.*, **10**, 195 (1965).
(46) G. J. Palenik, *Acta Crystallogr.*, **19**, 47 (1965).
(47) J. D. Sutor, *J. Chem. Soc.*, 1105 (1963).
(48) J. Donohue in "Structural Chemistry and Molecular Biology," A. Rich and N. Davidson, Ed., W. H. Freeman, San Francisco, Calif., 1968, p 459.
(49) G. A. Sim, *Annu. Rev. Phys. Chem.*, **18**, 57 (1967).
(50) J. C. Calabrese, A. T. McPhail, and G. A. Sim, *J. Chem. Soc. B*, 282 (1970).
(51) P. Coppens, *Acta Crystallogr.*, **17**, 573 (1964).
(52) R. West and C. S. Kraihanzel, *J. Amer. Chem. Soc.*, **83**, 765 (1961).
(53) K. Morokuma, *J. Chem. Phys.*, **55**, 1236 (1971).
(54) V. Sasisekharan, *Acta Crystallogr.*, **12**, 897 (1959).
(55) G. N. Ramachandran, G. Ramakrishnan, and C. M. Venkatachalam, in "Conformation of Biopolymers," Vol. 2, G. N. Ramachandran, Ed., Interscience, New York, N. Y., 1967, p 429.
(56) S. Krimm, K. Kuroiwa, and T. Rebane, in ref 56, p 439.
(57) S. Krimm and K. Kuroiwa, *Biopolymers*, **6**, 401 (1968).
(58) D. Poland and H. A. Scheraga, *Biochemistry*, **6**, 3791 (1967).
(59) W. J. Dulmage and W. N. Lipscomb, *Acta Crystallogr.*, **4**, 330 (1951).
(60) R. E. Hoffman and D. F. Hornig, *J. Chem. Phys.*, **17**, 1163 (1949).
(61) F. V. Shallcross and G. B. Carpenter, *Acta Crystallogr.*, **11**, 490 (1958).
(62) G. C. Turrell, W. D. Jones, and A. Maki, *J. Chem. Phys.*, **26**, 1544 (1957).
(63) T. J. V. Findlay, J. S. Keniry, A. D. Kidman, and V. A. Pickles, *Trans. Faraday Soc.*, **63**, 846 (1967).
(64) P. J. Berkeley and M. W. Hanna, *J. Chem. Phys.*, **41**, 2530 (1964).
(65) M. A. Mesubi, Ph.D. Thesis, Kansas State University, 1972.
(66) T. Gramstad and O. Vikane, *Spectrochim. Acta, Sect. A*, **28**, 2131 (1972).
(67) P. J. Berkeley and M. W. Hanna, *J. Amer. Chem. Soc.*, **86**, 2990 (1964).
(68) G. R. Wiley and S. I. Miller, *J. Amer. Chem. Soc.*, **94**, 3287 (1972).
(69) K. W. Jolley, L. M. Hughes, and I. D. Watson, *Aust. J. Chem.*, **27**, 287 (1974).
(70) J. P. Sheridan, D. E. Martire, and Y. B. Tewari, *J. Amer. Chem. Soc.*, **94**, 3294 (1972).

Electronic Spectra of Aromatic Hydrocarbon Anions and Cations in the CNDO/S Model

Poul Jørgensen* and Jens Christian Poulsen

Department of Chemistry, Aarhus University, DK-8000 Aarhus C., Denmark (Received March 5, 1974)

The electronic spectra of some aromatic hydrocarbon radical anions and cations have been calculated within a model of complete neglect of differential overlap using spectroscopically determined parameters (CNDO/S). It was found that the σ–π interaction is of minor importance in the calculations and that the systems can as well be described in a pure π model.

Electronic spectra of conjugated hydrocarbon radical anions and cations have received an increasing experimental[1-4] as well as theoretical[5,6] interest. Theoretical treatments have concentrated on applications based on the Pariser-Parr-Pople (PPP) model where the anions and cations receive identical theoretical treatment.[7,8] The experimental spectra show strong similarities too, but differences exist. Explicit consideration of the σ–π interaction gives theoretically different spectra and we decided to examine the applicability of the CNDO/S model in describing the experimental differences. Recently the CNDO/S model has been applied on free π radicals and π radical anions,[9] but in contrast to ref 9 which used a traditional open shell configuration interaction (CI) procedure[10] we will use the grand canonical (mono excited) configuration interaction (GCCI) approximation.[5] We obtain molecular orbitals under the assumption that the unpaired electron in spatial molecular orbital k on the average is equally distributed between the $k\alpha$ and the $k\beta$ spin orbital each having an occupancy of 1/2 electron.[11] The excitation energies are obtained by performing the configuration interaction consistent with the determination of the molec-

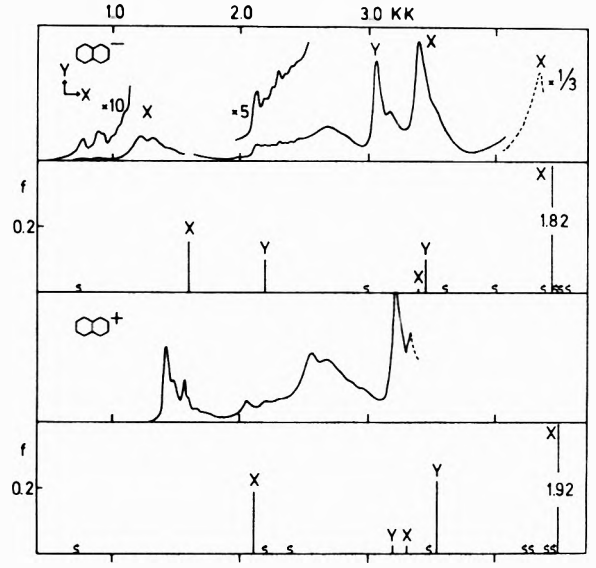

Figure 1. Comparison of experimental and calculated excitation spectrum of the naphthalene anion and cation. The experimental spectrum is taken from ref 1 and 2 while the moment directions are obtained from ref 3. In the theoretical spectrum the ordinate indicates the oscillator strength f calculated in the dipole length approximation. The wavy lines with arrows indicate forbidden transitions.

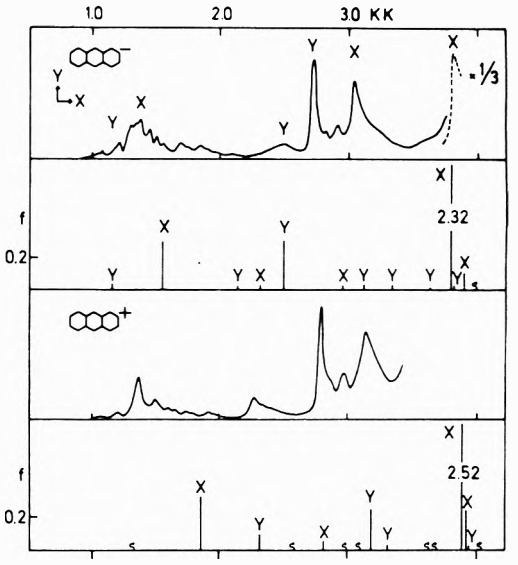

Figure 2. Comparison of experimental and calculated excitation spectrum of the anthracene anion and cation. The experimental spectrum is taken from ref 1 and 2 while the moment directions are obtained from ref 3. In the theoretical spectrum the ordinate indicates the oscillator strength f calculated in the dipole length approximation. The wavy lines with arrows indicate forbidden transitions.

ular orbitals. This corresponds to diagonalizing the grand canonical monoexcited configuration interaction matrix[5]

$$A_{(kl)(k'l')} = \delta_{kk'}\delta_{ll'}(\nu_l - \nu_k)(\epsilon_k - \epsilon_l) + (\nu_l - \nu_k)(\nu_{l'} - \nu_{k'})[(kl|l'k') - (kk'|l'l)] \quad (1)$$

ν_k is the occupation number of spin orbital k with orbital energy ϵ_k. The index (kl) refers to an excitation from the lth to the kth molecular spin orbital. In case of a closed shell system where the occupation numbers are integers eq 1 reduces to the standard monoexcited configuration interaction approximation. A detailed description of the GCCI method can be found in ref 5.

Figures 1-3 show the electronic excitation spectra calculated for three hydrocarbon anions and cations. The agreement between theory and experiment seems satisfactory and comparable to the agreement obtained in ref 9. The theoretical spectrum of the naphthalene and anthracene anion shows a strong and a medium peak in the x direction at about the experimental peaks of 3.6 and 1.3 kK. The rather complex structure in the experimental spectrum from about 2.5 to 3.1 kK is also present in the calculated spectra although a direct assignment of individual lines is difficult. For the biphenyl anion the experimental and the theoretical spectra are dominated by two strong peaks and the assignment is unique.

Experimental differences between the spectra of the conjugated anions and cations seem, however, not to be reproduced. The shift should be caused by the σ-π interaction. This interaction will be examined by performing a π electron PPP calculation with the CNDO/S π parameters. These resemble very much those used in a standard PPP calculation.[12] The electron repulsion integrals are obtained from the Mataga-Nishimoto formula[13] with one-center integrals for carbon of 11.11 eV. The resonance integrals are determined from[14]

$$\beta_{\mu\nu}^{\pi} = (\beta_\mu^0 + \beta_\nu^0)KS_{\mu\nu}/2 \quad (2)$$

where β_μ^0 is a parameter characterizing atom μ. $S_{\mu\nu}$ is the

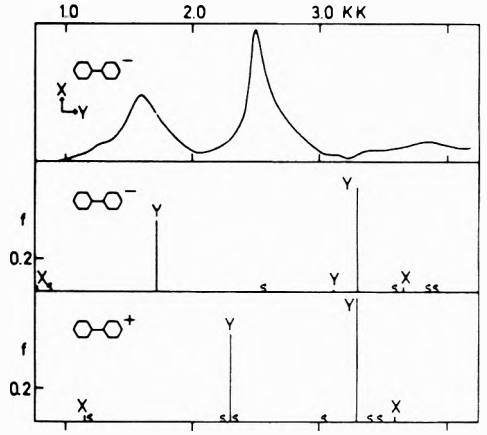

Figure 3. Comparison of the experimental and calculated excitation spectrum for the biphenyl anion. The experimental spectrum is taken from ref 4.

overlap between atom μ and ν, and K is a constant of 0.585. The constant K is introduced only for spectroscopic applications of the CNDO/S model. A value of 2.44 eV which is close to the one used in standard PPP calculations is obtained for the resonance integral between two carbon atoms at a distance of 1.40 Å. The use of eq 2 to calculate resonance integrals leads to consideration of nonneighbor resonance integrals in CNDO/S π parameters. The nonneighbor resonance integrals are excluded in the standard PPP model. We performed PPP calculations both with and without the nonneighbor resonance integrals. Exclusion gives identical spectra for the anion and cation in the PPP model and in the GCCI scheme.[8] In Tables I and II the configurational energies relative to the ground state and the GCCI excitation spectrum are given for the naphthalene anion and cation in the CNDO/S model and in the PPP model with and without consideration of the nonneighbor resonance integrals. The differ-

TABLE I:[a] Configurational Energies Relative to the Ground State, Oscillator Strength, and Moment Direction for the Naphthalene Cation and Anion

Cation		Cation and anion, PPP without nonneighbor resonance integrals	Anion	
CNDO/S	PPP with nonneighbor resonance integrals		PPP with nonneighbor resonance integrals	CNDO/S
7.6	4.8	5.3	4.0	6.3
22.4 $\sigma-\pi^*$				
22.8 (0.84) x	22.1 (0.57) x	20.0 (0.52) x	16.7 (0.46) x	17.0 (0.62) x
24.5 $\sigma-\pi^*$				
34.9 (0.68) y	34.0 (0.45) y	26.9 (0.37) y	22.2 (0.32) y	23.1 (0.46) y
			29.8	30.8
35.0 (0.46) y	35.1 (0.30) y	37.0 (0.32) y	35.0 (0.30) y	35.0 (0.46) y
35.8		39.4		36.5 $\pi-\sigma^*$
36.3 (0.88) x	38.7 (0.58) x	41.7 (0.61) x	39.8 (0.62) x	38.0 (0.96) x
42.1 (0.86) x	40.0 (1.46) x	41.7 (1.43) x	38.9 (1.37) x	40.5 (0.80) x
43.3	43.9			

[a] Excitation energies are in kK. The numbers in parentheses are the oscillator strengths calculated in the dipole length approximation, x and y indicate the direction of the transition moment, and $\sigma-\pi^*$ denotes the nature of the transition.

TABLE II:[a] Grand Canonical Configuration Interaction Spectrum for the Naphthalene Anion and Cation

Cation		Cation and anion, PPP without nonneighbor resonance integrals	Anion	
CNDO/S	PPP with nonneighbor resonance integrals		PPP with nonneighbor resonance integrals	CNDO/S
7.3	4.6	5.0	3.7	6.0
21.5 (0.20) x	20.9 (0.17) x	23.4 (0.19) x	15.7 (0.16) x	16.2 (0.16) x
22.1 $\sigma-\pi^*$				
24.2 $\sigma-\pi^*$				
32.6 (0.006) y	31.0 (0.02) y	25.7 (0.11) y	21.2 (0.10) y	22.1 (0.10) y
35.1 $\sigma-\pi^*$			29.5	30.5
35.6 (0.22) y	34.3 (0.02) y	36.5 (0.16) y	34.6 (0.13) y	34.5 (0.14) y
33.3 (0.02) x	35.2 (0.20) x	36.8 (0.04) x	34.3 (0.26) x	34.3 (0.0006) x
42.9	43.4	39.0		36.2 $\pi-\sigma^*$
43.0 $\sigma-\pi^*$				40.7 $\pi-\sigma^*$
44.4 $\sigma-\pi^*$				42.9
44.8	44.4			44.2
45.6 (1.92) x	44.9 (1.94) x	46.8 (1.88) x	44.4 (1.76) x	44.7 (1.84) x

[a] Excitation energies are in kK. The numbers in parentheses are the oscillator strengths calculated in the dipole length approximation, x and y indicate the direction of the transition moment, and $\sigma-\pi^*$ denotes the nature of the transition.

ence between the CNDO/S calculations and the PPP calculations with CNDO/S π parameters are small compared to the difference obtained in the two different PPP calculations with and without inclusion of nonneighbor resonance integrals. The $\sigma-\pi$ interaction is thus unimportant in CNDO/S and calculated differences between the anions and cations are caused by reparameterization of the PPP model.

No $\sigma-\sigma^*$ type transitions were considered in the CNDO/S calculational procedure. The configurational energy for the lowest $\sigma-\sigma^*$ state was found to be more than 9 eV and the considered frequency region is thus hardly expected to be influenced by these transitions.

The main difference between the PPP and the CNDO/S model is that CNDO/S includes symmetry forbidden $\sigma-\pi^*$ and $\pi-\sigma^*$ transitions. The CNDO/S model reproduces the main feature of the spectra of individual hydrocarbon radical ions but no definite advantage is obtained relative to use a pure π model.

The calculations have been carried out with a modified version of QCPE program no. 174.[15]

Acknowledgments. We are indebted to Professor Jan Linderberg and Dr. Jens Oddershede for helpful and stimulating discussions.

References and Notes

(1) T. Shida and S. Iwata, *J. Amer. Chem. Soc.*, **95**, 3473 (1973), and references therein.
(2) G. J. Hoijtink, N. H. Yelthorst, and P. J. Zandstra, *Mol. Phys.*, **3**, 533 (1960).
(3) P. Balk, G. J. Hoijtink, and J. W. H. Schreurs, *Recl. Trav. Chim. Pays-Bas*, **76**, 907 (1957).
(4) K. H. J. Buschow, J. Dieleman, and G. J. Hoijtink, *J. Chem. Phys.*, **42**, 1993 (1965).
(5) P. Jørgensen, *J. Chem. Phys.*, **57**, 4884 (1972).
(6) R. Zahradnik and P. Carsky, *J. Phys. Chem.*, **74**, 1235, 1240, 1249 (1970).
(7) H. C. Longuet-Higgins and J. A. Pople, *Proc. Phys. Soc., Ser. A*, **68**, 591 (1955).
(8) P. Jørgensen and J. Bellum, *Mol. Phys.*, **26**, 725 (1973).
(9) H. M. Chang and H. H. Jaffe, *Chem. Phys. Lett.*, **23**, 146 (1973).
(10) A. Ishitani and S. Nagakura, *Theor. Chim. Acta*, **4**, 236 (1966).
(11) S. F. Abdulnur, J. Linderberg, Y. Öhrn, and P. W. Thulstrup, *Phys. Rev. A*, **6**, 889 (1972).
(12) See, e.g., R. G. Parr, "Quantum Theory of Molecular Electronic Structure," W. A. Benjamin, New York, N. Y., 1964.
(13) N. Mataga and K. Nishimoto, *Z. Phys. Chem. (Frankfurt am Main)*, **13**, 140 (1957).
(14) J. Del Bene and H. H. Jaffe, *J. Chem. Phys.*, **48**, 1807, 4050 (1968); **49**, 1221 (1968); **50**, 1126 (1969).
(15) H. H. Jaffe and J. Del Bene, QCPE Program No. 174.

Monte-Carlo Model of Micelle Formation

Heinz Christen and Hans Friedrich Eicke*

Institute for Physical Chemistry of the University, CH-4056 Basel, Switzerland *(Received October 22, 1973; Revised Manuscript Received April 1, 1974)*

A statistical molecular interpretation of micelle formation and the corresponding energy of nucleation was made with the help of a Monte-Carlo model using a two-dimensional liquid lattice. With the help of a computer program a phase transition is created which is applied to the formation of micelles. A consideration of the fluctuations in this simulation allows the determination of local variations in density, which are directly correlated with the energy and frequency of nucleation. Number ($\langle N_n \rangle$) and weight ($\langle N_w \rangle$) average molecular sizes as function of the number of weighed-in monomers (per lattice) are calculated. In this connection a hysterisis loop of $\langle N_w \rangle$ is predicted corresponding to formation and decomposition of micelles. Finally, since the nucleation process of micelle formation may be considered as a cooperative phenomenon a quantitative relation between the cooperativity parameter and the energy of nucleation is derived.

Introduction

The formation of micelles has been often treated with the help of the so called "multiple equilibrium model"[1-4] in which several types of particles from monomers to *n*mers are considered. In many cases another possible approximate interpretation of micelle formation is to view the micellization as a phase change since its thermodynamical behavior resembles in many respects that of systems with two macroscopic homogeneous phases (see Discussion[5]). An indication for the phase concept is the jump-like change of a measurable quantity which follows the transformation in many aqueous and nonaqueous colloidal solutions.[6] Furthermore vapor-pressure osmometric and light-scattering measurements in nonaqueous solutions of some ionic surfactants (Aerosol OT, AY, di-2-ethylhexylphosphate sodium salt)[7] indicate a considerable monodispersion of the micellar phase. This finding is an important hint with respect to the phase model. The experimental observations on nucleation in a series of nonaqueous colloidal solutions below the critical micelle concentration (cmc) give additional evidence.

In a recent paper[8] on the nucleation process in which the phase model has been applied to the micelle formation of ionic surfactants in apolar media it was demonstrated that the free energy change ΔG as a function of the number of colloidal monomers n shows a maximum at $n = 3$ (see Figure 1) corresponding to the existence of premicellar aggregates and a minimum at $n = 16$ indicating the stability of the micelles under the experimental conditions. It could be shown experimentally that this micelle size is representative for a number of these surfactants in apolar solvents. The maximum of $\Delta G(n)$ was assumed to represent a potential barrier of the free energy which has to be overcome by the surfactant molecules in order to build up the micelle. The experimental observations of these premicellar aggregates (= subunits) below the cmc could be correlated well with this potential barrier and the corresponding aggregates have been interpreted as nuclei. The size of the nuclei is given by the number n of monomers corresponding to the maximum height of the potential barrier which (in this picture) describes the free energy of nucleation. The model permits an estimation of the size of the micelle and of the micellar nucleus and a determination of the free energy of formation of the nucleus, which satisfactorily agrees with the above-mentioned experiments, e.g., on Aerosol OT or AY in apolar solvents.

The aim of this paper is to simulate a phase change with the help of the Monte-Carlo method. This statistical simulation based on simple model assumptions should provide a simple approach to the molecular process of nucleation and micellization consistent with available experimental observations on ionic surfactants in apolar media. Furthermore it should yield an explanation for the origin of the energy necessary to overcome the above-mentioned potential barrier which could not be given in ref 8.

It should be noted that the following procedure has not been based on particular assumptions with respect to particle interactions as is often done[9,10] and thus it is more easily applicable to different physical processes originating from fluctuation phenomena.

Computer Experiment

(*a*) *Physical Model.* According to the statistical phenomenon the model to be proposed should contain parameters to describe the frequency of collisions of monomers, and subunits, and furthermore the probabilities for their aggregation and decomposition. One suitable parameter, ΔG, the amount of free energy necessary to overcome the above-mentioned potential barrier is connected with the local fluctuation ΔN in the concentration of particles.

Thus one has to find a relation between the fluctuations ΔG and ΔN in a particular subsystem where a nucleation or a micellation process is to be investigated. The mean square of the fluctuation of the free energy can be calculated in the subsystem. Thus squaring and averaging $\Delta G = V\Delta P - T\Delta S$ yields

$$\langle \Delta G^2 \rangle = V^2 \langle \Delta P^2 \rangle + T^2 \langle \Delta S^2 \rangle \qquad (1)$$

where the mixed term on the right-hand side of eq 1 disappears because of the independence of the fluctuations ΔP and ΔS. In order to get a rough estimate of the order of magnitude of the mean square fluctuations $\langle \Delta G^2 \rangle$ and its functional dependence on N, the following derivation is based on the ideal gas Thus

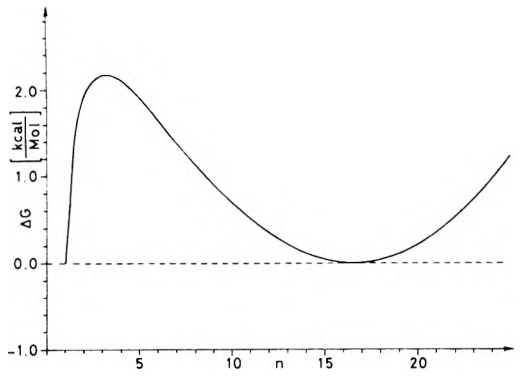

Figure 1. Variation of the free energy change ΔG (kcal mol^{-1}) as a function of the number of aggregating monomers n (see ref 8) at the cmc 5×10^{-4} M.

$$\langle \Delta G^2 \rangle = \frac{c_p}{c_v} \frac{(PV)^2}{\langle N \rangle} + \frac{5}{2} \langle N \rangle (kT)^2 \qquad (2)$$

or

$$\langle \Delta G^2 \rangle = \langle N \rangle (kT)^2 \left(\frac{c_p}{c_v} + \frac{5}{2} \right) = \frac{25}{6} \langle N \rangle (kT)^2 \qquad (3)$$

From expression 3 the mean fluctuation $\langle \Delta G^2 \rangle^{1/2}$ may be obtained

$$\langle \Delta G^2 \rangle^{1/2} = \frac{5}{\sqrt{6}} kT \langle N \rangle^{1/2} = \frac{5}{\sqrt{6}} kT \left[(N - \langle N \rangle)^2 \right]^{1/2} \qquad (4)$$

which shows the expected relation between the fluctuations of the free energy and the number of particles within the particular subvolume (V). In the frame of this rough approximation the absolute amount of the mean free energy fluctuation with respect to 1 mol yields at room temperature $\langle \Delta G^2 \rangle^{1/2} \simeq 2$ kcal mol^{-1}.

In contrast to the above thermodynamical fluctuation treatment the Monte-Carlo model provides information about a single event in a particular subvolume and at a definite moment. Thus the connection between the number of particles and the free energy change (eq 4) can be evaluated by sampling and averaging the single events. It is tacitly assumed that the same proportionality exists between the free energy change and the number of particles observed at a single event as between the corresponding average magnitudes. Consequently the momentary value of the free energy and particle fluctuations, ΔG^* and $(N - \langle N \rangle)$, respectively, are interrelated by

$$\Delta G^* = s(N - \langle N \rangle) \qquad (5)$$

where s is a proportionality constant which depends explicitly on the type of the intermolecular interaction.

Now this fluctuation energy is available, if within the fixed small volume a micelle or a colloidal nucleus is being built up. In other words nuclei can only be formed if a local excess of particles exists, whereas the subsequent formation of micelles may even proceed with $(N - \langle N \rangle) < 0$, *i.e.*, if the momentary number of particles N is smaller than the temporary mean value $\langle N \rangle$.

The subvolume V may be interpreted physically as a region where the molecular interactions start to become responsible for aggregation or decomposition. To obtain statements about the distribution of aggregates of definite sizes in the solution, information on the probabilities of formation and decomposition of aggregates is necessary. Within the frame of the Monte-Carlo model this information can be derived from a comparison between the free energy values $\Delta G(n)$ (describing the stability of different colloidal aggregates) and the fluctuation energy ΔG^*.

Suppose two aggregates a and b in solution with the association numbers n and m are interacting with each other in such a way that a redistribution of the number of particles per aggregate is possible. With the assumption that the interaction results in not more than two new aggregates, the following cases are possible ($m > n$, $[\cdots]$ = integer value)

a	b
$m + n$	0
$m + n - 1$	1
⋮	⋮
m'	n'
⋮	⋮
$\left[\frac{m+n}{2}\right]$	$m + n - \left[\frac{m+n}{2}\right]$

The free energy of formation of the new (redistributed) aggregates (n',m') may be determined from the $\Delta G(n)$ plot (see Figure 1), *i.e.*

$$\Delta G_{\text{formation}} = \Delta G(n) + \Delta G(m) - \Delta G(n') - \Delta G(m') \qquad (6)$$

ΔG^* is the upper limit of $\Delta G_{\text{formation}}$ and the number of monomers in the new aggregates will comply with a probability distribution.

The Monte-Carlo program will thus be capable of making a choice with respect to the redistribution of the number of monomers per aggregate (n',m') for two interacting aggregates under the explicit consideration of the probabilities of all possible distributions.

(*b*) *Simulation of Micelle Formation in the Computer Experiment.* The Monte-Carlo method appears to be particulary suited to realize the above proposed model of aggregation, since its technique gives a direct imitation of the physical behavior of the system. Since only equilibrium properties of the system will be investigated it was unnecessary to apply the more elaborate molecular dynamical method.[11]

Essentially, the simulation has to fulfil three requirements: (1) a liquid solution with N_0 solvent molecules and N_1 colloidal monomers, (2) the Brownian motion (diffusion), and (3) intermolecular interactions between the solute particles. The liquid is modeled with the help of a two-dimensional lattice[12] represented by a $\lambda \times \lambda$ matrix. The lattice sites are "filled" with the numbers 0 and 1, where "zero" represents a solvent molecule, and "one" a dissolved monomer. The distribution of these numbers over the lattice is random, *i.e.*, determined by a random number R[13] between 0 and 1. If the random number ranges between $0 < R \leq N_0/(N_0 + N_1)$, "zero" will be chosen, and for $N_0/(N_0 + N_1) < R \leq 1$ the lattice site will be occupied by 1. The matrix generated in this way will approximately contain $\lambda^2 N_1/(N_0 + N_1)$ "ones" for large values of λ.

Since a particular pair potential of the intermolecular interactions has not been considered in this model, the Brownian motion and diffusion have explicitly to be simulated in the Monte-Carlo program. In reality these motions would be a consequence of the particle interactions. By simple means these diffusion processes, which are necessary for the intermixing of the single matrix elements, may be simulated in this two-dimensional lattice model. Each element at a lattice site should be capable of inter-

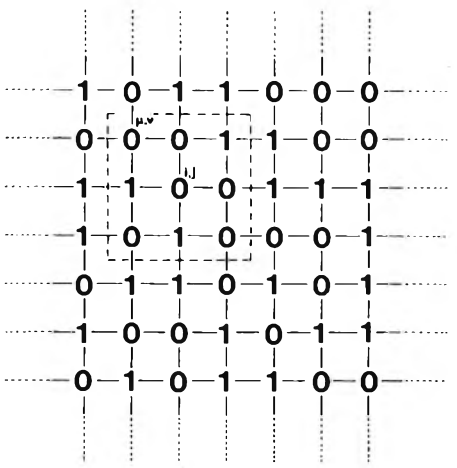

Figure 2. Two-dimensional matrix (i,j) as a model solution. (μ,ν) matrix is the subregion ($k = 1$) for which the fluctuations are calculated.

changing with one of its four neighbors. The selection of a neighboring site can then be made with the help of the random number generator by dividing its interval $\{0,1\}$ into four equal ranges. (It should be pointed out in this connection that the sequence of selecting the matrix elements within the λ^2 sites should be random. The numerical experiments have shown, however, that a regular row by row treatment leads to the same results.)

The procedure used to include the interaction between solute particles is to permit neighboring aggregates to exchange particles. The redistribution is determined (see section a) by the free energy difference $\Delta G' = \Delta G^* - \Delta G_{\text{formation}} > 0$. The momentary fluctuation ΔG^* is calculated in the simulation program by counting the number of particles around each lattice site $a(i,j)$ $(i,j \neq 0)$ within a square subregion of the lattice, Figure 2. The subregion contains the elements $a(\mu,\nu)$ where

$$\mu = i - k, i - k + 1, \ldots i, \ldots i + k$$

and

$$\nu = j - k, j - k + 1, \ldots j, \ldots j + k \qquad (7)$$

i.e., the $(2k + 1)^2$ elements of the immediate neighborhood of the central particle $a(i,j)$. For the present the size of this subregion, *i.e.*, the value of the parameter k, has not been fixed. It has to be determined by comparison with experimental results. In the physical picture k can be imagined to be the mean particle separation at the cmc.

The momentary occupation N in the subregion is the sum of all lattice sites therein occupied by "1." The mean occupation is determined by the equation

$$\langle N \rangle = \frac{N_1}{N_0 + N_1} (2k + 1)^2 \qquad (8)$$

from which the momentary deviation $N - \langle N \rangle$ may be easily derived.

The dependence of the relative fluctuations of the number of particles on the parameter k may be evaluated from the frequency distribution of the momentary deviations of many subregions within the model solution. The standarized frequency distribution of the relative particle fluctuations $(N - \langle N \rangle)/\langle N \rangle$ (referring to the same number of measurements) for $k = 3$, and $k = 5$ have been plotted in Figure 3. The graph demonstrates by the narrowness of the computer simulated distribution that large subregions show comparatively less relative fluctuations than the small regions. It should be mentioned that this well-

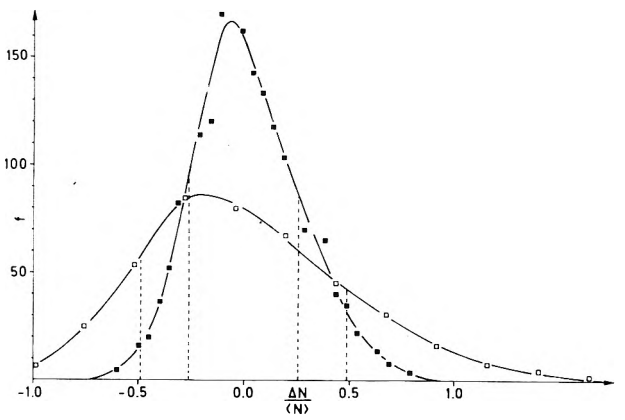

Figure 3. Frequency distribution (f) of relative fluctuations: subregion $k = 3$(□) and $k = 5$(■). The mean relative fluctuations corresponding to these k values are $(\langle \Delta N^2 \rangle / \langle N \rangle^2)^{1/2} = [\int_{-\infty}^{\infty} f(\Delta N/\langle N \rangle)^2 \, d(\Delta N/\langle N \rangle) / \int_{-\infty}^{\infty} f \, d(\Delta N/\langle N \rangle)]^{1/2} = 0.49$ ($k = 3$) and 0.26 ($k = 5$).

known fact is correctly simulated by the computer program.

The inner loop of the iteration process within the simulation program is responsible for the redistribution of the number of particles within the aggregates (after the collision) which may increase or reduce the aggregation number of monomers per lattice site. Since the selection of a redistribution is determined by the free energy difference

$$\Delta G_i' = \Delta G^* - \Delta G_{\text{formation}} \quad (i = 1 \ldots (m + n)/2)$$

these $[(m + n)/2]$ energy values are calculated for each central particle of a subregion, using the ΔG(aggregation number) values (see eq 6) derived from Figure 1. Among the l positive energy values $\Delta G_i'$ one value is chosen with the help of a random number R. To be sure that this frequently repeated selection leads to a Boltzmann distribution the interval $\{0,1\}$ of the random number generator will be divided into l subintervals determined by the intersections p_k $(k = 1 \ldots l - 1)$ which can be calculated according to

$$p_k = \sum_{i=1}^{k} \left[\exp(\Delta G_i'/kT) / \sum_{i=1}^{l} \exp(\Delta G_i/kT) \right] \qquad (9)$$

i.e.

$$p_k - p_{k-1} = \exp(\Delta G_k/kT) / \sum_{i=1}^{l} (\Delta G_i/kT)$$

If the random number falls in one of these subintervals $p_{k-1} < R \leq p_k$, the choice is made in favor of the kth distribution.

Efficiency of the Monte-Carlo Model

The results of the computer experiment are shown in Figures 5-8. In Figure 5 weight and number averages of particle size have been plotted linearly against the number of weighed-in monomers. The curve corresponding to $\langle N_w \rangle$ shows a typical run of a micelle forming system. The steepness of the transition region of the plot depends on the extent of the fluctuation in the subsystem as indicated by the parameter s (see eq 5). Thus the smaller the fluctuation the steeper the transition from monomers to micelles due to the energy necessary to form a nucleus. The variation of this parameter is demonstrated in Figure 6. s may be thought to change with temperature as can be seen from eq 4 since it was assumed that the proportionality constants between the mean fluctuation of the free en-

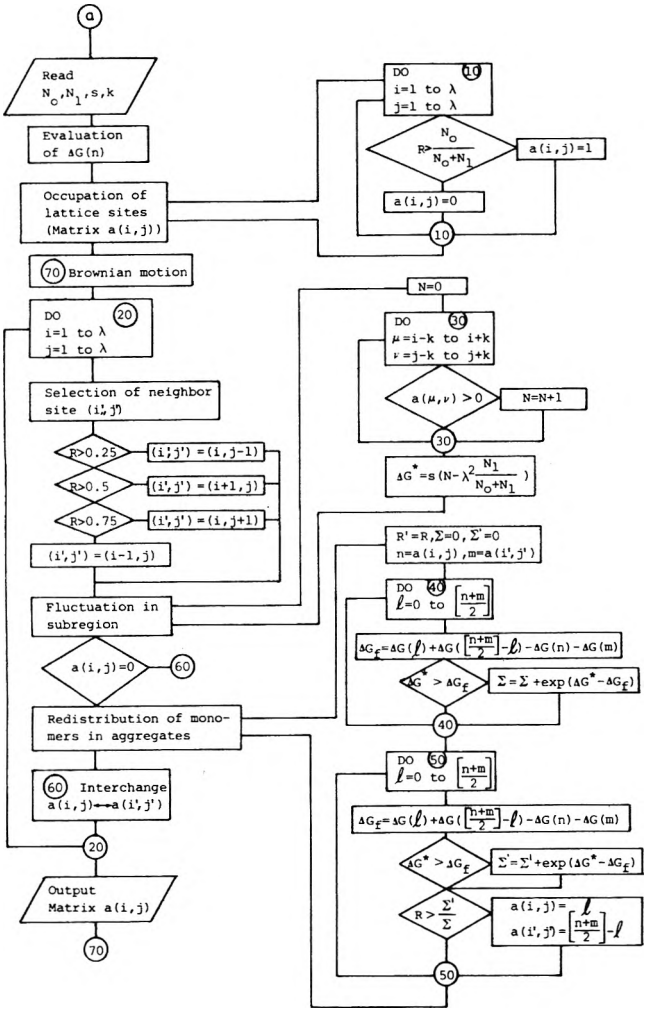

Figure 4. Flow chart of the Monte-Carlo program: R = random number, all the other symbols are explained in the text.

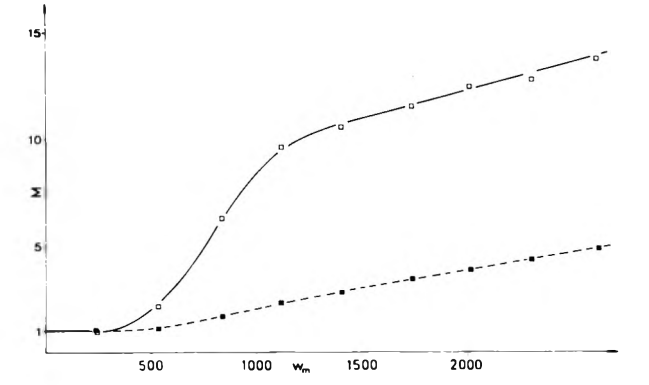

Figure 5. Weight (□) and number (■) average particle size as a function of the number of weighed-in monomers (W_m). M is given in monomer units: s = 0.5 (see eq 5 and text), k = 3.

ergy and the number of particles are the same as for the momentary values.

The lower curve in Figure 5 shows the plot of the number average $\langle N_n \rangle$ particle size against the number of weighed-in monomers. The graph ($\langle N_n \rangle$) appears to be rather flat in the concentration region considered in this figure. The plot should show (in principle) the same curvature as $\langle N_w \rangle$ but at considerably higher weighed-in concentrations since a sharp phase change was assumed. An

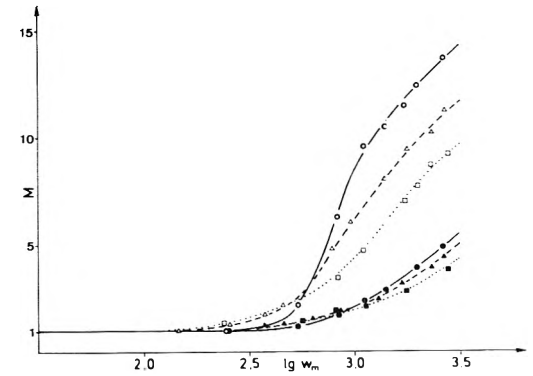

Figure 6. Weight (○,△,□) and number (●,▲,■) average particle size as a function of the logarithm of weighed-in monomers (log W_m). M in monomer units: s = 0.5 (○,●), 1.0 (△,▲), 2.0 (□,■), k = 3 (see eq 5 and text).

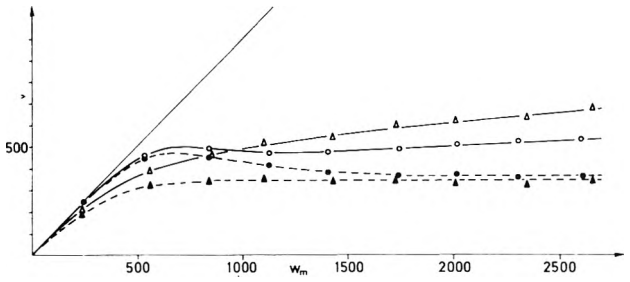

Figure 7. Number (ν) of monomers (▲,●) and of all particles (△,○) *vs.* number of weighed-in monomers (W_m): s = 0.5 (○,●), 2.0 (△,▲) k = 3 (see eq 5 and text).

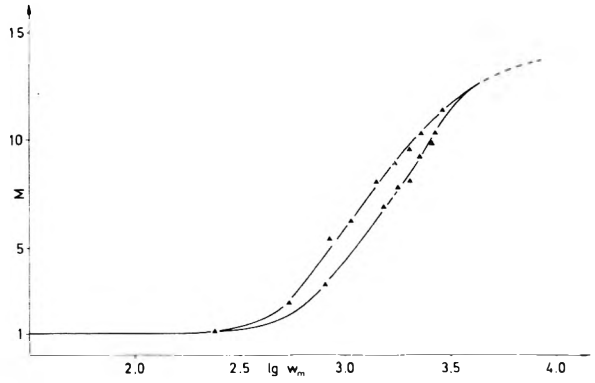

Figure 8. Weight average particle size *vs.* the logarithm of number of weighed-in monomers (log W_m). All values refer to a constant time interval after changing the monomer concentration: s = 1.0 and k = 3 (see eq 5 and text).

application of the so-called "multiple equilibrium" would automatically shift the transition region of $\langle N_n \rangle$ to lower weighed-in concentrations, *i.e.*, near to the $\langle N_w \rangle$ transition region as found, for example, in a paper by Corkill, *et al.*[4]

The parameter k which was introduced to describe the size of the "subvolume" of this two-dimensional model solution has been kept constant in the present results. Physically, the parameter k describes the region of interaction between the particles (monomers and/or aggregates). Strictly speaking it is a mean interaction distance since this range increases with the size of the colloidal particle.

According to Figure 3 larger k values correspond to a sharper distribution of the momentary fluctuations, *i.e.*, the momentary fluctuations are more nearly equal to the mean fluctuations. Thus at large values of the parameter k the mean fluctuations determine the nucleation process, whereas at low k values the broad distribution curve indi-

cates that a number of molecules possess enough energy on account of intense momentary fluctuations to form a nucleus. In the first case the proportionality constant s will consequently influence only the level of the mean fluctuation. The steepness of the transition region (between monomers and micelles) is therefore not expected to be changed. In contrast to the first case, s determines in the second instance the distribution of molecules supplied with sufficient energy to build up nuclei. This results in a change of the steepness of the transition region as is actually observed (see Figure 6).

A plot of the number of particles against the number of weighed-in monomers (Figure 7) for two values of the parameter s shows an interesting detail. The curves (○ = monomers, ● = all particles) corresponding to the smaller s value (less fluctuations) possess at $W_m \approx 500$ significant maxima in the number of particles (ν). Due to the small fluctuations, only a few molecules can be supplied with sufficient energy to form a micellar nucleus. This leads to an accumulation of monomers as was to be expected. The limiting slopes of the $\langle N_w \rangle$ curves are determined by the final sizes of the aggregates, *i.e.*, 16 monomeric particles.

An additional supersaturation-like behavior may be derived from Figure 6 where the $\langle N_w \rangle$ curve corresponding to the lowest s value tends to flatten after a jump-like increase of M. The less steep part of the curve is due to the increasing amount of micelles in the solution. At large numbers of weighed-in monomers the $\langle N_w \rangle$ curves must tend to the limit $M = 16$. These observations have been experimentally verified with a number of ionic surfactants in apolar solvents.[6] Finally, a computer experiment has been performed with respect to possible kinetic experiments which demonstrates the appearance of a hysteresis loop while building up and decomposing the micelles (Figure 8). The weighed-in concentration of monomers was stepwise increased (or decreased, respectively) and the apparent molecular weight, which occured after a definite time interval, calculated and plotted. This procedure does not lead to an equilibrium distribution. However, the graph may indicate that the rates of composition and decomposition of a micelle are different due to the assumption that the micelle formation has been based on a nucleation process in this model (see Figure 1 and ref 8).

Statistical Interpretation of Cooperativity

It should be mentioned, however, that in particular the curves of Figure 6 may be interpreted in a different way. They could be regarded as describing the difficulty of overcoming a potential barrier in forming a micellar nucleus. This aspect of the problem leads to the conception of a cooperative phenomena (see Figure 1 and ref 14), *i.e.*, the formation of a nucleus is more difficult than its subsequent growth to a micelle.

The cooperativity parameter σ which serves as a measure for the difficulty of the initial step of a process compared with those following is a number between 0 and 1.[15] It seems possible, however, to relate the parameter s, which was introduced in eq 5 as a proportionality constant to σ. Thus the relation

$$s^{(2)}/s^{(1)} = \ln 1/\sigma \qquad (10)$$

would conform to the meaning of σ. $s^{(1)}$ and $s^{(2)}$ are, respectively, arbitrary reference values (1) and any value between zero and infinity (2). The s values given in Figure 6 correspond to the three cooperativity parameters 0.136, 0.368, and 0.607, respectively. The relation given in eq 10, therefore, permits simple interpretation of σ as a measure of the difficulty in overcoming the potential barrier in the micellation process.

Preliminary testing of the Monte-Carlo program was carried out on a PDP 9 computer. The final results were obtained with a CDC 3200 and a UNIVAC 1108 computer at the computing center of the University of Basel.

Acknowledgment. We thank Mr. H. Hammerich for preparing the figures.

References and Notes

(1) H. Kempter and R. Mecke, *Naturwissenschaften*, **27**, 583 (1939).
(2) I. Prigogine and R. Defay, "Chemical Thermodynamics," Longmans, Green and Co., London, 1954.
(3) H. G. Elias, "The Study of Association and Aggregation via Light-scattering," in "Ligh Scattering from Polymer Solutions," M. B. Huglin, Ed., New York, N. Y., 1971.
(4) J. M. Corkill, J. F. Goodman, T. Walker, and J. Wyer, *Proc. Roy. Soc., Ser. A*, **312**, 243 (1969).
(5) D. G. Hall *Trans. Faraday Soc.*, **66**, 1351 (1970).
(6) H. F. Eicke and V. Arnold, *J. Colloid Interface Sci.*, **46**, 101 (1974).
(7) H. F. Eicke and H. Christen, *J. Colloid Interface Sci.*, **46**, 417 (1974).
(8) H. F. Eicke and H. Christen, *J. Colloid Interface Sci.*, in press.
(9) N. Metropolis, A. W. Rosenbluth, M. N. Rosenbluth, A. H. Teller, and E. Teller, *J. Chem. Phys.*, **21**, 1087 (1953).
(10) W. Wood, *J. Chem. Phys.*, **48**, 415 (1968).
(11) I. R. McDonnald and K. Singer, *Chem. Brit.*, **9**, 54 (1973).
(12) L. J. Schaad, *J. Amer. Chem. Soc.*, **85**, 3588 (1963).
(13) D. E. Knuth, "The Art of Computer Programming," Vol. II, Addison-Wesley, Reading, Mass., 1969.
(14) F. Oasawa and M. Kasai, *J. Mol. Biol.*, **4**, 10 (1962).
(15) D. Winkelmair, *Arch. Biochem. Biophys.*, **147**, 509 (1971).

Molecular Structure Effect on the Diffusion of Heptane Isomers

Eli Grushka* and Paul Schnipelsky

Department of Chemistry, State University of New York at Buffalo, Buffalo, New York 14214 (Received January 7, 1974)

The diffusion coefficients of eight heptane isomers in He were measured by the chromatographic broadening technique. As was the case with octane isomers, it was found that the diffusion coefficient increased with branching. The diffusion trend can be explained, at least in a qualitative manner by Giddings' shielding theory. It was found that the number and position of methyl groups greatly influence the magnitude of the diffusion coefficient. Group diffusion values calculated from the methyl groups agreed with previous calculation. Also, a relationship between diffusion coefficients and critical volumes was found. The relationship is similar to that obtained for octane isomers. The physical importance of that phenomenon is not yet clear. However, it can be used in estimating critical values from diffusion data.

The study of mass transport phenomena, molecular interactions, and the physical parameters describing molecular geometry all can be aided by the accurate determination of the diffusion coefficients of the molecules. In order to predict accurate values of these diffusion coefficients many theoretical approaches have been tried.[1-3]

Most of the success of these estimating equations, whether founded on theory or empirically determined, has been with small molecules. This is because most of the theoretical estimating methods as well as some of the empirical methods are firmly couched in a spherical model of the molecule. Both the "hard sphere, elastic collision" model and the Chapman-Enskog theory with various intermolecular interaction parameters depend upon spherical geometry and force field assumptions to yield reasonable results. Other models are available such as the rough sphere model by Bryan,[4] the loaded sphere, and the spherocylindrical model by Dahler, *et al.*,[5-8] and the rigid ovaloids model proposed by Ishida.[9] These models probably describe polyatomic molecules more realistically than the spherical models. These models, however, are often so complex that meaningful computations of molecular interaction parameters are intractable. In some cases, cross-sectional collisional integrals are not available for calculations.

Due to these difficulties, relatively little work has been done on large molecules. Some of the work done up to now on polyatomic molecules is by Watts,[10-14] Haung,[15] Humpheys and Mills,[16] and Wakeham and Slater.[17] These workers center little attention on molecular geometry. Little work appears on the effect of structural isomerism on diffusion. Fuller, Ensley, and Giddings,[18] Grushka and Maynard,[19] and Vandensteendam and Piekarski[20] have focussed attention on the effects of molecular geometry on diffusion using the chromatographic methods.

There has been some confusion on the effects of structural isomerism on the diffusion. Ubbelhode's work[21,22] shows some inconsistencies. Lugg,[23] Haung,[15] and Watts[14] show more confusion about the effects of branching on diffusion. These inconsistencies are discussed in detail by Grushka and Maynard.[19]

The exact nature of the geometric contributions to diffusion is difficult to determine although insights can be obtained experimentally as evidenced by Grushka and Maynard's study on the effect of branching on octane isomers' diffusion coefficients.[19] This work is a continuation of that preliminary study. It is the purpose of this work to establish whether or not geometric factors contribute in a predictable manner to diffusion coefficients. For this purpose, the diffusion of heptane isomers in He was measured. In addition, Hirschfelder, Curtiss, and Bird[24] have suggested that the Lennard-Jones 6-12 interaction parameters (ϵ, σ) could be extracted from accurate diffusion data. Binary diffusion would be the transport phenomenon of choice for the determination of ϵ and σ because to a first approximation heteromolecular interactions are the only ones that occur as opposed to other transport phenomena (thermal conductivity, viscosity, etc.) which have large homomolecular interactions.

The diffusion measurements were done using the chromatographic method as suggested by Giddings[25] and improved by Grushka and Maynard.[19] The chromatographic method, in general, was recently reviewed by Maynard and Grushka.[26]

The mathematical correlations between chromatographic zone width and diffusion coefficients follow. The mass balance equation describing the solute dispersion in a fully developed laminar flow is given by

$$\frac{\partial c}{\partial t} - D_{AB}\left[\frac{\partial^2 c}{\partial x^2} + \frac{1}{r}\frac{\partial}{\partial r}\left(r\frac{\partial c}{\partial r}\right)\right] + 2\bar{v}\left[1 - \left(\frac{r}{r_0}\right)^2\right]\frac{\partial c}{\partial x} = 0 \tag{1}$$

$\bar{v}$ is the cross-sectional coverage velocity, r_0 is the radius of the tubing, t is time, x is the axial coordinate, and c is the concentration of the organic vapor solute. This equation is rigorously correct for a straight tube. However, in a coiled tube where the ratio of the coil radius to the tube is very large, secondary flow phenomena are unimportant and eq 1 can be utilized. The boundary conditions for the system are no mass transport of solute through the walls of the column, and the radial concentration gradient is zero at the center of the tube. The initial conditions are injection profile in the form of a delta function and $c = 0$ at $t = 0$. The solution to this equation is given by

$$c_{x,t} = A\left[\frac{D_{eff}t}{L^2}\right]^{-1/2} \exp\left[-\frac{(x - \bar{v}t/L)^2}{4D_{eff}t}L^2\right] \tag{2}$$

L is the length of the column and A is a constant related to the initial c, and D_{eff} is the effective dispersion coefficient given by[27]

$$D_{eff} = D_{AB} + (r_0^2\bar{v}^2/48D_{AB}) \tag{3}$$

The modified gaussian given by eq 2 tends to a pure gaussian as $D_{eff}/\bar{v}L$ becomes small.[28] The variance (in

TABLE I: Diffusion Coefficients (cm^2/sec) of Heptane Isomers in He at 100.0 ± 0.10° and at 760 mm

Compound	Bp, °C	D_{AB}[a]	Relative deviation, %
n-Heptane	98.42	0.3544	0.62
3-Methylhexane (3MH)	92.0	0.3586	0.36
2-Methylhexane (2MH)	90.0	0.3626	0.54
2,4-Dimethylpentane (2,4DMP)	80.5	0.3635	0.27
2,2-Dimethylpentane (2,2DMP)	79.20	0.3720	0.11
2,3-Dimethylpentane (2,3DMP)	89.8	0.3758	0.61
3,3-Dimethylpentane (3,3DMP)	86.06	0.3843	0.59
2,2,3-Trimethylbutane (2,2,3TMB)	80.9	0.3858	0.32

[a] Diffusion coefficients are corrected to 1 atm pressure.

length units) is given by

$$\sigma^2 = \frac{2D_{AB}L}{v} + \frac{r_0^2 \bar{v} L}{24 D_{AB}} \quad (4)$$

In chromatographic theory, the plate height H, is defined as

$$H = \sigma^2 / L \quad (5)$$

It is evident upon substitution of eq 5 into 4 and rearrangement that

$$D_{AB} = \left(\frac{\bar{v}}{4}\right)\left[H \pm \sqrt{H^2 - r_0^2/3}\right] \quad (6)$$

Since H, $\bar{v}$, and r_0 are experimentally obtained variables, the diffusion coefficient can be calculated from the chromatogram. Possible sources of errors and their elimination were discussed elsewhere.[19]

Experimental Section

Apparatus. The apparatus was similar to that described by Grushka and Maynard.[19] Temperature gradients were held to <0.2° and the temperature at any point was held at ±0.1°. The column used was 316 stainless steel with a radius of 0.270 ± 0.002 cm i.d. and a length of 3051.1 cm. The injection system and oven were identical with that used by Grushka and Maynard[19] except that a precision bearing assembly was installed to maintain a uniform fan speed throughout the analysis time.

The data system was controlled by a sequencer of novel design described by Schnipelsky, Solsky, and Grushka.[29]

Reagents. The solutes studied, purchased from Chemical Samples Co., were (a) *n*-heptane (99.9%), (b) 2-methylhexane (99%), (c) 3-methylhexane (99%), (d) 2,2-dimethylpentane (99.9%), (e) 2,3-dimethylpentane (99.9%), (f) 2,4-dimethylpentane (99.9%), (g) 3,3-dimethylpentane (99%), and (h) 2,2,3-trimethylbutane (99.9%). The methane used was Matheson high purity (99.97% pure). The carrier gas was commercially available Grade A helium dried through a molecular sieve and preheated. Air used for the flame ionization detector was dried over Drierite and through a molecular sieve.

Procedure. The sequencer activated the injection and started the timing sequence of the sequencer. A punch and a digitizer were activated by the sequencer at a predetermined time interval from the injection point. At the end of a run the punch and digitizer were turned off and another injection was made. At least ten runs were collected for each diffusion determination. The carrier velocity was about 2 cm/sec. The retention time of the solutes was about 1500 sec.

Results and Discussion

Approximately 300 points were taken in the central portion of the peak. Between 50 and 100 points were taken on either side of the peak. These points were used to establish the baseline and correct for any drift which might have occurred. The overall accuracy of the system and the data treatment were discussed before.[19] Only the diffusion coefficients obtained by least squares, fitting a Gaussian to the experimental data, are given in the paper.

In order to test the reproducibility of the system we examined the diffusion of methane in He at 100°. The D_{AB} value was 1.002 ± 0.005 cm^2/sec. Previous values[19] were 1.000 ± 0.003 cm^2/sec at 1.5 cm/sec and 1.006 ± 0.007 cm^2/sec at 3.0 cm/sec. The agreement is well within the experimental error.

Diffusion of Heptane Isomers in He. The data for the heptane isomers were obtained from at least 10 replicate runs for each isomer. Data points were eliminated only when they fell outside the requirements for a student "t" test at the 95% confidence interval. At no time were more than two points eliminated. The diffusion coefficients of eight heptane isomers in He are shown in Table I. The value of D_{AB} obtained for heptane is in good agreement with that of Vandensteendam and Piekarski.[20] The excellent precision should be noted. It is comparable to our previous study.[19]

As with the octane isomers,[19] as the branching of the molecules increases, so does the diffusion coefficient. In order to confirm the order of diffusion coefficients of 2-methylhexane and 3-methylhexane, the measurements were repeated. The coefficients obtained were the same (within experimental error) for each of the isomers. Thus, it is seen that D_{AB} for 2-methylhexane is, indeed, larger than that of 3-methylhexane. An explanation of this will be given shortly.

In Table I the boiling points of the various isomers are also given. No exact correlation can be found between the diffusion coefficients and the boiling points although in general an inverse relationship exists. This indicates that estimating equations using boiling points such as suggested by Arnold[30] should be used with caution.

An explanation of the order of diffusion coefficient of 2-methylhexane and 3-methylhexane can perhaps be explained by using Giddings[18] shielding theory. Space filling models of these molecules clearly demonstrate that the longer straight chain portion of the 2-methylhexane (*i.e.*, *n*-butyl) can be more effective in shielding the methyl side group than the 3-methylhexane straight chain (*i.e.*, *n*-propyl) portion. The result is that the methyl group of the 2-methylhexane contributes less to the diffusion volume of the molecules. These two isomers, however, do not present a simple picture. Alternatively to the above discussion the following can be made. Because of its proximity to the end of the chain the methyl in the 2-methylhexane shields a smaller portion of straight chain than the methyl group on the other isomer. This would seem to give a diffusion order which is reversed to that found ex-

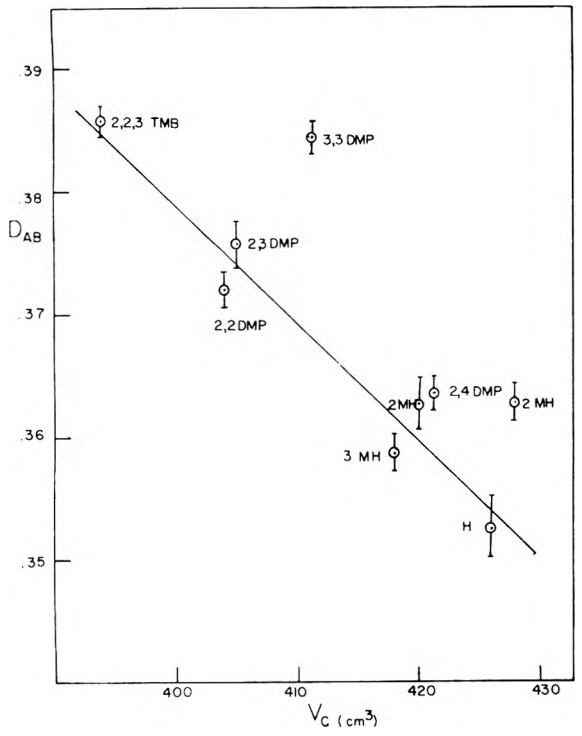

Figure 1. Relationship between diffusion coefficients and critical volumes.

perimentally. At this point all we can say is that the experimental values coupled with space filling models indicate perhaps that the first of the two explanations is the most plausible.

It is interesting to note that with the heptanes, as well as the octanes,[19] the diffusion coefficients of the 2,4-dimethylalkane are smaller than either the 2,3-dimethylalkane or 2,2-dimethylalkane. In fact, Table I indicates that as the two methyl side groups are closer together the diffusion coefficients increase. In terms of the Giddings' shielding theory[18] it can be said that when the two methyl groups are close, the linear portions of the molecule shield the two methyl groups more effectively, thus reducing their contribution to the diffusion coefficient. The diffusion coefficient of the 3,3-dimethylpentane is the highest of any other dimethylpentane. Perhaps, an explanation lies in the fact that the two ethyl groups (on either side of the molecule center where the methyls are located) can be quite effective in shielding. Using space filling molecular models, it is easily seen that the 3,3-dimethylpentane can assume a more compact form than any of the other dimethylpentanes. Another important point is the shielding of one methyl group by the other. As the two groups get closer together the mutual shielding becomes more effective.

The diffusion values of the 3,3-dimethylpentane and the 2,2,3-trimethylbutane are rather close. The two isomers have roughly the same molecular dimensions.

In Table II the group diffusion volumes for the methyl groups are given for all the branched isomers. The method of calculation of the group diffusion volumes and their importance are described elsewhere.[19] Again, it is noticed that the methyl group diffusion volume is dependent on the position and number of the methyl units.

We assumed that with dimethyl or trimethyl isomers the diffusion volume of each methyl unit in an isomer is equivalent. Most likely, this assumption is invalid. Nevertheless, we shall use this value as a first approximation. With the octane isomers some of the diffusion volumes for each CH_3 group were[19] 3-methylheptane, 26.2 cm^3; 2,4-dimethylheptane, 24.2 cm^3; 2,3-dimethylhexane, 20.5 cm^3; and 2,2,4-trimethylpentane, 18.7 cm^3. From Table II we see that for the same group position in the heptane isomers the diffusion volumes of the methyl groups are roughly in 10% agreement. Note, however, that the CH_3 diffusion volume contribution of the 2,2,3-trimethylbutane is larger than that of 3,3-dimethylpentane. This observation might indicate, as mentioned before, the more pronounced shielding effect of the ethyl group on either side of the center of the dimethylpentane isomer. It is stressed at this point that the above arguments remain only speculation, and must be checked with additional systems.

TABLE II: Group Diffusion Volumes of CH_3 Groups

Compound	V_{CH_3}, cm^3 (of each methyl group)
3MH	25.79
2MH	23.16
2,4DMP	21.19
2,2DMP	19.32
2,3DMP	18.00
3,3DMP	14.57
2,2,3TMB	16.23

The above arguments give support to Giddings' shielding theory and give hope that numerical values for shielding constants can be derived from the data.

Relationship to Critical Volume It was observed previously[19] that a linear relationship exists between the diffusion coefficients and the critical volumes of the octane isomers. Figure 1 shows the relationship between the two parameters for the eight heptane isomers. For 2-methylhexane we found two confliting critical volumes: 420[31] and 428.[2] The value of 420 was chosen in fitting the data to a straight line. Not included in the fitting was the critical volume of 3,3-dimethylpentane, since that value, obtained from ref 2, is calculated from an estimating equation. In fact, Figure 1 might indicate that the estimated critical volume of 3,3-dimethylpentane is too large and a smaller volume is more realistic. A similar observation was made with one of the octane isomers.[19] Plots such as Figure 1 can aid, then, in a better estimation of critical values, at least in some cases.

The slope of the line is −0.558. The correlation coefficient is 0.884. With our octane isomer data, the slope of the line was −0.613. The two values are within 10%. At this point, we do not know if the slope of the line has any physical significance other than being a fitting parameter. We did not try to fit other curves to the data.

Summary

The data presented here, together with the octane data,[19] indicate definite trends in the behavior of the diffusion coefficients. It seems that as the molecular branching increases so does the diffusion coefficient. The shielding theory of Giddings[18] can, at least in a qualitative manner, explain this trend. This is particularly so since the position of the side group in the molecule can have a marked effect on the diffusion coefficient.

The concept of *group* diffusion volumes can be valid, and it can be utilized in the F.S.G. estimating equation.[18] However, additional data are needed to get more reliable values for the group contribution in terms of their number and position. Also, a relationship seems to exist between critical volumes and diffusion data.

Since diffusion coefficients can be utilized in obtaining intermolecular forces, we are now engaged in studying the temperature dependence of D_{AB}. This data, to appear in a subsequent publication, will deal with parameters such as collision cross section and potential well depth.

References and Notes

(1) S. Bretsznajder, "Prediction of Transport and Other Physical Properties of Fluids," Pergamon Press, New York, N. Y., 1971, p 329.
(2) R. C. Reid and T. K. Sherwood, "The Properties of Gases and Liquids," McGraw-Hill, New York, N. Y., 1966
(3) T. R. Marrero and E. A. Mason, *J. Chem. Phys. Ref. Data*, **1**, 3 (1972).
(4) G. H. Bryan, *Brit. Assoc. Rep.*, 83 (1894).
(5) J. S. Dahler and N. F. Sather, *J. Chem. Phys.*, **38**, 2363 (1962).
(6) S. I. Sandler and J. S. Dahler, *J. Chem. Phys.*, **43**, 1750 (1965).
(7) S. I. Sandler and J. S. Dahler, *J. Chem. Phys.*, **46**, 3520 (1967).
(8) S. I. Sandler and J. S. Dahler, *J. Chem. Phys.*, **47**, 2621 (1967).
(9) Y. Ishida, *Phys. Rev.*, **10**, 305 (1971).
(10) H. Watts, *Can. J. Chem.*, **49**, 67 (1971).
(11) M. Cowie and H. Watts, *Can. J. Chem.*, **44**, 74 (1971).
(12) R. W. Elliot and H. Watts, *Nature (London), Phys. Sci.*, **234**, 98 (1971).
(13) R. F. Bar and H. Watts, *J. Chem. Eng. Data*, **17**, 45 (1972).
(14) R. W. Elliot and H. Watts, *Can. J. Chem.*, **50**, 31 (1972).
(15) T. C. Havas, F. J. F. Yang, C. J. Haung, and C. H. Kuo, *J. Chromatogr.*, **70**, 13 (1972).
(16) A. E. Humphreys and A. Mills, *Nature (London), Phys. Sci.*, **238**, 46 (1972).
(17) W. A. Wakeham and D. H. Slater, *Nature (London), Phys. Sci.*, **239**, 109 (1972).
(18) E. N. Fuller, K. Ensley, and J. C. Giddings, *J. Phys. Chem.*, **73**, 3679 (1969).
(19) E. Grushka and V. R. Maynard, *J. Phys. Chem.*, **77**, 1437 (1973).
(20) C. Vandensteendam and S. Piekarski, *J. Chim. Phys.*, **70**, 600 (1973).
(21) G. A. McD. Gummings and A. R. Ubbelohde, *J. Chem. Soc.*, 3751 (1953).
(22) J. K. Clarke and A. R. Ubbelohde, *J. Chem. Soc.*, 2050 (1957).
(23) G. A. Lugg, *Anal. Chem.*, **40**, 1022 (1968).
(24) J. O. Hirschfelder, C. F. Curtiss, and R. B. Bird, "Molecular Theory of Gases and Liquids," Wiley, New York, N. Y., 1954, p 580.
(25) J. C. Giddings and S. L. Seager, *J. Chem. Phys.*, **33**, 1579 (1960).
(26) V. R. Maynard and E. Grushka, *Advan. Chromatogr.*, in press
(27) G. Taylor, *Proc. Roy. Soc., Ser. A*, **219**, 186 (1953).
(28) O. Levenspiel and W. K. Smith, *Chem. Eng. Sci.*, **6**, 227 (1957).
(29) P. N. Schnipelsky, J. Solsky, and E. Grushka, *J. Chromatogr. Sci.*, in press.
(30) J. H. Arnold, *Ind. Chem.*, **22**, 1091 (1930).
(31) Phillips Reference Data for Hydrocarbons and Petro-Sulfur Compounds, Phillips Petroleum Co., Bulletin No. 521, 1962.

Effect of Ion Pairs on the Relaxation of Ionic Atmospheres[1a,b]

Stefan Highsmith and Ernest Grunwald*

Chemistry Department, Brandeis University, Waltham, Massachusetts 02154

(Received January 9, 1974)

Publication costs assisted by the Petroleum Research Fund and Brandeis University

A recent theory by Onsager and Provencher which includes the effects of ion association on the relaxation of the ionic atmosphere in electrolytic solutions has been confirmed by capacitance and conductance measurements of solutions of i-Am_4NNO_3 in 1-octanol and 1,2-dichloroethane. This theory supplants the classical treatment by Debye and Falkenhagen and has some significant consequences: it allows one to determine the rates of ion association and dissociation for rates from 0.05 to 1 times the diffusion-controlled rate by capacitance measurements; and it modifies the limiting slope, S_Λ, in the Onsager expression for equivalent ionic conductance. The dissociation constant for i-Am_4NNO_3 in 1-octanol at 25° was 2.86×10^{-5} M.

Subsequent to earlier work by Gilkerson,[1c] Onsager and Provencher (OP) have derived a theory[2] according to which the relaxation of an ionic atmosphere is speeded up by the presence of ion pairs, because the association-dissociation of the ions provides an additional relaxation mechanism. This theory has far-reaching consequences for the prediction of interionic effects on irreversible processes in electrolytic solutions whenever ion pairs are present. It is no longer sufficient merely to know the ionic strength (I); one must also know the rate constant (k_a) for the association of the free ions. Thus, in the presence of ion pairs, the limiting slope S_Λ in the expression for the equivalent ionic conductance,[3] $\Lambda = \Lambda_0 - S_\Lambda I^{1/2}$, may not be set equal to the Onsager limiting slope for a strong electrolyte. As a consequence, all conductometric ion-pair association constants calculated using the interionic attraction theory in the traditional way should be at least somewhat in error.

It is clearly desirable to test the OP theory.[2] That is best done by isolating the interionic effects and measuring them as directly as possible. We report here a study of both the conductance and capacitance of tetraisoamylammonium nitrate (i-Am_4NNO_3) in 1-octanol which, in conjunction with similar data for 1,2-dichloroethane (DCE),[4] confirms the theory.

The test of the OP theory depends primarily on the measurement of the capacitance; the conductance is used mainly to obtain the ion-pair dissociation constant. The specific capacitance of an electolytic solution differs from that of the pure solvent owing to (a) electric dipoles of the ion pairs and noncentric free ions; (b) "freezing" of solvent dipoles by the electrolyte;[5] and (c) the 90° out-of-phase component of the ionic conductance. It will now be shown that under our conditions, a and b are small compared to c.

Measurements were made at electrolyte concentrations ranging up to 2.5×10^{-4} F, corresponding to ionic strengths up to 7.5×10^{-5} M. The static permittivity (ϵ_0) of 1-octanol at 25° is 9.88. Assuming the dipole moment of i-Am_4NNO_3 ion pairs to be 14.3 D (same as in chloroben-

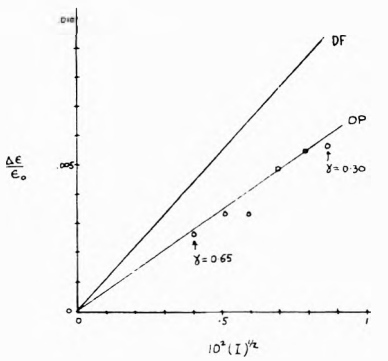

Figure 1. Experimental change in permittivity ($\Delta\epsilon/\epsilon_0$) of *i*-$Am_4NNO_3$ in 1-octanol plotted as a function of the square root of the ionic strength. Solid lines are predicted by the DF theory (μ = 0.0) and the OP theory (μ = 0.31).

zene[4]), the change in *static* permittivity $\Delta\epsilon$ owing to a is 6 × 10^{-3} at the highest concentration. $\Delta\epsilon$ owing to b is about -3×10^{-3}, estimated roughly from data at high frequencies for strong electrolytes in methanol.[5] By contrast, $\Delta\epsilon$ owing to c is predicted by the OP theory to be in the range 0.03–0.09, depending on the value of k_a. In the following, effects a and b will therefore be neglected.

The maximum value of $\Delta\epsilon$ predicted by the OP theory, for the case that either $k_a = 0$ or the free-ion fraction γ is unity, corresponds to that predicted by the classical Debye–Falkenhagen (DF) theory[6,7] (which does not allow for ion association). As k_a increases toward the diffusion-controlled limit, $\Delta\epsilon$ drops to 0.340 times the maximum value. A complete test of the OP theory would require independent knowledge of k_a. Our test consists of showing that when γ is small, $\Delta\epsilon$ is distinctly smaller than predicted by the DF theory and can be reproduced by the OP theory with a plausible assumed value for k_a. Moreover, as γ approaches unit, $\Delta\epsilon$ approaches the value predicted by the DF theory. The frequency dependence of $\Delta\epsilon$, though measured with low accuracy, conforms to that predicted by the OP theory.

$\Delta\epsilon$ in 1-Octanol. In this section we let $\Delta\epsilon_w$ denote the change in permittivity at angular frequency $2\pi f = w$. We shall continue to use $\Delta\epsilon$ to denote the limit of $\Delta\epsilon_w$ as $w \to 0$.

A general expression for $\Delta\epsilon_w$ has been given by Onsager and Provencher.[2,8] However, when γ is small, the general and rather complicated expression reduces simply to (1), with parameters as defined in 2–6.

$$\frac{\Delta\epsilon_w}{\epsilon_0} = \frac{7.002 \times 10^5\sqrt{I}(1 + a\sqrt{1 + y^2} - \sqrt{2aR})}{(\epsilon_0 T)^{3/2}\sqrt{2aR}([1 - a]^2 + a^2y^2)} \quad (1)$$

$$a = 1/2 + \mu \quad (2)$$

$$\mu = k_a/A = k_a\epsilon_0/(1.130 \times 10^{10}\Lambda_0) \quad (3)$$

$$y = w\tau/2a \quad (4)$$

$$\tau = \epsilon_0/4\pi L_{esu} = 8.85 \times 10^{-14}\epsilon_0/L \quad (5)$$

$$R = 1 + \sqrt{1 + y^2} \quad (6)$$

Here A is the theoretical rate constant for the diffusion-controlled combination of opposite univalent point charges; τ is the Maxwell relaxation time for the ionic atmosphere (τ neglects relaxation by the association–dissociation mechanism); and L_{esu} or L is the conductivity of the electrolytic solution, in esu cm^{-1} or siemens cm^{-1}, respectively. According to graphs given by OP, eq 1 is a useful approximation even when γ is as high as 0.5, and thus should apply to our data in 1-octanol.

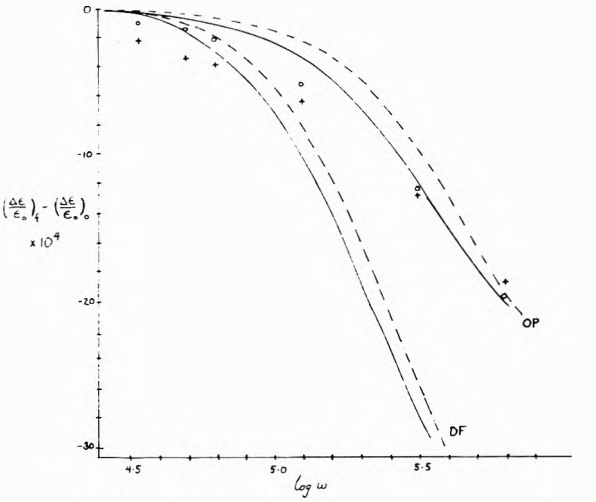

Figure 2. Experimental dispersion of the change in permittivity ($\Delta\epsilon_w/\epsilon_0$) of *i*-$Am_4NNO_3$ in 1-octanol as a function of frequency. Circles and solid lines are experimental and predicted values (DF and OP theories) for 4.84 × 10^{-5} F solution. Crosses and dotted lines are for 7.416 × 10^{-5} F solution.

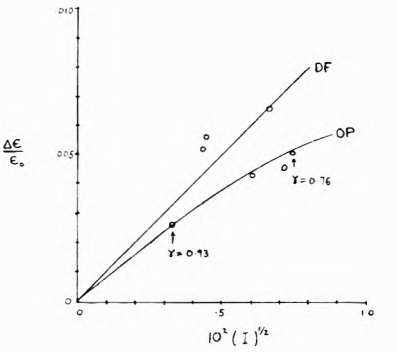

Figure 3. Experimental change in permittivity ($\Delta\epsilon/\epsilon_0$) of *i*-$Am_4NNO_3$ in DCE plotted as a function of the square root of the ionic strength. Solid lines are predicted by the DF theory (μ = 0.0) and the OP theory (μ = 0.31).

Our results for *i*-Am_4NNO_3 in 1-octanol are plotted in Figures 1 and 2. Figure 1 shows $\Delta\epsilon$ *vs.* $I^{1/2}$, as well as theoretical curves for μ = 0.3 and μ = 0.0. Figure 2 shows $\Delta\epsilon_w$ *vs.* log w for two selected concentrations, as well as theoretical curves for μ = 0.3 and μ = 0.0. The fit of the OP theory with μ = 0.3 is quite satisfactory and clearly superior to that of the DF theory (μ = 0.0). At higher ionic strengths, the fit of $\Delta\epsilon_w$ *vs.* log w is less impressive, especially at frequencies below 10 kHz, probably due to double-layer effects.

$\Delta\epsilon$ in 1,2-Dichloroethane. Results for *i*-Am_4NNO_3 in DCE at 25°, reported by Effio and Grunwald,[4] are interpreted in terms of the OP theory in Figure 3. (The required values of γ are calculated using an ion-pair dissociation constant reported by Tucker and Kraus.)[9] Since γ under these conditions varies between 0.93 and 0.76, eq 1 does not apply and the prediction of $\Delta\epsilon$ is based on graphs given by Onsager and Provencher.[2] A theoretical curve is shown for μ = 0.3 as well as the straight line predicted for μ = 0.0. The experimental points have considerable scatter but suggest that μ is intermediate between 0.0 and 0.3.

Conductivity in 1-Octanol. The conductivity of *i*-Am_4NNO_3 in 1-octanol was measured at 25° in the con-

centration range from 6×10^{-7} to 2.5×10^{-4}. The data were first treated by the method of Fuoss and Kraus,[10] with a conventional Onsager limiting slope. Results are $K_d = 2.81 \times 10^{-5}$, $\Lambda_0 = 4.03$, and $S_\Lambda = 40.45$. These results permitted preliminary estimates of the ionic strength for the examination of $\Delta\epsilon$ and led to $\mu = 0.3$. Recalculation on the basis of the OP theory, using $\mu = 0.3$, then led to $K_d = 2.86 \times 10^{-5}$, $\Lambda_0 = 4.01$, and $S_\Lambda = 38.35$. In this case the effect of neglecting the ionic association on K_d and Λ_0 is tolerably small, considering the experimental error.

Association-Dissociation Behavior of i-Am_4NNO_3. The dissociation constant of 2.86×10^5 obtained in 1-octanol may be compared with the value of 1.20×10^{-4} reported[9] in the nearly isodielectric solvent DCE. However, as pointed out by Denison and Ramsey,[11] ion-pair dissociation constants for quaternary ammonium salts in DCE are about an order of magnitude greater than one might expect on the basis of the macroscopic permittivity, perhaps because solvent molecules near the ions can assume the more polar gauche conformation. Thus the value obtained in 1-octanol appears to be "normal."

If the OP theory can be accepted, then the parameter μ permits evaluation of the rate constant k_a for ionic association (eq 3). Using $\mu = 0.31$, k_a is thus found to be 1.43×10^9 sec^{-1} M^{-1} for $i\text{-}Am_4N^+ + NO_3^-$ in 1-octanol at 25°. From this value and that obtained for K_d, we then find that the rate constant k_d for ion-pair dissociation in this system is 4.09×10^4 sec^{-1} at 25°.

From a broader point of view, these results indicate that the measurement of $\Delta\epsilon$ provides a convenient method for measuring rate constants for ionic association. Roughly speaking, the range of μ in which quantitative results can be obtained for k_a is 0.05–1.0. However, there are experimental constraints. In particular, it is desirable to have a fairly viscous medium so that the ionic conductivity is small even at moderate ionic strengths. 1-Octanol is a good choice in this respect; its viscosity coefficient, $\eta = 0.076$ at 25°, about ten times that of water.

Experimental Section

$i\text{-}Am_4NNO_3$ was prepared as described in ref 4. 1-Octanol was twice distilled under reduced pressure with a head temperature of about 100°. Center fractions were collected each time and stored in the dark under N_2. Solutions were prepared by weighing samples of the salt and solvent, using a drybox.

Capacitance and conductance measurements were done as described in ref 4.

References and Notes

(1) (a) Acknowledgment is made to the donors of the Petroleum Research Fund, administered by the American Chemical Society, for partial support of this research. We also thank the Rosenstiel Fund of Brandeis University for partial support and the National Institutes of Health for a postdoctoral fellowship to SH. (b) It is a pleasure to thank W. R. Gilkerson for a helpful discussion. (c) W. R. Gilkerson, *J. Phys. Chem.*, **66**, 669 (1962).
(2) L. Onsager and S. W. Provencher, *J. Amer. Chem. Soc.*, **90**, 3134 (1968).
(3) H. S. Harned and B. B. Owen, "The Physical Chemistry of Electrolytic Solutions," 3rd ed, Reinhold, New York, N. Y., 1958.
(4) E. Grunwald and A. Effio, *J. Solution Chem.*, **2**, 373 (1973).
(5) J. B. Hasted and G. W. Roderick, *J. Chem. Phys.*, **29**, 17 (1958).
(6) P. Debye and H. Falkenhagen, *Phys. Z.*, **29**, 401 (1928).
(7) H. Falkenhagen and G. Kelbg in "Modern Aspects of Electrochemistry," Vol. 2, J. O'M. Bockris, Ed., Butterworths, London, 1959.
(8) Equations 31a and 31b in the paper by Onsager and Provencher (ref 2) contain a minor error; the coefficients of χ_R and χ_I should be divided by 2.
(9) L. M. Tucker and C. A. Kraus, *J. Amer. Chem. Soc.*, **69**, 455 (1947).
(10) R. M. Fuoss and C. A. Kraus, *J. Amer. Chem. Soc.*, **55**, 1019 (1933).
(11) J. T. Denison and J. B. Ramsey, *J. Amer. Chem. Soc.*, **77**, 2615 (1955).

Vaporization of Reactive Salts[1a]

R. T. V. Kung and R. Roberts*[1b]

Department of Engineering and Applied Science, Yale University, New Haven, Connecticut 06520

(Received January 31, 1973; Revised Manuscript Received December 7, 1973)

Publication costs assisted by the Office of Naval Research

Tang and Fenn have recently reported that single crystal ammonium perchlorate vaporized into two molecules, ammonia and perchloric acid. Their results with compressed perchlorate powder indicated decomposition into several species. By a change in their experimental arrangement we have shown that pressed ammonium perchlorate and monofluoroammonium trifluoromethylsulfonate also undergo simple two species vaporization without decomposition. Our results with the latter material also constitute additional evidence for the existence of H_2NF.

Introduction

The vaporization of salts at low pressures in a molecular beam apparatus has been used by Tang, *et al.*,[2] and Tang and Fenn[3] for the identification of the species subliming from a solid. In their experiments base heating was used so that there was a decreasing temperature gradient, from the bulk to the surface. In this arrangement the vapors from pressed powder samples of ammonium perchlorate (AP) apparently reacted before leaving the sample and did not give a velocity spectrum corresponding to two species formation as obtained from a single crystal. The

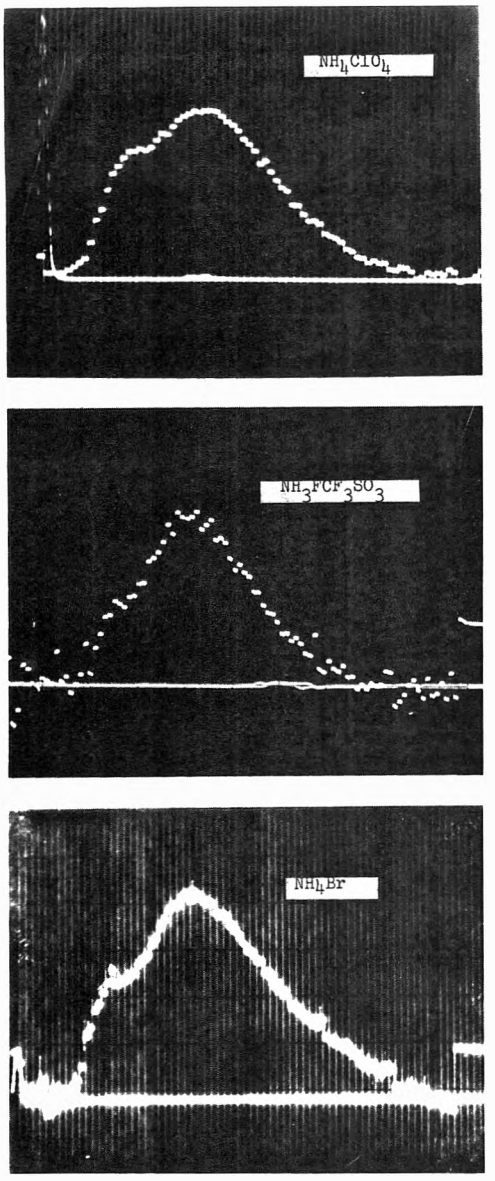

Figure 1. Oscilloscope traces of velocity distribution, mass *vs.* arrival time, for (a) NH_4ClO_4, (b) $[FNH_3][CF_3SO_3]$, (c) NH_4Br.

spectrum obtained indicated a mixture of low molecular weight compounds. To demonstrate that this was truly due to reaction within the pores, as suggested in ref 3, and to simulate more closely solid propellant combustion conditions, experiments with powdered AP were undertaken using surface heating. The technique was then extended to the study of monofluoroammonium trifloromethylsulfonate $[FNH_3]^+[CF_3SO_3]^-$, I,[4] to determine whether additional evidence for the existence of H_2NF could be obtained.

The background for earlier studies on AP vaporization has been reviewed by Tang and Fenn.[3] In a recent review[5] of the decade of effort on oxidizer chemistry, 1955–1965, involving much research on NF chemistry, no mention was made of H_2NF although the related compounds HNF_2 and NF_3 were discussed fully. Colburn[6] also has noted that monofluoroamine has not been characterized. Earlier Ruff[7] and Schmeisser and Sartori[8] claimed evidence for the existence of H_2NF based on the products obtained on the electrolysis of ammonia–ammonium fluoride mixtures and of ammonium fluoride, respectively. Ruff presented

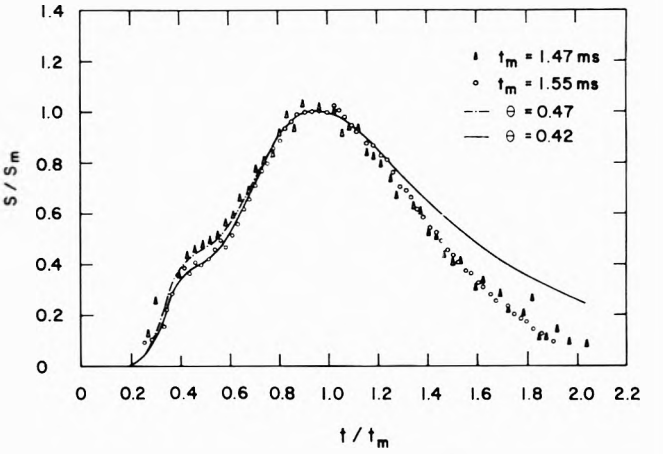

Figure 2. Normalized signal (signal intensity/maximum signal intensity) *vs.* relative arrival time (time/time of maximum signal).

evidence for the existence of H_2NF but the characterization was incomplete. However, both agree that the substance prepared was unstable and hazardous. Later work on the electrolysis, reviewed in ref 5, gave no evidence for H_2NF although more modern techniques of separation and identification were used.

Since the work of Tang and Fenn established the two species vaporization of some ammonium salts it was hypothesized that the sublimation of I would either be molecular or dissociative. The latter would lead to H_2NF in the vapor phase. Ionic dissociation into H_3NF^+ and CF_3SO^- was ruled out because of the expectation that H_2NF would be of lower basicity than NH_3 in view of the following order of basicities deduced from the known chemistry of the related molecules: NH_3 > (H_2NF) > HNF_2 > NF_3. No salts of proton acids have been reported for HNF_2 and NF_3. In addition, the latter is reported to show only weak association with strong acids, such as BF_3.[9] In the mass spectrum of I,[4] H_2HF^+ is the primary N,F containing ion and H_3NF^+ was not present. H_2NF^+ could be either the primary ion from electron impact with H_2NF or a fragment from dissociative ionization of I. It seemed likely that TOF measurements could distinguish between these two possibilities.

The major change in the experimental arrangement of Tang and Fenn[3] was the provision for radiative surface heating. Otherwise the technique and data reduction were as they described. The present experiment consisted in vaporizing a material from a pressed (10,000 psi) pellet, 3 to 4 mm by 10 mm, whose surface was heated by a focused iodine vapor lamp. The vapor passed through a collimating slit (2 mm), a chopper, a second collimating slit (4 mm). A Bayard-Alpert flow-through ionization detector, located 42.5 cm from the chopper, recorded the number density of molecules arriving as a function of time. Time zero was obtained from a photocell exposed to a light when the chopper wheel was in the "open" position. The general procedure was tested by time-of-flight (TOF) measurements with ammonium bromide. Two peaks were obtained corresponding to NH_3 and HBr, Figure 1c. In order to determine the amount of decomposition during surface heating, experiments were made with pellets of compressed AP powder. The results (Figure 1a) were not distinguishable from those obtained with single crystals by Tang and Fenn[3] and showed only NH_3 and $HClO_4$.

There was no evidence of the further decomposition which they found with the compressed powder.

Similar experiments were conducted with I. The resulting TOF distribution is shown in Figure 1b. It is apparent that all three substances show a two species vaporization mechanism.

Data on I were fitted to curves representing the sum of two Maxwellian distributions corresponding to two different masses with the mass ratio of 150:35 at the same temperature as shown in Figure 2 and given by

$$s/s_m = [\theta(m_L/m_H)^2(t_m/t)^4 \exp[-2(t_m/t)^2(m_L/m_H) + 2] + (t_m/t)^4 \exp[-2(t_m/t)^2 + 2]]N^{-1}$$

and

$$N = \theta(m_L/m_H)^2 \exp[-2(m_L/m_H) + 2] + 1$$

where s_m and t_m are, respectively, the signal intensity and arrival time at the most probable velocity of the heavier mass, m_H. The term θ is the ratio of detector sensitivity for the lighter mass, m_L (NH_2F), to that for the heavier mass (HSO_3CF_3). There are no data from which θ can be determined *a priori*. The values which best fit the data range between 0.42 and 0.47. The arrival time, t_m, was adjusted so that the calculated signal maximum fitted the oscillogram maximum in terms of arrival time. The departures from the curve at longer times, *i.e.*, slower molecules, are most likely due to self-scattering effects. Although no independent temperature measurement was obtained, the work by Tang and Fenn[7] supports the generally accepted concept that molecules evaporating freely from a surface have a Maxwellian velocity distribution corresponding to the surface temperature. On this basis, the range of surface temperatures (T_s) for I was between 420 and 460°K. These values were deduced from $t_m = x(m_H/kT_s)^{1/2}$ where x is the distance from the chopper to the detector. The uncertainty in T_s is about ±10°K, and originates mainly from the uncertainty of ~10 μsec in time zero. The curve fit in Figure 2 and the high improbability of a two species vaporization process giving other than the assumed mass ratio leads to the conclusion that I undergoes a two species dissociative vaporization and that one of these species most probably is H_2NF.

The results with pressed powder AP definitely establish the advantage of surface heating to avoid interstitial reaction of subliming materials whose vapors can readily react or decompose as a result of gas-gas or gas-surface collisions. The use of surface heating of I and time-of-flight mass resolution of the vaporizing species also has given additional evidence for the probable existence of H_2NF.

Acknowledgment. The authors are deeply grateful to Professor J. B. Fenn for his suggestions and valuable discussions. The authors also wish to thank Fluorchem, Inc. of Pasadena, Calif., for furnishing the sample of monofluoroammonium trifluoromethylsulfonate. One of us, R. R., wishes to thank the Office of Naval Research and Yale University for the opportunity of making his participation in this research possible.

References and Notes

(1) (a) Supported in part by the Office of Naval Research through Project SQUID. (b) Visiting Fellow, on advance training from the Office of Naval Research. Current address, Office of Naval Research, Arlington, Va. 22217.
(2) S. Tang, R. J. Gallagher, and J. B. Fenn, *Entropie*, **42**, 51 (1971).
(3) S. P. Tang and J. B. Fenn, *J. Phys. Chem.*, **77**, 940 (1973).
(4) V. Grakauskas and K. Baum, private communication.
(5) E. W. Lawless and I. C. Smith, "Inorganic High-Energy Oxidizers," Marcel Dekker, New York, N. Y., 1968.
(6) C. B. Colburn, *Advan. Fluorine Chem.*, **3**, 108 (1963).
(7) O. Ruff and L. Staub, *Z. Anorg. Allg. Chem.*, **198**, 32 (1931).
(8) M. Schmeisser and P. Sartori, *Angew. Chem.*, **71**, 523 (1959).
(9) A. D. Craig, *Inorg. Chem.*, **3**, 1628 (1964).

Electrical Conductances of Some Aqueous Rare Earth Electrolyte Solutions at 25°. I. The Rare Earth Perchlorates[1]

F. H. Spedding* and J. A. Rard

Ames Laboratory USAEC and Department of Chemistry, Iowa State University, Ames, Iowa 50010 *(Received October 23, 1973; Revised Manuscript Received February 27, 1974)*

Publication costs assisted by the U. S. Atomic Energy Commission

The electrical conductances of aqueous solutions of $La(ClO_4)_3$, $Pr(ClO_4)_3$, $Nd(ClO_4)_3$, $Sm(ClO_4)_3$, $Gd(ClO_4)_3$, $Tb(ClO_4)_3$, $Dy(ClO_4)_3$, $Ho(ClO_4)_3$, $Er(ClO_4)_3$, $Tm(ClO_4)_3$, and $Lu(ClO_4)_3$ were measured over the concentration range of approximately 0.004 *m* to saturation at 25°. The equivalent conductances of the rare earth perchlorates, at constant molality, were found to decrease smoothly from $La(ClO_4)_3$ to $Lu(ClO_4)_3$ below 2.5 *m*. A prominent two-series effect appears in the equivalent conductances by 3.0 *m* and is discussed in terms of a change in the inner-sphere cation hydration number and the occurrence of water sharing between the rare earth and perchlorate ions.

Introduction

Aqueous rare earth salt solutions differ from each other mainly because of a slight change in the cation radius across the rare earth series due to the lanthanide contraction. The rare earths therefore form a good series of trivalent salts for the study of the variation of transport and

thermodynamic properties as a function of ionic size. This laboratory is involved in the study of these properties for the rare earth chlorides, perchlorates, and nitrates from dilute solution to saturation and this paper represents one of these studies.

A number of thermodynamic,[2-7] transport,[3,4,8-11] and spectral properties[12-17] have been measured for aqueous rare earth chloride and perchlorate solutions. Irregularities in these properties as a function of the rare earth cation have given rise to a model in which the light and heavy rare earth ions have different inner-sphere hydration numbers, with the rare earth ions from Nd^{3+} to Tb^{3+} being mixtures of the two hydrated forms.

The electrical conductance of an electrolyte solution is influenced by ion-solvent and ion-ion interactions. It is usually assumed that the perchlorate ion does not complex with metal ions although, at high concentrations, outer-sphere complexes have been suggested.[16-25] The concentration dependence of the electrical conductance of the rare earth perchlorate solutions was studied in order to investigate the effect of the changing cationic hydration upon the chemical properties of the rare earth ion-water system. To extend this investigation to include the role of anion hydration and anion-cation interactions, subsequent papers will deal with the aqueous rare earth chloride and nitrate systems.

Experimental Section

Preparation of Solutions. The stock solutions were prepared by the method of Spedding, Pikal, and Ayers.[5] All dilutions were prepared by weight from concentrated stock solutions and conductivity water and all weights were corrected to vacuum. The stock solutions were microfiltered to remove suspended silica particles and then carefully analyzed.

Stock Solution Analyses. The concentrated stock and saturated solutions were analyzed by both EDTA[26] and sulfate methods.[5] Different analyses on the same stock agreed to ±0.1% or better in terms of molality.

Equipment. The Leeds and Northrup conductance bridge assembly described by Dike[27] was used for all of the resistance measurements. All bridge resistors were calibrated and lead resistance corrections were made. The pH's were measured with glass and saturated NaCl-calomel electrodes (saturated KCl-calomel electrodes are erratic in perchlorate solutions).

The cells used in this research were of the capillary type recommended by Jones and Bollinger,[28] were platinized by the method of Jones and Bollinger,[29] and were calibrated using Jones and Prendergast's standards.[30] The cells all had cell constants in the range of 250 to 300 cm^{-1}.

Experimental Procedure. The resistances of three or four samples of each dilution were measured and the average resistances, with few exceptions, are reliable to ±0.02%. Resistances of solutions below 0.01 *m* were measured in parallel with some bridge resistors and are reliable to only ±0.2%. The oil bath temperature was controlled to 24.99 ± 0.01°.

Prolonged contact between the platinum electrodes and concentrated rare earth perchlorate solutions occasionally resulted in the oxidation of the electrode surfaces as evidenced by a large frequency dependence in the measured resistance. This oxidation was eliminated by periodic treatments with dilute $FeSO_4$-H_2SO_4, followed by soaking with HCl and, finally, conductivity water.

Errors and Data Treatment

The equivalent conductances were calculated from the equation

$$\Lambda = \frac{10^3 L}{N} = \frac{(10^3 + mM)L}{3md} \quad (1)$$

where L is the specific conductivity of the solution corrected for the solvent conductivity, N is its normality, m is its molal concentration, M is the molecular weight of the salt (IUPAC values of 1969), and d is the density of the solution. The density data of Spedding and coworkers[31] were fitted to fifth-order polynomials in terms of molality and these equations were used to calculate the densities of the corresponding solutions studied in this research. These density polynomials are of the form

$$d = \sum_{i=0}^{5} A_i m^i \quad (2)$$

and the coefficients are listed in Table I.[32]

The equivalent conductance results from 0.1 *m* to saturation were fitted to seventh-order least-squares polynomials using statistical weighting factors. These fits were performed on an IBM 360 computer using double precision to avoid round off errors. The resulting equations are of the form

$$\Lambda = \sum_{i=0}^{7} B_i m^{i/2} \quad (3)$$

The difference between the experimental and calculated conductances was usually less than 0.02 ohm^{-1} cm^2 $equiv^{-1}$ except for an occasional deviation as large as 0.05 ohm^{-1} cm^2 $equiv^{-1}$. The larger deviations tend to occur at low concentrations where the actual conductance is quite large. The probable errors above 0.05 *m* were calculated to range from less than 0.01 to 0.05 ohm^{-1} cm^2 $equiv^{-1}$, with the smaller errors occurring for the more concentrated solutions, so the polynomials fit within experimental error.

The conductance data are reported in Table II[32] and the conductance polynomial coefficients are given in Table III. The saturated solution molalities to be used with eq 2 and 3 are listed in Table IV. The equivalent conductances are reported in units of $(absolute\ ohm)^{-1}$ cm^2 $equivalent^{-1}$. The equivalent conductance and the concentration data are generally uncertain in the fourth figure but were reported to five places in most cases since the internal consistency of the data is greater than its absolute accuracy.

The purpose of obtaining these polynomial fits was to calculate relative per cent differences defined as

$$\frac{\Lambda_{RE(ClO_4)_3} - \Lambda_{Lu(ClO_4)_3}}{\Lambda_{Lu(ClO_4)_3}} \times 100 \quad (4)$$

where RE represents the rare earth of interest. These per cent differences enable one to examine the small but real differences between the various rare earth perchlorates.

The dilute solution conductances of eight of the rare earth perchlorates have been measured by Spedding and Jaffe.[9] As previously mentioned, the conductances of the most dilute solutions reported here are reliable to 0.2%. The data of Spedding and Jaffe should be reliable to 0.1% in this region so our data should agree with theirs to 0.3% for each salt in the overlapping region. Graphical comparison indicated that all but La agreed within this limit and La fell only slightly outside.

TABLE III: Conductance Polynomial Coefficients for Perchlorates

Salt	B_0/B_4	B_1/B_5	B_2/B_6	B_3/B_7
$La(ClO_4)_3$	113.755644	−133.865051	250.664759	−362.979281
	300.887992	−150.716050	42.4226658	−5.03245629
$Pr(ClO_4)_3$	112.709943	−125.819473	225.023065	−319.880772
	258.876234	−127.191732	35.4473810	−4.18715132
$Nd(ClO_4)_3$	112.384826	−120.223678	203.032449	−281.684257
	223.493003	−109.039229	30.5627797	−3.64653777
$Sm(ClO_4)_3$	113.722978	−137.885487	265.889823	−390.941918
	324.737789	−159.774179	43.5348830	−4.97352759
$Gd(ClO_4)_3$	112.999666	−138.635838	267.818563	−398.119408
	335.126600	−166.361377	45.5448518	−5.22309077
$Tb(ClO_4)_3$	112.587096	−138.758261	264.905446	−389.083116
	321.478887	−155.696784	41.5842113	−4.67045271
$Dy(ClO_4)_3$	111.619667	−130.573806	233.247016	−330.125866
	260.679872	−120.672584	31.1075186	−3.40584028
$Ho(ClO_4)_3$	110.683936	−126.733062	221.014053	−312.945925
	247.840798	−115.303952	29.9547094	−3.31212709
$Er(ClO_4)_3$	111.544708	−136.164521	254.363940	−370.218577
	301.044753	−142.937823	37.5419784	−4.17157148
$Tm(ClO_4)_3$	111.635535	−135.829207	249.703539	−359.186533
	288.410556	−135.342338	35.2439817	−3.89428363
$Lu(ClO_4)_3$	111.039291	−132.602462	239.210493	−341.648847
	271.376036	−125.953311	32.5628478	−3.58761827

TABLE IV: Aqueous Rare Earth Perchlorate Molal Solubilities at 25°

Rare earth	Molality	Rare earth	Molality
La	4.7601	Dy	4.6016
Pr	4.6955	Ho	4.6241
Nd	4.6851	Er	4.6185
Sm	4.6401	Tm	4.6173
Eu	4.6334	Yb	4.6044
Gd	4.6089	Lu	4.6335
Tb	4.6073		

Results

To the scale of graphs allowed here little difference could be seen between the equivalent conductances of adjacent rare earth perchlorates so relative per cent difference curves are used to illustrate the data in Figures 1 and 2. Gd is plotted on both graphs as a common reference. The Lu data, on this type of plot, fall along the molality axis.

Below 2.5 *m* the curves plotted in Figures 1 and 2 show that the conductances are cleanly separated and occur in the sequence of the atomic numbers of the rare earths. Above 2.5 *m* some crossovers occur. In order to clarify the trends represented by the crossings, plots were made of the relative per cent differences at constant molality. In Figure 3 the relative per cent differences are given at 1.0 and 2.0 *m* for both the chlorides[33] and perchlorates and in Figures 4 and 5 plots are given for the perchlorates at higher concentrations. The similarity of the rare earth chloride and perchlorate data below 2.0 *m* should be noted here. The viscosity data included on these plots are that of Spedding, Shiers, and Rard.[34]

The radius of the rare earth cation decreases as the atomic number of the rare earth increases and the radius of the rare earth ion together with its first hydration sphere should also decrease across the series. As a result the surface charge density of the smallest hydrated cations should be largest. The smaller hydrated cations should therefore bind water in the second and higher hydration spheres more strongly and the total hydration of the cations should increase from La to Lu. The total hydration sphere is involved in electrolytic conductance so

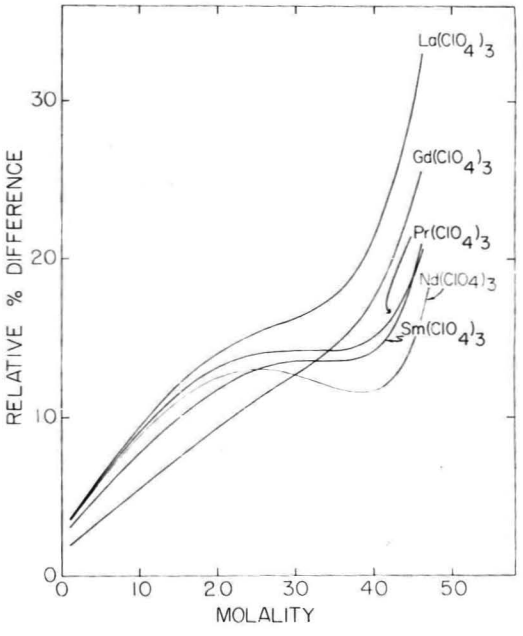

Figure 1. Per cent differences in equivalent conductances relative to $Lu(ClO_4)_3$ for some light and middle rare earth perchlorates.

the cation mobility, at constant concentration, should decrease with an increase in the rare earth atomic number. If the amount of complexation changes little across the rare earth series, then the perchlorate ion contribution to conductance should be similar, at equal concentrations, for all of the rare earth perchlorate solutions, so the cation mobilities determine the order of the electrolytic conductances. The above explanation is adequate to account for the trends in conductance and viscosity below 2.5 *m*. The assumption of increasing total hydration has also been used to explain aqueous rare earth chloride water activity data.[35]

Above 2.5 *m*, the conductance data begin to form two distinct series and this effect is well established by 3.0 *m*. For the rare earth perchlorates the isomolal conductances decrease from La to Nd, rise to Tb, and then decrease

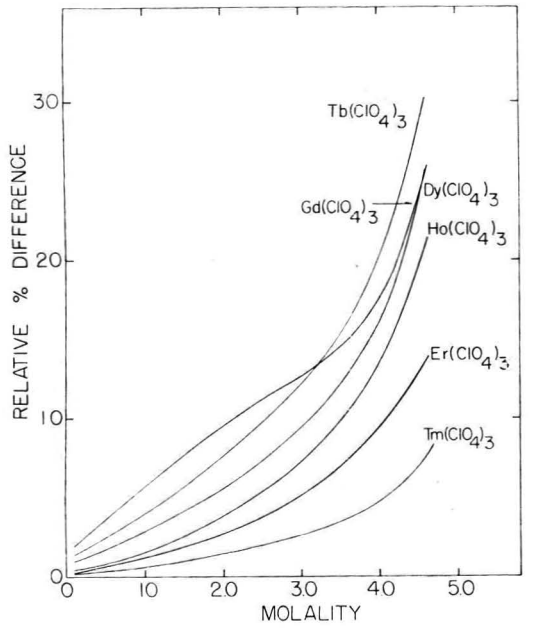

Figure 2. Per cent differences in equivalent conductances relative to $Lu(ClO_4)_3$ for some middle and heavy rare earth perchlorates.

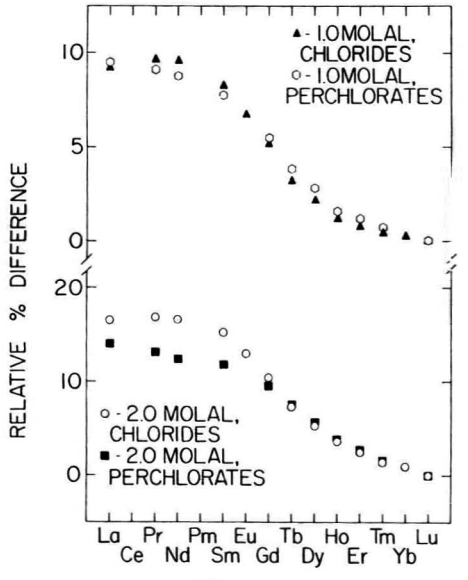

Figure 3. Relative per cent differences in equivalent conductances at constant molality for the rare earth perchlorates and chlorides.

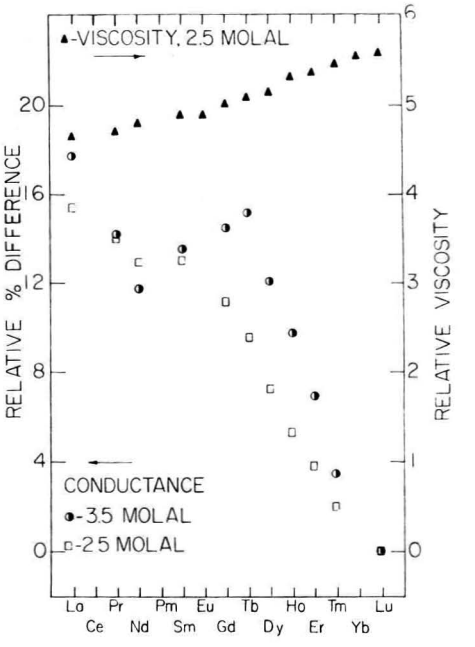

Figure 4. Relative per cent differences in equivalent conductances and relative viscosities at constant molality for the rare earth perchlorates.

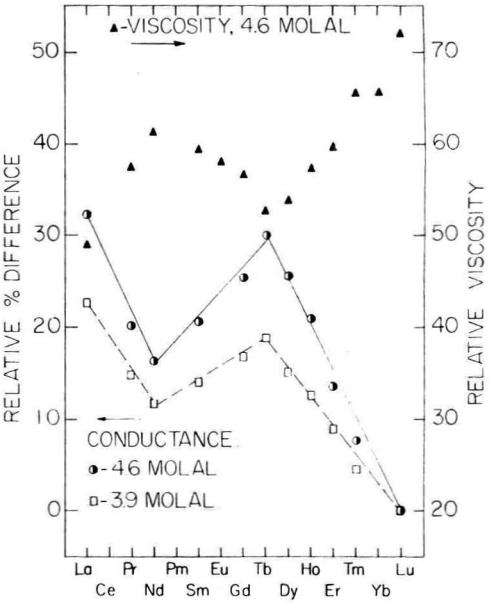

Figure 5. Relative per cent differences in equivalent conductances and relative viscosities at constant molality for the rare earth perchlorates.

smoothly to Lu. The viscosity data given in Figure 5 also reflect this trend.

Assume that by 3.0 *m* too little water remains in the rare earth perchlorate solutions to separately satisfy the inner-sphere hydration needs of all the ions. Then, by this concentration some inner-sphere water will be shared between the anions and cations and outer-sphere ion pairing will result. When the inner-sphere hydration shift occurs between Nd and Tb the water liberated from the inner hydration sphere should be less firmly bound. In the very concentrated solutions, where nearly all the water is bound to the inner spheres of one or more ions, the addition of a less firmly bound water to the system should allow these hydrated ions to slip past each other more readily, and will result in a viscosity decrease for the rare earth perchlorates following Nd. This will give rise to a gradual increase in the isomolal conductance for the rare earth perchlorates, which occur between Nd and Tb, relative to the lighter rare earths. The end result is a prominent two-series effect in the concentrated perchlorate solution electrical conductances. The assumption that the rare earth and perchlorate ions retain a layer of water between them is supported by X-ray diffraction data for a nearly saturated rare earth perchlorate solution.[17]

This two-series effect is quite distinct by 3.0 *m* for the perchlorates but does not appear by 3.5 *m* in the rare earth chlorides. It thus appears that water is bound more strongly in the perchlorate system than in the chloride at equal molalities. Although the generally made assumption is that the perchlorate ion interacts only weakly with water, some aspects of ir[25,36] and Raman[16] data have

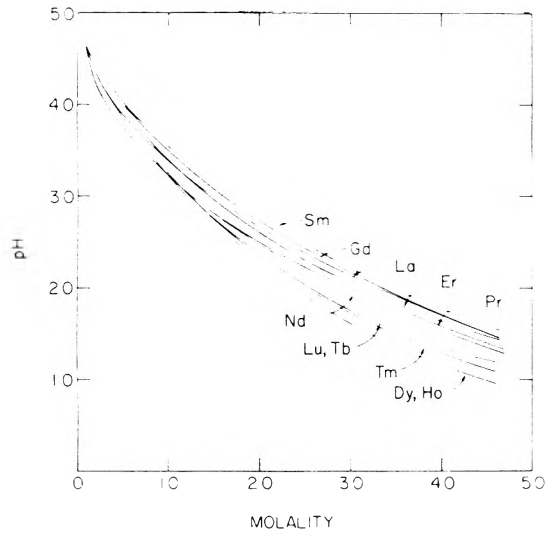

Figure 6. The pH's of the rare earth perchlorates as a function of the molality.

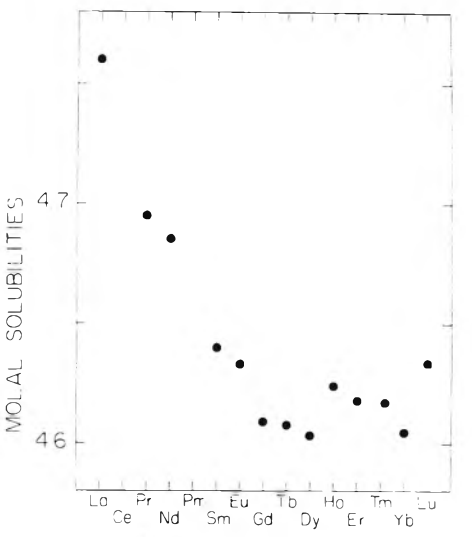

Figure 7. Solubilities of the aqueous rare earth perchlorates at 25°.

been explained in terms of perchlorate ion–water interaction. In addition, the activities of water in concentrated rare earth perchlorate[37] and uranyl perchlorate[38] solutions have been found to be considerably lower than for the corresponding chloride salt solutions. While some of this difference will result from the greater amount of complexation in the chloride solutions, more extensive perchlorate ion hydration can explain the rest.

The pH's of the rare earth perchlorate solutions are shown as a function of the molality in Figure 6. At the highest concentrations the pH's are reliable only to 0.15 unit due to drift.[39] The solutions studied contained stoichiometric rare earth perchlorates in conductance water. At equilibrium a number of ionic species are present in these solutions including various outer-sphere complexes and hydrolysis products. These hydrolyzed species are as much of a part of the solutions as the unhydrolyzed species and they cannot be eliminated from solutions of stoichiometric salts. Unless the pH is carefully controlled in the stock solutions, the resulting solutions will no longer be two-component systems. By measuring data on solutions of the stoichiometric salts, results are obtained which can be readily reproduced at other laboratories.

Since the pH's are fairly low in concentrated solutions the possibility must be considered that the two-series effect was caused by the conductance of the hydrogen ions. The pH can be defined as $-\log a_H$, where a_H is the molal ionic activity of the hydrogen ion in the solution of interest.[40] Individual ionic activities are not experimentally measurable and relating the pH to the actual molality of the hydrogen ion requires certain assumptions. The hydrogen ion contribution to conductance will be considered near saturation since the pH's are lowest there. The mean molal activity coefficients of several rare earth perchlorates have been measured and are 800 or larger at 4.6 m.[37] It is reasonable to assume that the activity coefficient of the hydrogen ion is in excess of unity in these solutions so a_H can be considered as a liberal upper limit for the hydrogen ion concentration. The pH's of the 4.6 m solutions are one or greater. Consider 1000 g of water with its 4.6 mol of rare earth perchlorate and its estimated upper limit of 0.1 mol of hydrogen ions. The hydrogen ion conductance in this solution can be estimated by Walden's rule

$$\Lambda \approx \Lambda^0(n_0/n) \tag{5}$$

where n/n_0 is the relative viscosity of the solution and Λ^0 is the limiting conductance of the hydrogen ion. The relative viscosity of the solution is about 60 and Λ^0 is 430 ohm^{-1} cm^2 equiv^{-1}.[41] The total conductance of the 0.1 mol of hydrogen ions in this solution will be (0.1)(430)(1/60) = 0.72 ohm^{-1} cm^2. Walden's rule frequently gives a low estimate for the conductance. Water sharing in highly viscous solutions should extensively disrupt the hydrogen ion conductance chain mechanism so the Walden's rule estimate could also be high. Even if some cancellation of errors occurs, the value of 0.72 ohm^{-1} cm^2 is still probably high. This same solution will contain 3(4.6) = 13.8 equiv of rare earth perchlorate with an experimental equivalent conductance of 3.5 ohm^{-1} cm^2 equiv^{-1}. The total conductance of the rare earth perchlorate, after subtracting the hydrogen ion value, will be (13.8)(3.5) − 0.7 = 47.6 ohm^{-1} cm^2. The hydrogen ion contribution to conductance is therefore 1.5% or less. There is a 32% change in conductance across the series at 4.6 m and a 15% change between Nd and Tb. It seems unlikely that the hydrogen ion conductance could be causing this much change especially since the hydrogen ion contribution to conductance will be shifting all of the curves in the same direction. Additional evidence for this is the fact that the pH does not follow the same regular sequence as the total equivalent conductances. The viscosities are even less dependent on the pH and they also exhibit the two-series behavior between the same concentrations. One may conclude that the two-series effect is real and not caused by hydrolysis.

An interesting finding of this research is that the inner-sphere two-series effect shows up in the conductance from 3.5 m to saturation between Nd and Tb. These are the same two rare earth ions between which the coordination change is believed to occur at infinite dilution.[5] This implies that no significant dehydration occurs with increasing concentration. Karraker[14] observed a change in the spectral behavior of Nd in the presence of a large excess of monovalent electrolyte. The large excess of anions present in his system could cause greater amounts of complexes to form than are present in solutions of the stoi-

chiometric salts. This may partially account for the observed spectral modification.

In Figure 7 the molalities of the saturated rare earth perchlorate solutions are shown and the numerical values of these concentrations can be found in Table IV. It should be noted that saturation occurs when approximately 12 waters remain for each rare earth perchlorate unit.

Acknowledgments. The authors would like to thank Mr. J. L. Derer and Dr. A. Habenschuss for assistance with the computer programming, and Mr. L. E. Shiers for preparing the conductivity water and for furnishing the density polynomial fits. Some of the saturated solution analyses were performed by Drs. J. L. Baker and J. P. Walters in the course of their own research. Thanks are due to Dr. J. E. Powell's group for preparing the rare earth oxides and to Mr. P. Palmer for providing the rare earth metals used as EDTA standards. The authors also thank Dr. A. Habenschuss for a critical reading of the manuscript.

Supplementary Material Available. Tables I and II, listings of the density coefficients and conductance data will appear following these pages in the microfilm edition of this volume of the journal. Photocopies of the supplementary material from this paper only or microfiche (105 × 148 mm, 24× reduction, negatives) containing all of the supplementary material for the papers in this issue may be obtained from the Journals Department, American Chemical Society, 1155 16th St., N.W., Washington, D. C. 20036. Remit check or money order for $4.00 for photocopy or $2.00 for microfiche, referring to code number JPC-74-1435.

References and Notes

(1) This paper is based, in part, on the Ph.D. Dissertation of J. A. Rard, Iowa State University, Ames, Iowa, Feb 1973.
(2) F. H. Spedding, P. E. Porter, and J. M. Wright, *J. Amer. Chem Soc.*, **74**, 2781 (1952).
(3) F. H. Spedding and G. Atkinson in "The Structure of Electrolytic Solutions," W. J. Hamer, Ed., Reinhold, New York, N. Y., 1959, Chapter 22.
(4) V. W. Saeger and F. H. Spedding, IS-338, unclassified AEC report, Ames Laboratory, Ames, Iowa, 1960.
(5) F. H. Spedding, M. J. Pikal, and B. O. Ayers, *J. Phys. Chem.*, **70**, 2440 (1966).
(6) F. H. Spedding and K. C. Jones, *J. Phys. Chem.*, **70**, 2450 (1966).
(7) J. P. Walters and F. H. Spedding, IS-1988, unclassified AEC report, Ames Laboratory, Ames, Iowa, 1968.
(8) F. H. Spedding, P. E. Porter, and J. M. Wright, *J. Amer. Chem. Soc.*, **74**, 2778 (1952).
(9) F. H. Spedding and S. Jaffe, *J. Amer. Chem. Soc.*, **76**, 884 (1954).
(10) F. H. Spedding and J. L. Dye, *J. Amer. Chem. Soc.*, **76**, 879 (1954).
(11) F. H. Spedding and M. J. Pikal, *J. Phys. Chem.*, **70**, 2430 (1966).
(12) W. B. Lewis, J. A. Jackson, J. F. Lemons, and H. Taube, *J. Chem. Phys.*, **36**, 694 (1962).
(13) L. O. Morgan, *J. Chem. Phys.*, **38**, 2788 (1963).
(14) D. G. Karraker, *Inorg. Chem.*, **7**, 473 (1968).
(15) K. Nakamura and K. Kawamura, *Bull. Chem. Soc. Jap.*, **44**, 330 (1971).
(16) L. Gutierrez, W. C. Mundy, and F. H. Spedding, *J. Chem. Phys.*, accepted for publication.
(17) F. H. Spedding and L. L. Martin, unpublished X-ray diffraction data.
(18) A. R. Olson and T. R. Simonson, *J. Chem. Phys.*, **17**, 1322 (1949).
(19) J. Sutton, *Nature (London)*, **169**, 71 (1952).
(20) L. J. Heidt and J. Berestecki, *J. Amer. Chem. Soc.*, **77**, 2049 (1955).
(21) L. H. Sutcliffe and J. R. Weber, *Trans. Faraday Soc.*, **52**, 2225 (1956).
(22) M. M. Jones, E. A. Jones, D. F. Harmor, and R. T. Semmes, *J. Amer. Chem. Soc.*, **83**, 2038 (1961).
(23) M. Alei, Jr., *Inorg. Chem.*, **3**, 44 (1964).
(24) Z. Libus and T. Sadowska, *J. Phys. Chem.*, **73**, 3229 (1969).
(25) G. Brink and M. Falk, *Can. J. Chem.*, **48**, 3019 (1970).
(26) F. H. Spedding, P. F. Cullen, and A. Habenschuss, *J. Phys. Chem.*, **78**, 1106 (1974).
(27) P. H. Dike, *Rev. Sci. Instrum.*, **2**, 379 (1931).
(28) G. Jones and G. M. Bollinger, *J. Amer. Chem. Soc.*, **53**, 411 (1931).
(29) G. Jones and D. Bollinger, *J. Amer. Chem. Soc.*, **57**, 280 (1935).
(30) G. Jones and M. J. Prendergast, *J. Amer. Chem. Soc.*, **59**, 731 (1937).
(31) F. H. Spedding, L. E. Shiers, M. A. Brown, J. L. Derer, D. L. Swanson, and A. Habenschuss, unpublished density data.
(32) See paragraph at end of paper regarding supplementary material.
(33) F. H. Spedding, J. A. Rard, and V. W. Saeger, *J. Chem. Eng. Data*, to be submitted for publication.
(34) F. H. Spedding, L. E. Shiers, and J. A. Rard, unpublished viscosity data.
(35) F. H. Spedding and H. O. Weber, unpublished activity data.
(36) P. Dryjanski and Z. Kecki, *Rocz. Chem.*, **43**, 1053 (1969); **44**, 1141 (1970).
(37) F. H. Spedding, J. A. Rard, H. O. Weber, and L. E. Shiers, unpublished activity data.
(38) R. A. Robinson and C. K. Lim, *J. Chem. Soc.*, 1840 (1951).
(39) W. H. Beck, J. Caudle, A. K. Covington, and W. F. K. Wynne-Jones, *Proc. Chem. Soc.*, (*London*), 110 (1963).
(40) R. G. Bates, "Determination of pH Theory and Practice," 2nd ed, Wiley, New York, N. Y., 1973.
(41) R. A. Robinson and R. H. Stokes, "Electrolyte Solutions," 2nd ed, revised, Butterworths, London, 1965.

COMMUNICATIONS TO THE EDITOR

Dielectric Response by Real Time Analysis of Time Domain Spectroscopy Data

Publication costs assisted by the Materials Science Program, Brown University, with support from the National Science Foundation.

Sir: Considerable interest has developed recently in use of time domain spectroscopy (TDS) for study of dielectric relaxation processes in the time range 10^{-7} to 10^{-11} sec. One observes reflected or transmitted signals as a function of time after incidence of a voltage pulse on a dielectric sample, but in most methods[1] the dielectric response function can be determined only by numerical Fourier analysis and other transformations. An exception is Fellner-Feldegg's thin sample method,[2] which yields the derivative of the response function directly, but as van Gemert[3] has shown is inaccurate unless the sample thickness and, as a result, the observed signal are very small. We present here some of the results of an analysis which is much less restricted and gives the response function without specific assumptions as to its form by simple numerical methods.

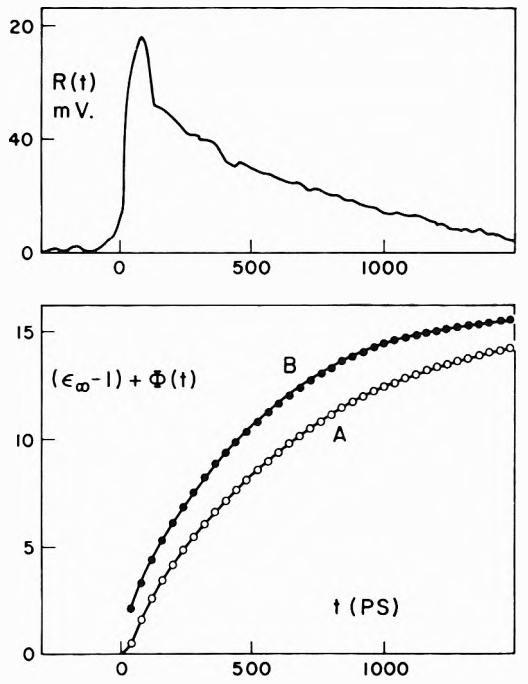

Figure 1. Upper graphic shows reflected voltage $R(t)$ from a 7.8-mm sample of 1-butanol at 22° for a 240-mV applied step voltage, using a Hewlett-Packard Type 181 TDR system with 40-psec rise time. Lower trace shows (A) dielectric response function calculated from thin sample formula (integral of eq 2) and (B) response function from finite sample formula (eq 3).

For a dielectric sample of thickness d placed in a coaxial line terminated in its characteristic impedance, solution of the propagation equations through terms of order d^2 relates the dielectric response function $\epsilon_\infty + \Psi(t)$ to the incident voltage pulse $V_0(t)$ and reflection $-R(t)$, $t > 0$, by

$$\frac{d}{dt}\int_0^t dt'[(\epsilon_\infty - 1)\delta(t - t') + \dot{\Psi}(t - t')][V_0(t') - R(t')] = \frac{2c}{d}R(t) + 2\frac{dR(t)}{dt} \quad (1)$$

where c is the speed of propagation in the empty, loss free line and $\delta(t)$ is the Dirac delta function for an instantaneous response $\epsilon_\infty - 1$.

If $R(t)$ is neglected in comparison to $V_0(t)$ and $dR(t)/dt$ compared to $cR(t)/d$, then for a step voltage $V_0(t) = V_0$, $t > 0$, one obtains Fellner-Feldegg's first-order result

$$(\epsilon_\infty - 1)\delta(t) + \dot{\Psi}(t) = \frac{2c}{d}\frac{R(t)}{V_0} \quad (2)$$

The observed response can only approximate the impulse $(\epsilon_\infty - 1)\delta(t)$ at short times because of the finite reflection time $2d\sqrt{\epsilon_\infty}/c$ in the sample, but more serious at longer times is the error from assuming that the sample voltage is $V_0(t)$ rather than $V_0(t) - R(t)$. For a considerable range of sample lengths and other parameters, this error can be satisfactorily corrected by using eq 2 as an approximation in the correction term of eq 1. For a step voltage, this gives on integration

$$(\epsilon_\infty - 1) + \Psi(t) = \frac{2c}{d}\int_0^t dt'\,\frac{R(t')}{V_0} + \frac{2c}{d}\int_0^t dt'\,\frac{R(t')}{V_0}\frac{R(t - t')}{V_0} + \frac{2R(t)}{V_0} \quad (3)$$

This result requires only simple numerical integration of $R(t)$ and its self convolution to obtain $\Psi(t)$, and has been found to work very well. As an example, the observed response for a 7.8-mm sample of 1-butanol at 22° is shown as the upper curve in Figure 1, and the two lower curves are the results for $(\epsilon_\infty - 1) + \Psi(t)$ from the thin sample formula and from the present analysis. Although both the latter are well fitted by Debye functions $\Psi(t) = (\epsilon_0 - \epsilon_\infty)[1 - \exp(-t/\tau)]$, the time constant τ from the uncorrected curve is 720 psec (1 psec = 10^{-12} sec), some 40% larger than values in the range 500–540 psec from transform analysis and steady-state results. The present analysis gives $\tau = 530$ psec in much better agreement.

This value is essentially the same as that given by an approximate formula derived by van Gemert *assuming* Debye relaxation; his formula can be obtained as a special case of eq 3. The static permittivity $\epsilon_0 = 17.2$ in the limit $t \to \infty$ and the high-frequency value $\epsilon_\infty = 3.2$ from analysis of short time response also agree well with other results.

The advantages of the present treatment are that the response function $\Psi(t)$ can be obtained with satisfactory accuracy for a considerable range of sample thickness and other parameters without specific assumptions about its form and without numerical Fourier transformations. The analysis has been generalized to take account of finite ohmic sample conductivity and finite rise times; similar methods have also been developed for a finite dielectric sample terminating a coaxial line. These will be presented in detail later.

Acknowledgments. This work was supported by the Brown University Materials Science Program and the National Science Foundation. I am indebted to T. G. Copeland for the computer program for numerical integrations, and to Dr. M. J. C. van Gemert for a copy of his paper[3] on analysis of the thin cell method in advance of publication.

References and Notes

(1) For a review and further references, see A. Suggett in "Dielectric and Related Molecular Processes," Vol. 1, Chemical Society, London, 1972, p 100.
(2) H. Fellner-Feldegg, *J. Phys. Chem.*, **76**, 2116 (1972).
(3) M. J. C. van Gemert, *J. Chem. Phys.*, submitted for publication.

Chemistry Department **Robert H. Cole**
Brown University
Providence, Rhode Island 02912

Received April 1, 1974

Comments on the Paper, "Flash Photolysis of Aromatic Sulfur Molecules," by F. C. Thyrion

Publication costs assisted by the American Cyanamid Company

Sir: In his above-mentioned paper,[1] Thyrion reports transient absorptions with maxima around 300 nm upon flash photolysis of aromatic thiols, disulfides, and sulfoxides in ethanol and cyclohexane solutions.

The author correctly assigns these transients to RS· radicals. He fails to mention, however, that similar results

have been reported in the pulse radiolysis[2] and the flash photolysis[3] of mercaptoethanol in aqueous solution at high pH. In the flash photolysis case, we have explicitly stated that we consider the 300-nm transient absorption as arising from the RS· radical. Our assignment has recently been verified by pulse radiolytic studies.[4]

Only the RS· transient which is rather insensitive toward oxygen is observed in nonpolar solvents such as cyclohexane. In polar solvents such as water the radical anion, $RSSR^-$, is observed as an additional transient. In the case of aliphatic thiols the absorption of the radical anion occurs around 420 mn, while for thiophenol the maximum is at 470 nm. The transient radical anions have a rather high extinction coefficient and are therefore readily observed, provided the solution is properly deoxygenated and the pH is adjusted to provide a sufficient concentration of RS^- anions.

Thyrion states in his paper: "The assignment of the absorption bands to a phenylsulfur radical is in contradiction with that postulated by Caspari and Granzow who observed a transient spectrum with maximum at ~420 nm identified as arising from the $RSSR^-$ radical anion upon photolyzing aqueous solutions of thiophenol." Since none of the transient spectra reported by Thyrion was obtained in aqueous solution, it is obviously not possible to compare the two studies. A minor flaw is the incorrect quotation of an absorption maximum for the thiophenol transient at 420 nm instead of 470 nm.

References and Notes

(1) F. C. Thyrion, *J. Phys. Chem.*, **77**, 1478 (1973).
(2) W. Karmann, A. Granzow, G. Meissner, and A. Henglein, *Int. J. Radiat. Phys. Chem.*, **1**, 395 (1969).
(3) G. Caspari and A. Granzow, *J. Phys. Chem.*, **74**, 836 (1970).
(4) M. Z. Hoffman and E. Hayon, *J. Phys. Chem.*, **77**, 990 (1973).

Chemical Research Division **Albrecht Granzow**
American Cyanamid Company
Bound Brook, New Jersey 08805

Received September 13, 1973

Reply to Comments on the Paper, "Flash Photolysis of Aromatic Sulfur Molecules," by A. Granzow

Sir: We thank Caspari and Granzow[1] for correcting the absorption maximum they observed in aqueous solutions of thiophenol at 470 nm and not at 420 nm as reported in our work.

We wish to make some further comments. (1) Thiophenol has been photolyzed in H_2O–EtOH (2:1) solutions at various pH's and in all cases the short and long wavelength bands were observed. The only difference observed in increasing the pH was an increase of the optical density. This can be explained by a higher absorption of flash light by the parent compound. (2) It was first thought that a radical ion produced the long wavelength band but this hypothesis was ruled out when considering the decay curves and the decrease of transient concentrations with an increase of parent compound concentrations. (3) The longer flash duration in the experiment of Caspari and Granzow may be responsible of the discrepancy between the results. (4) The comparison between flash photolysis and pulse radiolysis results can be made only with great care since the primary processes are likely different.

References and Notes

(1) G. Caspari and A. Granzow, *J. Phys. Chem.*, **74**, 836 (1970).

Laboratoire de cinétique chimique **F. C. Thyrion**
B-1348 Louvain-La-Neuve, Belgium

Received March 19, 1974

On the Use of the van't Hoff Relation in Determinations of the Enthalpy of Micelle Formation[1]

Publication costs assisted by the National Institutes of Health

Sir: There is considerable interest today in hydrophobic bonds. Since the outstanding thermodynamic characteristic of such bonds is the sizable temperature dependence of the enthalpy change that accompanies their formation, interest has grown in the determination of this enthalpy. One possible route to this goal is through study of detergent micelles.

Unfortunately, although a quite general thermodynamic analysis of micellar solutions has been made,[2,3] implementation of the equations is not possible because they involve various quantities that are unmeasurable at the present time. There is a particular property of micellar solutions, the critical micelle concentration (cmc), that *can* be very readily and precisely measured. Consequently, there is a need for methods of interpretation of that quantity in terms of the thermodynamic properties of the micellar solution.

Various viewpoints are available that make such an interpretation possible,[4] includingone described earlier by us[5-7] that comes under the rubric of "quasistatistical mechanical" methods.[2] In that method, attention is focused upon the reaction

$$A_1 + A_{\hat{N}} = A_{\hat{N}+1} \qquad (1)$$

wherein A_1 is a detergent monomer and $A_{\hat{N}}$ is a micelle containing $\hat{N}$ monomers, $\hat{N}$ being the number of detergent monomers in the micelle of size most probable at the concentration, temperature, and pressure of the cmc measurement; and it is shown that the standard free-energy change (infinitely dilute reference state) of reaction 1 may be estimated by

$$\Delta\bar{G}_{\hat{N}}^{\infty} = RT \ln (\text{cmc}) \qquad (2)$$

Experimental determination of the temperature dependence of the cmc is customarily then interpreted in the usual way, *i.e.*, through the van't Hoff relation, to provide the standard enthalpy of reaction 1.[8] However, since the more general thermodynamic analyses show that macroscopic, operational van't Hoff relations fail in this system if the micelle number is temperature dependent,[3] the question arises whether the quasistatistical mechanical method under scrutiny is consistent with that result. We are thus driven to analyze closely the temperature dependence of $\Delta\bar{G}_{\hat{N}}^{\infty}$. In the following, we demonstrate that the two approaches are consistent and therefore that such use of the van't Hoff relation is in principle incorrect. We also show that in practice numerical values of enthalpies so obtained may be very wrong.

Consider a micelle containing $\hat{N}$ monomers. In the ab-

sence of external fields, its change in standard (infinitely dilute reference state) partial molal Gibbs free energy is described by

$$d\bar{G}_{\hat{N}}^{\infty} = \bar{V}_{\hat{N}}^{\infty}\,dP - \bar{S}_{\hat{N}}^{\infty}\,dT + \left(\frac{\partial \bar{G}_{\hat{N}}^{\infty}}{\partial \hat{N}}\right)_{T,P} d\hat{N} \quad (3)$$

wherein the last term accounts for possible gain or loss of monomers, since the most probable micelle may change with temperature. A similar relation holds for the micelle containing $\hat{N} + 1$ monomers, while for monomer itself

$$d\bar{G}_1^{\infty} = \bar{V}_1^{\infty}\,dP - \bar{S}_1^{\infty}\,dT_1 \quad (4)$$

For reaction 1, then

$$d(\Delta\bar{G}_{\hat{N}}^{\infty}) = \Delta\bar{V}_{\hat{N}}^{\infty}\,dP - \Delta\bar{S}_{\hat{N}}^{\infty}\,dT + \left[\frac{\partial(\bar{G}_{\hat{N}+1}^{\infty} - \bar{G}_{\hat{N}}^{\infty})}{\partial \hat{N}}\right]_{T,P} d\hat{N} \quad (5)$$

from which we see that the temperature coefficient of $\Delta\bar{G}_{\hat{N}}^{\infty}$ is

$$\left(\frac{\partial \Delta\bar{G}_{\hat{N}}^{\infty}}{\partial T}\right)_P = -\Delta\bar{S}_{\hat{N}}^{\infty} + \left[\frac{\partial(\bar{G}_{\hat{N}+1}^{\infty} - \bar{G}_{\hat{N}}^{\infty})}{\partial \hat{N}}\right]_{T,P}\left(\frac{\partial \hat{N}}{\partial T}\right)_P \quad (6)$$

Substituting $-\Delta\bar{S}_{\hat{N}}^{\infty} = (\Delta\bar{G}_{\hat{N}}^{\infty} - \Delta\bar{H}_{\hat{N}}^{\infty})/T$ and eq 2 into eq 6 we find

$$RT^2\left[\frac{\partial \ln (\mathrm{cmc})}{\partial T}\right]_P = -\Delta\bar{H}_{\hat{N}}^{\infty} + T\left[\frac{\partial(\bar{G}_{\hat{N}+1}^{\infty} - \bar{G}_{\hat{N}}^{\infty})}{\partial \hat{N}}\right]_{T,P}\left(\frac{\partial \hat{N}}{\partial T}\right)_P \quad (7)$$

The left-hand side of eq 7 is the experimental quantity, and, as eq 7 shows, gives $\Delta\bar{H}_{\hat{N}}^{\infty}$ by a van't Hoff relation only if $(\partial\hat{N}/\partial T)_p$ is zero, *i.e.*, only if the most probable micelle number is independent of temperature. In general, we do not expect this to be the case, so the temperature coefficient of the cmc cannot be used to obtain heats of micelle formation.

The physical reason why the van't Hoff relation fails here is perfectly plain. If we measure a cmc at two different temperatures, and use eq 2 to calculate the two free-energy changes, those free-energy changes refer to two different chemical reactions, $A_1 + A_{\hat{N}(T_1)}$ *fr*= $A_{\hat{N}(T_1)+1}$ in one case, and $A_1 + A_{\hat{N}(T_2)} = A_{\hat{N}(T_2)+1}$ in the other. These two reactions are only the same if $\hat{N}$ is temperature independent.

The question remaining is whether the last term of eq 7 is numerically very significant. Sufficient information does not exist to decide the question unequivocally, but we can make the following rough computation as an enlightening estimate.

Although no good theoretical expression exists for the *total* standard Gibbs free-energy change of reaction eq 1, the *electrical part* of the standard free-energy change for an ionic micelle in the absence of added salt is[4]

$$\Delta\bar{G}_{\hat{N}}^{\infty} = N_A \hat{N} e^2/\epsilon b \quad (8)$$

wherein N_A is Avogadro's number, e the protonic charge, ϵ the solvent dielectric constant, and b the micellar radius. Assuming constant radius, the last term of eq 7 thus becomes, in magnitude $(N_A T e^2/\epsilon b)(\partial\hat{N}/\partial T)_p$. Using $T \simeq 300°K$, $e = 4.8 \times 10^{-10}$ esu, $\epsilon \simeq 80$, $b \simeq 2$ nm, and converting to calories, we find for this term $(6.3 \times 10^4)(\partial\hat{N}/\partial T)_p$. The only relevant measurements we have been able to find of the temperature dependence of micelle number are those of Debye,[9] which give a magnitude of ~0.4 for $(\partial\hat{N}/\partial T)_p$. Thus, the magnitude of the electrical part of the last term of eq 7 is $\sim 2.5 \times 10^4$ cal. For ionic micelles, experiments show that the left-hand side of eq 7 is nearly zero at room temperature, so that $\Delta\bar{H}_{\hat{N}}^{\infty}$ as determined from the van't Hoff relation (*i.e.*, by neglecting the last term of eq 7) may be grossly in error even if the total free energy is only a few per cent of the electrical part.

It is unfortunately not really possible to take the offending term into account since the result is so sensitive to its value and experimental errors in measuring $\hat{N}$ are such that a value of 0.4 for $(\partial\hat{N}/\partial T)_p$ is barely distinguishable from zero over the accessible temperature range. It would seem that the only valid way of assessing micellar enthalpies lies in the use of calorimetry.

References and Notes

(1) This investigation was supported by Research Grant No. GM-20064 from the Division of General Medical Sciences, U.S. Public Health Service.
(2) T. Hill, "Thermodynamics of Small Systems," Vol. 2, W. A. Benjamin, New York, N.Y., 1964.
(3) D. Hall and B. Pethica in "Nonionic Surfactants," M. Schick, Ed., Marcel Dekker, New York, N.Y., 1967.
(4) E. Anacker in "Cationic Surfactants," E. Jungermann, Ed., Marcel Dekker, New York, N.Y., 1970.
(5) M. Emerson and A. Holtzer, *J. Phys. Chem.*, **69**, 3718 (1965).
(6) M. Emerson and A. Holtzer, *J. Phys. Chem.*, **71**, 1898 (1967).
(7) M. Emerson and A. Holtzer, *J. Phys. Chem.*, **71**, 3320 (1967).
(8) Numerous references by a variety of authors could be given here as the procedure is commonplace, but we prefer to point an accusing finger only at ourselves: see ref 7, then, as a typical example.
(9) P. Debye, *Ann. N. Y. Acad. Sci.*, **51**, 575 (1949).

Department of Chemistry
Washington University
St. Louis, Missouri 63130

Alfred Holtzer*
Marilyn F. Holtzer

Received March 8, 1974

Hydrogen Bonding of Phenol in Carbon Tetrachloride. The Use of Activity Data to Evaluate Association Models

Publication costs assisted by the National Science Foundation

Sir: In spite of numerous studies which have been made of the self-association of phenol, there is still considerable disagreement regarding the nature of molecular aggregates of phenol which exist in organic solvents.[1,2] In the case of the volatile aliphatic alcohols methanol and *tert*-butyl alcohol, a combination of infrared and nmr spectral data and vapor pressure results provides evidence that trimers and larger polymers are present in solutions in CCl_4 and hydrocarbon solvents, even at concentrations well below unit molarity.[3,4] On the other hand, recent measurements of the physical properties of solutions of phenol in CCl_4 and cyclohexane at concentrations up to or exceeding 1 *M* have been interpreted in terms of association models limited to dimerization and/or trimerization.[1,5-8] In the present communication we provide thermodynamic evidence which can be used to discriminate among various classes of association models purported to represent the state of phenol aggregation in organic solvents.

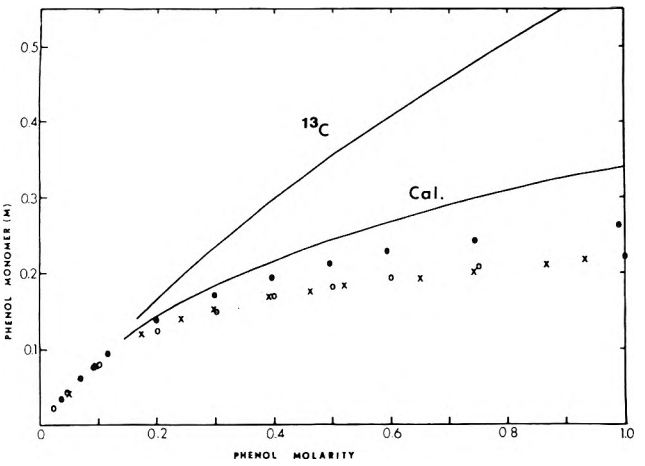

Figure 1. Phenol monomer concentration as a function of total phenol concentration: ^{13}C curve calculated by using $K_2 = 0.57$ M^{-1} at 27° (0.901 m^{-1} from Table III, ref 5); Cal. curve calculated by using $K_3 = 5.6$ M^{-2} at 25° from calorimetric data of ref 1; ● phenol monomer concentration at 29.1° from absorbance data of ref 2; × phenol monomer inferred from activity data (this work) using limiting relationship $C_M(\text{phenol}) = a(\text{phenol})/2.87$; O phenol monomer concentration at 20.7° from absorbance data of ref 2.

TABLE I: Activity of Phenol in CCl_4 at Several Concentrations at 21.0°

C^a	a^b	C	a
1.080	0.637	0.390	0.482
0.934	0.626	0.297	0.435
0.867	0.602	0.240	0.403
0.743	0.578	0.173	0.343
0.650	0.552	0.095	0.227
0.520	0.525	0.050	0.121
0.462	0.506		

[a] Molar concentration of phenol in CCl_4. [b] Ratio of vapor concentration of phenol above phenol–CCl_4 solutions (determined spectrally in the vicinity of 270[4] nm) to vapor concentration above solid phenol at 21.0°.

Vapor pressure methods have been shown to be uniquely powerful in evaluating alternative models for the association of alcohols.[3,4] Unfortunately, phenol is not volatile enough to permit use of conventional vapor pressure methods in this connection. However, the large absorption of phenol vapor in the ultraviolet region makes it possible to determine activities of phenol from absorbance measurements on phenol vapor above organic solutions of the compound; reliable results can be obtained even at partial pressures of phenol on the order of 100 μ or less. Some initial results are reported here for solutions of phenol in CCl_4. Table I lists values of phenol activity (expressed as a ratio of the partial pressure of phenol to the vapor pressure of pure solid phenol) in CCl_4 solutions at 21.0°.

Values of phenol monomer concentration derived from our measurements[9] are plotted in Figure 1 along with the concentration of phenol monomer inferred from several types of data for phenol–CCl_4 solutions in the temperature range 20–29°. The present activity results are in excellent agreement with the near-infrared results of Whetsel and Lady.[2] Both our results and those of Whetsel and Lady are also in reasonable agreement with values derived from partition-water solubility data[10] and with phenol activities derived from total vapor pressure measurements on phenol–CCl_4 solutions by use of the Gibbs–Duhem equation.[11] However, our results cannot be reconciled with either the interpretation of Nakashima, *et al.*,[5] of ^{13}C nmr measurements on phenol–CCl_4 solutions or with the 1-3 interpretation of calorimetric measurements[1] at phenol concentrations exceeding about 0.15 *M*. Both the 1-2 and 1-3 interpretations of these latter sets of data lead to calculated phenol monomer concentrations which increase much too rapidly with total phenol concentration to be consistent with activity measurements. We also note that the numerous pmr studies using models which limit phenol association only to trimer (*e.g.*, ref 7 and 8) would produce curves similar to that for the calorimetric curve in Figure 1.

In view of the relation between thermodynamic activity values and the concentration of phenol monomer in solution it is essential that any association model for phenol solutions be consistent with reliable activity results. This restriction arises from the basic assumption (made in all spectral and classical studies of phenol association) that Henry's law is obeyed by each of the individual phenol species. Under this assumption, values of the concentration of phenol monomer obtained from various association models should vary linearly with the thermodynamic activity. Relatively few types of physical measurements used to date on hydrogen-bonding systems can provide a directly observable quantity related to the activity of the monomeric species. Two methods which have been used are measurements of absorbance at the monomer hydroxyl stretching frequency[12] and vapor pressure measurements on alcohol–hexadecane solutions.[3,4] The results of our work provide a direct measurement of phenol activity in anhydrous phenol–CCl_4 solutions in the concentration range 0 → 1.0 *M*. At phenol pressures not exceeding about 300 μ it is highly improbable that significant quantities of associated phenol are present in the vapor and thus we expect the concentration of phenol vapor over phenol–CCl_4 solutions to be directly proportional to the monomer concentration of dissolved phenol.

All association models which have been used to describe phenol polymerization must be reducible, directly or indirectly, to monomer *vs.* total concentration curves. It is obvious that a common curve (at fixed temperature and solvent) should be obtained from reliable physical data of all types if a realistic model has been applied to fit the data. The marked discrepancies among the curves in Figure 1 clearly indicate that not all of the interpretations represented are meaningful. The directness of our measurements and the close agreement of our data with those of Whetsel and Lady[2] lead us to conclude that the concentrations of phenol monomer derived from our measurements and those of Whetsel and Lady are upper limiting values.

Phenol association models which are limited to dimerization[5] and/or trimerization[1,7,8] can be rejected as being physically unrealistic. More generally, we think that no single associated species model (*e.g.*, monomer–trimer or monomer–tetramer) is useful except in quite restricted ranges of phenol concentration. A careful numerical analysis of the infrared data of Whetsel and Lady and consideration of our activity results convinces us that no model yet proposed for representing the association of phenol in CCl_4 is as satisfactory as the monomer–trimer–sequential polymer model discussed previously.[4,14]

Acknowledgment. We wish to express our appreciation for support of this work by the National Science Foundation through Grants No. GP-33519X and GP-43307.

References and Notes

(1) E. M. Woolley, J. G. Travers, B. P. Erno, and L. G. Hepler, *J. Phys. Chem.*, **75**, 3591 (1971).
(2) K. B. Whetsel and J. H. Lady, "Spectrometry of Fuels," Plenum Press, New York, N. Y., 1970, pp 259–279.
(3) E. E. Tucker, S. B. Farnham, and S. D. Christian, *J. Phys. Chem.*, **73**, 3820 (1969).
(4) E. E. Tucker and E. D. Becker, *J. Phys. Chem.*, **77**, 1783 (1973).
(5) T. T. Nakashima, D. D. Traficante, and G. E. Maciel, *J. Phys. Chem.*, **78**, 124 (1974).
(6) E. M. Woolley and L. G. Hepler, *J. Phys. Chem.*, **76**, 3059 (1972).
(7) A. J. Dale and T. Gramstad, *Spectrochim. Acta, Sect. A*, **28**, 639 (1972).
(8) Y. S. Bogachev, L. K. Vasianan, N. N. Shapetko, and T. L. Alexeeva, *Org. Magn. Resonance*, **4**, 453 (1972).
(9) Monomer concentrations were derived from our activities from the slope of a plot of activity *vs.* monomer concentration from Whetsel and Lady's data at 20.7°. The reason for this procedure is that we have few low concentration data and thus considerable error would be involved in determining the intercept of a plot of activity concentration *vs.* phenol concentration. Plots of our activity *vs.* monomer concentrations derived from ^{13}C and calorimetric measurements are markedly nonlinear.
(10) J. R. Johnson, S. D. Christian, and H. E. Affsprung, *J. Chem. Soc.*, 1 (1965). J. R. Johnson, Ph.D. Dissertation, University of Oklahoma, 1966.
(11) J. Chevalley, *Bull. Soc. Chim. Fr.*, 510 (1961).
(12) It is probable, as has been suggested,[13] that there is at least a small degree of overlap at the monomer frequency from end hydroxyl groups of a polymer(s). Consequently, infrared results might be expected to lead to values of monomer concentration which are somewhat too large, particularly at the higher phenol concentrations.[2] In any case, monomer concentrations derived from infrared data on phenol solutions should represent upper limiting values; other spectral and thermodynamic results should be expected to yield monomer concentrations no larger than these.
(13) F. A. Smith and E. C. Creitz, *J. Res. Nat. Bur. Stand.*, **46**, 145 (1951).
(14) E. E. Tucker and E. Lippert, "High Resolution NMR Studies of Hydrogen Bonding," in Recent Advances in Hydrogen Bonding, P. Schuster, G. Zundel and C. Sandorfy, Ed., North-Holland Publishing Co., Amsterdam, in press.

Department of Chemistry
Oklahoma University
Norman, Oklahoma 73069

Edwin E. Tucker*
Sherril D. Christian
Lung-Nan Lin

Received March 11, 1974

Comments on the Paper, "A Study of the Formation of Negative Ions in Nitric Oxide and the Interaction of NO with H^- and O^- from Water," by S. K. Gupta and C. E. Melton

Publication costs assisted by the U. S. Department of Commerce National Oceanic and Atmospheric Administration

Sir: We wish to point out that a recent paper by Gupta and Melton[1] contains very serious errors concerning the negative ion NO^- and its chemistry. The first point concerns the reaction (with the original equation numbering)

$$H^- + NO \longrightarrow NO^- + H \qquad (7)$$

which Gupta and Melton find to have the extremely large rate constant 4×10^{-9} cm^3 molecule^{-1} sec^{-1} and which they therefore assume to be exothermic, from which they deduce that the electron affinity of NO exceeds that of atomic hydrogen which is 0.75 eV. The electron affinity of NO is now very well established by several methods to be less than 0.1 eV. The most precise determination is that of Siegel, *et al.*,[2] in which a value EA(NO) = 0.024 + 0.010 or −0.005 eV was determined by photodetachment electron spectroscopy. McFarland, *et al.*,[3] studied the collisional detachment of NO^- in eight gases in a temperature variable flowing afterglow system. The detachment rate in CO established that EA(NO) < 0.046 eV and for each of the eight gases it was established that EA(NO) < 0.11 eV. Parkes and Sugden,[4] using a drift tube, measured both the attachment rate in NO

$$e + 2NO \longrightarrow NO^- + NO \qquad (6)$$

and its' reverse and from detailed balancing they deduce EA(NO) = 0.028 eV, in agreement with the Siegel, *et al.*, value. The detachment rate constant of Parkes and Sugden agreed closely with that of McFarland, *et al.*, using a completely different experimental technique. Additionally, using endothermic reaction thresholds, Hughes, *et al.*,[5] have recently shown that EA(NO) < 0.1 eV. Berkowitz, *et al.*,[6] that EA(NO) < 0.5 eV, and Lecmann and Herschbach[7] that EA(NO) ~ 0. It has been known for some time from the demonstrated exothermicity of the charge-transfer reaction

$$NO^- + O_2 \longrightarrow O_2^- + NO \qquad (1)$$

that EA(NO) < EA(O_2) = 0.46 eV.[8] The few earlier experiments which gave large NO electron affinities have now been fully discredited. Thus there is no doubt that reaction 7 is in fact very endothermic and cannot occur at thermal energies. Moreover, the reaction of H^- with NO has been studied directly and found not to charge transfer but rather to associatively detach

$$H^- + NO \longrightarrow HNO + e + 1.4 \text{ eV} \qquad (2)$$

with a rate constant $k_2 = 4.6 \times 10^{-10}$ cm^3/sec.[9] The concluding statement in ref 1 that "NO reacts with H^- to produce H atoms and is thus a source of free radicals" is therefore erroneous and should not be propagated in radiation chemistry.

The second point we make concerns the manner of formation of NO^-. Gupta and Melton propose the termolecular collision (6). Although not noted by them this rate constant has been measured by a number of workers (as discussed in ref 3), the most reliable measurement being that of Parkes and Sugden[4] who obtained a value $k_6 = 8 \pm 2 \times 10^{-31}$ cm^6/sec at 300°K. Very little NO^- could have been made this way in the 360°K ion source of Gupta and Melton because of the rapid collisional detachment of NO^- by NO. The maximum possible NO^- production by attachment would be the equilibrium value

$$[NO^-] = K[NO][e] \qquad (3)$$

At 360°K, the equilibrium constant is 7.7×10^{-20} cm^3 and at 10^{-2} Torr NO pressure that maximum NO^- density would be 2.6×10^{-5}[e] where [e] refers to themal electrons. Presumably the energetic beam electrons would undergo three-body attachment to a much less extent.

It seems likely that the NO^- is produced in the well-known reaction

$$O^- + N_2O \longrightarrow NO^- + NO \qquad (5)$$

which has a rate constant of 2.5×10^{-10} cm^3/sec at 300°K.[10] Gupta and Melton's statement that they had purified the NO to impurity levels no greater than a few ppm is not convincing. Our experience is that the N_2O cannot be removed from NO to this extent by the distillation described and that substantially improved purification techniques only remove N_2O to about the part per thousand level.[11] We are aware that others have experienced the same difficulty.

The third point we raise concerns Gupta and Melton's reaction

$$O^- + 2NO \longrightarrow NO + NO_2^- \qquad (4)$$

for which they deduce $k_4 = 7.6 \times 10^{-27}$ cm^6/sec. This is

an unreasonably large rate constant on its face but in any case it is known that (4) cannot occur because O^- rapidly reacts with NO in a binary reaction,[8,12]

$$O^- + NO \longrightarrow NO_2 + e \quad (8)$$

with $k_8 = 2 \times 10^{-10}$ cm^3/sec. If there is a sufficient NO_2 impurity in the NO then several fast processes are known to occur

$$NO^- + NO_2 \longrightarrow NO_2^- + NO \quad (9)$$

$k_9 = 7.4 \times 10^{-10}$ cm^3/sec^3

$$e + NO_2 \xrightarrow{M} NO_2^- \quad (10)$$

$k_{10} \sim 4 \times 10^{-11}$ cm^3/sec,[13] and

$$O^- + NO_2 \longrightarrow NO_2^- + O \quad (11)$$

with $k_{11} = 1.6 \times 10^{-9}$ cm^3/sec.[11] However, NO_2 is relatively easy to remove from NO and NO_2^- production has been observed previously to arise from NO^- in NO by several groups and the mechanism for this has not yet been satisfactorily explained.[3]

References and Notes

(1) S. K. Gupta and C. E. Melton, *J. Phys. Chem.*, **77**, 2594 (1973).
(2) M. W. Siegel, R. J. Celotta, J. L. Hall, J. Levine, and R. A. Bennett, *Phys. Rev. A*, **6**, 607 (1972).
(3) M. McFarland, D. B. Dunkin, F. C. Fehsenfeld, A. L. Schmeltekopf, and E. E. Ferguson, *J. Chem. Phys.*, **56**, 2358 (1972).
(4) D. A. Parkes and T. M. Sugden, *J. Chem. Soc., Faraday Trans. 2*, **68**, 600 (1972).
(5) B. M. Hughes, C. Lifshitz, and T. O. Tiernan, *J. Chem. Phys.*, **59**, 3162 (1973).
(6) J. Berkowitz, W. A. Chupka, and D. Gutman, *J. Chem. Phys.*, **55**, 2733 (1971).
(7) K. Lacmann and D. R. Herschbach, *Chem. Phys. Lett.*, **6**, 106 (1970).
(8) F. C. Fehsenfeld, E. E. Ferguson, and A. L. Schmeltekopf, *J. Chem. Phys.*, **45**, 1844 (1966).
(9) D. B. Dunkin, F. C. Fehsenfeld, and E. E. Ferguson, *J. Chem. Phys.*, **53**, 987 (1970).
(10) R. Marx, G. Mauclaire, F. C. Fehsenfeld, D. B. Dunkin, and E. E. Ferguson, *J. Chem. Phys.*, **58**, 3267 (1973).
(11) D. B. Dunkin, M. McFarland, F. C. Fehsenfeld, and E. E. Ferguson, *J. Geophys. Res.*, **76**, 3820 (1971).
(12) J. L. Moruzzi, J. W. Ekin, and A. V. Phelps, *J. Chem. Phys.*, **48**, 3070 (1968).
(13) B. H. Mahan and I. C. Walker, *J. Chem. Phys.*, **47**, 3780 (1967).

Aeronomy Laboratory — **E. E. Ferguson***
NOAA Environmental Research Laboratories — **F. C. Fehsenfeld**
Boulder, Colorado 80302 — **Carleton J. Howard**

Received November 12, 1973

Reply to Comments of E. E. Ferguson, F. C. Fehsenfeld, and C. J. Howard on the Paper, "A Study of the Formation of Negative Ions in Nitric Oxide and the Interaction of NO with H^- and O^- from Water," by S. K. Gupta and C. E. Melton[1]

Publication costs assisted by the University of Georgia

Sir: Perhaps the most interesting aspect of science is the fact that physical and chemical reactions are under no obligation to occur in accord with the preconceived ideas of scientists. This principle is illustrated by the nitric oxide water system and the comments of Ferguson, *et al.* These investigators state that the negative ion charge transfer reaction

$$H^- + NO \longrightarrow H + NO^- \quad (1)$$

does not occur in the H_2O–NO system. We find by direct experimental observation that NO^- is indeed formed in the system by a charge transfer reaction.[2] In our experiments, a marked increase in the abundance of NO^- was observed when NO was added to a pure H_2O system and irradiated with low-energy electrons. The ionization efficiency curve for NO^- was found to be identical with that for H^- from H_2O. Furthermore, the abundance of NO^- was observed to decrease with increasing repeller field, consistent with the behavior of an ion produced by an ion–molecule reaction. Thus, we concluded that NO^- was formed by a charge transfer reaction of H^- with NO. It should be pointed out, however, that the thermodynamic analysis used by Ferguson, *et al.*,[2] to void our experimental data does not apply to the H_2O–NO system. This is true because H^- formed from H_2O may have a maximum kinetic energy of 2 eV.[3] Furthermore, our conclusions about the value of the electron affinity of NO is invalid for the same reason. Ferguson, *et al.*, claim that H^- reacts with NO according to the scheme

$$H^- + NO \longrightarrow HNO + e^- + 1.4 \text{ eV} \quad (2)$$

Even if H^- and NO react by this mechanism, the charge transfer reaction between H^- and NO would not be precluded because the reactions represent two independent processes.

Concerning the production of extremely small concentration of NO^- in pure NO, our results support production by the termolecular reaction

$$e^- + 2NO \longrightarrow NO + NO^- \quad (3)$$

We cannot accept the explanation of Ferguson, *et al.*, that NO^- is formed by the reaction

$$O^- + N_2O \longrightarrow NO^- + NO \quad (4)$$

if this were true, the ionization efficiency curve for NO^- would be identical with that for O^-/NO (Figure 1, ref 1). In sharp contrast, we found the small amount of NO^- formed in pure NO to be independent of the electron energy in support of reaction 3.

Finally, in the case of NO_2^- formation in pure NO at high pressures ($\sim 10^{-2}$ Torr), we state again that the occurrence of the reaction

$$O^- + 2NO \longrightarrow NO + NO_2^- \quad (5)$$

was established by standard experimental techniques. Here again, Ferguson, *et al.*, dismiss the above reaction in favor of the associative detachment reaction

$$O^- + NO \longrightarrow NO_2 + e^- \quad (6)$$

with a rate constant $k_3 = 2 \times 10^{-10}$ cm^3/sec. However, they failed to note that the reaction 6 was studied at thermal energies. Under the conditions existing in our experiments where, in addition to the initial kinetic energy acquired by O^- ion the DA process from H_2O, 2 eV addition kinetic energy was applied to the ion by the ion repeller electrode, an associative detachment reaction at the relatively high energy of our experiments is unlikely to occur.

References and Notes

(1) Supported by the U. S. Atomic Energy Commission under Contract No. AT-(38-1) 640 with the University of Georgia.

(2) S. K. Gupta and C. E. Melton, *J. Phys. Chem.*, **77**, 2594 (1973).
(3) C. E. Melton, *J. Chem. Phys.*, **57**, 4218 (1972).

Department of Chemistry — **Satish K. Gupta**
University of Georgia — **Charles E. Melton***
Athens, Georgia 30602

Received January 10, 1974

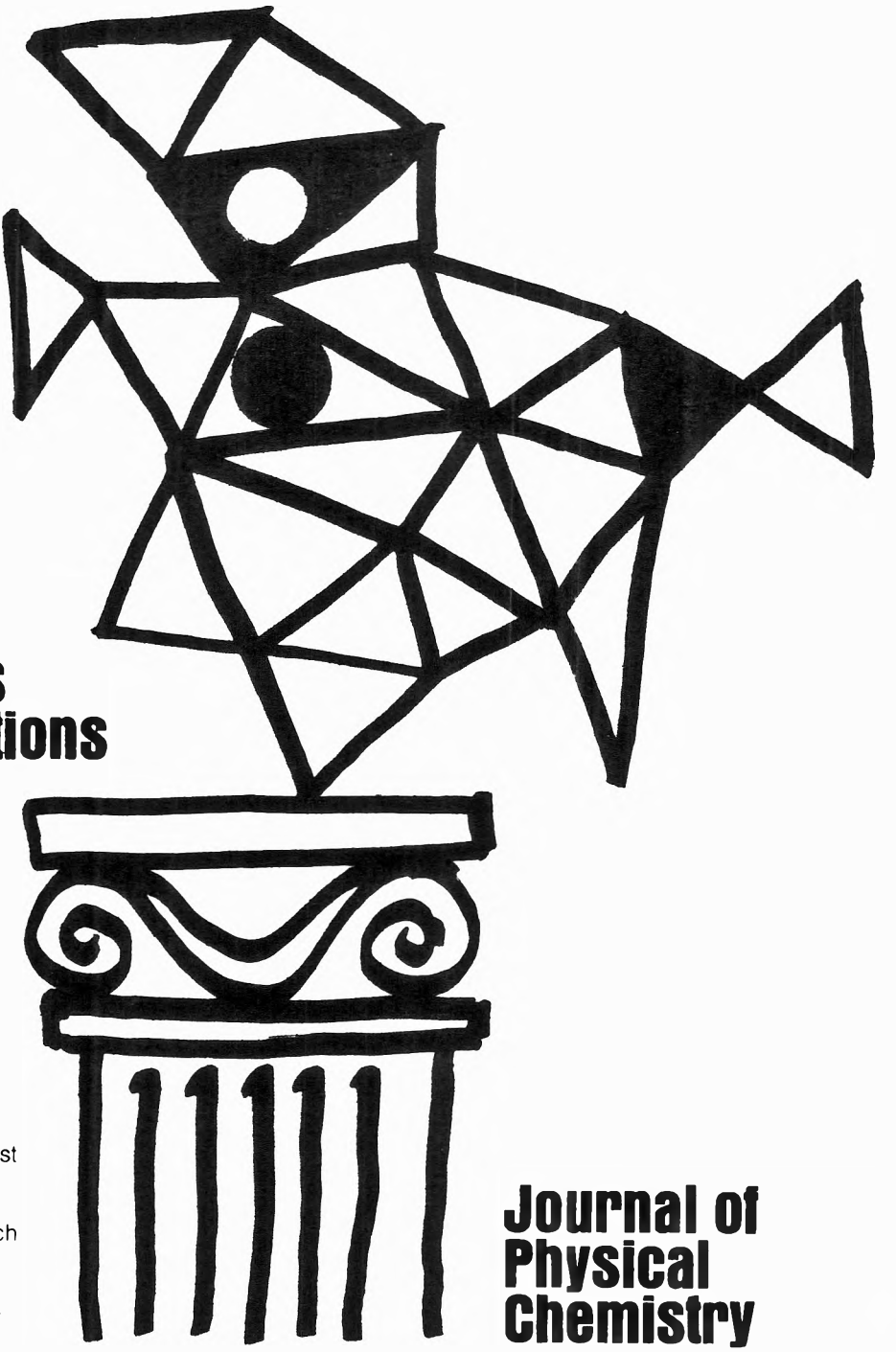

New concepts new techniques new interpretations

. . . together with valuable reports on classical areas

They are all waiting for you between the covers of our well-balanced JOURNAL OF PHYSICAL CHEMISTRY. Whatever your particular interest in physical chemistry, you'll find the JOURNAL's broad range of experimental and theoretical research reports are relevant and beneficial to your work. Each biweekly issue brings you an average of 30 authoritative, comprehensive reports on fundamental aspects of atomic and molecular phenomena, as well as timely notes, communications and reports plus the proceedings of selected symposia.

Join your fellow physical chemists who rely on JPC as an excellent biweekly source of data in both new and classical areas. Just complete and return the form to start your own subscription.

. . . *another ACS service*

Journal of Physical Chemistry

The Journal of Physical Chemistry
American Chemical Society
1155 Sixteenth Street, N.W.
Washington, D.C. 20036

1974

Yes, I would like to receive the JOURNAL OF PHYSICAL CHEMISTRY at the one-year rate checked below:

	U.S.	*Canada***	*Latin America***	*Other Nations***
ACS Member One-Year Rate*	☐ $20.00	☐ $25.00	☐ $25.00	☐ $26.00
Nonmember	☐ $60.00	☐ $65.00	☐ $65.00	☐ $66.00

Bill me ☐ Bill company ☐ Payment enclosed ☐

Air freight rates available on request.

Name _____

Street _____ Home ☐ Business ☐

City _____ State _____ Zip _____

*NOTE: Subscriptions at ACS member rates are for personal use only. **Payment must be made in U.S. currency, by international money order, UNESCO coupons, U.S. bank draft, or order through your book dealer.

Molecular Sieve Zeolites

ADVANCES IN CHEMISTRY SERIES No. 101 and 102

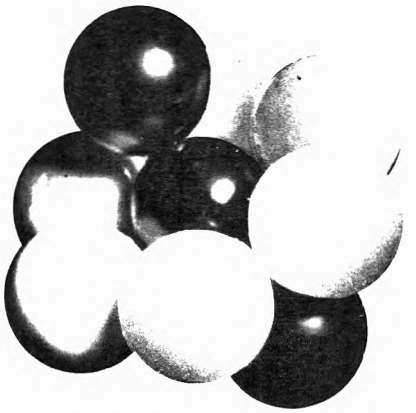

Seventy-seven papers from a symposium co-sponsored by the Divisions of Colloid and Surface Chemistry, Petroleum Chemistry, and Physical Chemistry of the American Chemical Society and Worcester Polytechnic Institute, Edith M. Flanigen and Leonard B. Sand, co-chairmen.

Do you need a group of substances that can remove radioactive isotopes from nuclear wastes, remove ammonia from secondary sewage effluents, remove sulfur dioxide from waste gases, foster formation of actinides, or disrupt bacterial cells? These and many other possibilities are available through research on molecular sieve zeolites. For example, they are used for separating hydrogen isotopes . . . solubilizing enzymes . . . carrying active catalysts in curing of plastics . . . transporting soil nutrients in fertilizers . . . filtering tars from cigarette smoke.

"Molecular Sieve Zeolites" reports recent advances in this rapidly developing field. Volume I offers 41 papers devoted to the synthesis, structure, mineralogy, and modification of sieve zeolites. These are followed in Volume II by 36 papers discussing sorption and catalysts.

Volume I: 526 pages with index	Cloth	(1971)	$16.00
Volume II: 459 pages with index	Cloth	(1971)	$16.00
No. 101 and 102 ordered together			$30.00

Postpaid in U.S. and Canada; plus 40 cents elsewhere.
Set of L.C. cards with library orders upon request.

Other books in the ADVANCES IN CHEMISTRY series on colloid chemistry include:

No. 95 Cellulases and Their Applications
Twenty-five papers stress the practical application of cellulolytic systems in biochemistry, animal nutrition, textiles, forest product utilization. Topics include new mechanisms for cellulose degradation, the cellulase complex, structure and morphology of cellulase, a commercial enzyme process and wood-derived products as nutritional sources.
470 pages with index Cloth (1969) $14.50

No. 87 Interaction of Liquids at Solid Substrates
Twelve papers survey recent research on solid/liquid interaction, including work on "coupling agents," adhesion of polymers, organic/inorganic interfaces, ultrasonic impedometry. Four more papers are concerned with heparinized surfaces at the blood/material interface.
212 pages with index Cloth (1968) $9.50

No. 84 Molecular Association in Biological and Related Systems
Nineteen articles survey and report new work on molecular association in fat digestion, in soap systems, in membrane constituents, and in mixed monolayers. Other topics include bile salt micelles, lipid monolayers and membranes, and a definitive review of biological membrane structure.
308 pages with index Cloth (1968) $10.50

No. 79 Adsorption from Aqueous Solution
Fifteen papers discuss thermodynamic and kinetic aspects of adsorption phenomena and the results of studies on a variety of adsorbate-adsorbent systems.
212 pages with index Cloth (1968) $10.00

No. 63 Ordered Fluids and Liquid Crystals
Twenty-two studies on characterization, properties, and occurrence of these phenomena in many substances such as tristearin, *p*-azoxyanisole, mono- and di-hydric alcohols, phospholipids, and polypeptides.
332 pages with index Cloth (1967) $11.50

No. 43 Contact Angle, Wettability, and Adhesion
Surface chemistry studies. Relation of equilibrium contact angle to liquid and solid constitution, contact angle as a thermodynamic property, surface energy estimation from contact angle. Contact angle hysteresis, relationship between wetting and adhesion.
389 pages with index Cloth (1964) $10.50

No. 33 Solid Surfaces and the Gas-Solid Interface
Thirty-seven papers from the Kendall Award Symposium honoring Stephen Brunauer. Theory and techniques for studying surface phenomena.
381 pages with index Cloth (1961) $12.00

Order from: **Special Issues Sales**
American Chemical Society, 1155 16th Street, N.W., Washington, D.C. 20036